Nitric Oxide Donating Furoxan Derivatives and Ruthenium(II) Complexes as Anticancer and Antibacterial Agents

by

Shireen H. Jozi

B.Sc., Simon Fraser University, 2016

Thesis Submitted in Partial Fulfillment of the
Requirements for the Degree of
Master of Science

in the
Department of Chemistry
Faculty of Science

SIMON FRASER UNIVERSITY
Summer 2018

Approval

Name:	**Shireen H. Jozi**
Degree:	**Master of Science (Chemistry)**
Title:	**Nitric Oxide Donating Furoxan Derivatives and Ruthenium(II) Complexes as Anticancer and Antibacterial Agents**
Examining Committee:	**Chair:** **Robert A. Britton** Professor
	Charles J. Walsby Senior Supervisor Associate Professor
	Vance E. Williams Supervisor Associate Professor
	Jeffrey J. Warren Supervisor Assistant Professor
	Tim Storr Internal Examiner Associate Professor
Date Defended/Approved:	August 27, 2018

Abstract

Ruthenium(II)-arene complexes were combined with furoxan (1,2,5-oxadiazole 2-oxide) moieties to generate new anticancer and antibacterial drug candidates. Previous studies have shown that Ru(II) organometallic complexes can exhibit significant anticancer activity with low levels of side-effects. Furoxans are heterocyclic molecules capable of releasing nitric oxide (NO), which can induce apoptosis or necrosis. Therefore, furoxans were employed as ligands for Ru(II)-arene complexes to design new drug candidates. Furoxan derivatives were synthesized with different substituents (-NO_2, -H, -OCH_3, -OPh, -SPh, -SOPh, -SO_2Ph), which were found to affect the amount of NO released. NO release was quantified via electron paramagnetic resonance (EPR) spectroscopy. The complexes were found to donate more NO than the ligands; the highest concentration of NO was donated by the complex containing (-SO_2Ph) substituent. Furthermore, antibacterial assays were performed, and the complexes exhibited higher cytotoxicity than the corresponding ligands. This work also reports the synthesis of a new heterobimetallic complex combining a Ru(II)-arene with a gold(III) compound.

Keywords: Nitric oxide; Furoxan; Ruthenium(II) anticancer complexes; Gold(III) anticancer complexes; heterobimetallic complexes; EPR

إهداء

إلى أغلى ما أملك .. أمي وأبي

وإلى من كان وسيبقى قدوتي في العلم .. إلى روح العالم أحمد زويل

Acknowledgements

The author would like to thank her senior supervisor Dr. Charles Walsby for his supervision during research and assistance in editing this work. In addition, the author acknowledges the supervisory committee: Dr. Vance Williams and Dr. Jeffrey Warren for their helpful comments. Furthermore, the author acknowledges Walsby research group; especially, the former member, Dr. Changhua Mu who assisted in the EPR measurements and provided his insight into the protocol used in the antibacterial assay described in Chapter 2. He also assisted in collecting crystal structure data for the novel Ru(II)-arene complex addressed in Chapter 3 – *Thank you Changhua for your support and friendship*. The author also acknowledges other collaborating graduate students: Declan McKearney from Leznoff research lab at SFU, who performed X-ray diffraction analysis on several compounds and solved the novel crystal of Ru(Pterpy)Cl_3 described in Chapter 3; Dr. Ryan Roberts from Leznoff research lab at SFU, who performed the X-ray fluorescence analysis described in Chapter 3.

The author acknowledges the National Cancer Institute for their acceptance to test four of the furoxan derivatives. The author also acknowledges: Dr. Brian Patrick from UBC for collecting crystal structure data for the Ru(II)-arene complex described in Chapter 2; Dr. Andrew Lewis for acquiring ^{1}H-^{15}N HMBC on the first furoxan derivative L1(-NO_2); Hongwen Chen for acquiring mass spectra; Dr. Eric Ye and Colin Zhang for their assistance in acquiring NMR on the 600 MHz instrument. Furthermore, the author would like to thank all the staff, technicians, and the research groups in the Department of Chemistry at SFU for their general assistance.

Finally, the author would like to thank the following professors from her undergraduate and graduate studies at SFU who were supportive and inspiring – *I know none of you will read this or even remember me, but I wrote it because I want to remember you*: Dr. Natalia Kouzniak – for teaching me not to give up; Dr. Gabriel Oba – for attending his lectures without being registered in his course; Dr. Pete Wilson – for inspiring many students to major in chemistry; Dr. George Agnes – for his patience when I was a slow marker during my first TAship; Dr. Dev Sharma – for being supportive and asking me to stay positive.

Table of Contents

List of Tables

List of Figures

List of Abbreviations

ACN	Acetonitrile
Damp	2-[(dimethylamino)methyl]phenyl
DBU	1,8-diazabicyclo(5.4.0)undec-7-ene
DCM	Dichloromethane
DMF	N,N-dimethylformamide
DMSO	Dimethyl sulfoxide
DNA	Deoxyribonucleic acid
DPPH	2,2-diphenyl-1-picrylhydrazyl
EDRF	Endothelium-Derived Relaxing Factor
eNOS	Epithelial Nitric Oxide Synthase (also called NOS III)
EPR	Electron Paramagnetic Resonance or Electron Spin Resonance (ESR)
eq	Equivalent(s)
ESDT	Ethylsarcosinedithiocarbamate
ESI-MS	Electrospray Ionization Mass Spectrometry
EtOH	Ethanol
FDA	Food and Drug Administration
GSH	Reduced Glutathione
GST	Glutathione S-transferase
GTN	Glyceryl trinitrate
HIV	Human Immunodeficiency Virus
HMBC	Heteronuclear Multiple Bond Correlation
HSQC	Heteronuclear Single Quantum Correlation
iNOS	Inducible Nitric Oxide Synthase (also called NOS II)
IR	Infrared
IUPAC	International Union of Pure and Applied Chemistry
MALDI-TOF	Matrix Assisted Laser Desorption Ionization – Time of Flight
MeOH	Methanol
MGD	N-(dithiocarbamoyl)-N-methyl-D-glucamine
MS	Mass Spectrometry
NADPH	Nicotinamide Adenine Dinucleotide Phosphate (reduced)
NAMI	New Antitumor Metastasis Inhibitor

NCI	National Cancer Institute
NHC	N-Heterocyclic Carbene
NMR	Nuclear Magnetic Resonance
nNOS	Neuronal Nitric Oxide Synthase (also called NOS I)
NOS	Nitric Oxide Synthases
PBS	Phosphate Buffered Saline
Pterpy	4'-(4-pyridyl)-2,2':6',2''-terpyridine
Quinpy	*N*-(8-quinolyl)pyridine-2-carboxamide
RA	Rheumatoid Arthritis
RAED	Ruthenium Arene Ethylenediamine
RAPTA	Ruthenium Arene (1,3,5-Triaza-7-phosphaadamantane)
RNS	Reactive Nitrogen Species
ROS	Reactive Oxygen Species
RR	Ribonucleotide Reductase
Rt	Room temperature
sGC	Soluble Guanylate Cyclase
SNP	Sodium nitroprusside
TEA	Triethylamine
terpy	2,2′:6′,2″-terpyridine
TLC	Thin Layer Chromatography
XRD	X-ray Diffraction
XRF	X-ray Fluorescence

Glossary

Acetylcholine	Neurotransmitter that carries signals between nerves and regulates muscle contraction.
Aconitase	An enzyme required in the Krebs cycle, contains a [4Fe-4S] cluster.
Active site	Also called the catalytic site; it is the part of the enzyme surface containing the amino acid residues that bind to the substrate to catalyse a specific reaction.
Angina	A medical condition characterized by the hardening of the blood vessels (coronary arteries) suppling oxygen to the heart muscle.
Angiogenesis	The development and differentiation of new blood vessels from pre-existing once.
Ascorbate oxidase	An enzyme catalyses the oxidation of ascorbate into dehydroascorbic acid.
Atherosclerosis	Narrowing of the arteries due to the presence of plaque (i.e., accumulation of fat, cholesterol, …etc.).
Apoptosis	Programmed cell death.
Azole	A five-membered heterocyclic compound containing one nitrogen atom and another heteroatom(s).
Bond order	The number of bonds between two atoms.
Cellular respiration	Metabolic reactions that convert nutrients into energy.
Cofactor	Inorganic ion required for the activity of enzyme(s); if the cofactor is an organic molecule then its called a coenzyme.
Complex I, II, IV	Proteins in the mitochondria required for cellular respiration.
Condensed heterocycles	A class of heterocyclic compounds that contain fused-ring(s); for example: quinoline.
Cytostatic cells	Cells that are not growing or dividing.
Cytotoxic	Being toxic to living cells.
Denitrification	A process performed by several bacterial strains; it is the reduction of nitrate to $N_{2(g)}$.
Endothelium	Single layer of cells found in the lining of organs and blood vessels.
Enzyme	A molecule (usually a protein) that catalyses reactions in biological systems.
Furoxan	1,2,5-oxadiazole 2-oxide; a five-membered heterocycle that can act as a nitric oxide donor.

Glial cells	The dominant type of cells in the central nervous system (i.e., brain and spinal cord) that support and act as insulators for the neurons (i.e., nerve cells that conduct electrical impulses).
Glutathione	A tripeptide (Cys-Glu-Gly) that helps in protecting the cells from reactive oxygen species (abbreviated GSH).
Glyceryl trinitrate	A medical drug used in the treatment of angina (abbreviated GTN).
Guanylate cyclase	Enzyme involved in muscle relaxation.
Half-life	The time required for the concentration of a reactant to decrease to half its original concentration.
HeLa cells	A cell line derived from cervical cancer cells.
Hydrophobic	A substance (or parts of) that is insoluble in water.
Hyperfine interaction	Interaction between electron spin and nuclear spin.
Hypoxic	Cells that are low in oxygen.
In situ	Synthesis of a compound in a reaction mixture; typically, compounds that are required as reaction intermediates, or difficult to isolate, or unstable are synthesized *in situ*.
In vitro	An experiment performed outside a biological system.
In vivo	An experiment performed in a whole or living organism.
Krebs cycle	The metabolic pathway that generates energy via aerobic respiration in the mitochondria.
Lumen	The cavity of an organ or blood vessel.
Macrophage	Immune cells that defend the body from microorganisms such as bacteria by engulfing and destroying them.
Mesoionic heterocycle	Five membered heterocycles belong to the non-benzenoid aromatics that has a dipolar structure with delocalized negative and positive charges; the term mesoionic combines the two terms (mesomeric and ionic).
Microorganism	An organism that can only be seen with a microscope; for example: bacteria.
Mitochondria	One of the components of the cell that is responsible for generating energy via a process known as cellular respiration.
Necrosis	Uncontrolled cell death; spreads cellular debris into the neighboring cells.
Neurodegeneration	The loss of function of the neurons due to alteration in their structure or their death.
Neurons	Nerve cells that conduct electrical impulses.

Neurotransmitter	A compound with low molecular weight whose function is to transmit nerve impulses.
Neutrophils	Immune cells in charge of destroying pathogens by ingesting them or by secreting specific enzymes.
Nitric Oxide Synthases (NOS)	A family of enzymes that synthesize nitric oxide from arginine in living systems. It contains three isoforms: nNOS (neuronal), iNOS (inducible), eNOS (endothelial).
Nitroglycerin	*see* glyceryl trinitrate.
Nitropress	A medical drug used to treat heart failure.
Nitrosyl complex	A transition metal complex that contains a NO ligand.
Normoxia	Normal level of oxygen.
Oxadiazole	A five-membered heterocyclic aromatic compound with the chemical formula $C_2H_2N_2O$.
Oxidative stress	A cellular state occurs when the rate of production of reactive oxygen species is higher than the rate of their degradation by antioxidants.
Oxygen-fixation hypothesis	The effect of oxygen on radiotherapy; this hypothesis postulates that molecular oxygen has affinity for electrons and can form the anionic superoxide radical ($O_2^{\cdot -}$), which damages the DNA.
Plasmodium	A genus of parasites that results in malaria.
Platelet	Blood cells that repair damaged blood vessels by forming clots.
Proteasomes	Protein complexes that hydrolyse unrequired proteins in the cell. Enzymes that assist proteasomes are called proteases.
Prototropy	A type of tautomerism that involves the migration of a proton between different parts of the molecule.
Purkinjie fibers	Specialized cardiac muscle cells in charge of conducting electrical impulses in the heart.
Reactive nitrogen species	Highly reactive products of nitric oxide (NO) reactions (abbreviated RNS).
Reactive oxygen species	Highly reactive chemical species that are produced from the partial reduction of molecular oxygen (abbreviated ROS).
Ribosomes	The organelles responsible for protein synthesis.
Selenols	Compounds containing the functional group R-Se-H.
Side-chain prototropic tautomerization	A specific form of prototropy that refers to the transfer of a proton between a ring and a side-chain.
Spin-trap in EPR	A molecule that traps the paramagnetic species and forms a stable spin-adduct that can be detected via EPR.

Sodium nitroprusside	*see* nitropress.
Superoxide dismutase	An enzyme catalyses the disproportionation (i.e., dismutation) reaction of superoxide, $O_2^{\cdot -}$, into oxygen, O_2, and hydrogen peroxide, H_2O_2.
Tautomerism	Coexistence of two or more molecular structures (i.e., tautomers or constitutional isomers) in an equilibrium due to their dynamic interconversion.
Thromboembolism	When a thrombus (i.e., clot) detaches from a blood vessel and travels into another location to plug a new vessel. For example, it can plug a vessel in the brain resulting in stroke.
Tumour	Abnormal mass of tissue caused by uncontrolled cell growth (i.e., cancer).
Vasodilation	Relaxation (dilatation) of blood vessels that causes the blood pressure to decrease.
Warburg effect	The anaerobic glycolysis and fermentation in the presence of oxygen; this phenomenon occurs in cancer cells.

“Weak people revenge.

Strong people forgive.

Intelligent people ignore.”

- Albert Einstein

Chapter 1. Introduction

Cancer is one of the major causes of death in Canada and in the world. During the next two decades, it is predicted that there will be 22 million new cancer cases worldwide.[1] The Canadian Cancer Statistics estimated that in 2017 there were 206,200 new cancer cases and 80,800 deaths from this disease in Canada.[2] There are three main types of cancer treatment: surgery, radiotherapy, and chemotherapy.[3-5] The first two methods can only remove solid tumours (i.e., localized cancer cells).[3, 5] However, migrating cancer cells, which are known as metastasized cells, cannot be treated by these approaches.[3, 5] In addition, surgery and radiotherapy cannot remove all cancer cells from solid tumours. Thus, there is a need to design chemotherapeutics that target these cells to provide complete cancer remission.

Metals have a variety of applications as chemotherapeutics due to their biological and chemical properties.[6-8] The behaviour of metal ions can be tuned by their coordinating ligands.[9-12] In one common example, DNA is the target for several metal-based anticancer therapeutics.[13] Metal ions are capable of interacting with DNA by coordinating to its basic nitrogen and oxygen atoms.[14] Furthermore, some metals are redox active and can generate radicals that create structural distortions in DNA.[15, 16] These distortions hinder cell division and therefore prevent propagation of cancer in the body.[17-19] In recent years, other novel approaches were developed to generate metal complexes that target cancer cells in different ways. For example, protein inhibitors and photoactivated complexes have garnered attention.[13, 20, 21]

1.1. Platinum-based chemotherapeutics

Platinum-based (Pt-based) chemotherapeutics are currently used in clinics against several forms of cancer.[22-24] They are considered the benchmark for metal-based anticancer compounds.[22, 25, 26] Cisplatin, *cis*-diamminedichloroplatinum(II), was the first reported Pt-based anticancer drug (**Figure 1.1**).[27] The United States Food and Drug Administration (FDA) approved the clinical use of this compound in 1978, and it is still used widely in modern chemotherapy.[22] It was first synthesized by Michele Peyrone in 1845, but its anticancer properties were not discovered until 1965 by Barnett Rosenberg.[28, 29] Cisplatin can enter the cell via passive diffusion and active transport (through membrane proteins).[30, 31] It can bind to DNA after chloride ligand exchange with water.[31] This results in structural distortions in the DNA and eventually cell death via apoptosis.[32] Cisplatin can also platinate the tubulin protein and thus prevent microtubule

assembly, a process that is required for cell division.[33] The main use of cisplatin is in the treatment of genitourinary tumours, such as testicular and ovarian cancers.[14] Further research has led to the development of other Pt-based compounds such as carboplatin, *cis*-diammine(1,1-cyclobutanedicarboxlyto-O,O')platinum(II), and oxaliplatin, (*1R,2R*-diaminocyclohexane)(oxalato-O,O')platinum(II) (**Figure 1.1**).[27] These drugs were approved for clinical use in the treatment of different forms of cancer, such as head and neck and lung cancers.[34] Although Pt-based drugs are effective chemotherapeutics, they cause several side-effects due to their low specificity. Side-effects include nephrotoxicity (i.e., toxicity in the kidneys), ototoxicity (i.e., toxicity in the ears) and nausea.[35-37] Furthermore, some cancer cells can become resistant to these drugs by activating more DNA repair mechanisms and/or by increasing the drug efflux rate.[36, 38, 39]

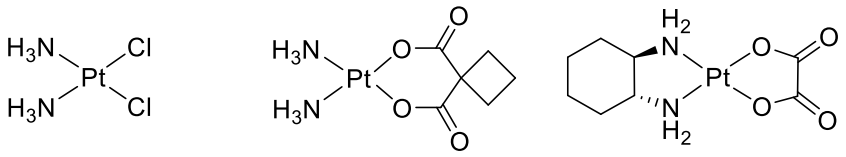

Figure 1.1. Pt(II)-based chemotherapeutics currently in clinical use.

1.2. Ruthenium(III)-based complexes

Toxicity, low selectivity, and acquired cellular resistance are major issues for Pt-based chemotherapeutics.[40-43] Therefore, researchers are investigating the anticancer activity of other metals.[44-46] A number of ruthenium-based (Ru-based) complexes exhibit anticancer activity and lower cytotoxicity than Pt-based drugs.[3, 47, 48] Ligand exchange rates for both platinum and ruthenium-based complexes are slow (typically one to two hours) which is comparable to the rate of cell division. This property of ligand exchange is one factor in these metal's anticancer activity.[49] Ru(III) complexes typically have a six-coordinate octahedral geometry and therefore have a greater variety of ligand combinations and isomers compared to the four-coordinate, square-planar geometry of Pt complexes.[50] This extends the potential to tune the properties of the compounds, giving more scope to target anticancer pathways.[51, 52] Moreover, the reduction of Ru(III) to Ru(II) does not change the geometry of the complexes, as opposed to the reduction of Pt(IV) to Pt(II), which changes the number of ligands and bond lengths.[50]

The first Ru(III)-based complex to enter clinical trials in 1999 was NAMI-A (**N**ew **A**ntitumour **M**etastasis **I**nhibitor-**A**), imidazolium *trans*-[tetrachloro-(dimethylsulphoxide)(1*H*-imidazole)ruthenate(III)] (**Figure 1.2**).[3, 53] NAMI-A was found to be 1000-fold less cytotoxic than cisplatin.[54] Tumour cells do not internalize this drug, instead, it interacts with membrane proteins, such as collagen.[55, 56] The membrane-binding mechanism of NAMI-A reduces the activity of certain enzymes in metastasized cells.[57] Therefore, NAMI-A is effective against metastasis as opposed to primary tumours.[55-59] Recently, NAMI-A was found to be effective against leukaemia; however, it has not yet been approved for clinical use.[60]

The second Ru-based compound to enter clinical trials was indazolium *trans*-[tetrachlorobis(1*H*-indazole)ruthenate(III)], which is commonly known as KP1019 (**Figure 1.2**).[50] Unlike NAMI-A, KP1019 can be internalized by cancer cells and therefore it is effective against primary tumours.[55] Both NAMI-A and KP1019 are able to bind to the most abundant protein in the serum, human serum albumin (hsA). These drugs also bind to human serum transferrin (hsT).[61, 62] Transferrin functions to deliver iron to the cell.[63] More transferrin receptors are found on the membrane of some tumour cells compared to the healthy ones, because these cells divide rapidly and thus require more nutrients, such as iron.[62] Therefore, both albumin and transferrin may play a role in carrying Ru(III) complexes to the targeted cancer cells.[64, 65]

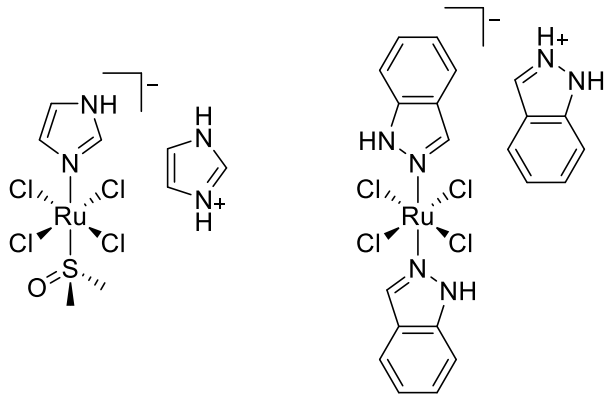

NAMI-A KP1019

Figure 1.2. Ru(III)-based anticancer complexes.

1.3. Ruthenium(II) piano-stool complexes

There have been significant developments in the field of Ru(II) organometallic anticancer therapeutics.[66-71] In particular, Ru(II)-arene piano-stool complexes (**Figure 1.3**) have shown promise in preclinical studies.[66, 72-75] These coordination compounds are designed with η^6-arene ring(s), which provide a stable piano-stool, pseudo-octahedral geometry, and act as a hydrophobic surface that increases the permeability of the complex across the cell membrane.[76]

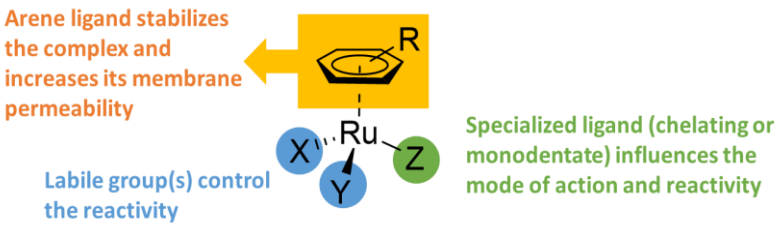

Figure 1.3. The general chemical structure of Ru(II)-arene complexes.

If these ligands are extended arene rings, such as dihydroanthracene, they can allow interactions with DNA via intercalation (i.e., stacking between base pairs).[64, 77] Typically, the arene used in these types of compounds is one of the following aromatic rings: benzene, hexamethylbenzene, tri-isopropylbenzene, cymene, or biphenyl.[66, 78] By examining several Ru(II)-arene complexes, researchers concluded that the lipophilicity of the arene ligand can impact the cytotoxicity of the compound.[66] Lipophilic complexes have better cell permeability, and thus are more likely to be internalized by cells.[66, 79] However, in a recent study the opposite effect was observed; replacing the arene ring, *p*-cymene, with less lipophilic benzoate resulted in higher cytotoxicity.[80] Benzoate has an electron withdrawing substituent (-OCO^{-}) on benzene making the ring less lipophilic than *p*-cymene which has electron donating alkyl groups. In addition, Ru(II)-arene complexes are characterized by having one or two labile group(s) and a monodentate ligand or chelating ligand.[66, 78]

There are two general types of Ru(II)-arene complexes that have become the focus of current research. The first of these are called RAPTA complexes and were developed by Dyson and co-workers.[81] RAPTA complexes with the general chemical formula [$Ru^{II}(\eta^6$-arene)X_2(PTA)] (PTA: 1,3,5-triaza-7-phosphaadamantane, X: leaving group, typically chloro ligand), are common Ru(II)-arene compounds that have lower toxicity than NAMI-A.[82] In 2001, the first member of this class of compounds, RAPTA-C, [Ru(η^6-p-cymene)Cl_2(PTA)], was reported.[83] This complex can

selectively damage the DNA in cancer cells while leaving healthy cells relatively unaffected, since it is only active at pH ≤ 7.[83] Tumour cells are hypoxic (i.e., low in oxygen), hence they have lower pH than the physiological (pH ≥ 7.4).[81] Furthermore, RAPTA-C was found to possess anti-metastatic activity (**Figure 1.4**).[84] On the other hand, the analogue of RAPTA-C, DAPTA-C [Ru(η^6-p-cymene)Cl_2(DAPTA)] (DAPTA: (3,7-diacetyl-1,3,7-triaza-5-phosphabicyclo[3.3.1]nonane)) exhibits anti-angiogenic activity (i.e., prevent the growth of new blood vessels at the tumour site).[85] The amphiphilic PTA ligand was found to increase the solubility of RAPTA complexes; however, this is limited by the nature of the coligands.[81] Researchers also reported that some RAPTA complexes exhibit antibacterial activity that does not correlate with their ability to damage DNA *in vitro* suggesting that the mechanism of action may not always involve DNA.[81]

It has been demonstrated that the chloro-ligand(s) in RAPTA compounds exchange with water (i.e., aquation or hydrolysis) when the chloride concentration in the environment is low. This process increases the biological reactivity of the complexes.[78, 81] Hydrolysis does not occur as readily in the blood plasma because the chloride concentration is high ([Cl^-] = 104 mM).[78] However, the intracellular and intranuclear systems have lower chloride concentration, [Cl^-] = 23 mM and 4 mM, respectively, which promotes aquation.[78] RAPTA compounds are the basis for the complexes described in this thesis, where DNA intercalating or nitric-oxide donating groups have been coordinated in place of the PTA ligand.

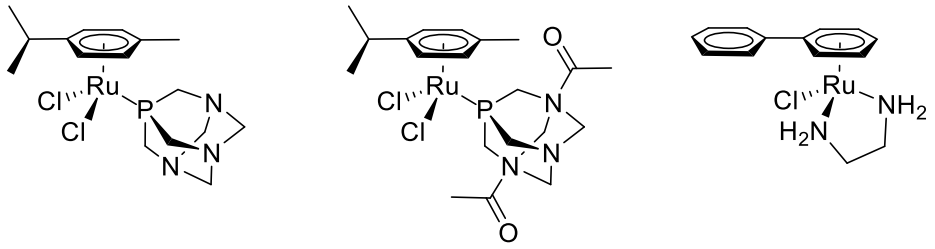

RAPTA-C DAPTA-C RAED

Figure 1.4. Chemical structures of anticancer Ru(II) piano-stool complexes.

The second type of anticancer Ru(II)-arene complexes is called RAED (**R**uthenium **A**rene **E**thylene**d**iamine) or [Ru(II)(η^6-arene)X(en)]. This family of compounds was first reported in 2001 by Sadler and co-workers.[86] RAED is effective against primary tumours, such as ovarian cancer, and reduces the development of lung metastasis (**Figure 1.4**).[86, 87] The cytotoxicity of these compounds was found to be affected by the hydrophobicity of the arene ring(s), the stability of the chelating ligand, and the ability of the halide leaving group to exchange with water.[64, 78]

Aquation influences the solubility of the complex and its electrostatic interaction with DNA.[64, 78] Another factor that impacts this process is the nature of the chelating ligand where electron donors enhance halide ligand exchange.[75] These Ru(II) piano-stool complexes can coordinate to guanine bases in DNA after aquation, which results in structural distortions and causes the cell to undergo apoptosis.[64, 87] Apoptosis is the goal of most chemotherapeutics because this process is less damaging to the surrounding healthy tissues in comparison to necrosis (i.e., uncontrolled cell death).[88]

1.4. Heterometallic ruthenium(II)-based anticancer chemotherapeutics

As described above, some Ru(II) complexes were found to exhibit anticancer properties *in vitro* and *in vivo*.[66, 77] Therefore, researchers began investigating the effect of adding another metal with anticancer properties to Ru(II) scaffolds. It is reasonable to expect better bioactivity when having multiple functional sites in the molecular structure of a single compound. The synergistic interaction of metal centres may also result in novel modes of action against cancer, and the nature and length of spacer groups can influence metal-metal interactions.[66, 89] In 1998, BBR3464 became the first multinuclear complex to enter clinical trials (**Figure 1.5 – a**).[90] It contains three Pt(II) centers and was found to interact electrostatically and covalently with DNA.[66] BBR3464 is active against gastric, ovarian, lung, and melanoma cancers. However, it was removed from clinical trails at Phase II.[14, 66, 90, 91]

Pt(II) was also combined with Ru(II) to generate a flexible binuclear complex capable of interacting with the DNA through two sites (**Figure 1.5 – b**).[92] The Ru centre has intercalative and electrostatic interactions with the DNA minor groove, while Pt(II) coordinates to the major groove.[92, 93] Trimetallic complexes, such as ruthenocene linked to Pt(II) or Au(I), have the potential of acting as anticancer, antimalarial, or anti-HIV therapeutics.[94] The ruthenocene complexes presented in **Figure 1.5 – c** exhibited anticancer activity against HeLa cells, a cell line derived from cervical cancer cells.[66, 94] The Ru(II)-arene scaffold has also been linked to other mononuclear complexes to generate active anticancer agents. **Figure 1.5 – d** shows the structure of Ru(II)-arene, analogous to RAPTA-C, linked to titanocene.[66, 95] This bimetallic compound was found to be cytotoxic in ovarian cancer cells and exhibited better activity than the mononuclear building blocks.[66, 95] In addition, Ru(II)-arene linked to *cis,cis,trans*-diamminedichloridobiscarboxylatoplatinum(IV) acts as a cisplatin prodrug.[66] Pt(IV) is reduced in cells to Pt(II) forming cisplatin and the axial spacer, 2-pyridinepropionate, dissociates.[66]

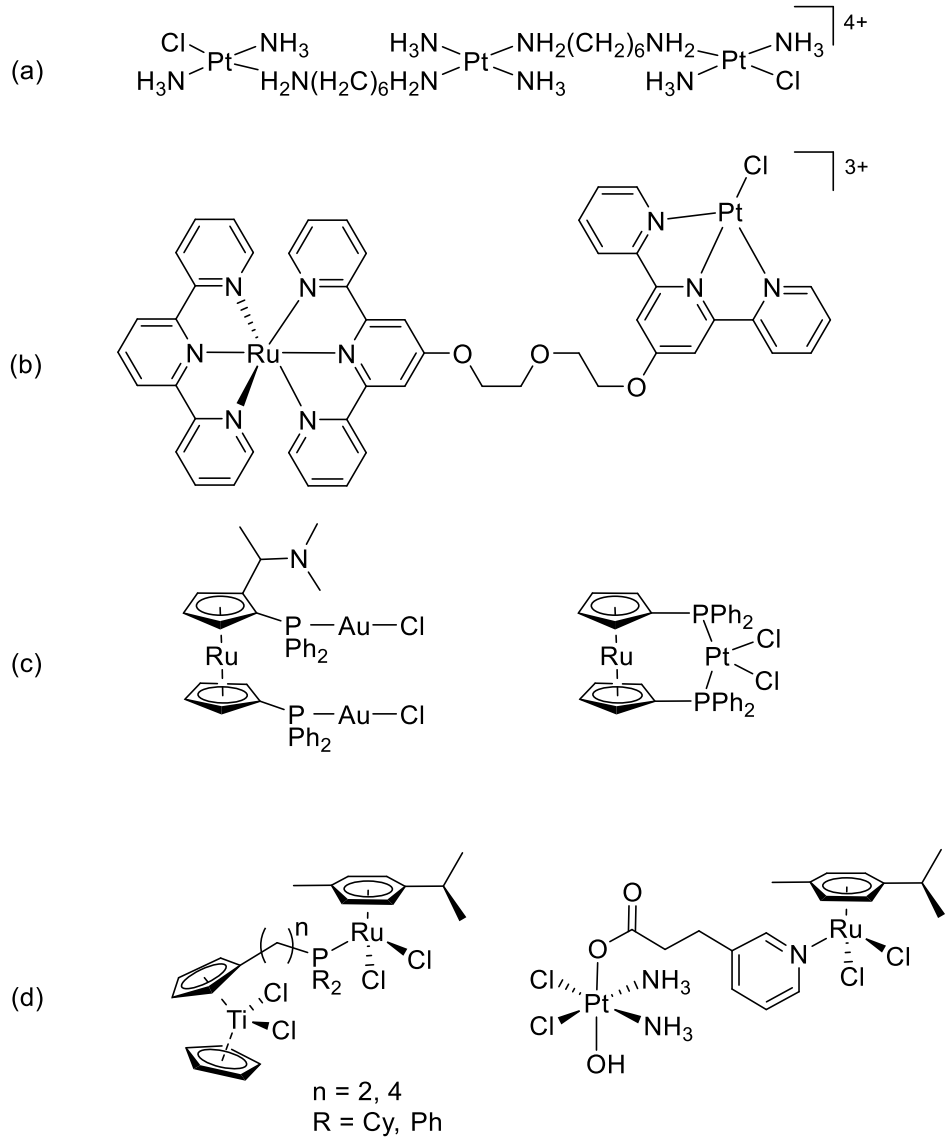

Figure 1.5. Chemical structure of some multinuclear chemotherapeutics.

1.5. Nitric oxide donors and their anticancer properties

Nitric oxide (NO) is an endogenous radical that has several biological functions.[96-99] The major role of NO is to act as a vasodilator* (i.e., relaxes the arteries in order to lower blood pressure).[97, 100] Thereby, nitric oxide regulates blood pressure and prevents heart attack and stroke.[100-102] Furthermore, NO is cytotoxic and genotoxic at high concentration. NO induces cell

* This topic is explained in Chapter 2.

death and inhibits metastasis in some forms of cancer, for example, pancreatic, liver, breast, ovarian, and skin.[100, 103-106] Low concentrations of NO (<300 nM) were found to assist in cancer cell proliferation and activate angiogenic factors.[105-107] At higher concentrations of NO (>300 nM), the rate of phosphorylation of a tumour suppressor transcription factor known as p53 increases.[105, 107, 108] Phosphorylation activates p53, which results in cytostasis (i.e., halts cell division or growth) or apoptosis (i.e., programmed cell death).[105, 108] Therefore, the bioactivity of NO in tumour cells is dependant on its concentration, the tumour site microenvironment, and the duration of exposure (**Figure 1.6**).[96, 97, 106] In addition, nitric oxide acts as a ligand and coordinates to different metals, such as iron and copper, present in metalloproteins.[105, 109, 110] For example, NO can inhibit cellular respiration by binding to the iron and copper present in cytochrome c oxidase (also known as complex IV) in the mitochondria.[96, 105] Furthermore, high concentration of NO can inhibit glycolysis (i.e., breakdown of glucose) in tumour cells.[105] Tumour cells produce energy from glycolysis followed by lactic acid fermentation.[111] This interesting phenomenon in cancer cell metabolism is known as the Warburg effect, which is defined as the anaerobic glycolysis and fermentation in the presence of oxygen, and was reported in 1920 by the Nobel laureate Otto Warburg.[111, 112]

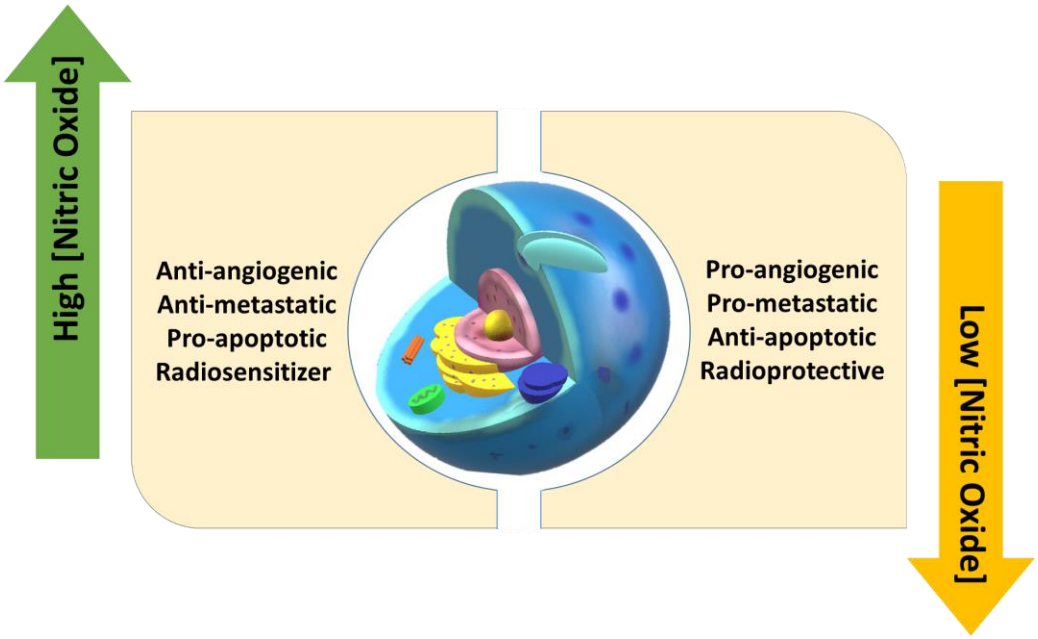

Figure 1.6. The effect of nitric oxide concentration on tumour cells.

Under normal levels of oxygen (i.e., normoxia), nitric oxide is synthesized from the amino acid L-arginine via enzymes known as nitric oxide synthases (NOS).[97] NO can also be produced from serum nitrite by deoxyhemoglobin.[113, 114] When the partial pressure of oxygen is low (i.e.,

hypoxia), NOS enzymes are deactivated, and the oxygen deficiency will trigger deoxyhemoglobin to reduce nitrite to NO.[97, 113, 114] Solid tumours, such as head and neck tumours, have regions of hypoxia. Although they tend to grow new blood vessels (i.e., angiogenesis), these vessels are not sufficient to supply blood to the tumour site, which drops the level of oxygen.[115, 116] The hypoxic regions in tumours are also radioresistant.[117-119] In radiotherapy, radiation is used to ionize biomolecules and generate electrons that undergo various reactions to form radicals.[120] Radicals can damage the DNA and/or other parts of the cancer cell.[120, 121] Oxygen was found to amplify the effect of radiation in cells.[120, 122] It has an affinity for electrons and can form the anionic superoxide radical ($O_2^{\cdot -}$), which damages DNA.[120, 122] The effect of oxygen on radiotherapy is known as the oxygen-fixation hypothesis.[121] This explains why hypoxic cells are less sensitive to radiation.[120]

Molecules other than oxygen also have an affinity for electrons, and thus can increase the sensitivity of tumour cells to radiotherapy.[120] Researchers have attempted to develop such molecules, which are known as radiosensitizers or radio-enhancers.[120] According to some experiments, nitric oxide was effective in radio-sensitizing hypoxic tumour cells.[106, 123-128] Other experiments refuted this observation.[97, 107, 129] Subsequently, researchers came to realize that whether or not NO acts as a radiosensitizer is dependant on the cellular environment and the concentration of NO.[97, 106, 107]

RRx-001, (1-bromoacetyl-3,3-dinitroazetidine), is a radiosensitizer that is selectively activated in hypoxic tumour cells to release nitric oxide (**Figure 1.7**).[97, 130, 131] This anticancer agent is currently in phase II clinical trails.[130] As stated earlier, deoxyhemoglobin acts as a reducing agent under hypoxia; thus, it reduces ($-NO_2$) substituents in RRx-001 and generates NO.[97] Furthermore, NO released by RRx-001 can dilate the blood vessels allowing oxygenation of the tumour cells.[132] As a result, RRx-001 is used in combination therapy studies as an agent to increase the sensitivity of tumour cells toward chemo and radiotherapy.[130] Researchers have anticipated using RRx-001 as a chemosensitizer in several other diseases, such as malaria and sickle cell anemia.[133, 134] Interestingly, RRx-001 is a dinitroazetidine derivative, which is a class of high energy compounds that was originally used in aerospace industry before being identified as a novel class of anticancer agents.[133]

Another NO donor drug, known as OKN-007 (2,4-disulfophenyl-tert-butylnitrone, **Figure 1.7**), is also in clinical trials.[135] This drug is effective against malignant glioma (i.e., brain tumour).[135] The mechanism of action of OKN-007 is still unknown, but, it is thought that it acts as a scavenger of free radicals.[135]

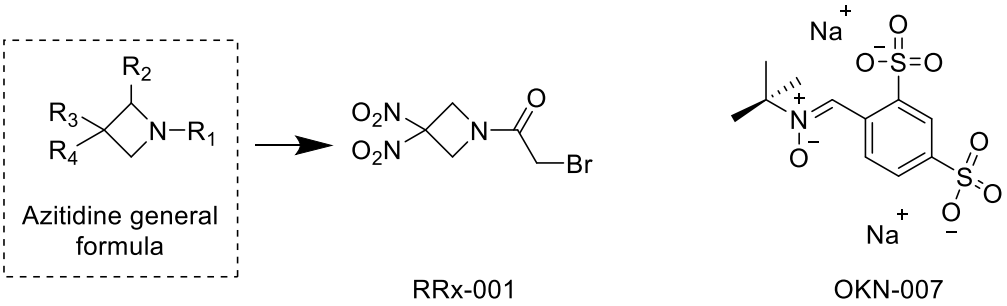

Figure 1.7. Nitric oxide anticancer agents currently in clinical trials.

In addition, researchers have synthesized ruthenium nitrosyl complexes to study their NO donating properties. Ruthenium complexes of the form *trans*-$[(NO)L(NH_3)_4Ru]^{3+}$ (L = an aromatic nitrogen heterocycle) function as vasodilators.[136] Since nitric oxide can inhibit tumour growth, some ruthenium nitrosyl complexes were found to exhibit anticancer activity, such as the trinuclear Ru complex presented in **Figure 1.8**.[78, 137] This cluster was found to exhibit cytotoxicity against melanoma cells.[137] Furoxan (1,2,5-oxadiazole 2-oxide) derivatives are nitric oxide donors that were used as ligands on Pt(II) complexes to generate molecular hybrids with pronounced cytotoxicity in colon and gastric cancer cell lines.[138] Other furoxan derivatives were found to be cytotoxic in sarcoma and mammary adenocarcinoma (**Figure 1.8**).[139]

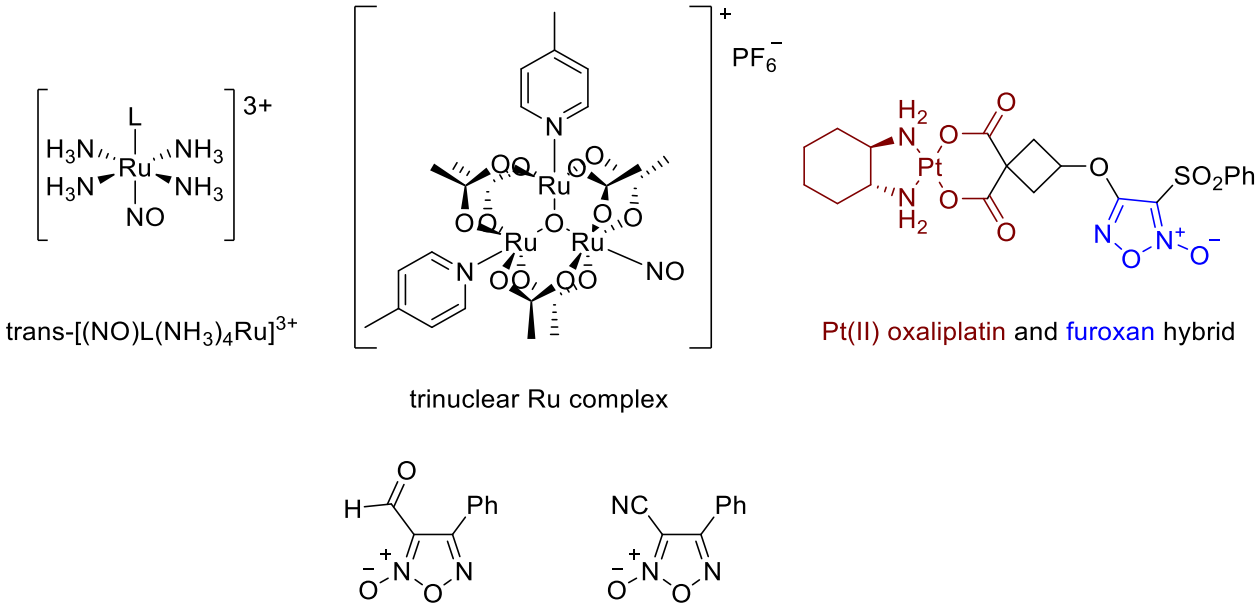

Figure 1.8. Nitric oxide releasing compounds with anticancer activity.

1.6. Antibacterial agents: historical overview and the application of nitric oxide donors

Antibacterial agents have a long history. In 1928, Sir Alexander Fleming discovered the world's first antibiotic, penicillin, which is a natural product used to treat several bacterial infections, such as pneumonia and scarlet fever.[140, 141] Afterword, Albert Schatz and Selman Waksman successfully isolated the natural product streptomycin, which was the first antibiotic to treat tuberculosis.[140] The period between the 1960s and 1990s witnessed the discovery of several synthetic drugs by medicinal chemists.[141] Nalidixic acid was the first quinolone antibacterial agent isolated as a by-product from the synthesis of chloroquine.[142] Although, the discovery of penicillin marks the world's first antibiotic, in 1910 the German scientist Paul Ehrlich was the first to introduce a synthetic compound with antimicrobial activity.[140] His compound, 3-amino-4-hydroxyphenylarsenic(I) (also known as arsphenamine, Salvarsan or compound 606), was found to be effective against syphilis and trypanosomiasis (**Figure 1.9**).[140] Arsphenamine is the world's first chemotherapeutic agent, initiating the concept of chemotherapy. Surprisingly, the structure of this compound was not confirmed until 2005 via electrospray ionization mass spectrometry.[143]

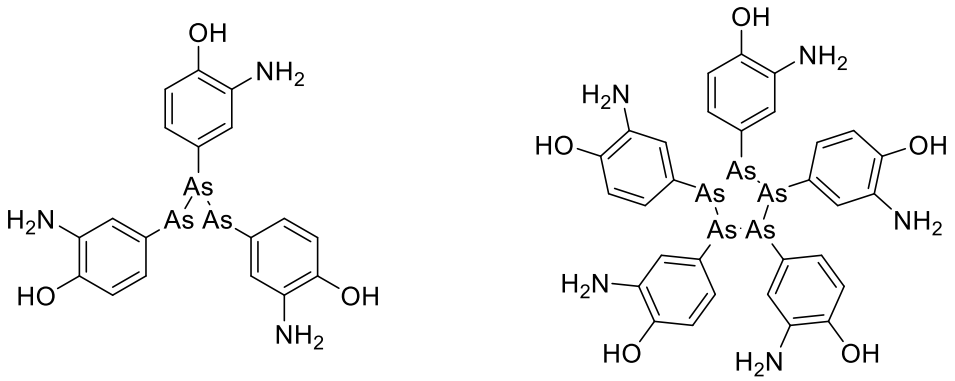

Figure 1.9. Arsphenamine is a mixture of a trimer and a pentamer of organoarsenic compounds.

Bacterial infections represent a global problem as microorganisms can develop resistance to a variety of antibiotics.[144, 145] There is a continuous demand for new drugs that can have different modes of action than the classical antibiotics to overcome bacterial resistance that resulted from drug overuse in the past.[146-148] The majority of the current antibiotics originate from natural products or their derivatives (i.e., semisynthetic).[141, 149] These compounds can target different parts of the bacterium including the cell wall, the ribosomes, or the DNA.[141] Natural products have proven to be effective antibiotics over the years, but they tend to be difficult to synthesize in the laboratory.[141] According to an analysis of FDA-approved drugs as of the year 2016, the antibiotics derived from microbes (i.e., bacteria and fungi) are 97% of all the antibacterial natural products.[150] Some, especially first-generation antibiotics, are metabolites (i.e., molecules used in metabolism) extracted from microbes.[141] These microorganisms have the genetic code to acquire resistance against their metabolites and can pass this code to the bacteria present in the environment.[141]

Recent research focuses on developing synthetic antibiotics that have unconventional targets.[141] Synthetic compounds need to have structural features that allow them to penetrate the bacterium cell wall since antibiotics rely on active transport (i.e., passing through transmembrane proteins) rather than diffusion.[149] An example of an unconventional antibiotic is tigecycline (**Figure 1.10**).[151] The FDA approved the clinical use of this drug in 2005.[151] Tigecycline is the first tetracycline in a new class of antibiotics known as glycylcyclines.[151] This semisynthetic drug is used to treat multi-drug resistant bacteria that have acquired an efflux pump and ribosomal protection.[151] **Figure 1.10** is a timeline illustrating some of the important discoveries and historical advancements in the field of antibiotics.

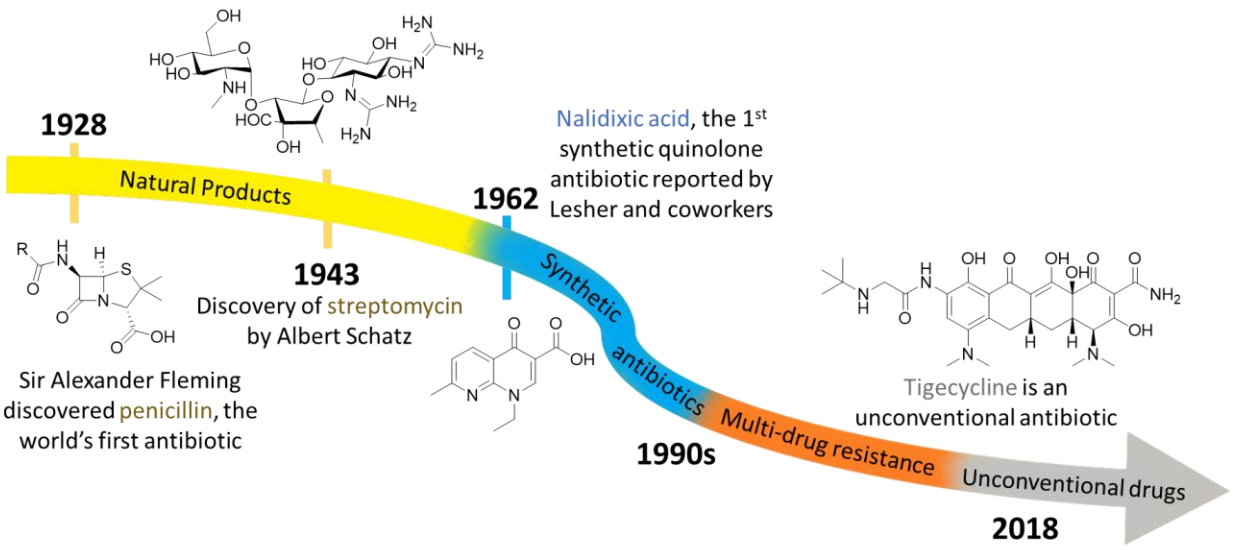

Figure 1.10. Timeline illustrating the historical development of antibiotics.

Endogenous nitric oxide is produced as an immunological response to pathogens.[152-154] NO and the products that result from its reaction with other molecules in the cell were found to exhibit antibacterial activity.[153] The products of NO reactions, such as S-nitrosothiols and peroxynitrites ($ONOO^-$), are known as Reactive Nitrogen Species (RNS) and have been found to mutate bacterial DNA by deaminating its nucleosides or promote strand breaks.[153] Since nitric oxide is generated in higher organisms as part of their immune defence mechanism, researchers anticipated that synthesizing NO-donors that may potentially exhibit activity against multi-drug resistant bacteria.[155] For example, nanoparticles were found to be effective scaffolds in carrying NO and delivering it to bacteria.[156, 157]

Relevant to this thesis are reports that furoxan derivatives can act as antibacterial agents since they are capable of releasing NO under physiological conditions.[158] For example, the benzofuroxan derivative presented in **Figure 1.11 – A** was found to be effective against several bacterial strains, such as Gram-positive *Staphylococcus aureus* and Gram-negative *Escherichia coli (E. coli)*.[159] The sulfonylhydrazone furoxan derivative, (*E*)-3-methyl-4-((2-tosylhydrazono)methyl)-1,2,5-oxadiazole 2-oxide, was also found to be effective against *E. coli* (**Figure 1.11 – B**).[160] Aside from their antibacterial activity, furoxan derivatives were found to be effective against viruses and parasites. **Figure 1.11 – C, D** shows two furoxan derivatives that are effective against *Trypanosoma cruzi* and *Plasmodium falciparum* (the malaria parasite).[161]

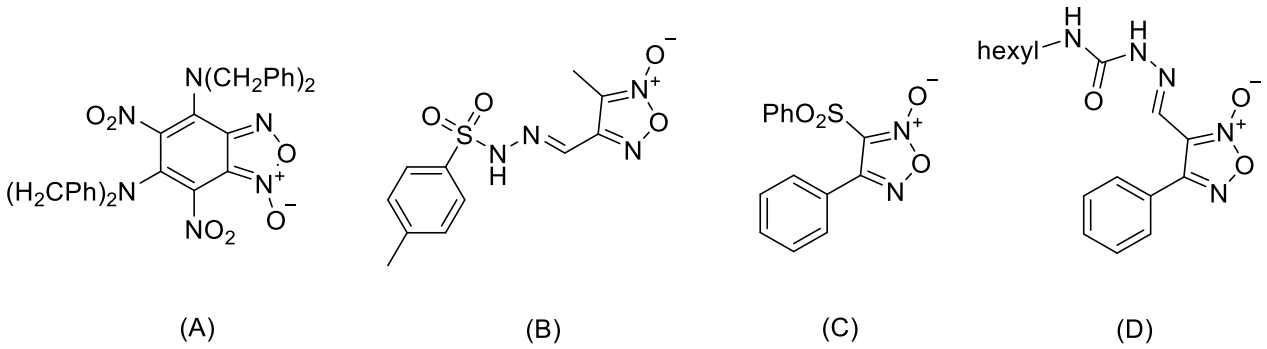

Figure 1.11. Antibacterial furoxan derivatives.

1.7. Gold in medicinal chemistry

Chrysotherapy (derived from the Greek word for gold, *chrysos*) or aurotherapy is the treatment of diseases using gold-based compounds.[162] The use of gold in medicine is dated back to 2500 B.C., where the Egyptians and Chinese used it in the treatment of some diseases, such as syphilis.[65, 162] However, it had a small contribution in formulating drugs, as early physicians faced tremendous difficulty in dissolving gold to generate soluble remedies.[163] Medieval alchemists solved this problem by developing potable gold, *aurum potabile*.[163] The utilization of gold in modern chemotherapeutics began in 1890, when Robert Koch discovered the role of gold cyanide in treating tuberculosis.[164] Gold cyanide, $[Au(CN)_2]^-$, also exhibits anti-HIV (**H**uman **I**mmunodeficiency **V**irus) activity.[165, 166] Several gold(I) thiolate salts were developed as anti-tubercular agents between 1925 and 1935.[164] In the 1920s, the physician Jacques Foresteir began examining the application of gold in the treatment of rheumatoid arthritis (RA), since the patients who were administered gold drugs during clinical trials, experienced reduced joint pain.[164] Several gold-based compounds were synthesized and tested against RA. Auranofin, $Et_3PAu^{I}SR$, (trade name Ridaura) and sodium aurothiomalate, $[Au^{I}\text{-}S\text{-}CH(CO_2Na)(CH_2CO_2Na)]_n$, (trade name Myochrysine) are gold(I) complexes used in clinics as anti-arthritic agents (**Figure 1.12**).[165] Auranofin which was synthesized by Sutton and co-workers, was approved for clinical use in 1985, and around the same year, reports showed that it exhibits antitumor activity due to its cytotoxicity.[164] Therefore, researchers began focusing on the synthesis of new Au(I) phosphine complexes, such as $[Au(d2pypp)_2]Cl$, to examine their role as anticancer agents (**Figure 1.12**).[164] Medicinal chemists were motivated to synthesize Au(III) complexes as potential anticancer chemotherapeutics, since Au(III) possesses the same square planar geometry as Pt(II) in

cisplatin. Furthermore, Au(III) and Pt(II) are isoelectronic (i.e., 8 electrons in d-orbitals) and thus might demonstrate the same biological activity. Recent studies have focused on applying auranofin and aurothiomalate in the treatment of several forms of cancer, such as chronic lymphocytic leukemia and lung cancer.[167]

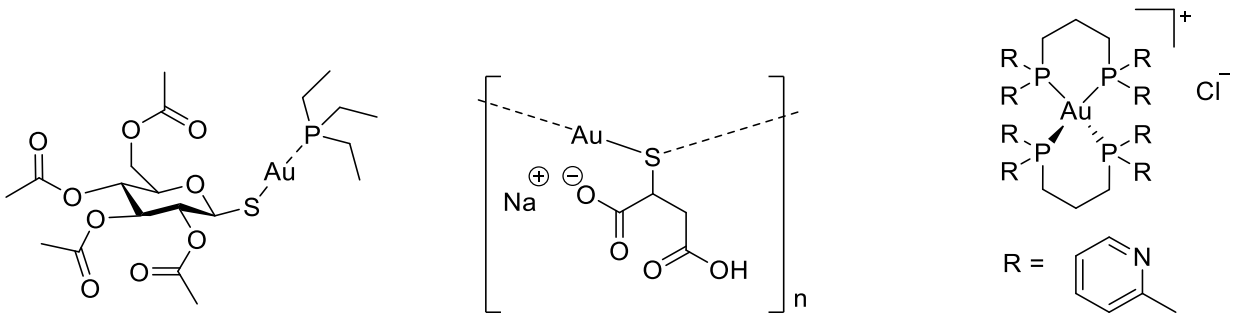

Figure 1.12. Common gold-based chemotherapeutics. Both auranofin and sodium aurothiomalate are used in clinics to treat arthritis.

The interest in using gold complexes as therapeutic agents stems from their ability to interact with thiol groups present in proteins, as well as, selenols present in enzymes like thioredoxin reductase.[164] Thioredoxin reductase is the enzyme responsible for regulating the redox reactions inside cells, thus it is the target of several chemotherapeutics.[164] Au(I) and Au(III) complexes can inhibit the activity of this enzyme because they have high affinity for cysteine and selenocysteine amino acids, which are present in its active site.[164] The inhibition of thioredoxin reductase, which is present in the mitochondria, leads to cell death.[164]

1.8. Gold(I) anticancer compounds

Gold(I)-based anticancer compounds are divided into two categories: 1) neutral complexes that possess linear geometry, such as auranofin and 2) positively charged complexes, such as [Au(d2pypp)$_2$]Cl, which was found to be selectively active against breast cancer.[164] Both categories were found to display the same mode of action. They target the mitochondria and cause oxidative stress, which leads to apoptosis.[164] Recent research focuses on synthesizing gold(I) complexes with N-heterocyclic carbene (NHC) ligands since these compounds were found

to be selectively cytotoxic against tumour cells.[168-170] Studies showed Au(I)-NHC complexes that are lipophilic and positively charged can accumulate more readily in cancer cells (i.e., have higher bioavailability), particularly in the mitochondria.[171] Coordination of highly lipophilic ligands, such as triphenylphosphine has been found to enhance mitochondrial uptake.[167] Examples of Au(I)-NHC complexes are presented in **Figure 1.13**.

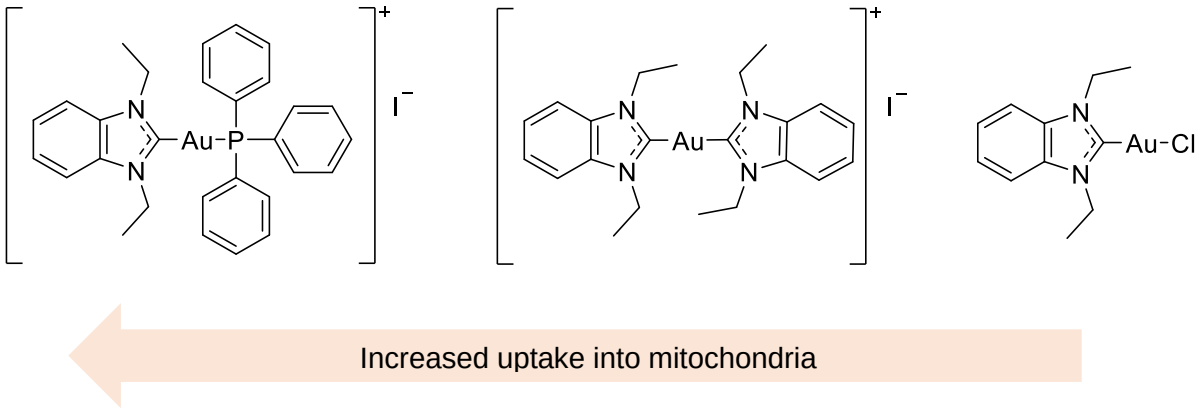

Figure 1.13. Examples of gold(I) N-heterocyclic carbene (NHC) complexes.

1.9. Gold(III) anticancer compounds

Gold(III) has a high reduction potential rendering it unstable in biological systems.[166] Most notably, gold(III) complexes can be reduced by glutathione (GSH) and ascorbic acid in physiological environments.[164] To address this issue, researchers used chelating ligands that stabilize gold in its (3+) oxidation state.[164] Examples of such complexes are presented in **Figure 1.14**. $[AuX_2(damp)]$, $[Au(ESDT)X_2]$,[†] and Au(III) meso-tetraphenylporphyrin are cytotoxic *in vivo* and *in vitro*.[164, 172] In addition, $[Au(dien)Cl]Cl_2$ is cytotoxic in the cisplatin-resistant ovarian cell line A2780.[173] $[Au(Quinpy)Cl]Cl_2$ and $[Au(terpy)Cl]Cl_2$[‡] were found to interact with DNA, demonstrating that the cytotoxicity of gold-based complexes may not always be attributed to their interaction with

[†] Damp = 2-[(dimethylamino)methyl]phenyl; ESDT = ethylsarcosinedithiocarbamate.

[‡] Quinpy = *N*-(8-quinolyl)pyridine-2-carboxamide; terpy = 2,2′:6′,2″-terpyridine.

the mitochondria.[166, 174] However, since most gold-based compounds do not target DNA, they could exhibit activity against cisplatin-resistant cells, due to their different mode of action.[167]

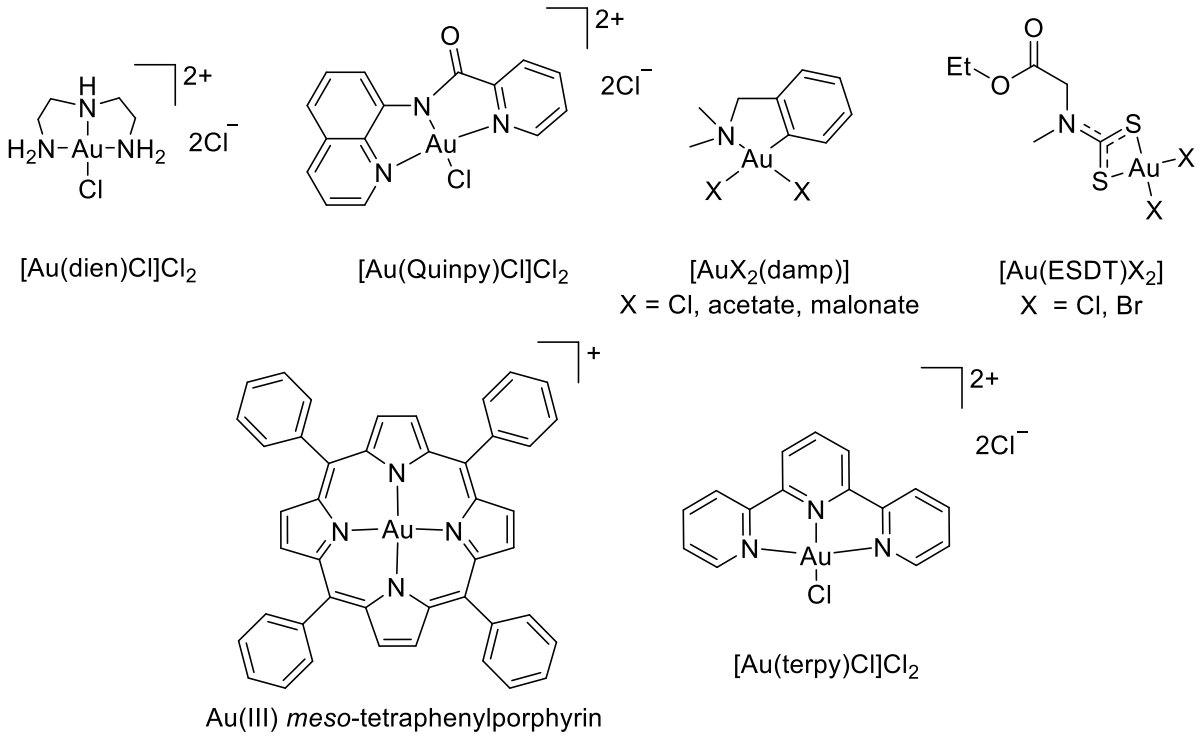

Figure 1.14. Gold(III) complexes exhibiting anticancer activity.[162, 164]

1.10. Research goals

The first two research chapters in this thesis will discuss the synthesis and characterization of: 1) novel nitric oxide releasing Ru(II)-arene complexes and their role as anticancer and antibacterial agents; 2) a heterobimetallic Ru(II)-arene–Au(I) complex and its potential use as a scaffold to build new multinuclear complexes. The compounds in both chapters were characterized by different methods including: Nuclear Magnetic Resonance (NMR) spectroscopy, Electrospray Ionization Mass Spectrometry (ESI-MS), Matrix Assisted Laser Desorption Ionization Time of Flight (MALDI-TOF), Infrared (IR) spectroscopy, and Electron Paramagnetic Resonance (EPR) spectroscopy.

The goal of **Chapter 2** is to develop a structure-activity relationship for a series of furoxan derivatives coordinated to a Ru(II)-arene moiety based on RAPTA-C. The furoxan derivatives were functionalized with electron donating groups (-OCH_3, -OPh, -SPh) or electron withdrawing groups (-NO_2, -SOPh, -SO_2Ph) or a standard (-H) (**Figure 1.15**). EPR spin-trapping was used to measure the NO-donating ability of the furoxan derivatives and the complexes. Furthermore, the antibacterial activity of all the compounds was evaluated *in vitro* using a turbidity assay. The National Cancer Institute (NCI) has accepted four of the furoxan derivatives, L1(-NO_2), L5(-SPh), L6(-SOPh), and L7(-SO_2Ph) for evaluation of anticancer activity using NCI 60 screening.

The goal in **Chapter 3** is to synthesize a heterobimetallic Ru(II)-arene complex with potential anticancer and/or antibacterial activity. The original proposal was to synthesize a Ru(II)-Cu(II) heterobimetallic complex. However, this effort failed after several attempts due to the reasons described later in the chapter. Consequently, an alterative metal with anticancer properties (i.e., gold(III)) was used (**Figure 1.16**). The chemical structure of the binuclear complex was confirmed via NMR, ESI-MS, and X-ray fluorescence (XRF) spectroscopy.

Chapter 4 concludes the research addressed in this thesis and suggests some future work.

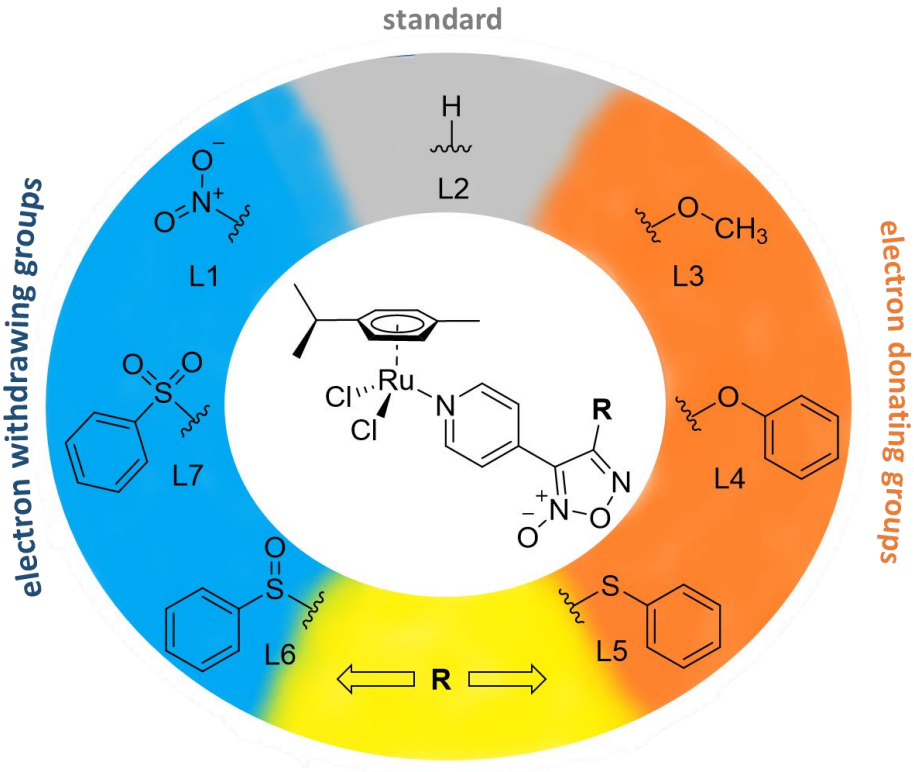

Figure 1.15. **General structure of the Ru(II)-arene nitric oxide donating complex and the substituents used to functionalize the furoxan ring.**

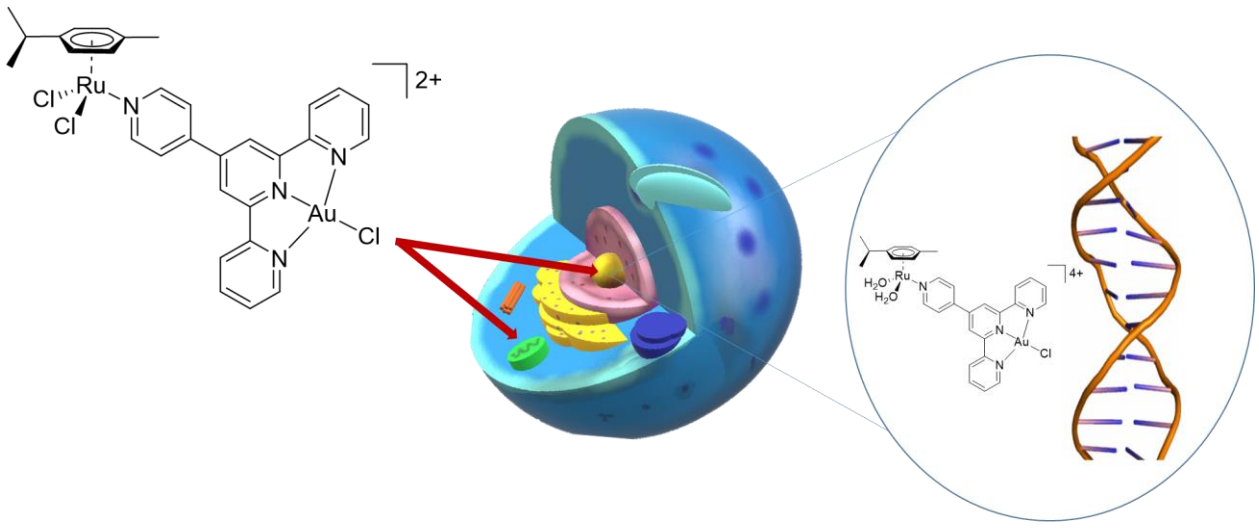

Figure 1.16. **Ru(II)-arene-Au(III) heterobimetallic complex and its potential targets in the cell. The compound is expected to inhibit thioredoxin reductase in the mitochondria due to the presence of Au(III). It may also migrate to the nucleus and damage the DNA.**

Chapter 2. Nitric Oxide Donating Ruthenium(II) Complexes as Anticancer and Antibacterial Agents

2.1. Introduction

During lightning strikes, N_2 and O_2 gaseous molecules react to form a colourless gas known as nitric oxide, NO,[§] **Figure 2.1**.[175] Nitric oxide is a free radical that can subsequently react with O_2 generating the toxic brown gas nitrogen dioxide, NO_2.[96] Therefore, NO was primarily considered an air pollutant until the discovery of its physiological role during the 1970s and 1980s.[96] It is now well established that NO is an endogenous molecule responsible for the dilation of smooth muscles in blood vessels.[176, 177] Consequently, NO regulates blood pressure and can be used to prevent the hardening of arteries caused by atherosclerosis and angina.[178, 179] These findings were made by three researchers: Robert Furchgott, Louis Ignarro, and Ferid Murad, who were awarded the Nobel Prize for Physiology and Medicine in 1998.[96, 180] Due to the biological importance of NO, it was named the molecule of the year by the journal *Science* in 1992.[178]

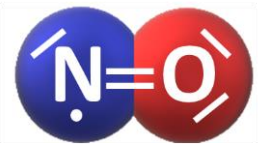

Figure 2.1. Chemical structure of nitric oxide.

Most radicals are reactive species owing to the fact that they possess unpaired electrons. NO is moderately reactive since the unpaired electron is delocalized over the nitrogen and oxygen atoms, with a higher probability of finding it on nitrogen (*ca.* 60%).[96] This explains why NO gas does not dimerize at room temperature and pressure.[181] The bond order of NO is 2.5 with a corresponding bond length equal to 1.154 Å, which is shorter than the double bond in nitroxyl anion (1.26 Å in NO^-) and longer than the triple bond in nitrosonium cation (1.06 Å in NO^+).[96, 182]

There are three enzymes (isoforms) in the human body responsible for the synthesis of NO. These enzymes are known as Nitric Oxide Synthases (NOS) and are found in several parts

[§] Although the molecule NO is commonly referred to as nitric oxide, the IUPAC nomenclature is nitrogen monoxide. By convention, chemists do not include a dot with the chemical formula to denote the presence of unpaired electron ($NO^{\cdot}$), whereas, biologists do.

of the body, thus they have different characteristics.[181, 183] Neuronal NOS (nNOS or NOS I) is found in the nervous system and generates NO that acts as a neurotransmitter (i.e., allows communication between neurons).[178, 181] Inducible NOS (iNOS or NOS II) is located in macrophages.[184] Macrophages are cells that belong to the immune system and defend the body by using NO as a cytotoxic agent.[178, 183] The concentration of NO synthesized by iNOS is relatively higher than that generated by the other two isoforms, and it is only induced to generate NO when a foreign molecule or microorganism is present in the body.[178, 184] The third type of NOS is endothelial NOS (eNOS or NOS III). Endothelial tissue is found in the lining of organs and blood vessels. NO released in this tissue acts as a vasodilator.[181] Since NO is a small lipophilic molecule, it has a high diffusion rate and can penetrate the membranes of the endothelium and muscle cells.[109] In the past, researchers referred to NO as EDRF (**E**ndothelium-**D**erived **R**elaxing **F**actor).[109] **Figure 2.2** illustrates how NO acts as a vasodilator. When NO binds to an enzyme called soluble Guanylate Cyclase (sGC), which is present in muscle cells, it activates it by changing the geometry of the iron(II) metal in the enzyme. The NO ligand pulls Fe(II) out of the plane of the porphyrin ring where it resides, resulting in the active conformation of sGC.[96, 109]

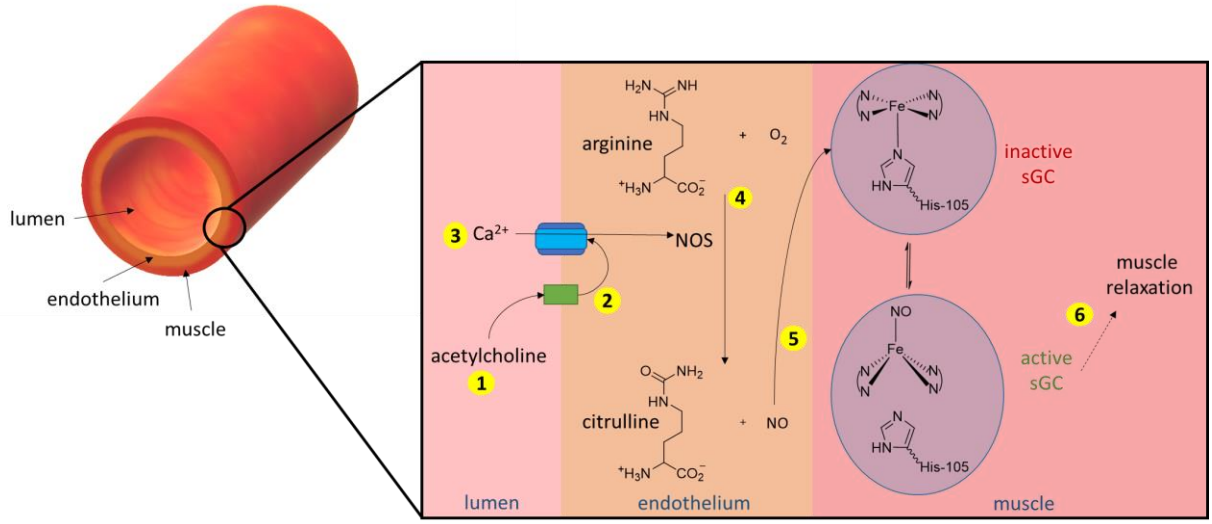

Figure 2.2. The role of NO as a vasodilator in blood vessels.[96, 176] 1) acetylcholine binds to its receptor protein in the endothelium, 2) this stimulates the entrance of Ca^{2+} and activates the enzyme eNOS, 3) eNOS oxidizes arginine and forms citrulline and NO, 4) NO binds to the enzyme soluble Guanylate Cyclase (sGC) and activates it, 6) after several steps that are initiated by the active sGC, the muscle relaxes resulting in a lower blood pressure.

Glyceryl trinitrate or nitroglycerin (GTN) and sodium nitroprusside or nitropress (SNP) are two drugs that were approved for clinical use to lower blood pressure, such as in the case of angina or heart failure, respectively (**Figure 2.3**).[176, 185, 186] GTN was synthesized in 1847 by Ascanio Sobrero, while the preparation of SNP was reported in 1848 when it was the first iron nitrosyl complex to be synthesized.[96, 180] It is remarkable that both compounds were used as vasodilation drugs before a link was made to the role of NO in biological systems and the ability of these compounds to release it.

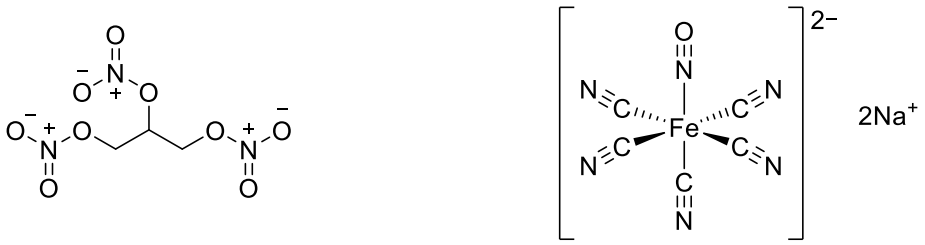

Figure 2.3. Chemical structure of the vasodilators GTN and SNP.

The medical applications of NO are not limited to its ability to regulate the blood pressure. NO can also inhibit platelet aggregation which is a condition that results in thromboembolic disorders.[187, 188] NO released by neurons targets glial cells, nerve terminals, and Purkinjie fibers (i.e., cardiac muscle cells that conduct electrical impulses in the heart).[109, 189] Researchers have proven that neurons containing nNOS are not susceptible to degradation from neurodegenerative diseases such as Alzheimer's disease.[109, 190]

Macrophages and neutrophils have cytotoxic activity since they are capable of releasing NO. [191-193] What makes NO toxic in this case is its high local concentration. The concentration of NO released by this defense mechanism is 100 times higher than that released from neuronal and endothelial cells.[109] This provides insight into the impact of the concentration of NO on its biological activity. The cytotoxicity of NO comes from its ability to damage iron-sulfur clusters in metalloproteins when it has a high concentration in the physiological environment.[183, 194, 195] In addition, elevated levels of NO allow it to react with superoxide radical, $O_2^{\cdot -}$, which is released from immune cells as part of their defense mechanism.[196] The reaction between these two radicals results in the formation of cytotoxic peroxynitrite anion, $ONOO^-$.[175, 197]

In the presence of tumour tissues, macrophages are stimulated to release NO.[198] Nitric oxide inhibits the enzyme aconitase, which is involved in the Krebs cycle (i.e., the metabolic pathway that generates energy via aerobic respiration in the mitochondria), and consequently reduces protein synthesis.[199] Complexes I and II in the electron transport chain of the mitochondria are also inhibited by NO, which impairs cellular respiration.[200] Therefore, tumour cells can struggle to survive in the presence of elevated NO concentration.

Nitric oxide also exhibits antimicrobial activity.[198, 201] It can inhibit the growth of the *Plasmodium* parasite, which is responsible for malaria.[198, 202] Furthermore, the origin of the effectiveness of nitrate and nitrite salts as food preservatives, is that they generate nitric oxide which interacts with metalloproteins, particularly, iron-containing proteins in microbes, and thus prevents their growth.[201] Although NO is toxic towards bacteria, it is an intermediate molecule in the denitrification pathway (i.e., the reduction of nitrate to $N_{2(g)}$) in bacterial cells, and it is maintained at a small steady-state concentration (≤ 60 nM).[203, 204]

This chapter will focus on the synthesis of new furoxan (1,2,5-oxadiazole 2-oxide) derivatives coordinated to Ru(II)-arene complexes to be used as anticancer and antibacterial agents. Furoxan is a five-membered aromatic heterocycle capable of releasing NO in the presence of thiols.[205-207] Therefore, the newly synthesized furoxan derivatives and their corresponding complexes are expected to donate nitric oxide under physiological conditions. There are four isomers of oxadiazole, illustrated in **Figure 2.4**. Furoxan is an azole that belongs to the class of N-oxide heterocycles that are characterized by the presence of the coordinate-covalent, also called dative, bond between nitrogen and oxygen.[208] This bond is indicated by an arrow or by using formal charges (N→O or N^{+}-O^{-}). X-ray crystallography revealed that the unsubstituted furoxan ring is planar and the N→O bond length is 1.240 Å.[209] This bond is characterized by strong absorption of infrared (IR) radiation at 1620 cm^{-1}.[209]

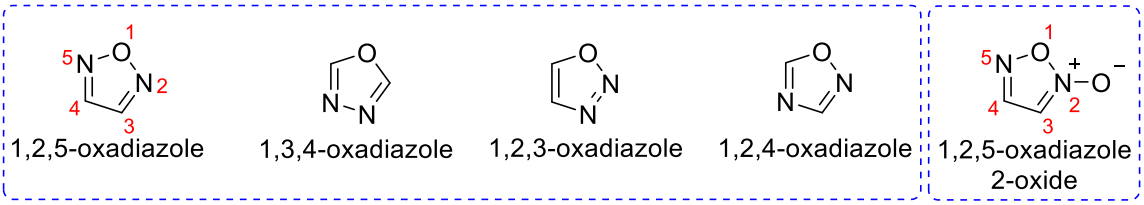

Figure 2.4. The four isomers of oxadiazoles and furoxan (1,2,5-oxadiazole 2-oxide).

Applications of furoxan derivatives vary with their substituents, which can impact the amount of NO released.[210-213] For example, furoxans used as vasodilators need to release less NO than those used to make high-energy explosive materials.[214, 215] **Figure 2.5** illustrates some of the applications of furoxan derivatives. For instance, 4-phenylfuroxan derivative is used as a neuroprotective agent for the central nervous system.[216] 4-phenyl-3-furoxancarbonitrile inhibits platelet aggregation *in vitro*, while CAS 1609 (4-hydroxymethyl-furoxan-3-carboxamide) acts as a vasodilator.[188, 217] In addition, furoxans can exhibit antibacterial activity. For example, (*E*)-3-methyl-4-((2-tosylhydrazono)methyl)-1,2,5-oxadiazole 2-oxide was found to be active against *E. coli*.[160] Furthermore, some benzofuroxans, which are condensed heterocycles, exhibit antileukemic activity.[218, 219]

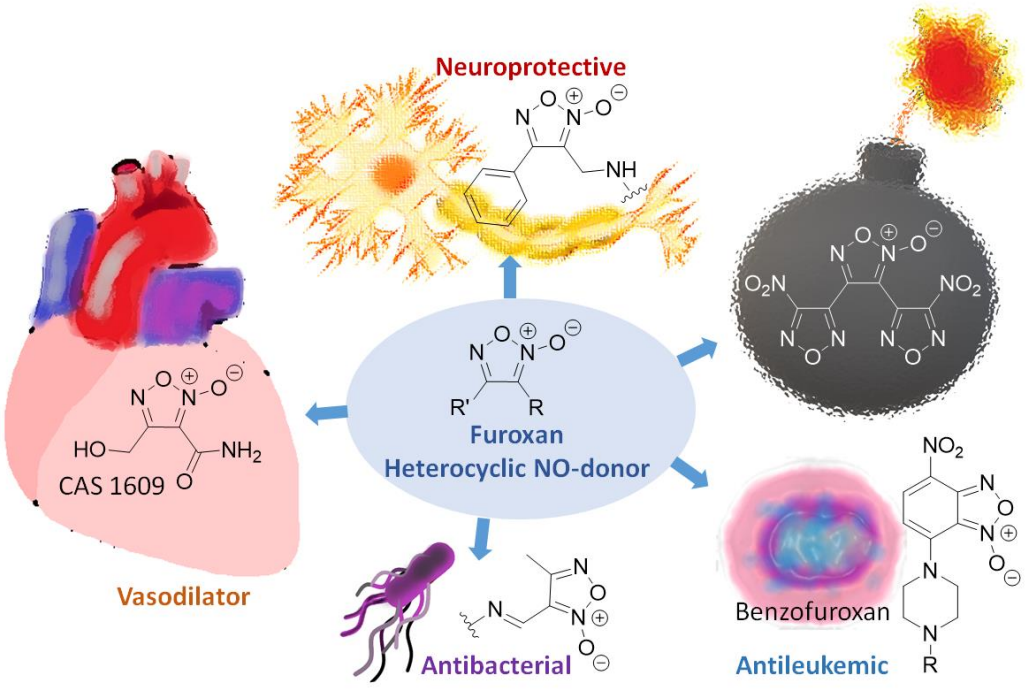

Figure 2.5. Applications of furoxan derivatives.

In this chapter, the syntheses and characterization of seven new furoxan ligands and their corresponding Ru(II)-arene complexes are described. The furoxan derivatives differ in the functional group at C4 (-NO_2, -H, -OCH_3, -OPh, -SPh, -SOPh, -SO_2Ph), and a pyridinyl group is appended at C3 to allow coordination to a Ru(II) center. The complexes have a piano-stool

geometry, as shown in **Figure 2.6**. The first two derivatives (-NO_2, -H) were obtained by following the Wieland approach for the synthesis of furoxans.[220] The other three derivatives (-OCH_3, -OPh, -SPh) were synthesized via nucleophilic aromatic substitution of the -NO_2 group. Finally, the sulfinyl (-SOPh) and the sulfonyl (-SO_2Ph) derivatives were obtained by oxidation of the thiol in the ligand with (-SPh) substituent.

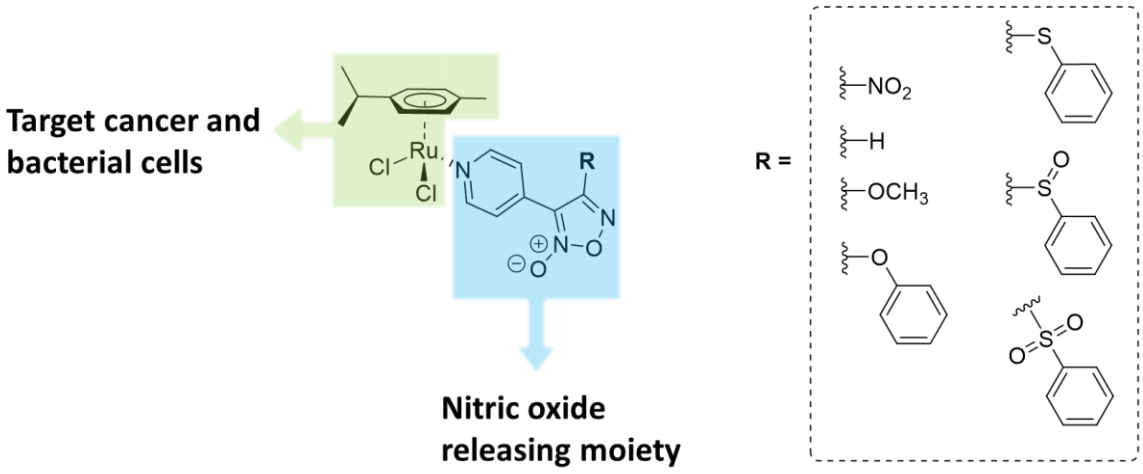

Figure 2.6. Design of the NO-releasing Ru(II)-arene complexes.

The amount of NO released by the complexes and their corresponding ligands was quantified via Electron Paramagnetic Resonance (EPR) spectroscopy using a spin-trapping technique. In addition, the antibacterial activity of all compounds was tested against Gram-positive and Gram-negative bacteria, *Bacillus subtilis* and *Escherichia coli*, respectively, using a turbidity assay. Four of the furoxan derivatives were submitted to the National Cancer Institute (NCI) to investigate their anticancer activity via NCI-60 screening.

In general, nitric oxide donors can either release NO spontaneously or require a specific reagent to mediate its release.[209] It has been found that some furoxan derivatives are able donate NO, detected as nitrite, without the assistance of thiols.[221] Nevertheless, most furoxan derivatives require thiols, and as such they can only donate NO in reducing biological environments.[222] Significant to this thesis is the observation that bacterial and tumour cells can exhibit reducing environments that are low in oxygen and high in glutathione.[223] Glutathione is a tripeptide containing the amino acid cysteine in which a thiol group is present.[223] Therefore, it is

hypothesized that the complexes and the ligands in this thesis could preferentially be activated in hypoxic cells.

Tautomerism and isomerization are common in some furoxan derivatives.[208, 209] This will also be discussed by comparing the new furoxan derivative (-NO_2) to its literature analogue, which differs only by the presence of a phenyl substituent as opposed to the pyridinyl functionality.[224, 225] The literature analogue is presented in **Figure 2.7**.

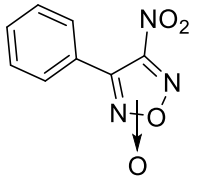

Figure 2.7. Relevant furoxan derivative synthesized previously by the literature.

2.2. Experimental

2.2.1. Materials and Methods

All reagents were purchased from Sigma-Aldrich, except for sodium *N*-(dithiocarbamoyl)-*N*-methyl-D-glucamine (MGD), which was purchased from Alfa Aesar and ruthenium(III) chloride trihydrate, $RuCl_3 \cdot 3H_2O$, from Pressure Chemical. All reagents were used as received. Nuclear Magnetic Resonance (NMR) spectra were recorded on a Bruker-AV (400, 500, or 600 MHz) instruments. Infrared (IR) spectra were recorded in the range of 4000-400 cm^{-1} using a PerkinElmer Spectrum Two FTIR Spectrometer equipped with a UATR Diamond/ZnSe ATR (Single Reflection). Mass spectra (positive and negative ion) were obtained on Bruker micrOTOF time-of-flight electrospray ionization mass spectrometer (ESI-MS). Electron Paramagnetic Resonance (EPR) spectra were obtained using a Bruker EMXplus spectrometer equipped with a PremiumX microwave bridge and HS resonator at X-band (9.3-9.4 GHz). Optical density was determined using a BioTek microplate reader. The growth of bacterial cultures was monitored with a Cary 1E UV-Visible spectrophotometer.

Note that elemental analysis of C, H, and N was not performed because this class of compounds tend to decompose readily and thus may lose the N→O moiety. The purity of the compounds ranges approximately between 90 – 97 % (determined from the ^{1}H NMR spectra). A change in the proton chemical shifts of the ligands' pyridyl substituent can confirm the coordination to the Ru(II)-arene moiety. **Figure 2.8** shows the stacked ^{1}H NMR spectra of L1(-NO_2) and C1(-NO_2). The pyridyl protons shift downfield when the ligand is coordinated to Ru(II) moiety. The assigned and integrated spectra for all the compounds can be found in **Appendix A**. Some of the ^{13}C NMR spectra may not contain the correct number of C atoms due to the low concentrations of the samples being tested. In addition, Ru(II) complexes have a characteristic isotopic pattern that can be seen in mass spectra (provided in Appendix A). C4(-OPh) was found to have several isotopic peaks. However, some complexes may not have this isotopic pattern, but will have a molecular weight similar to the compound of interest, and thus may not provide evidence of the indicated complex. While the author is confident in the structural assignment of all compounds and complexes described in this thesis, several of the complexes (C1-C7) were isolated and characterized as impure mixtures.

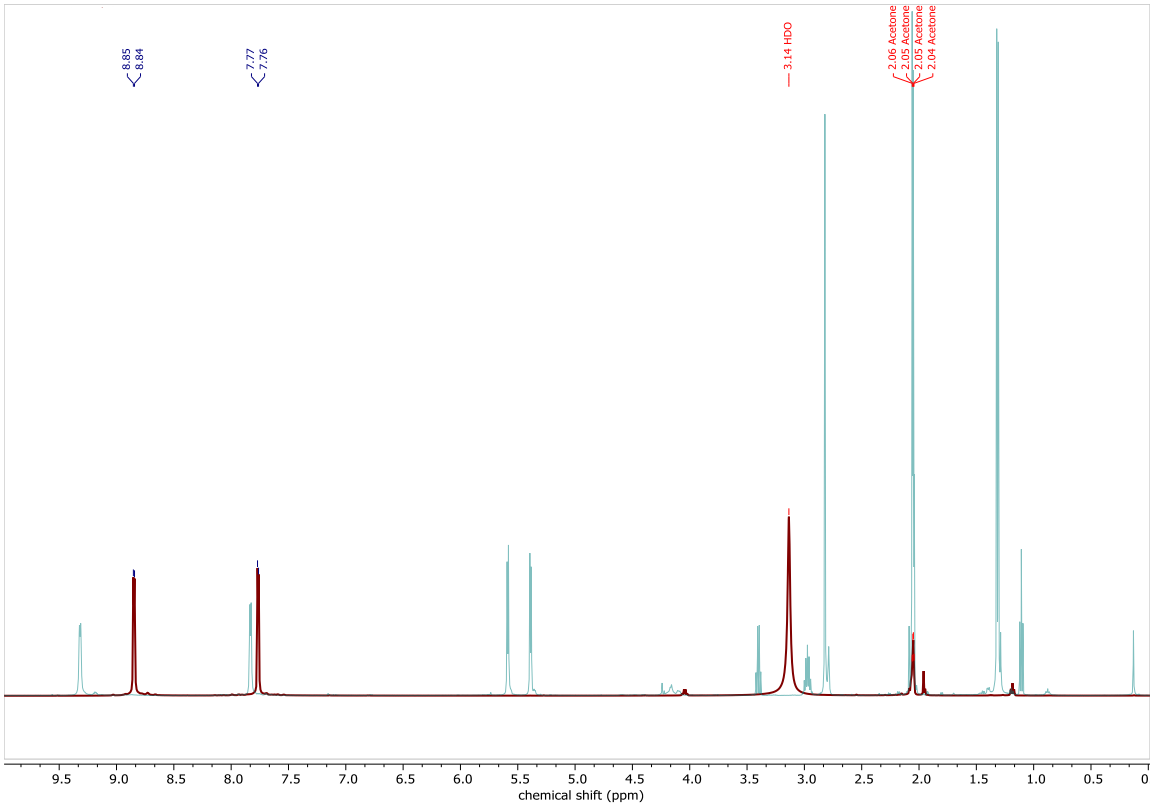

Figure 2.8. The stacked ^{1}H NMR spectra of C1(-NO_2) and its corresponding ligand.

2.2.2. Synthesis of 4-nitro-3-(pyridin-4-yl)-1,2,5-oxadiazole 2-oxide (L1)

Acetic acid (50 mL) was mixed with 4-vinylpyridine, C_7H_7N, (11 mL, 102 mmol) and the solution was placed in an ice-bath. Saturated aqueous solution of sodium nitrite, $NaNO_2$, (40 g, 580 mmol, dissolved in *ca.* 70 mL H_2O) was added dropwise over an hour. ***Caution: nitrogen dioxide gas, NO_2, will form, if large portions of $NaNO_2$ were added. NO_2 is toxic orange-brown gas. If formed, the gas evolution must cease before adding additional portions of the nitrite solution*.** The solution was left to stir for two hours in the ice-bath before warming to room temperature (23 °C) for an additional 16 h. The solution was then diluted with H_2O, followed by extraction with dichloromethane (5 × 200 mL). The organic extracts were washed with brine, dried over anhydrous magnesium sulfate, $MgSO_4$, then filtered and concentrated *in vacuo*. The crude product was purified via silica gel column chromatography using ethyl acetate as eluent to yield the product as a yellow-white precipitate. Yield: 5.0 g, 24 %. ^{1}H NMR (500 MHz, acetone-d_6) δ δ 8.85 (d, J = 5.1 Hz, 2H$_b$), 7.77 (d, J = 5.1 Hz, 2H$_a$). ^{13}C NMR (126 MHz, acetone) δ 151.77, 126.28, 123.41, 120.92, 117.32. Positive ESI-MS: calculated for $[M+H]^+$ 209.0311 and $[M-O+H]^+$ 193.0361; found, 209.0313 and 193.0363, respectively.

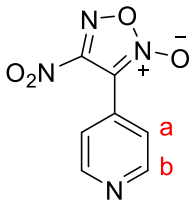

2.2.3. Synthesis of 3-(pyridin-4-yl)-1,2,5-oxadiazole 2-oxide (L2)

L2 was obtained as a side-product from the synthetic procedure of **L1** with modifications. The amount of $NaNO_2$ was half that for the synthesis of **L1** (20 g, 290 mmol). The amount of the other reagents was the same as that used for **L1**. The reaction was left to stir at room temperature (23 °C) for 6 h. The compound was purified by silica gel column chromatography using ethyl acetate as eluent. The product was obtained as a white precipitate. Yield: 0.5 g, 3.0%. ^{1}H NMR (400 MHz, DMSO-d_6) δ 8.82 – 8.62 (m, 2H$_b$), 7.73 – 7.56 (m, 3H$_{a+c}$). ^{13}C NMR (101 MHz, DMSO) δ 152.45, 150.56, 143.69, 138.36, 119.78. Positive ESI-MS: calculated for $[M+H]^+$ 164.0460 and $[M-O+H]^+$ 148.0511; found, 164.0458 and 148.0507, respectively.

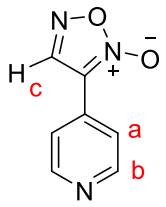

2.2.4. Synthesis of 4-methoxy-3-(pyridin-4-yl)-1,2,5-oxadiazole 2-oxide (L3)

L1 (0.1189 g, 0.572 mmol) was dissolved in methanol (20 mL). Potassium methoxide, $KOCH_3$ (0.0607 g, 0.866 mmol) was added to the solution. The reaction was left to stir at room temperature (23 °C) for 3 h. The yellow-white precipitate was filtered, rinsed with hexanes then dried *in vacuo*. Yield: 0.05 g, 50%. ^{1}H NMR (500 MHz, acetone-d_6) δ 8.85 (d, J = 6.4 Hz, 2H$_b$), 7.65 (d, J = 6.4 Hz, 2H$_a$), 3.78 (s, 3H$_c$). ^{13}C NMR (126 MHz, acetone) δ 151.17, 121.08, 56.66 (quaternary carbons were difficult to resolve). Positive ESI-MS: $[M\text{-}NO+H]^+$ calculated 164.0586, found 164.0473; $[M\text{-}O+H]^+$ calculated 178.0617, found 178.0596; $[M+H\text{-}NO\text{-}Me]^+$ calculated 152.0586, found 152.0695.

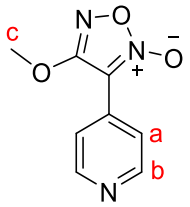

2.2.5. Synthesis of 4-phenoxy-3-(pyridin-4-yl)-1,2,5-oxadiazole 2-oxide (L4)

L1 (1.233 g, 5.93 mmol) was dissolved in dichloromethane (20 mL). Phenol (0.560 g, 5.95 mmol) and 1,8-diazabicyclo[5.4.0]undec-7-ene, (abbreviated: DBU) (896 µL) were mixed in a separate vial to obtain phenolate. Phenolate was then added to the **L1** solution. The resulting solution was left to stir at room temperature (23 °C) for 24 h. Reaction progress was monitored by TLC, with ethyl acetate as the elution solvent. The organic solution was washed with sodium bicarbonate, $NaHCO_3$ (5 × 5 mL), dried over anhydrous $MgSO_4$, then filtered and dried *in vacuo* to yield a yellow precipitate. **L4** tends to degrade into 4-cyanopyridine ($C_6H_4N_2$), which appears as colourless needle crystals so the product should be stored at low temperature (*ca.* -2 °C). Yield:

0.4 g, 26%. ^{1}H NMR (400 MHz, $CDCl_3$-*d*) δ 8.84 – 8.76 (m, $2H_b$), 7.60 – 7.51 (m, $2H_a$), 7.25 – 7.17 (m, $2H_c$), 6.93 – 6.80 (overlap, $3H_{d+e}$). ^{13}C NMR (101 MHz, $CDCl_3$) δ 156.30, 150.56, 129.70, 125.60, 120.94, 120.43, 116.26, 115.55. Positive ESI-MS: calculated for $[M\text{-}O+Na]^+$ 261.0522 and $[C_{13}H_{11}N_3O_4+ACN+Na]^+$ 337.0908; found 261.1105 and 337.0995, respectively.

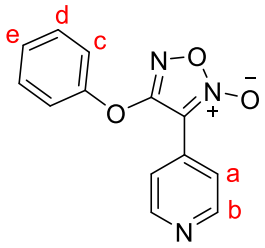

2.2.6. Synthesis of 4-(phenylthio)-3-(pyridin-4-yl)-1,2,5-oxadiazole 2-oxide (L5)

This procedure was similar to **L4**, but with appropriate modifications (thiophenol was used instead of phenol). The product was obtained as a white solid. Yield: 60%. ^{1}H NMR (400 MHz, acetone-d_6) δ 7.56 – 7.53 (m, $2H_b$), 7.47 – 7.44 (m, $2H_a$), 7.38 – 7.32 (overlap, $4H_{c+d}$), 7.30 – 7.27 (m, $1H_e$). ^{13}C NMR (101 MHz, acetone) δ 137.55, 136.22, 130.95, 129.88, 129.16, 128.42, 128.35, 127.7. Positive ESI-MS: calculated for $[M\text{-}O+H]^+$ 256.0544; found, 256.0464.

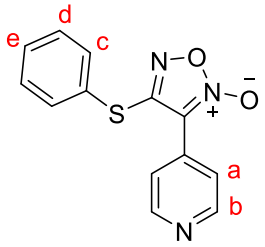

2.2.7. Synthesis of 4-(phenylsulfinyl)-3-(pyridin-4-yl)-1,2,5-oxadiazole 2-oxide (L6)

The literature procedure for the synthesis of the sulfinyl group was followed with modifications.[226] **L5** (0.267, 1.00 mmol) was dissolved in methanol (15 mL) then H_2O_2 (30%, 2 mL, 20 equivalent) and zirconium(IV) chloride, $ZrCl_4$ (1.61 g, 10 equivalent), were added to afford

a yellow-green solution. The reaction took around 10 minutes to reach completion. Reaction progress was monitored by TLC (ethyl acetate: hexanes, v/v, 3:7). Once the starting material was completely consumed, the reaction was quenched with water (15 mL) followed by extraction with chloroform (3 × 10 mL). Organic layers were combined and dried over anhydrous $MgSO_4$, filtered and dried *in vacuo*. The product was isolated as a clear, dense oil. Yield: 0.27 g, 94%. ^{1}H NMR (500 MHz, $CDCl_3$-*d*) δ 7.58 – 7.56 (m, $2H_b$), 7.48 – 7.40 (overlap, $3H_{d+e}$), 7.37 – 7.32 (overlap, $4H_{a+c}$). ^{13}C NMR (126 MHz, $CDCl_3$) δ 136.70, 133.72, 132.35, 131.51, 129.55, 129.95, 127.70, 125.53. Positive ESI-MS: calculated for $[M\text{-}O+H]^+$ 272.0488; found, 272.0522.

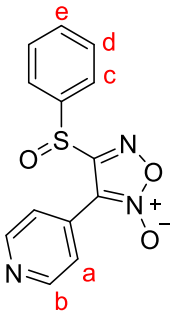

2.2.8. Synthesis of 4-(phenylsulfonyl)-3-(pyridin-4-yl)-1,2,5-oxadiazole 2-oxide (L7)

The literature procedure for the synthesis of sulfonyl group was followed with modifications.[226] **L5** (0.265, 1.00 mmol) was dissolved in methanol (15 mL) then H_2O_2 (30%, 4.0 mL, 40 eq) and $ZrCl_4$ (3.20 g, 20 eq) were added to afford a yellow-green solution. The reaction took 15 minutes to reach completion. Reaction progress was monitored by TLC (ethyl acetate: hexanes; v/v; 3:7). Once the starting material had disappeared the reaction was quenched with water (15 mL), followed by extraction with chloroform (3 × 10 mL). The organic layers were combined and dried over anhydrous $MgSO_4$, then filtered and dried *in vacuo*. The product was isolated as a clear, pale yellow dense oil. Yield: 0.28 g, 92%.^{1}H NMR (400 MHz, $CDCl_3$-*d*) δ 8.15 – 8.12 (m, $1H_b$), 7.93 – 7.77 (overlap, $3H_{d+e}$), 7.69 – 7.53 (overlap, $4H_{a+c+b'}$). ^{13}C NMR (101 MHz, $CDCl_3$) δ 133.94, 132.70, 132.31, 129.40, 129.12, 128.81, 128.25, 128.18. Positive ESI-MS: calculated for $[M\text{-}O+H]^+$ 288.0474; found, 288.0471.

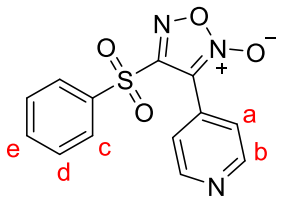

2.2.9. Synthesis of [Ru(η^6-*p*-cymene)Cl_2]$_2$

This complex was prepared according to the literature procedure.[227] Ruthenium(III) chloride trihydrate, $RuCl_3 \cdot 3H_2O$, (438 mg, 1.68 mmol) was dissolved in ethanol (20.0 mL) and α-phellandrene, $C_{10}H_{16}$, (3.40 mL, 20.9 mmol) was added. This solution was refluxed for 4 h. After cooling to *ca.* 0 ˚C for 12 h, red crystals were filtered, washed with cold ethanol (2 mL) and hexanes (2 mL), and dried *in vacuo*. Yield: 0.482 g, 94%. ^{1}H NMR (DMSO-d_6): δ 5.82 (d, *J* = 6.2 Hz, 2H, benzyl, *p*-cymene), 5.77 (d, *J* = 6.2 Hz, 2H, benzyl, *p*-cymene), 2.83 (septet, *J* = 6.9 Hz, 1H, isopropyl, *p*-cymene), 2.09 (s, 3H, methyl, *p*-cymene), 1.19 (d, *J* = 6.9 Hz, 6H, isopropyl, *p*-cymene).

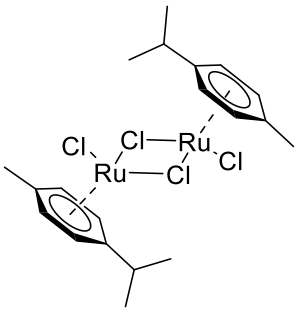

2.2.10. General synthetic procedure for the complexes

The chosen furoxan derivative (2 mmol) was dissolved together with [Ru(η^6-*p*-cymene)Cl_2]$_2$ (1 mmol) in methanol (20 mL). The solution was then left to stir at room temperature (23 °C) for 12 h. The solution was concentrated to *ca.* 2 mL under reduced pressure, then the product was filtered, rinsed with cold hexanes and dried *in vacuo*.

2.2.11. Synthesis of C1(-NO_2)

The product was obtained as an orange powder. Yield: 70 %. ^{1}H NMR (500 MHz, acetone-d_6) δ 9.32 (d, *J* = 6.0 Hz, 2H_b), 7.83 (d, *J* = 6.0 Hz, 2H_a), 5.59 (d, *J* = 5.8 Hz, 2H, benzyl, *p*-cymene), 5.39 (d, *J* = 5.8 Hz, 2H, benzyl, *p*-cymene), 2.97 (hept, *J* = 6.9, 1H, isopropyl, *p*-cymene), 2.05 (s, 3H, methyl, *p*-cymene), 1.32 (d, *J* = 6.9 Hz, 6H, isopropyl, *p*-cymene). ^{13}C NMR (126 MHz, acetone) δ 157.38, 126.78, 103.93, 84.14, 83.12, 22.53, 18.04. Positive ESI-MS showed a base peak at 565.0846, however it could not be assigned to any mass adduct containing the compound of interest. The isotopic pattern indicates the presence of Ru + 2Cl.

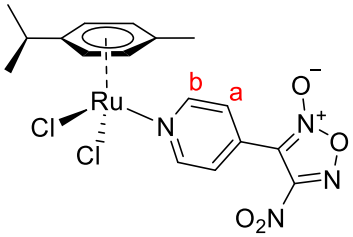

2.2.12. Synthesis of C2(-H)

The product was obtained as a white powder. Yield: 45%. ^{1}H NMR (400 MHz, DMSO-d_6) δ 8.73 (d, J = 5.1 Hz, 2H_b), 7.75 – 7.53 (m, 2H_a), 5.83 – 5.75 (two doublets, 4H, benzyl, *p*-cymene), 2.83 (hept, *J* = 6.9, 1H, isopropyl, *p*-cymene), 2.09 (s, 3H, methyl, *p*-cymene), 1.19 (d, *J* = 6.9 Hz, 6H, isopropyl, *p*-cymene). ^{13}C NMR (101 MHz, DMSO) δ 151.09, 119.94, 100.61, 86.82, 85.98, , 30.45, 21.98, 18.32. Negative ESI-MS: $[M\text{-}O\text{-}H]^-$ calculated 451.9876 found 451.9917; $[M\text{-}2NO\text{+formic acid-}H]^-$ calculated 453.9920, found 453.9903; [deoxygenated ligand-H]$^-$calculated 146.0360, found 146.0393.

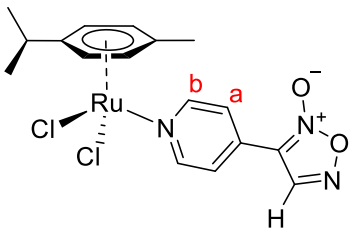

2.2.13. Synthesis of C3(-OCH_3)

The product was obtained as a yellow-orange precipitate. Yield: 50%. ^{1}H NMR (400 MHz, $CDCl_3$-*d*) δ 9.31 (d, *J* = 6.3 Hz, $2H_b$), 8.81(d, *J* = 6.3 Hz, $2H_a$), 5.26 (s, $3H_c$), 5.47 (d, *J* = 6.1 Hz, 2H, benzyl, *p*-cymene), 5.25 (d, *J* = 6.1 Hz, 2H, benzyl, *p*-cymene), 2.86 – 2.80 (m, 1H, isopropyl, *p*-cymene), 3.47 (s, $3H_c$), 2.13 (s, 3H, methyl, *p*-cymene), 1.31 (d, *J* = 6.8 Hz, 6H, isopropyl, *p*-cymene). ^{13}C NMR (101 MHz, $CDCl_3$) δ 155.84, 134.74, 126.85, 84.30, 82.89, 23.05, 18.84. Positive ESI-MS: reverse $[M+K]^+$= M_2 adduct, calculated $[M_2\text{-}CH_3\text{+}NH_4]^+$ 505.0414, found 505.3262.

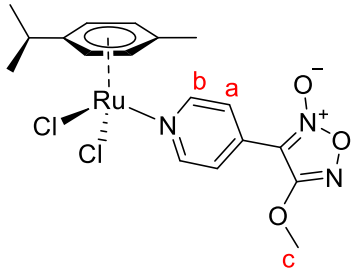

2.2.14. Synthesis of C4(-OPh)

The product was obtained as an orange powder. Yield: 32%. ^{1}H NMR (400 MHz, $CDCl_3$-*d*) δ 9.25 (t, *J* = 6.4 Hz, $2H_b$), 8.15 (d, *J* = 5.9 Hz, $1H_a$), 8.00 (d, *J* = 5.9 Hz, $1H_{a'}$), 7.49 (dt, *J* = 8.5, 6.9 Hz, $2H_c$), 7.45 – 7.27 (m, $3H_{d+e}$), 5.48 (d, *J* = 5.5 Hz, 2H, benzyl, *p*-cymene), 5.26 (d, *J* = 5.5 Hz, 2H, benzyl, *p*-cymene), 3.01 (m, 1H, isopropyl, *p*-cymene), 2.14 (s, 3H, methyl, *p*-cymene), 1.34 (d, *J* = 6.8 Hz, 6H, isopropyl, *p*-cymene). ^{13}C NMR (151 MHz, $CDCl_3$) δ 155.92, 152.19, 143.20, 134.05, 130.29, 126.81, 122.03, 120.19, 119.97, 119.43, 105.74, 83.12, 82.50, 30.84, 22.42, 18.46. MALDI-TOF: $[M\text{-}O\text{+}CH_3OH\text{+}H]^+$ calculated 578.0545, found 578.501.

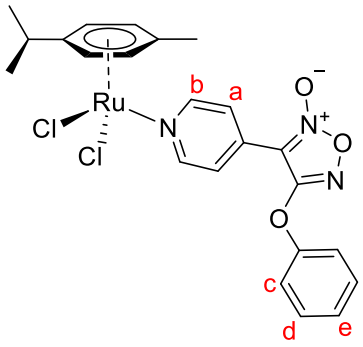

2.2.15. Synthesis of C5(-SPh)

The product was obtained as an orange powder. Yield: 25%. ^{1}H NMR (500 MHz, $CDCl_3$-*d*) δ 7.50-7.49 (overlap, $3H_{b+e}$), 7.32 – 7.29 (overlap, $4H_{a+c}$), 7.24 – 7.21 (m, $2H_d$), 5.47 (d, *J* = 5.9 Hz, 2H, benzyl, *p*-cymene), 5.33 (d, *J* = 5.9 Hz, 2H, benzyl, *p*-cymene), 2.92 (hept, *J* = 6.5 Hz, 1H, isopropyl, *p*-cymene), 2.16 (s, 3H, methyl, *p*-cymene), 1.28 (d, *J* = 6.5 Hz, 6H, isopropyl, *p*-cymene). ^{13}C NMR (101 MHz, $CDCl_3$) δ 137.23, 137.22, 129.17, 127.80, 127.78, 127.31, 127.29, 101.41, 96.89, 81.44, 80.73, 30.78, 22.28, 19.02. MALDI-TOF: [M] calculated 577.486 Da, found 577.055 Da.

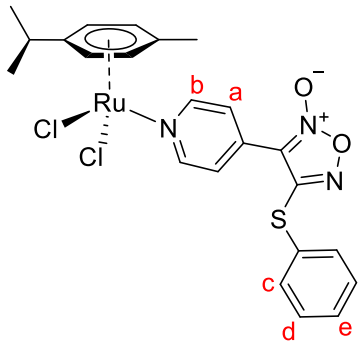

2.2.16. Synthesis of C6(-SOPh)

The product was obtained as a brown precipitate. Yield: 20%. ^{1}H NMR (500 MHz, $CDCl_3$-*d*) δ 8.07 – 8.05 (overlap, $4H_{a+b}$), 7.75 – 7.73 (overlap, $3H_{c+e}$), 7.58 – 7.55 (m, $2H_d$), 5.67 (d, *J* = 6.4 Hz, 2H, benzyl, *p*-cymene), 5.24 (d, *J* = 6.4 Hz, 2H, benzyl, *p*-cymene), 2.70 (hept, *J* = 8.3

Hz, 1H, isopropyl, *p*-cymene), 2.15 (s, 3H, methyl, *p*-cymene), 1.35 (d, *J* = 8.3 Hz, 6H, isopropyl, *p*-cymene). ^{13}C NMR (101 MHz, $CDCl_3$) δ 145.55,129.58, 129.25, 127.95, 81.46, 80.55, 31.46, 22.40, 19.07. MALDI-TOF: [M-O] calculated 576.9932 Da, found 576.602 Da

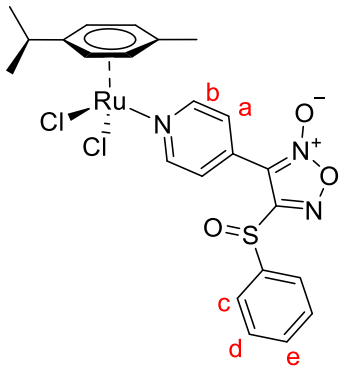

2.2.17. Synthesis of C7(-SO_2Ph)

The product was obtained as a brown precipitate. Yield: 30%. ^{1}H NMR (400 MHz, $CDCl_3$-*d*) δ 8.15 (d, *J* = 7.5 Hz, $1H_b$), 7.93 – 7.64 (overlap, $6H_{a+b'+c+e}$), 7.41 – 7.37 (m, $2H_{d'}$), 5.99 (d, *J* = 5.9 Hz, 2H, benzyl, *p*-cymene), 5.77 (d, *J* = 5.9 Hz, 2H, benzyl, *p*-cymene), 2.81 (hept, *J* = 6.5Hz, 1H, isopropyl, *p*-cymene), 2.22 (s, 3H, methyl, *p*-cymene), 1.31 (d, *J* = 6.5 Hz, 6H, isopropyl, *p*-cymene). ^{13}C NMR (101 MHz, $CDCl_3$) δ 137.04,134.79, 133.30, 132.91, 130.61, 130.19, 129.68, 128.95, 128.73, 127.20, 102.27, 98.24, 80.26, 79.08, 22.32, 19.03.

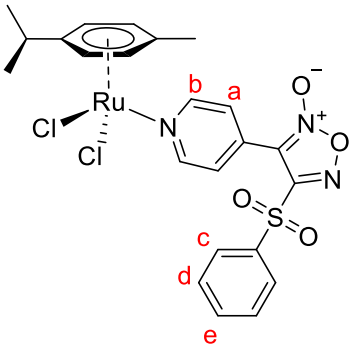

2.2.18. Ru(η^6-*p*-cymene)(Pyridine)Cl_2 – control

The compound was synthesized according to the literature procedure.[228] ^{1}H NMR (500 MHz, $CDCl_3$-*d*) δ 9.07 – 9.01 (m, $2H_b$), 7.74 (tt, J = 7.6, 1.6 Hz, $1H_c$), 7.34 – 7.28 (m, $2H_a$), 5.44 (d, *J* = 5.8 Hz, 2H, benzyl, *p*-cymene), 5.22 (d, *J* = 5.8 Hz, 2H, benzyl, *p*-cymene), 2.99 (hept, *J* = 6.5Hz, 1H, isopropyl, *p*-cymene), 2.10 (s, 3H, methyl, *p*-cymene), 1.31 (d, *J* = 6.5 Hz, 6H, isopropyl, *p*-cymene).

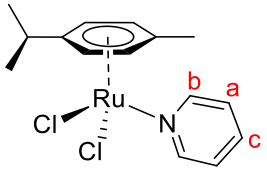

2.2.19. Synthesis of (nitro)(phenyl)-1,2,5-oxadiazole 2-oxide

The compound was synthesized according to the literature procedure.[220, 225] Styrene, C_8H_8 (5.0 mL, 44 mmol) was mixed with aqueous solution of $NaNO_2$ (20 g in *ca.* 30 mL H_2O) in acetic acid (25 mL). The solution was left to stir at room temperature (23 °C) for one hour. The white precipitate was filtered and washed with cold hexanes then dried *in vacuo*. Positive ESI-MS results are included in **Appendix A**.

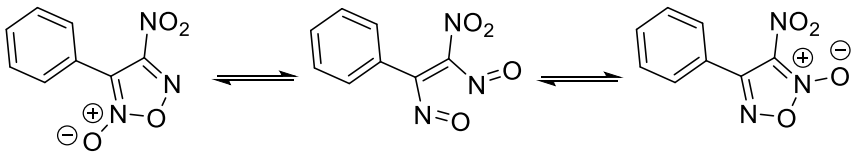

2.2.20. Summary of syntheses

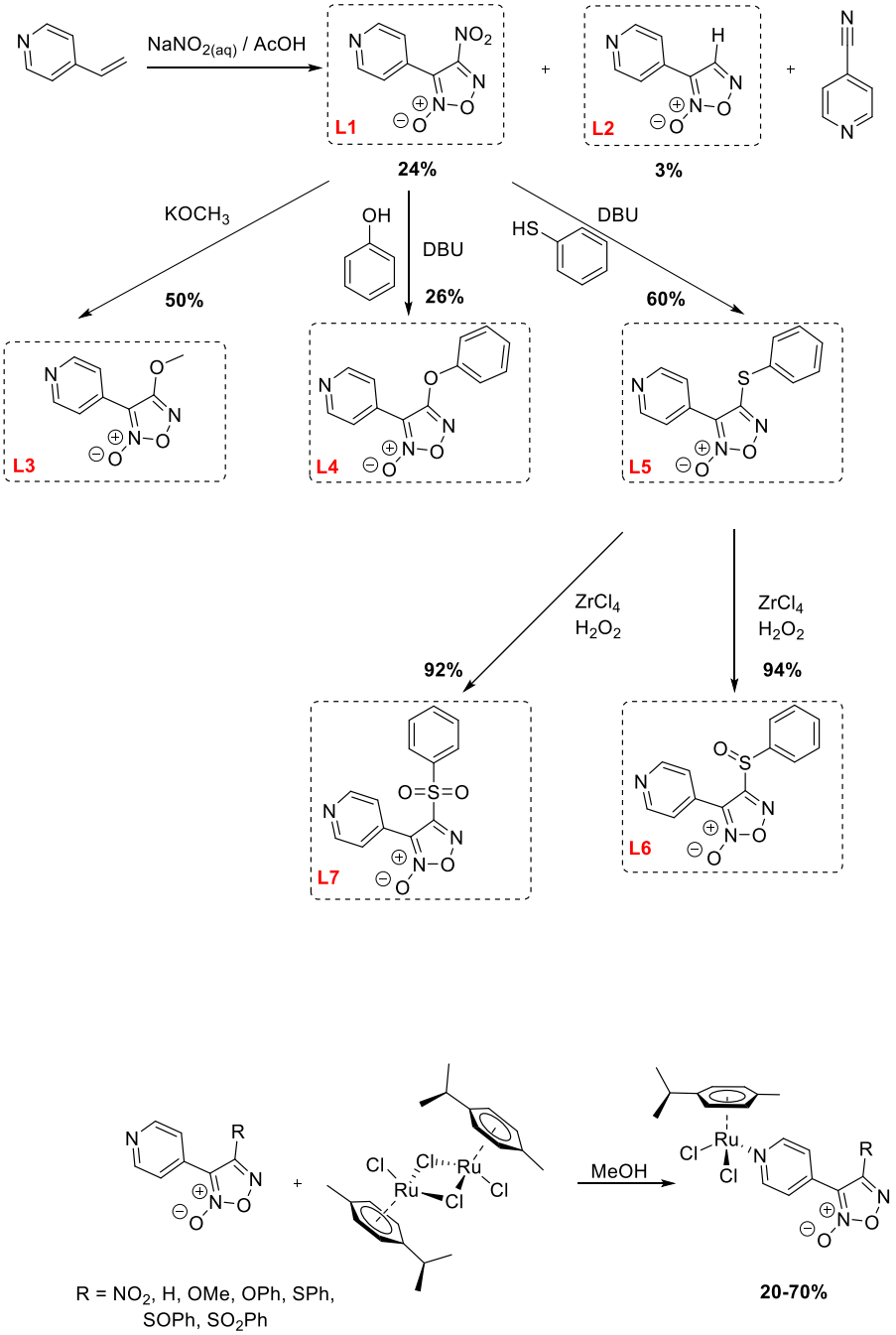

2.2.21. Crystal structure determination of C1 (decomposed)

X-ray diffraction was performed on a single crystal at the University of British Colombia. The data were collected using a Bruker Apex DUO diffractometer using Mo Kα radiation filtered with a Triumph monochromator. The strategy for automatic data collection was determined using COSMO. The crystal was oriented using Kappa geometry and was kept at 273 K during data collection. Using Olex2, the structure was solved with the olex2.solve structure solution program using Charge Flipping and refined with the olex2.refine refinement package using GaussNewton minimisation.[229, 230] Crystal Data for $C_{17}H_{21}Cl_2N_2ORu$ (M = 441.34 g/mol): triclinic, space group P-1 (no. 2), a = 7.2742(13) Å, b = 11.827(2) Å, c = 12.046(2) Å, α = 64.300(5)°, β = 89.453(5)°, γ = 77.446(5)°, V = 907.3(3) Å3, Z = 2, T = 273.15 K, μ(Mo Kα) = 1.163 mm-1, D_{calc} = 1.6155 g/cm3, 4361 reflections measured (3.94° ≤ 2Θ ≤ 56°), 4361 unique (R_{int} = 0.0000, R_{sigma} = 0.0623) which were used in all calculations. The final R1 was 0.0631 (I>=2u(I)) and wR2 was 0.1739 (all data).

2.2.22. Colour test for N-oxide heterocycles

This test was performed as described in the literature without modifications.[208, 231] In a test tube or round-bottom flask, *N*, *N*-dimethylaniline (0.2 mL) was mixed with concentrated HCl (0.05 mL) and the furoxan derivative (*ca*. 0.1 g). The solution was refluxed for 1 min. A blue-violet colour indicative of a positive test has developed. Ethanol (1 mL) may be added to the cooled solution if there is difficulty in observing the colour. This test was performed on L1(-NO_2) and L2(-H).

2.2.23. EPR spectroscopy and spin-trapping

Preparation of spin-trap complex, $Fe(MGD)_2$

The $Fe(MGD)_2$ complex was used to trap nitric oxide released by the compounds *in situ*. According to the literature, fresh stock solutions of this complex can be prepared in degassed phosphate buffered saline, (PBS), (purged with $N_{2(g)}$) using 1 equivalent of Mohr's salt, $(NH_4)_2Fe(SO_4)_2{\cdot}6H_2O$, and 5 equivalents of sodium *N*-(dithiocarbamoyl)-*N*-methyl-D-glucamine, (Na-MGD).[232] The final concentration of the spin-trap was 10 mM in the EPR samples.

Preparation of EPR samples

The compound to be studied for NO release was prepared in a mixture of degassed PBS and DMSO (49:1, v/v) to give a final concentration of 5 mM. The compound was mixed with the spin-trap, then a solution of reduced glutathione (abbreviated: GSH) prepared in degassed PBS

was added. The final concentration of GSH in the sample was 25 mM (i.e., 1 equivalent of compound was reacted with 5 equivalents of GSH). A 40 μL aliquot of the sample mixture was placed in a capillary tube that was sealed at one end. The capillary tube was placed inside an EPR tube, which was then sealed with Parafilm to reduce solvent evaporation.

Preparation of the DPPH standard

The stable organic radical, 2,2-diphenyl-1-picrylhydrazyl (DPPH), was used as a concentration standard. DPPH was dissolved in methanol to give a concentration of 4.77 μM, as determined using a NanoDrop™ 2000/2000c Spectrophotometer with measurement at 515 nm. A 40 μL aliquot of the DPPH solution was placed in a capillary tube sealed at one end. This capillary tube together with the capillary tube of the compound of interest were placed side-by-side in the EPR tube. The top of the EPR tube was sealed with Parafilm to reduce solvent evaporation.

Preparation of the S-nitrosoglutathione standard

S-nitrosoglutathione solution was used as a positive control for NO release. This solution was prepared following the literature procedure with some modifications.[233] The spin-trap $Fe(MGD)_2$ was mixed with 1 equivalent of sodium nitrite, $NaNO_2$, followed by 1 equivalent of GSH, and 500 equivalents of concentrated hydrochloric acid. The solution was prepared in a mixture of degassed PBS and DMSO (49:1, v/v). The final concentration of S-nitrosoglutathione in the EPR sample was 5 mM, and the spin-trap was 10 mM.

Experimental parameters used in EPR spectroscopy

Microwave power: 20 mM; modulation amplitude: 6.0 Gauss; modulation frequency: 100 kHz; time constant: 5.12 ms; sweep width: 70 Gauss; sweep time: 10.24 s; number of scans: 9.

2.2.24. Turbidity assay to investigate the antibacterial activity of the compounds

The complexes and the corresponding furoxan ligands were tested against Gram-positive *Bacillus subtilis* (*B. subtilis*) and Gram-negative *Escherichia coli* (*E. coli*) bacteria. Turbidity measurements were performed as described in the literature with some modifications.[75] The assay was conducted in sterile 96-well Thermo Scientific microplates. Using a BioTek microplate reader, the growth of bacteria was monitored by measuring the absorbance at 620 nm every 10

minutes for 12 hours at 37 °C. The broth, Luria-Bertani (ThermoFisher Scientific), was prepared using distilled-deionized water supplied by a Millipore Milli-Q deionization system. The broth, pipette tips, and glassware were autoclaved for 20 minutes in a wet cycle.

The assay was performed as follows. A single colony was inoculated into broth (15 mL) and incubated at 37 °C while shaking (200 rpm) for 16 hours. Afterward, additional broth was added (25 mL) and the bacteria was left in the incubator for 2 hours, then the optical density at 620 nm (OD_{620}) was measured (0.7 – 0.8) in a 1 mL cuvette. Stock solutions of the compounds were prepared in DMSO (1%) and broth (99%). The compound concentration was in the range of 20-300 μg/mL for the ligands and 20-400 μg/mL for the complexes. The assays were performed in 4 replicates, using 25 μL of compound and 175 μL of culture in each well. Three negative controls were used: solvent control (DMSO: broth, 1:99, v/v), broth control, and culture control (culture: broth, 7:1, v/v). The final volume of solution in each well was 200 μL.

2.3. Results and Discussion

2.3.1. Synthesis

The Wieland reaction is a three-step, one-pot synthesis,[**] where the π-bond of an alkene undergoes radical reactions that result in the formation of the aromatic heterocycle, furoxan.[225] Takayama and co-workers proposed the mechanism outlined below (**Scheme 1**):[225]

$$NaNO_2 \xrightarrow{H^+} HNO_2 + Na^+$$

$$2HNO_2 \rightarrow H_2O + NO + NO_2$$

[**] Note that in the proposed mechanism (Scheme 1) five steps are outlined. Furoxan forms in the third step; however, the proton is later substituted with a nitro group.

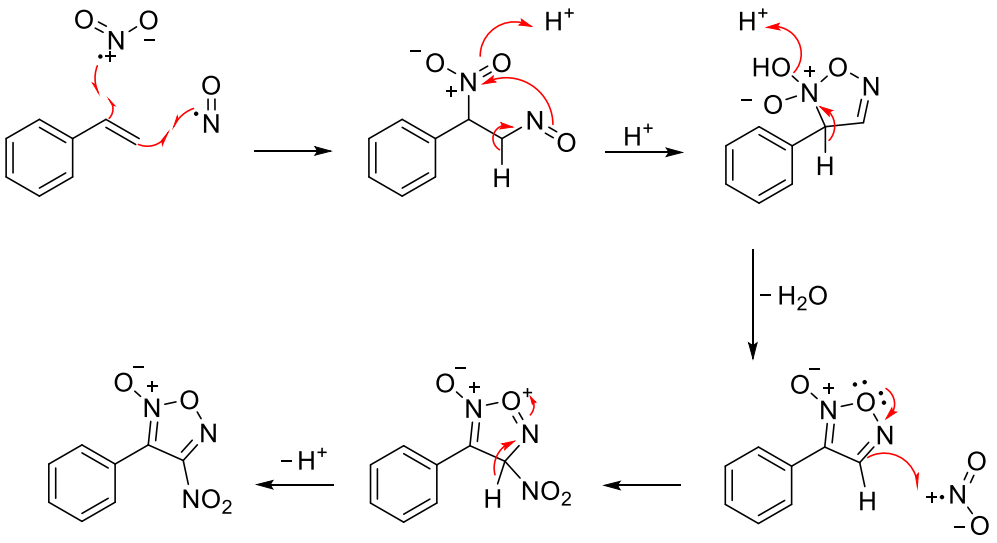

Scheme 1. Proposed reaction mechanism for the synthesis of furoxan ring from a vinyl group and $NaNO_2$ under acidic conditions.[225]

Under acidic conditions $NaNO_2$ forms nitrous acid. At pH < 5.0, nitrous acid will dissociate and form dinitrogen trioxide, N_2O_3.[201] This molecule generates two radicals, NO and NO_2, which react with the alkene in the first step.[225] However, another mechanism for this reaction has been suggested.[234] In the first step (**Scheme 2**), the alkene (**a**) reacts with NO_2 to form a carbon-nitrogen bond. The aryl radical (**b**) then reacts with NO to form pseudonitrosite (**c**) which loses water and forms furoxan (**d**).[234]

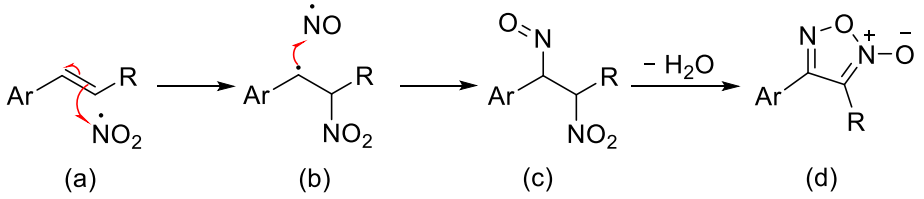

Scheme 2. An alternative reaction mechanism for the formation of furoxan.[234]

The two mechanisms predict different outcomes for the position of the exocyclic oxygen relative to the aryl group. The first reaction mechanism (**Scheme 1**) depicts what occurs during the synthesis of the new furoxan derivative L1(-NO_2).[225, 235] The position of the nitrone group relative to the aryl group can be determined using Heteronuclear Multiple Bond Correlation

spectroscopy, (HMBC, *see section 2.3.3*). Based on the spectrum, the pyridinyl substituent was found at C3.

Matsubara and co-workers reported that the presence of water in the reaction mixture during furoxan synthesis will generate α-nitrooxime (**Scheme 3 – c**) as a by-product. Water can attack the dinitrosoalkene resonance contributor (**a**) to form pseudonitrosite (**b**) which tautomerizes to form α-nitrooxime (**c**). This might explain the low yield of L1(-NO_2) synthesis (**Scheme 3**).[234]

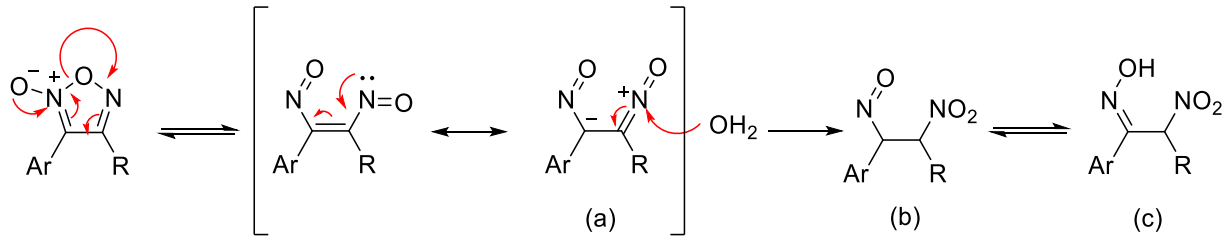

Scheme 3. Proposed mechanism for the synthesis of α-nitroxime by-product.[234]

Furoxans are stable in acid but are sensitive to bases.[209] 1,8-Diazabicyclo[5.4.0]undec-7-ene (DBU) was used as a base in the nucleophilic substitution reactions employed in the syntheses of L4(-OPh) and L5(-SPh). DBU is a strong base (pK_a = 12 in H_2O) that can deprotonate phenol and thiophenol. In addition, DBU cannot act as a nucleophile, under the experimental conditions and therefore, will not compete with the nucleophiles present in solution and result in side-products.[236] It is important to note that, L1(-NO_2) was used to synthesize L4(-OPh) and L5(-SPh), instead of L2(-H), not only because the yield of L1(-NO_2) was higher than L2(-H), but also because L2(-H) is a monosubstituted furoxan derivative that is unstable in the presence of bases. Previous studies have found that 4 and 3-monosubstituted furoxans can produce α-hydroxyimino nitrile oxide and α-nitro nitriles, respectively (**Scheme 4**).[209]

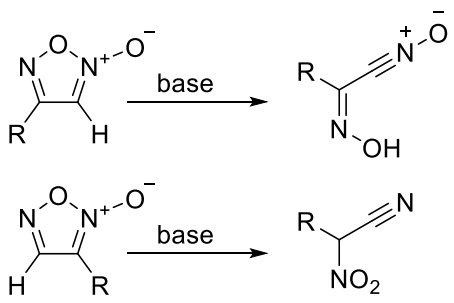

Scheme 4. Degradation reactions of monosubstituted furoxans under basic conditions.[209]

Physical characterization

The general physical properties of furoxans tend to be defined by their substituents. If both substituents on the furoxan ring are alkyl groups, then the compound will be a colourless liquid.[209] If both substituents are aryl groups, or an aryl and an alkyl group, then the compound is obtained as a white solid.[209] These physical features help in confirming the identity of the compounds. It was observed that all the furoxan derivatives synthesized in this work were obtained as white-yellow solids, except those that contain sulfur (L5, L6, and L7), which were light yellow liquids at room temperature (*ca.* 20-23 °C). However, they formed a solid at a low temperature (when placed in the fridge or freezer). This demonstrated that the compounds L5, L6, and L7, could be obtained as solids with low melting points.

Chemical characteristics and nucleophilic substitution reactions of furoxans

The six π-electrons in furoxan – two (C=N) and the lone pair of O – are delocalized; therefore the system is aromatic. Furoxans are mesoionic heterocycles (i.e., contain a dipolar structure with delocalized negative and positive charges) since they have a dipolar group (N→O). The resonance forms of mesoionic heterocycles are characterized by not having neutral structures.[237] In furoxans, a positive charge is delocalized on the ring while the exocyclic oxygen carries a negative charge. The positive charge makes furoxan susceptible to nucleophilic attack. The mesoionic structures and the general resonance form are illustrated below (**Scheme 5**):

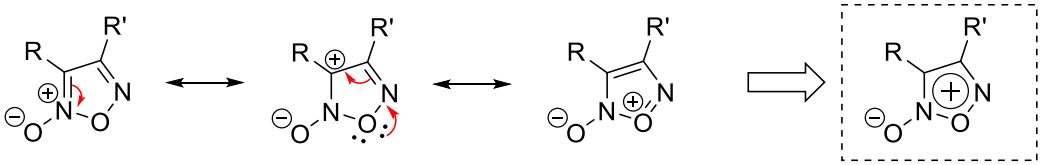

Scheme 5. Mesoionic structures of furoxan.

The N atom in the (N→O) group acts as σ-donor, and NO has a π-orbital that can accept electrons.[208] Therefore, backdonation from the exocyclic oxygen can occur and two mesoionic structures are obtained where both charges are present in the ring (**Scheme 6**):

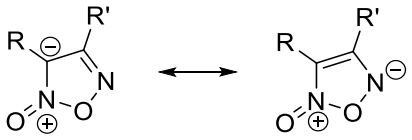

Scheme 6. Additional mesoionic structures of furoxan.

Synthesis of L3(-OCH$_3$) via nucleophilic substitution versus methylation reaction

A two-step synthetic route for the formation of methylated furoxan derivatives has been reported.[238] In the first step, a nucleophilic substitution reaction of the nitro group in 4-nitrofuroxan with hydroxide is performed.[238] Sodium hydroxide, NaOH, is used as the source of nucleophilic OH^- in a solvent mixture containing H_2O and tetrahydrofuran. 4-Hydroxyfuroxan forms in the first step and will undergo a side-chain prototropic tautomerization.[238] Tautomerization is defined as the coexistence of two or more molecular structures (i.e., tautomers or constitutional isomers) in an equilibrium due to their dynamic interconversion.[239] Prototropy is a type of tautomerism that involves the migration of a proton between different parts of the molecule.[239] Side-chain prototropic tautomerization is a specific form of prototropy that refers to the transfer of a proton between a ring and a side-chain.[238] In the second step, 4-hydroxyfuroxan is treated with a methylation reagent, such as methyl iodide, CH_3I, or dimethyl sulfate, $(CH_3O)_2SO_2$, to form a methylated furoxan.[238] The second step results in the formation of two regioisomers O-Me and N-Me, with O-Me being the predominant product (**Scheme 7**).[238] Therefore, the drawback of this synthetic pathway is the formation of two regioisomers both capable of releasing NO. Since this

work is aimed to synthesize furoxans that differ only in the substituent at the 4-position with no other structural differences, a different procedure was employed in the formation of the methylated furoxan derivative. In this procedure, the 4-nitrofuroxan (L1) was treated with potassium methoxide, $KOCH_3$, and by a nucleophilic substitution reaction the methylated furoxan derivative (L3) has formed in one step. This reaction workup is similar to the procedure reported in 1927 by Ponzio.[240]

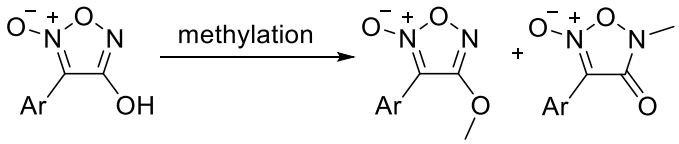

Scheme 7. Formation of two regioisomers during the methylation reaction of 4-hydroxyfuroxan.[238]

Thiophenol versus phenol reactivity

Thiophenol, PhSH, is more acidic than phenol, PhOH. The pK_a of PhSH in water is 6.5, while the pK_a of PhOH is 10.0, which implies that the S-H bond is relatively weak.[241] This feature of thiols makes them more reactive nucleophiles than alcohols.[242] The only concern in using thiols in the nucleophilic substitution reaction to form L5(-SPh), is the formation of disulfide bonds. Nevertheless, it is known that thiols can form salts, therefore by reacting PhSH with DBU a white salt will form (**Figure 2.9**) and can be reacted with L1(-NO_2). This minimizes the self-reaction of the thiols. In addition, it was found that the nitro substituent (in L1) is a good leaving group when thiolates are used as nucleophiles.[242] Alcohols can be used as reaction solvents since they are weaker nucleophiles and thus will not compete with thiols.[242]

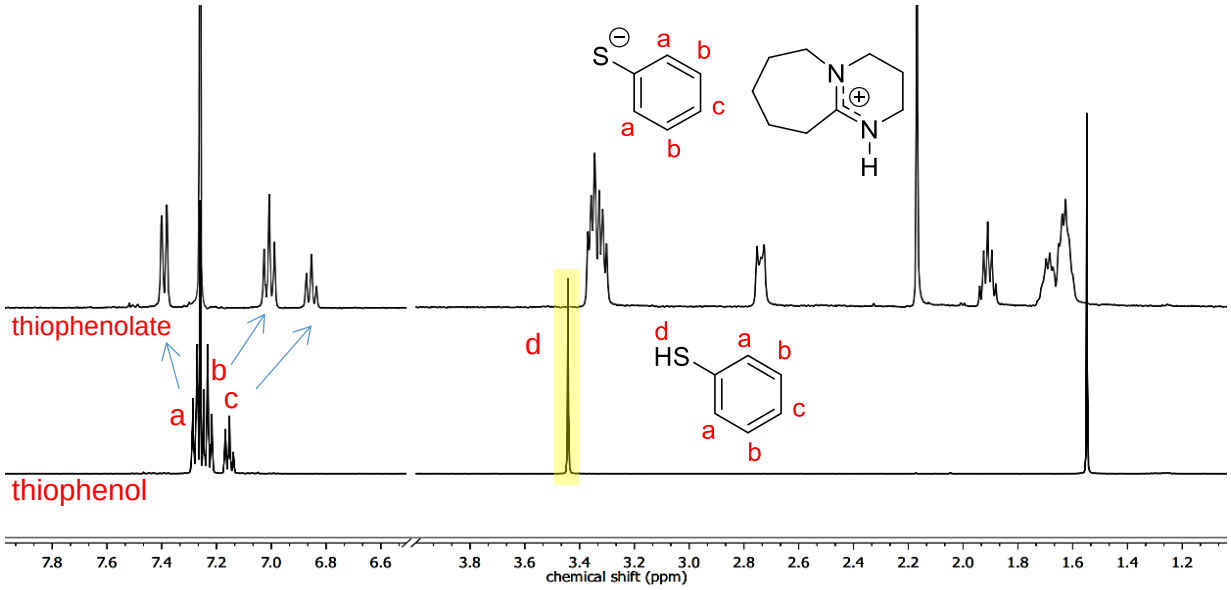

Figure 2.9. ^{1}H NMR spectrum of thiolate compared to thiol.

Oxidation reaction of L5(-SPh)

Oxidation of sulfides requires the presence of excess H_2O_2 and a long reaction time.[243] Heat might be effective in increasing the rate of the reaction.[243] However, since thermal isomerization is possible (*see section 2.3.3*), zirconium(IV) chloride, $ZrCl_4$, was used as a catalyst. In this reaction, aqueous H_2O_2 (30 %) is used as an oxidizing agent in the presence of methanol as a co-solvent. A more concentrated H_2O_2 solution (50-80%) can be used with acetic acid as a co-solvent, if a metal catalyst is not available. The oxidation of sulfide to sulfoxide is faster than the oxidation of sulfoxide to sulfone.[241, 243] A stacked ^{1}H NMR plot (internal standard is $CDCl_3$) of L5(-SPh), L6(-SOPh), and L7(-SO_2Ph) is presented in **Figure 2.10**. As can be seen from the spectra, the multiplicity and the chemical shifts change upon oxidation. When the thiol is oxidized, it becomes an electron withdrawing group and therefore the signals are deshielded in L6(-SOPh) and L7(-SO_2Ph) with respect to L5(-SPh). The spectrum of L6(-SPh) contains minor impurities, however since the spectrum does not contain signals in the same region as L7(-SO_2Ph), then the reaction was successfully terminated at the first oxidation step. The L7(-SO_2Ph) spectrum also contains minor impurities, but these are not in the region of L5(-SPh) or L6(-SOPh). A spectrum of L5(-SPh) is also provided in deuterated acetone in **Appendix 1**, since $CDCl_3$ signal overlaps with the compound signals. Therefore, it is possible to stop the reaction at the first oxidation step to form sulfoxide as the sole product, by adding water to dilute the peroxide, before the second oxidation step; the reaction progress needs to be monitored with TLC. Alternatively, one

equivalent of oxidizing agent can be used to ensure the reaction will stop at the first oxidation step.[241] The reaction mechanism in **Scheme 8** illustrates how H_2O_2 acts as an electrophilic oxidant.[241]

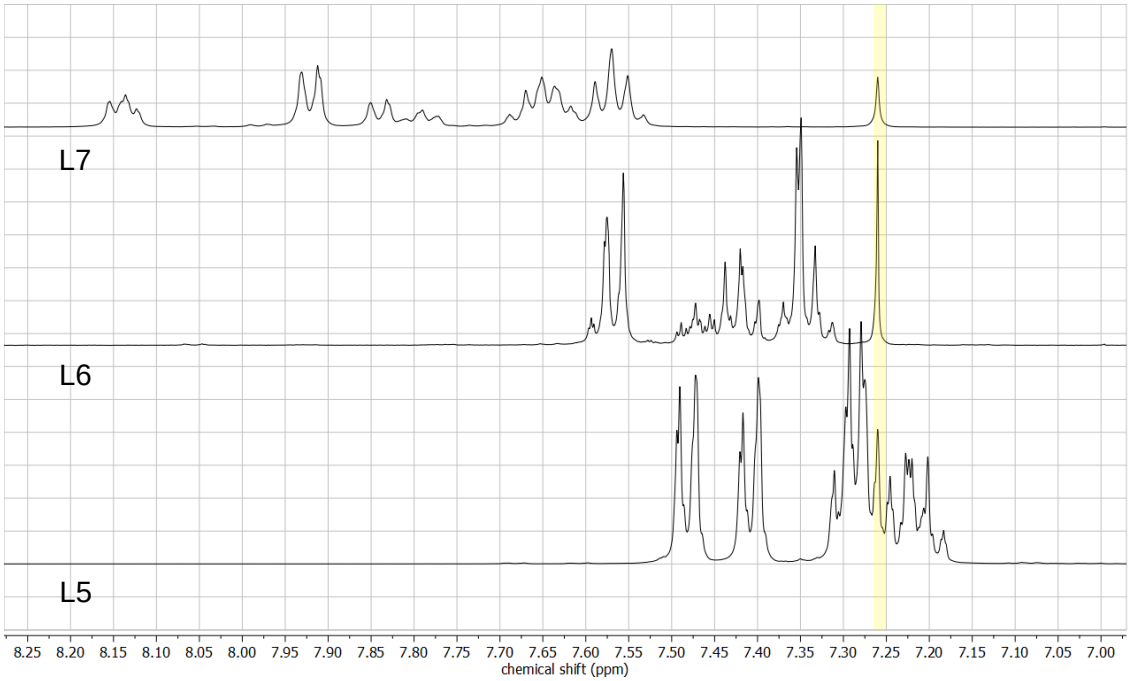

Figure 2.10. A stacked ^{1}H NMR spectra of L5(-SPh), L6(-SOPh), and L7(-SO_2Ph) in $CDCl_3$.

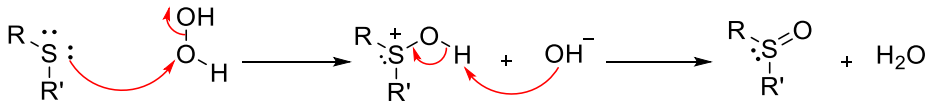

Scheme 8. Oxidation of thiol by H_2O_2.[241]

Colour test for N-oxide moiety in furoxans

In 1959, Katritzky and Coats reported a color test for the N-oxide moiety.[231] N-oxides act as oxidizing agents. They can oxidize *N*,*N*-dimethylaniline under acidic conditions into crystal violet and methyl violet.[††] A blue colour indicates a positive test of N-oxide, however, it may turn violet after reflux, because as the solution cools down, it absorbs moisture from air.[244] In general, treating *N*,*N*-dimethylaniline with inorganic oxidizing agents, such as $Cu(NO_3)_2$ and H_2O_2, forms crystal violet via oxidative N-dealkylation.[231] Oxidative N-dealkylation occurs when tertiary amines are oxidized at the α-carbon resulting in the removal of the alkyl group.[245] The proposed mechanism is illustrated in **Scheme 9**.[245] In addition, if the N-oxide compound contains a nitro substituent, like the L1(-NO_2) furoxan derivative, an orange-red colour solution will form, because it is believed that the nitro group can give rise to a charge transfer with dimethylaniline.[231] This test was performed on L1(-NO_2) and L2(-H). As can be seen in **Figure 2.11**, an orange-red solution was obtained from the former ligand (**a**), while the latter exhibited a blue colour (**b**) which turned violet (**c**) a few minutes after cooling the reaction to room temperature, 23 °C.

This colour test is useful when synthesizing novel compounds, since it can quickly – within one minute – indicates the presence (or absence) of N-oxide moiety. With respect to furoxan derivatives, ^{1}H and ^{13}C NMR spectroscopy are effective in determining the structure of hydrocarbons, while ^{17}O and ^{15}N HMBC can prove the presence of heteroatoms. However, the latter two experiments are time consuming and may require isotopic labelling. A ^{1}H-^{15}N HMBC (**Appendix A**) experiment was performed on L1(-NO_2) and was only able to detect the presence of the pyridyl nitrogen, while the two nitrogen atoms in furoxan are far from the protons and thus were not observed. Mass spectrometry can also assist in confirming the structure from the molecular weight but for furoxans fragmentation to lose the exocyclic oxygen can be a problem.[246-250] Indeed, there are alternative methods and analyses to prove the structure, particularly, X-ray diffraction (XRD). However, it may not always be likely to obtain a single crystal of an N-oxide novel compound. Therefore, this colour test is useful in proving the presence of N-oxide.

[††] The detailed mechanism of this reaction is not clear.

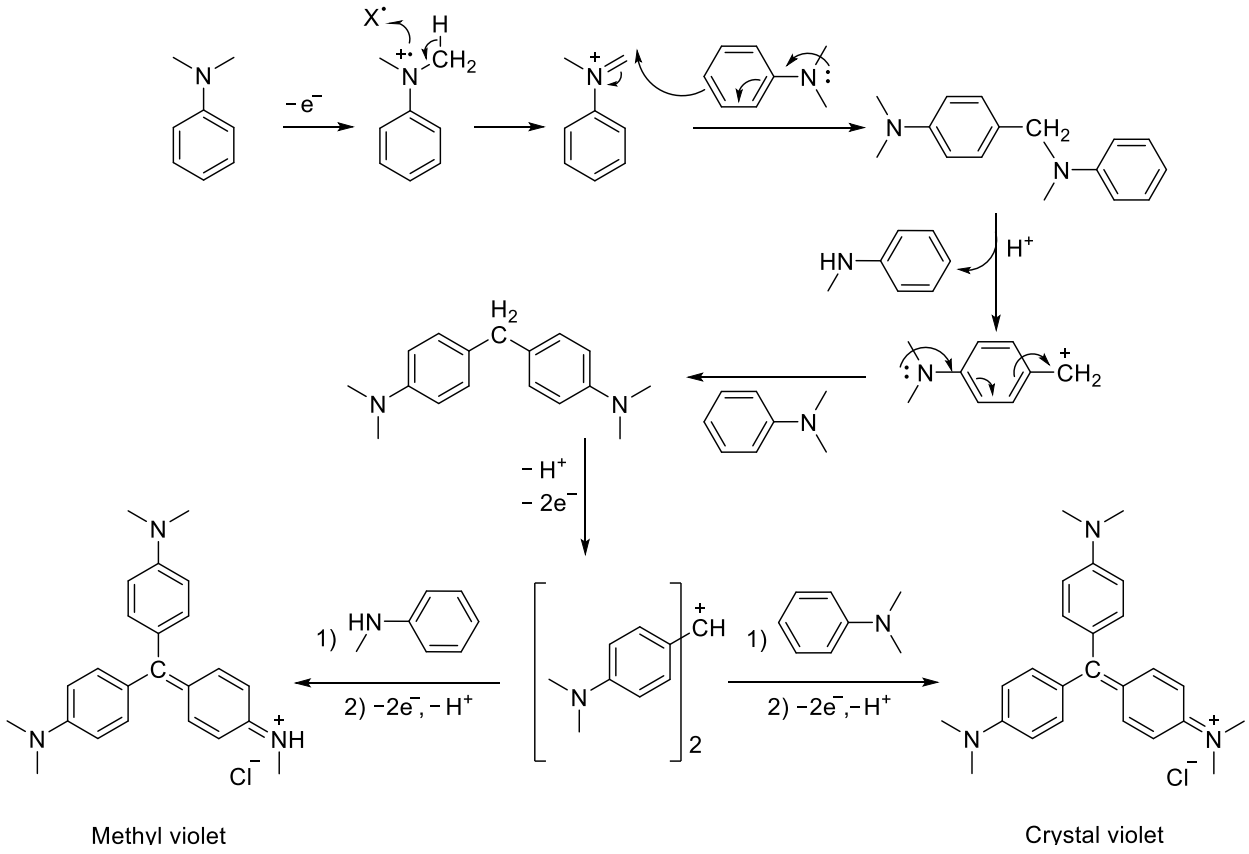

Scheme 9. Proposed mechanism for the synthesis of crystal violet and methyl violet.[245]

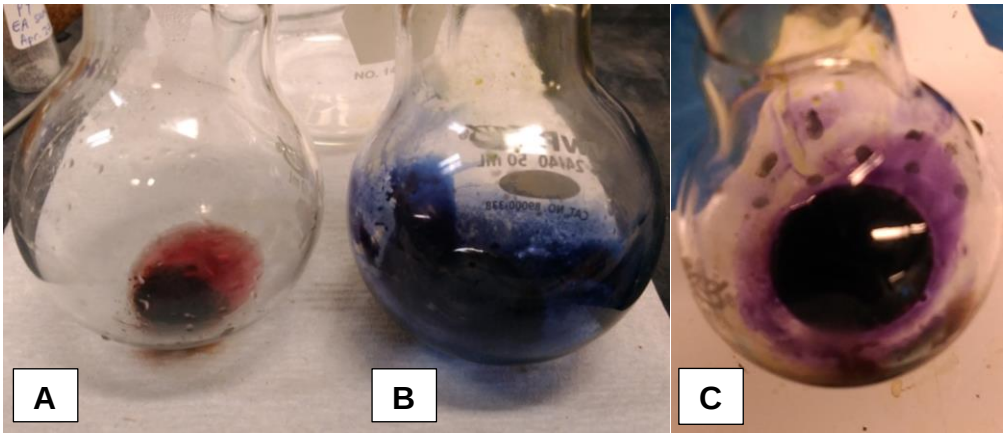

Figure 2.11. Colour test for N-oxide. A) colour test performed on L1(-NO_2); B) colour test performed on L2(-H); C) same test as in (B) but after cooling to room temperature.

2.3.2. Infrared spectroscopic analysis

Characteristic infrared (IR) absorptions of the (=N→O) bond in furoxan are observed in the regions 1200-1300 cm^{-1} and 850-950 cm^{-1}.[209, 251] However, having a nitro group in the compound can interfere with the signal at 1200-1300 cm^{-1}. A doublet is typically observed in the region (1410-1475 cm^{-1}) which corresponds to (O-N→O).[251] In addition, the two C=N stretching frequencies in the furoxan ring can be observed in the regions (1600-1625 cm^{-1}) and (1500-1600 cm^{-1}).[251] The IR spectra of L1(-NO_2) and its corresponding Ru(II) complex are provided below (**Figure 2.12** and **Figure 2.13**). The IR spectrum of L4(-OPh) is also provided in **Figure 2.14.** The IR spectra of the other compounds are not provided as different functional groups in these compounds can interfere with the signals characteristic of the furoxan moiety. This section is meant to elucidate the usefulness of IR spectroscopy in identifying bonds or groups in the furoxan ring that cannot be inferred using other spectroscopy techniques such as NMR and mass spectrometry. Nevertheless, IR spectroscopy should not be used as a primary tool in identifying the chemical structure of these compounds.

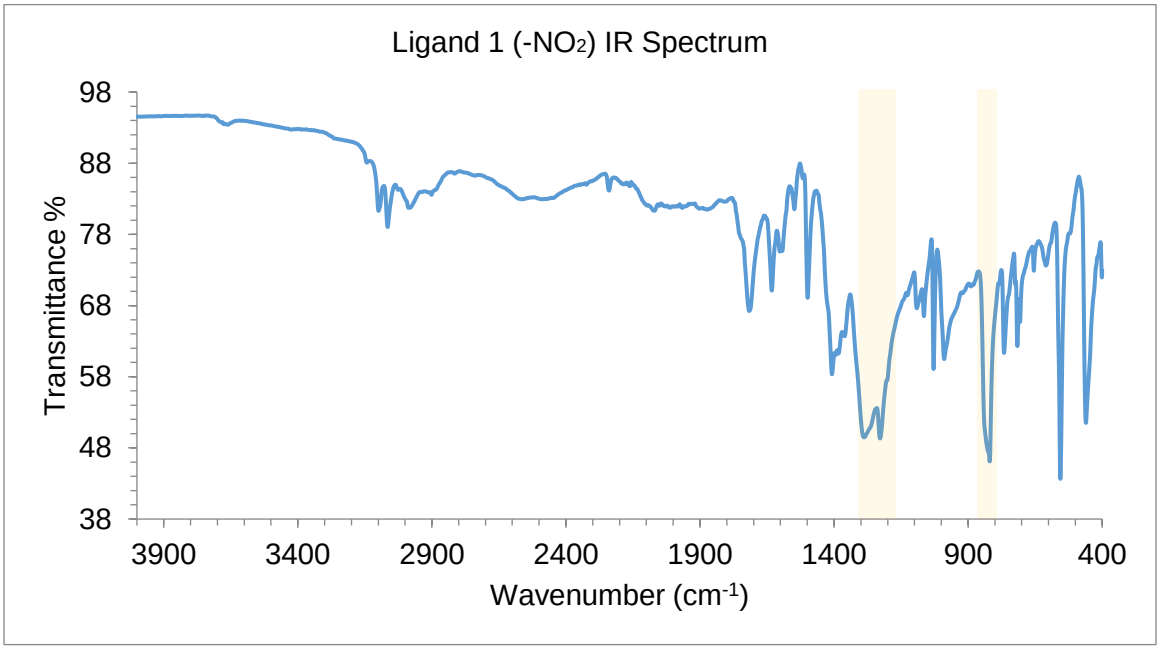

Figure 2.12. IR Spectrum of L1(-NO_2). The characteristic regions of (=N→O) absorption are highlighted.

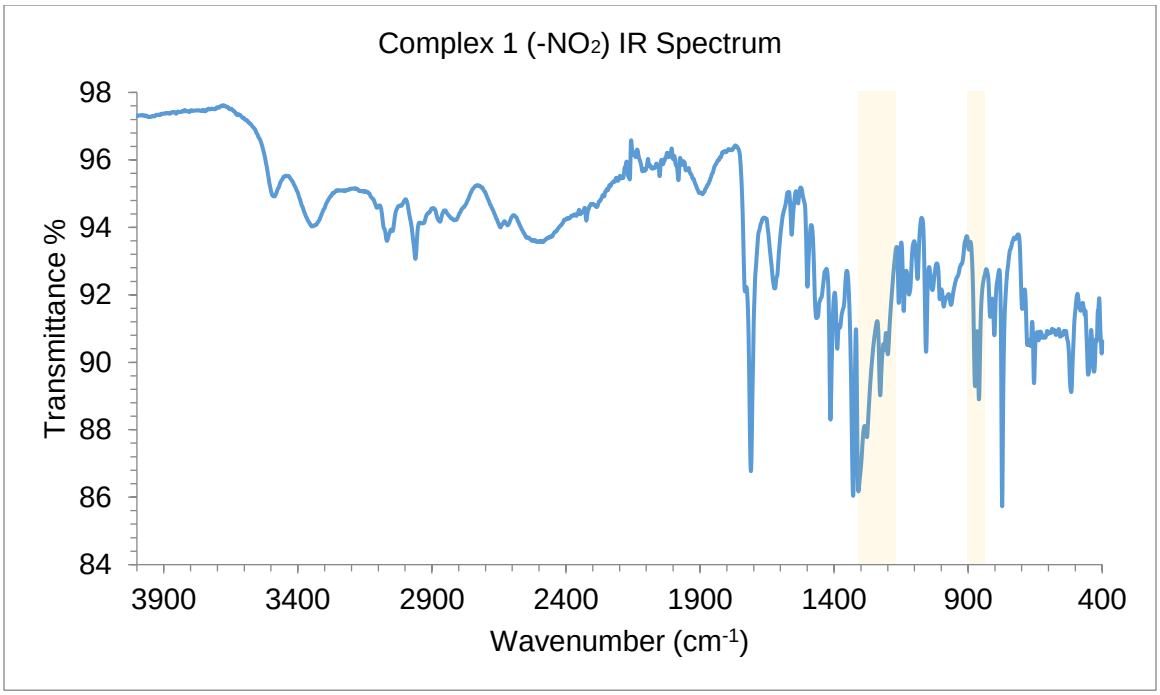

Figure 2.13. IR Spectrum of C1(-NO_2). The characteristic regions of (=N→O) absorption are highlighted.

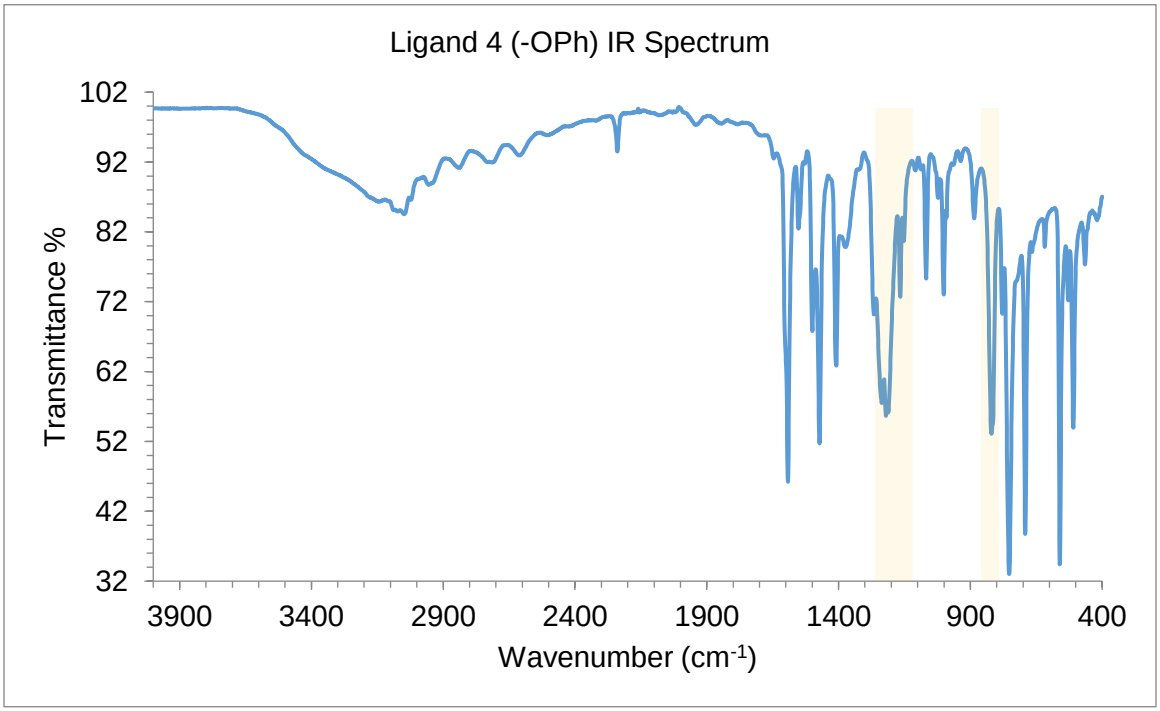

Figure 2.14. IR Spectrum of L4(-OPh). The characteristic regions of (=N→O) absorption are highlighted.

2.3.3. Isomerization of furoxans

Thermal isomerization is a common phenomenon in furoxans.[208] It is very likely to observe structural isomerization if the substituents on the furoxan ring are electron-donors.[209] These substituents were found to lower the energy barrier for isomerization.[209] Electron-donating groups favour the 4-position of the furoxan ring but electron-withdrawing groups will not always favour the 3-position.[209] Researchers have found that one of the best methods to distinguish between furoxan isomers is to use NMR spectroscopy. The C and H nuclei in the substituents are more shielded when N-oxide moiety is closer to them since N-oxide has a shielding effect. In other words, if a substituent is in the 3-position (closer to an N-oxide), the ^{13}C and ^{1}H NMR signals will appear upfield with respect to the signals corresponding to the same nuclei in the other isomer. The shielding effect is more pronounced in the C and H nuclei positioned near the spatial environment of N-oxide functionality.[209] Photo-isomerization is also observed in furoxans and is dependant on the wavelength of light.[209]

Since furoxan synthesis reactions are regiospecific, thermal isomerization is useful in obtaining regioisomers that are difficult to synthesize. Refluxing one isomer of furoxan at high temperature in solvents such as toluene or benzene will form dinitrosoalkene intermediate through which the exocyclic oxygen atom can transform from one nitrogen to the other.[252] Both isomers can be isolated as pure products via chromatographic separation.

The position of the exocyclic oxygen on the furoxan ring (the type of isomer) can be determined by using Heteronuclear Multiple Bond Correlation (HMBC) spectroscopy.[246] **Figure 2.15** shows the HMBC spectrum for L4(-OPh). Since H_a in the pyridinyl group correlates to the quaternary carbon that has a chemical shift of ~116 ppm, then the N→O group is closer to the pyridinyl substituent (the pyridinyl substituent is in position 3, while the phenoxy substituent is in position 4). This assignment was made following the literature method in assigning the type of furoxan isomer.[246]

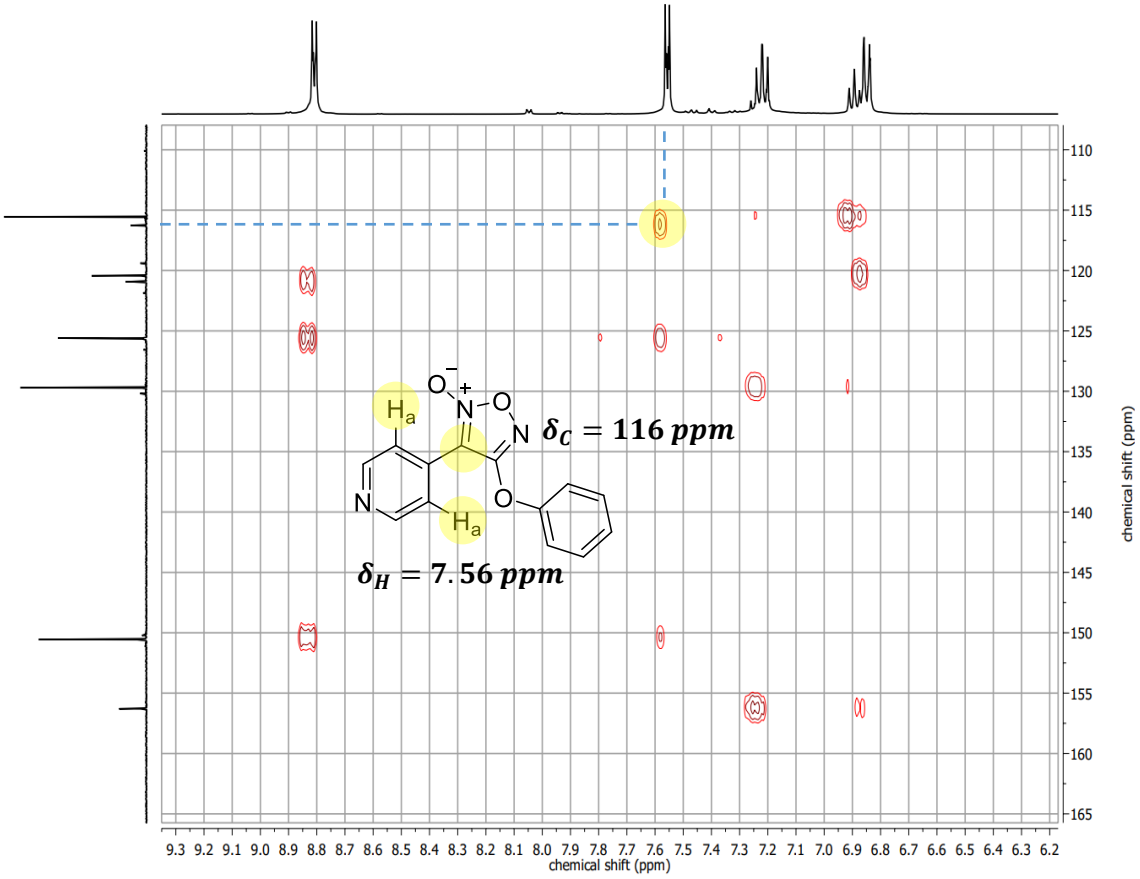

Figure 2.15. Determining the isomer of the furoxan L2(-OPh) via HMBC spectroscopy.

Several furoxans are known to exhibit thermal isomerization at room temperature.[208] The NMR spectra of these compounds cannot be resolved, because it is a mixture of two isomers and the intermediate state (**Scheme 10**).[208] Heteronuclear Single Quantum Coherence (HSQC) can be used to determine whether or not the furoxan derivatives exhibit isomerization. The HSQC spectra for L1(-NO_2) and its analogus structure (with a phenyl instead of a pyridyl substituent) are presented in **Figure 2.16**. HSQC does not show which isomer is present, however it indicates whether the molecule isomerizes. The complexity of the spectrum increases with the number of molecules (isomers and intermediate) present.

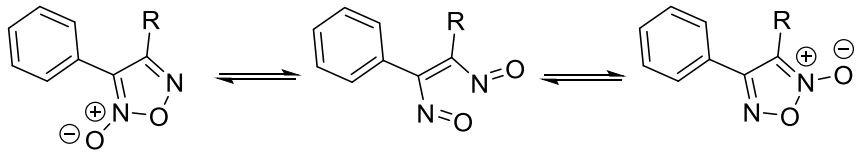

Scheme 10. Isomerization of furoxan.[208]

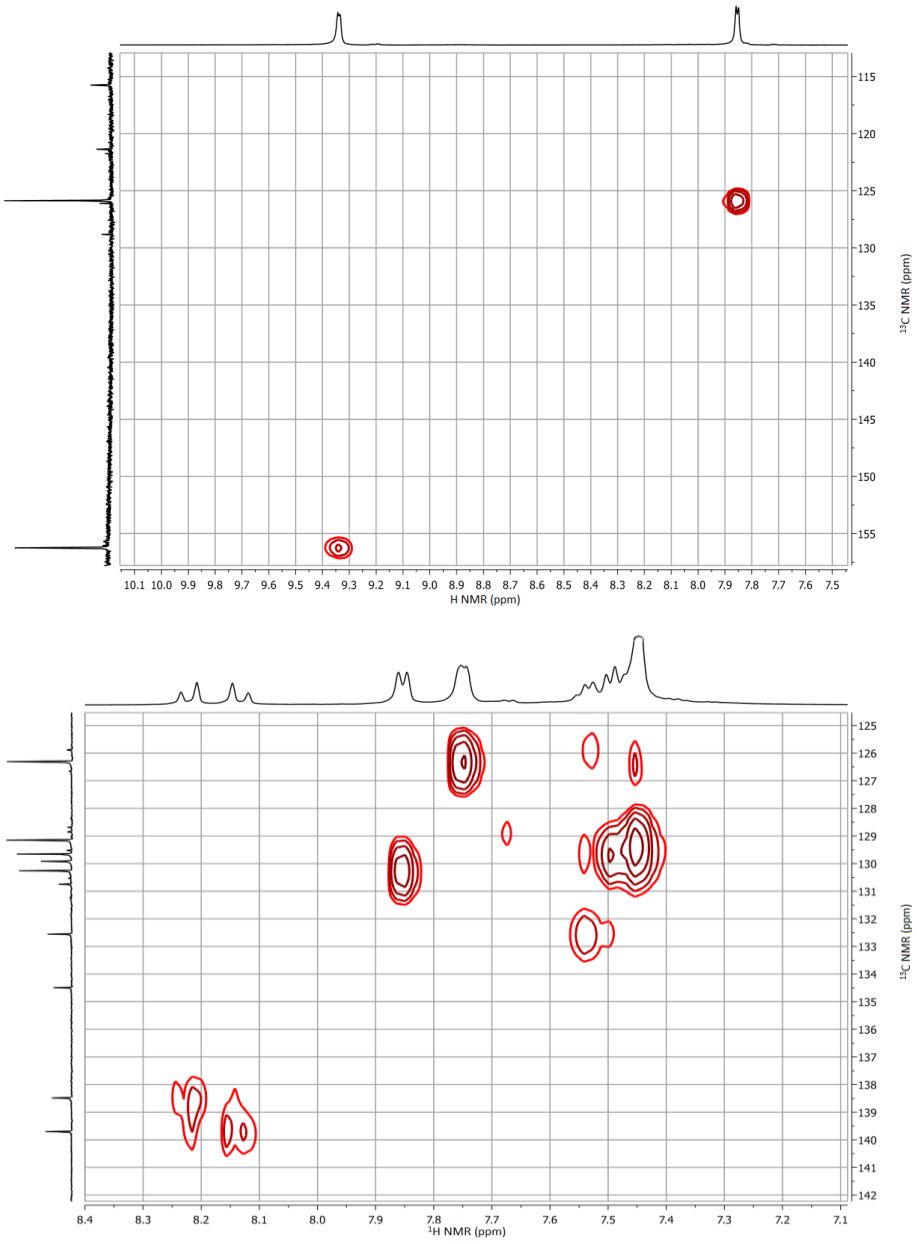

Figure 2.16. HSQC spectra for L1(-NO_2) (top) and its analog (nitro)(phenyl)-1,2,5-oxadiazole 2-oxide (bottom).

2.3.4. Nitric oxide detection via electron paramagnetic resonance

Principles of electron paramagnetic resonance (EPR)

Electron paramagnetic resonance (EPR), also known as electron spin resonance (ESR), is a spectroscopic method used to study the structure and electronic properties of paramagnetic species (i.e., species that have unpaired electron(s)).[253] An unpaired electron has a magnetic dipole that can interact with an external magnetic field, B.[253] The magnetic dipole can be aligned with or against the applied magnetic field, and therefore an unpaired electron can be in one of two energy states (i.e., quantized).[253] The splitting in energy that is caused by the interaction between the electron magnetic dipole and the external magnetic field is known as the Zeeman effect (**Figure 2.17**).[253] Since a single unpaired electron has a spin-angular momentum quantum number of 1/2, the "up" and "down" spin states are m_s = —1/2 (lower energy), and m_s = +1/2 (higher energy), respectively. For a transition to occur the resonance condition, $h\upsilon = B\beta_e g_e$, must be satisfied so that photon energy equals the Zeeman splitting, where h = Planck's constant, υ = the light frequency, g_e is the electron g value, β_e is the Bohr magneton and B is the applied magnetic field.‡‡ The observed transition is detected as an EPR signal.[253] The signal is an absorption spectrum but it is plotted by the acquisition software as the first derivative.

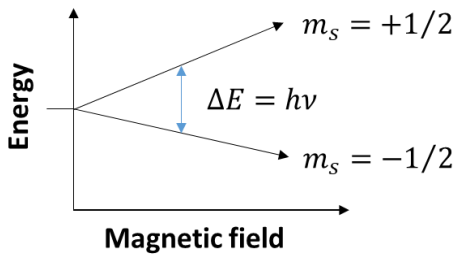

Figure 2.17. Single electron energy splitting due to Zeeman effect.

The energy of EPR transitions is described by the following equation:

$$\Delta E = h\upsilon = B\beta_e g \qquad 2.1$$

‡‡ The magnetic field can be measured in Tesla (T) – SI unit, or Gauss (G) – cgs unit. 1 T= 10000 G

The effect of the local environment is parameterized by the g value (g), which varies from free electron g_e = 2.0023 due to the effect of local magnetic field contributions from the paramagnetic compound, so that the resonance condition is defined as $h\upsilon = B\beta_e g$.[253] When acquiring the EPR spectrum of a compound, the microwave frequency, υ, is held constant while the magnetic field, B, is swept over a specific range.[253] Therefore, from the above equation only B is changing, and at a specific value of B, the product of $B\beta_e g$ will equal the energy required for an EPR transition of a single electron. The following figure is a block diagram that elucidates the main parts of an EPR spectrometer (**Figure 2.18**). The sample in the EPR tube is placed inside the cavity which is positioned between two magnetic poles. Microwave radiation is directed to the cavity via a waveguide.

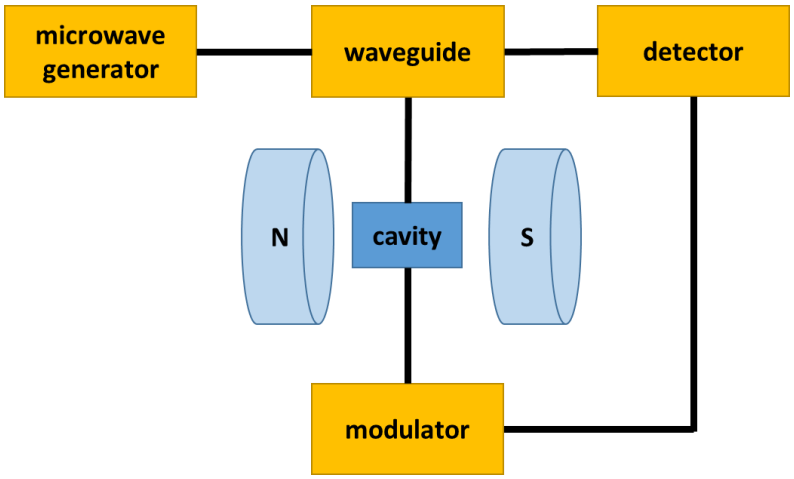

Figure 2.18. Block diagram illustrates the main parts of the EPR spectrometer.

Mode of nitric oxide release by furoxan

There are several classes of NO donors. Some compounds, such as organic nitrates and nitrites, hydroxy amine, and hydroxamic acid generate nitric oxide *in vivo* due to specific enzymes.[178] Enzymes capable of catalysing the release of NO are glutathione S-transferase (GST), NOS, guanylate cyclase, xanthine oxidase, and catalyse, to name a few.[178] Other classes of NO donors such as syndonimine, C-nitroso compounds and oximes do not require the presence of enzymes and release NO when exposed to light, heat, metals (Fe^{3+}, Cu^{2+}), thiols, or when the pH of their environment is altered.[178] Furoxans were found to generate the NO radical

in the presence of thiols.[178, 209] Therefore, NO quantification via EPR was performed in the presence of reduced glutathione (GSH).

GSH is the most abundant thiol in cells with concentrations ranging between 0.5–10 mM.[254] Cancer cells often have elevated concentrations of GSH.[255] Therefore, furoxans are more likely to release NO in tumour cells than in healthy cells. It has been suggested that thiolates can attack the 3 and/or the 4 positions on the furoxan ring resulting in the release of NO.[158, 256] However, some furoxans might experience the nucleophilic attack primarily at the 3 position (**Scheme 11**).[158, 205] Apoptosis can then be triggered by the elevated concentration of NO and the reduced concentration of GSH in the cell. The depletion of GSH induces apoptosis in several forms of cancer including pancreatic and lung cancers.[257-260] GSH acts as an ROS scavenger, thus its depletion can potentially increase the concentration of ROS and lead to cell death.[66]

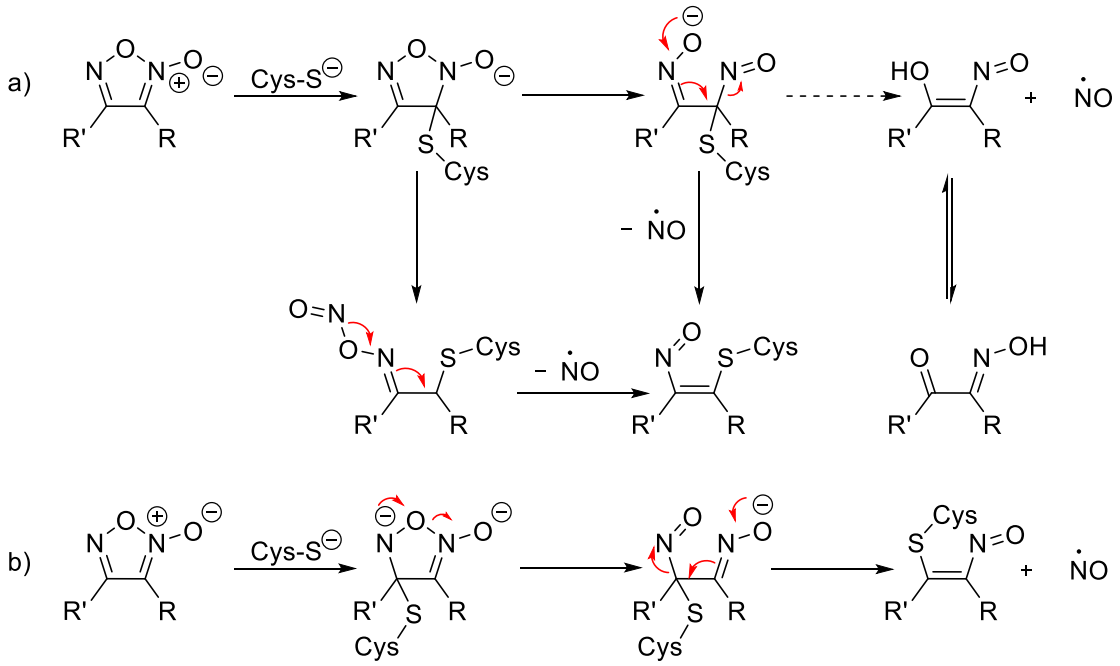

Scheme 11. Proposed mechanisms for nitric oxide release from furoxan upon its reaction with thiolate at the 3-position (a), and at the 4-position (b).[158, 205]

Introduction to spin-trapping

Nitric oxide can act as a ligand since it has an affinity for many metal ions, such as Fe, Co, Mn, Cu, and Ru. It can exist in bent, bridged and linear coordination geometries.[185] When NO has a bent geometry, it has a nitroxyl anion (NO^-) character (sp^2 hybridized) and metal-to-ligand charge transfer is observed.[185, 261] A linear binding geometry results in a nitrosonium cation, NO^+, character (sp hybridized) and ligand-to-metal charge transfer can occur. [185, 261] Nitrosyl complexes of hemoglobin have a bent bond angle of (145°).[262] The Fe-N-O bond is bent due to the hybridization of the orbitals in NO.[262]

In general, Fe(II) complexes have a high affinity for nitric oxide in solution. The resulting complexes are paramagnetic and can be studied by EPR.[262] Isotopic labelling of the nitrogen nucleus in NO was performed to prove that NO released from NO-donors becomes a ligand in the spin-adduct (the iron nitrosyl complex).[263] A spin-trap is a molecule that traps the paramagnetic species and forms a stable spin-adduct that can be detected via EPR.[264] Herein, the spin-trap is synthesized from Mohr's salt and a ligand containing a dithiocarbamate group. Mohr's salt, $(NH_4)_2Fe(SO_4)_2 \cdot 6H_2O$, forms the octahedral aquo Fe(II) complex, $[Fe(H_2O)_6]^{2+}$, when dissolved in H_2O. The sodium N-methyl-D-glucamine dithiocarbamate (MGD) salt is a water soluble molecule that exchanges with the aquo ligands of $[Fe(H_2O)_6]^{2+}$ to form a square planar complex, $Fe(MGD)_2$, which acts as a spin-trap for nitric oxide (**Figure 2.19**). For one equivalent of Fe(II), five equivalents of MGD are required to drive the reaction forward.[263] The rate constant of NO binding to $Fe(MGD)_2$ is high (1 to 5 × 10^8 $M^{-1}s^{-1}$), therefore, NO is more likely to form the spin-adduct than undergo side reactions.[263]

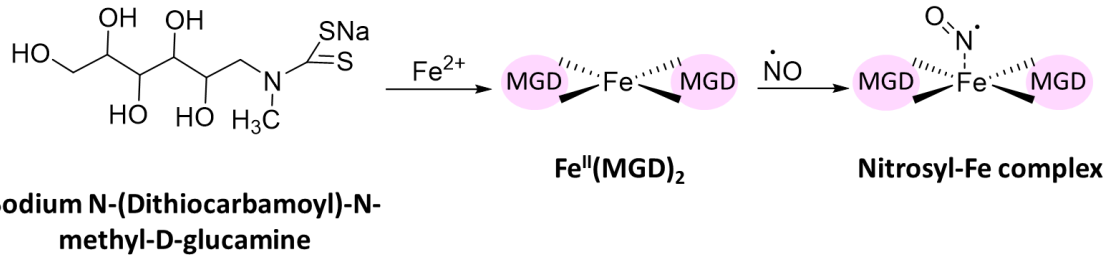

Figure 2.19. Formation of spin-adduct. MGD reacts with Fe^{2+} to form a square planar complex that can then react with nitric oxide radical to form the spin-adduct, nitrosyl-Fe complex.

Since NO has an unpaired electron in its π^* orbital, it is a paramagnetic molecule that can be detected using EPR. Nitric oxide in the gas phase can be measured directly by EPR. However, it cannot be directly detected in solution or biological environment, and spin-trapping is required to observe a clear NO signal.[263] One reason NO cannot be detected in solution is that the angular momentum of the unpaired electron (*L*) can couple with the angular momentum of the nitric oxide molecule, which influences the paramagnetic character and results in a broad signal.[181] In addition, the concentration of NO in physiological systems is relatively low and performing experiments that mimic this environment will require having low concentration of NO-donors. Therefore, the amount of NO released by these compounds might be lower than the detection limit of the EPR instrument, making it hard to prove whether the compounds of interest are capable of donating NO.[263] It has also been noted that the low solubility of NO in water prevents it from being detected by EPR spectroscopy; nevertheless, it can be detected when it is trapped by the Fe(II) complex at room temperature.[265, 266] Thus it is necessary to use the spin-trapping method when measuring NO in biological systems or in solution.

The spin of the unpaired electron of NO interacts with the nuclear spin of nitrogen (^{14}N, 99.632%, I = 1) resulting in what is known as hyperfine interaction. Since I = 1, the z component of the nuclear spin angular momentum vector has three orientations defined by M_I = —1, 0, +1. As a result, the hyperfine interaction of the unpaired electron with ^{14}N in NO leads to a three-line spectrum. **Figure (2.20)** shows the EPR spectrum acquired from the spin-trapping experiment with C1(-NO_2). From the middle spectral line, the g-value can be determined using the following equation:

$$g = \frac{h\upsilon}{B\beta_e} \qquad 2.2$$

B is the magnetic field at the centre of the spectrum (3387.7 G = 338.77 mT) which defines the g value. Experiments were performed using X-band frequency, υ = 9.67 GHz, that yields an experimental g-value of 2.039. This value is in agreement with the literature g-value of NO spin-adduct, which is reported to be 2.04.[263] The hyperfine splitting constant is the distance between the EPR lines which was found to be (a_N = 12.5 G), also in agreement with the literature.[233]

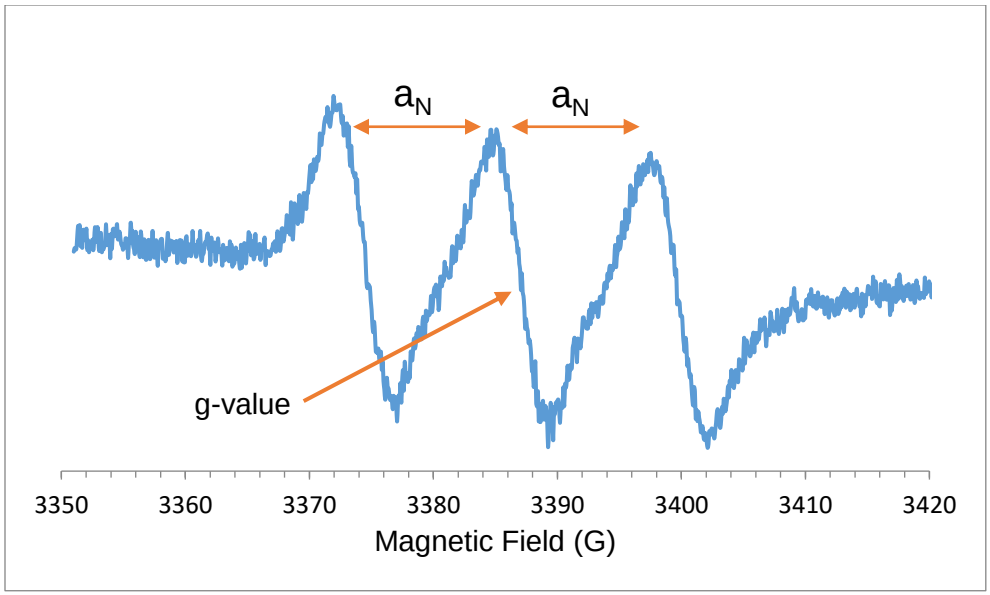

Figure 2.20. EPR spectrum of C1(-NO_2) complex.

The reaction between GSH and the compounds was investigated at pH 7.4, under an inert atmosphere in PBS. One disadvantage of using $Fe(MGD)_2$ as a spin-trap is that the solution must be deoxygenated prior to mixing the spin-trap with the NO-donor.[263] The presence of oxygen in solution can oxidize Fe(II) to Fe(III) and generate reactive oxygen species (ROS). Under physiological conditions, NO has a relatively short half-life due to several different reactions.[109] In the presence of superoxide anion, NO is oxidized to give the peroxynitrite anion which then isomerizes to form nitrate, NO_3^-.[109] However, NO can also oxidize to form nitrite, NO_2^-. Both nitrate and nitrite are stable end products.[198, 205] It is important to note that if nitrite and/or S-nitrosothiols are present in solution, then they will be reduced to NO by the $Fe(MGD)_2$ spin-trap with the production of the ferric complex, $[Fe(MGD)_2]^+$.[263] These reactions are slower than the formation of the NO spin-adduct.

Determining NO release from EPR signal intensity

To quantify the amount of paramagnetic species in a sample, the acquired EPR spectrum (the first derivative) is doubly integrated to measure the area under the absorption spectrum.[263] In other words, the area under the absorption curve is proportional to the number of unpaired electrons (**Figure 2.21**).[263] The value obtained from the second integral is compared with a standard that has a signal in the same magnetic field region as the compound of interest.[263] In this work, 2,2-diphenyl-1-picrylhydrazyl (DPPH) was used as an internal standard. Preliminary

EPR spectra were acquired for all the complexes and the corresponding ligands without the standard to check if they release nitric oxide. **Figure 2.22** shows the spectra from complexes 1, 3, and 4.

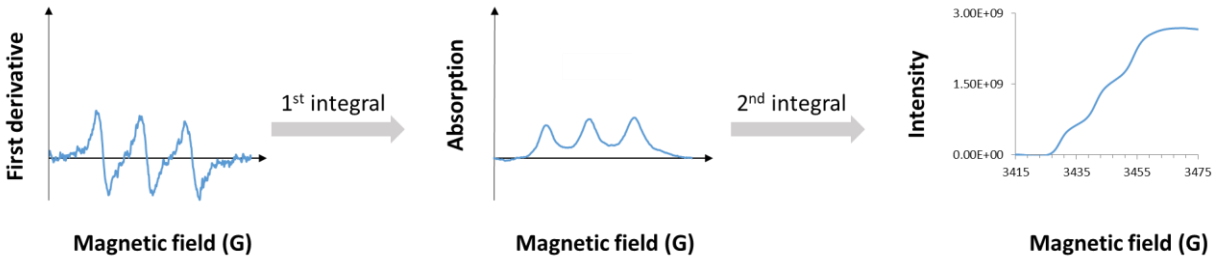

Figure 2.21. Determining the amount of NO from the intensity of the EPR spectrum.

As shown in **Figure 2.22**, one hour following mixing with excess GSH (5 equivalents of GSH), C1(-NO_2) released the highest amount of NO. C4(-OPh) released a very small amount of NO and C3(-OCH_3) which did not release any NO. The EPR spectra from the samples were measured over several hours. The intensity of the signal from C1(-NO_2) remained constant over time, thus only the spectrum from the first hour is shown in the figure. C4(-OPh) released 1.3 times more NO after 6 hours than after the first hour. Finally, C3(-OCH_3) did not exhibit any EPR signal until around the eighth hour. The intensity of this signal was then comparable to that of C4(-OPh). To better compare the amount of NO released by these compounds, the intensity of the signals was determined by double integrating the spectra. The results of measuring the signal intensities over the first two hours are presented in **Figure 2.23**.

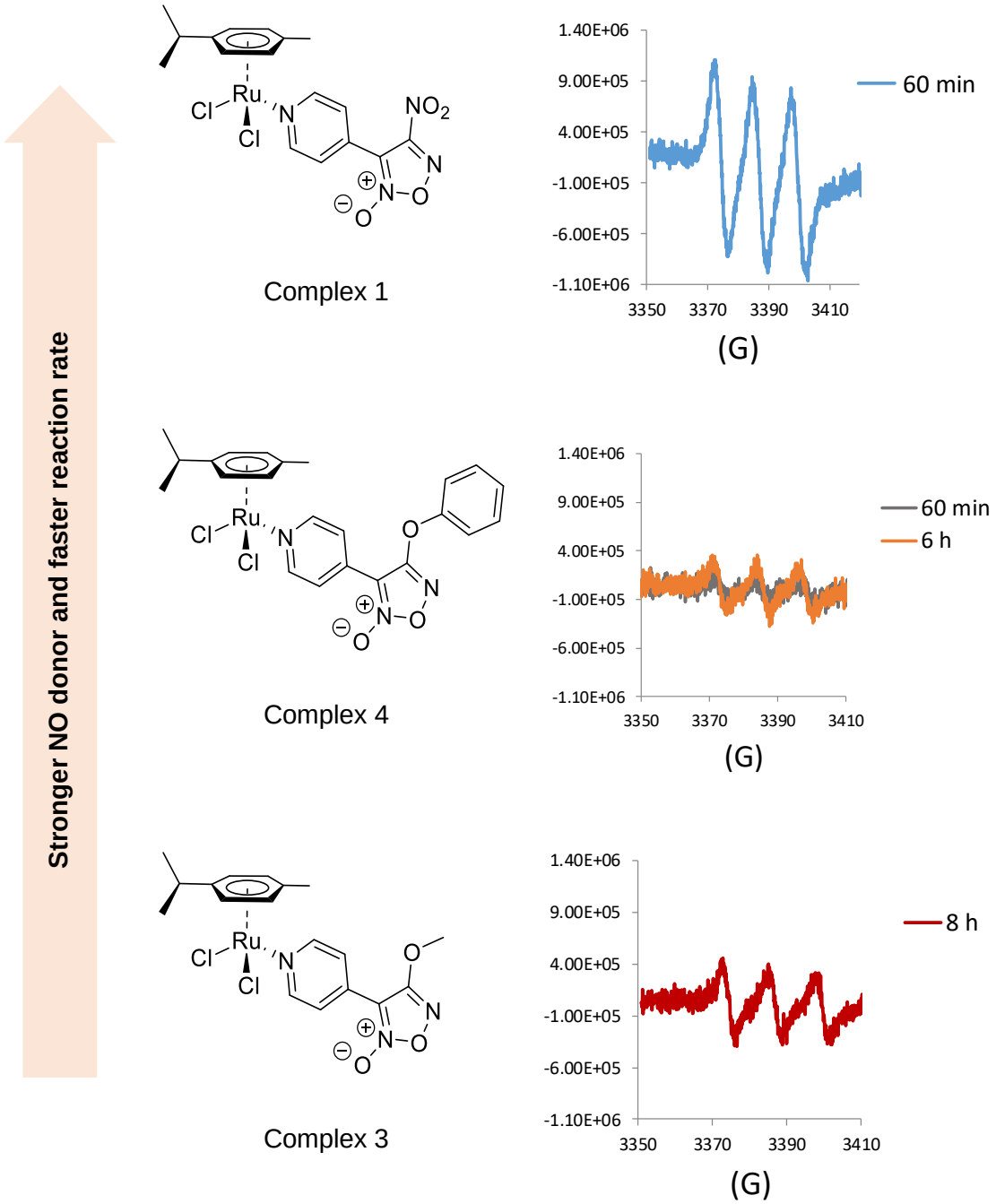

Figure 2.22. **EPR spectra acquired from reacting 1 equivalent of the complexes with 5 equivalents of reduced GSH under physiological conditions (37 °C, pH 7.4, in PBS). Although the vertical axis, which has arbitrary units, is typically removed from EPR spectra, it is included above to indicate the difference in the intensity of the signals.**

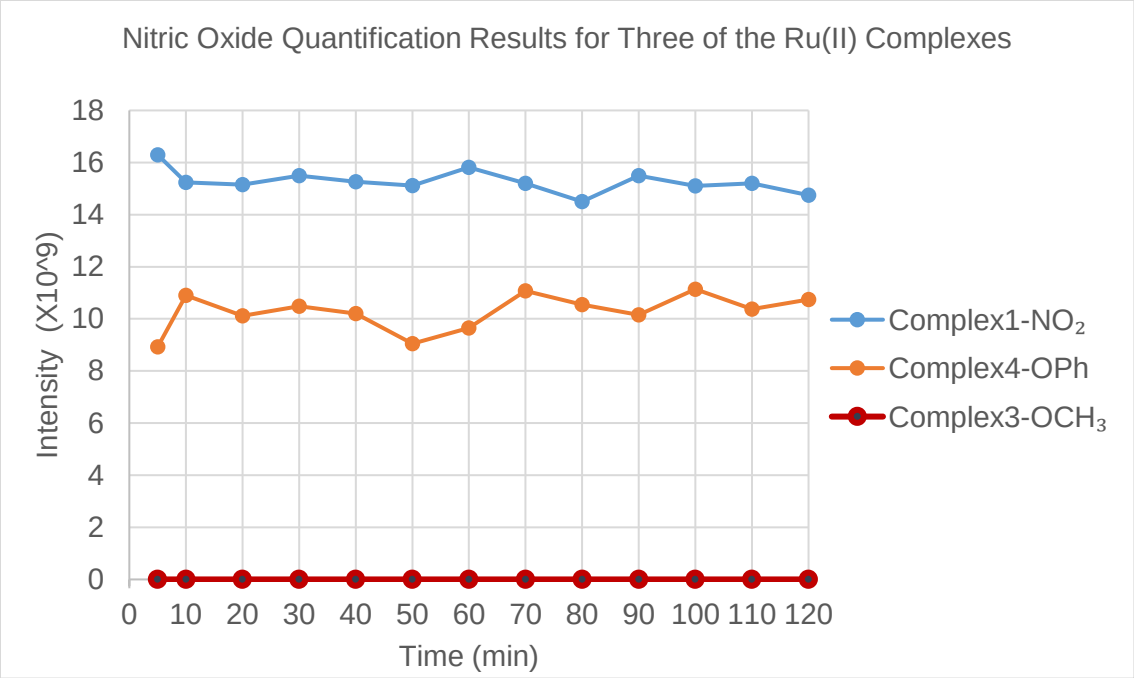

Figure 2.23. Comparison of the amount of NO released from complexes 1, 3 and 4 determined by plotting the intensity from the second integral of the EPR signal over two hours.

Following the same method of analysis, the amount of nitric oxide was also quantified for the rest of the complexes. **Figure 2.24** shows the intensity determined from double integrating the EPR spectra of all the complexes. The order in terms of the amount of nitric oxide they release is as follows:

C7(-SO_2Ph) > C1(-NO_2) > C5(-SPh) > C4(-OPh) > C2(-H) > C6(-SOPh) > C3(-OCH_3)

Stronger NO-donor

Since the complexes are different only in terms of their substituents on the furoxan ring, the electronic effect of these groups can assist in rationalizing the results. Electron withdrawing substituents (-NO_2 and -SO_2Ph) lower the electron density on the furoxan ring, making it electrophilic, and thus more susceptible to nucleophilic attack by the thiolate group of GSH. The substituents (-SPh) and (-OPh) are electron donors since they have atoms capable of donating lone pairs, sulfur and oxygen, respectively; however, they can also donate electrons to the phenyl ring. Based on the results obtained above, it is speculated that these substituents (-SPh and -

OPh) donate electrons to the phenyl ring and thus the furoxan rings are still susceptible to nucleophilic attack by thiolate and release more nitric oxide than the reference complex, C2(-H). Similar to the sulfonyl substituent, the sulfinyl substituent is an electron withdrawing group.[267] Therefore, complex C6(-SOPh) was expected to release more nitric oxide than the reference complex,C2(-H), yet it did not. This might be caused by the presence of the phenyl ring. The sulfinyl substituent possibly cannot withdraw electrons simultaneously from both, the phenyl and the furoxan, rings.[§§] Finally, the methoxy substituent acts as an electron donor in C2(-OCH_3) and therefore increases the electron density on the furoxan ring, making it less susceptible to nucleophilic attack by thiolate.

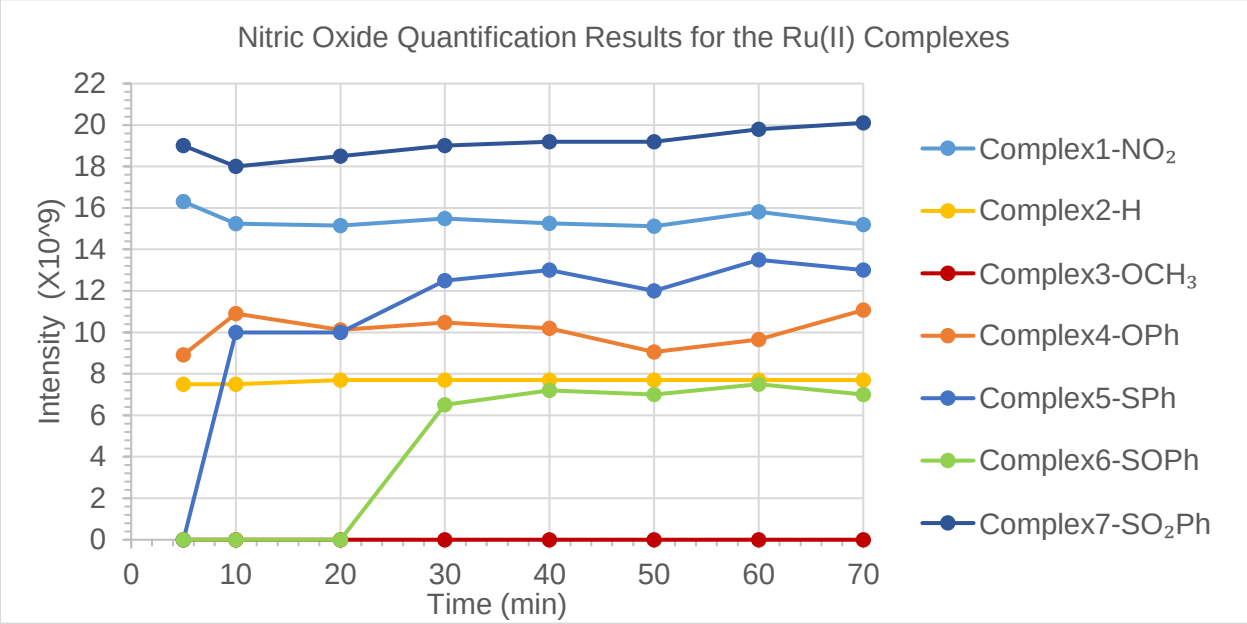

Figure 2.24. Comparing the intensity values obtained from quantifying the amount of nitric oxide released by the complexes.

The EPR spectra of the furoxan derivatives and their corresponding complexes are presented in **Table 1.** Under the same conditions the furoxan ligands were found to release less nitric oxide than the complexes. This could result from the absence of the Ru(II) metal centre, which can act as a Lewis acid and withdraw electrons from the pyridyl substituent. The intensity values obtained from the double integral of the EPR spectra are provided in **Figure 2.25**. The

[§§] This is based on the author's speculations

signals for L2(-H), L3(-OCH_3), and L6(-SOPh) were weak, thus those were not integrated and are not presented in the figure.

Table 1. EPR spectra of the furoxan derivatives and their corresponding complexes.

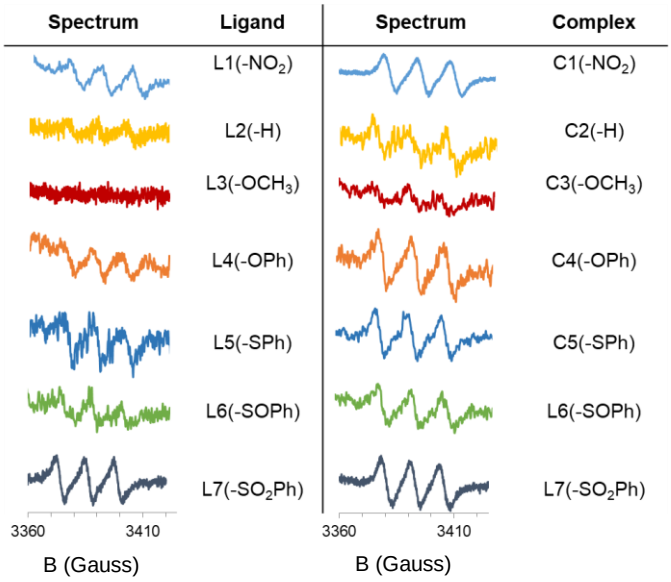

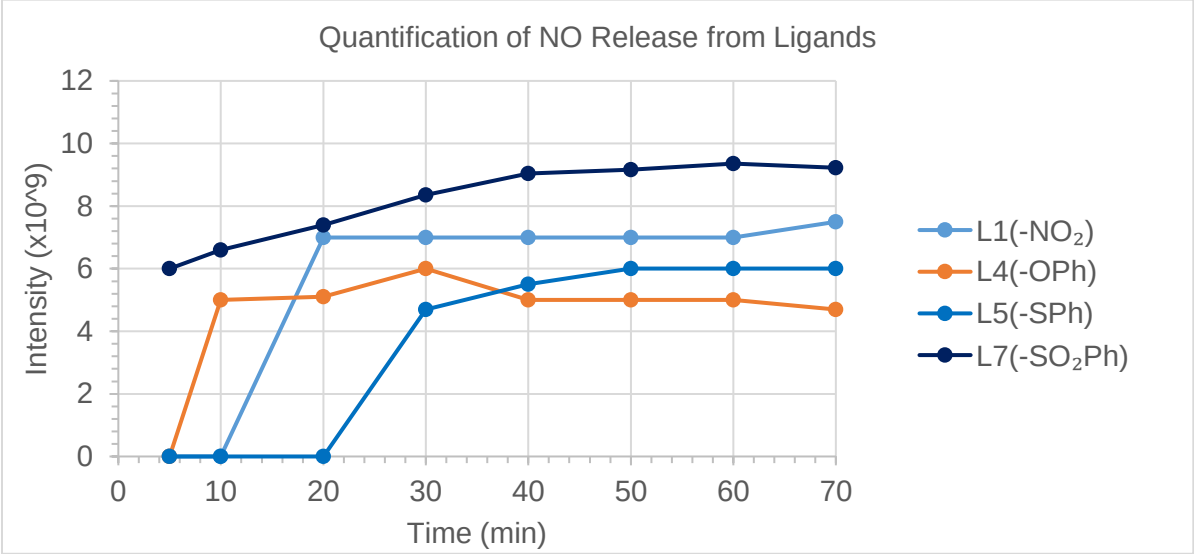

Figure 2.25. Comparing the intensity values obtained from quantifying the amount of nitric oxide released by the ligands.

Is reduced glutathione required for NO release by the complexes?

It was important to confirm that the furoxans selectively released nitric oxide in the presence of thiolate (from GSH). Therefore, the EPR spectra were acquired for three of the complexes: C1(-NO_2), C3(-OCH_3), and C4(-OPh) without reacting them with GSH. C3(-OCH_3) and C4(-OPh) did not release any nitric oxide (EPR silent), and C1(-NO_2) released approximately 3 times less nitric oxide than in the presence of GSH (**Figure 2.26**). This indicates that C1(-NO_2) is less selective in terms of its reactivity than the other two complexes.

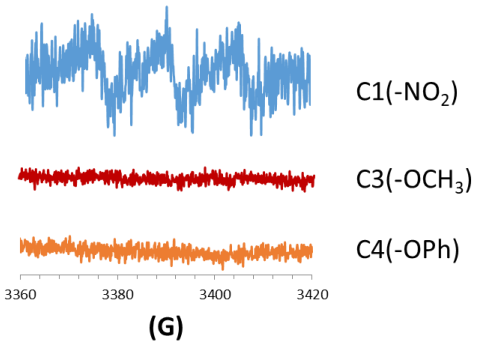

Figure 2.26. EPR spectra from spin-trapped NO in the absence of GSH for complexes C1, C3, and C4.

The aim of this research was to synthesize complexes that will be selectively activated in tumour cells, thus C1(-NO_2) is not a good candidate. The GSH-independent reactivity of this complex brings up some questions. What is the mechanism by which nitric oxide is released? What happens if it was reacted with one equivalent of GSH as opposed to excess GSH (5 equivalents)? The author speculates that the GSH-independent release of NO was mediated by the -NO_2 group, which can undergo side-reactions under physiological conditions. When the complex was reacted with one equivalent of GSH, the amount of nitric oxide released was comparable to that obtained from reacting the complex with excess GSH (**Figure 2.27**).

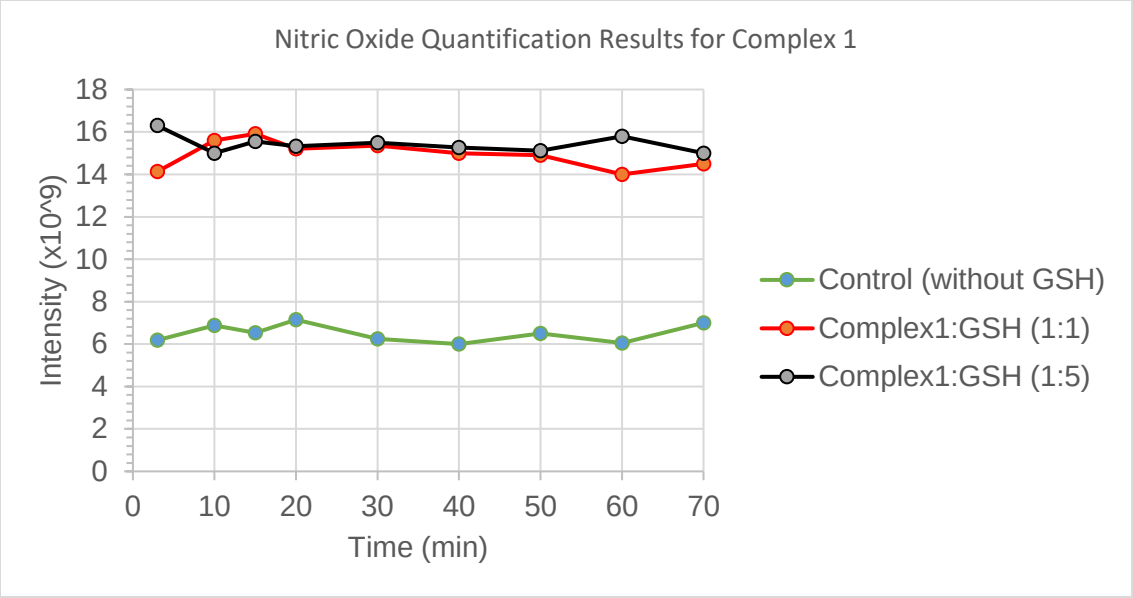

Figure 2.27. Assessing NO release by C1(-NO_2) under different amounts of GSH.

Quantifying the amount of NO by calibrating it against a standard

To determine the concentration of nitric oxide released by the complexes, the stable radical DPPH (g = 2.0037), was used as a standard (**Figure 2.28**).[268]

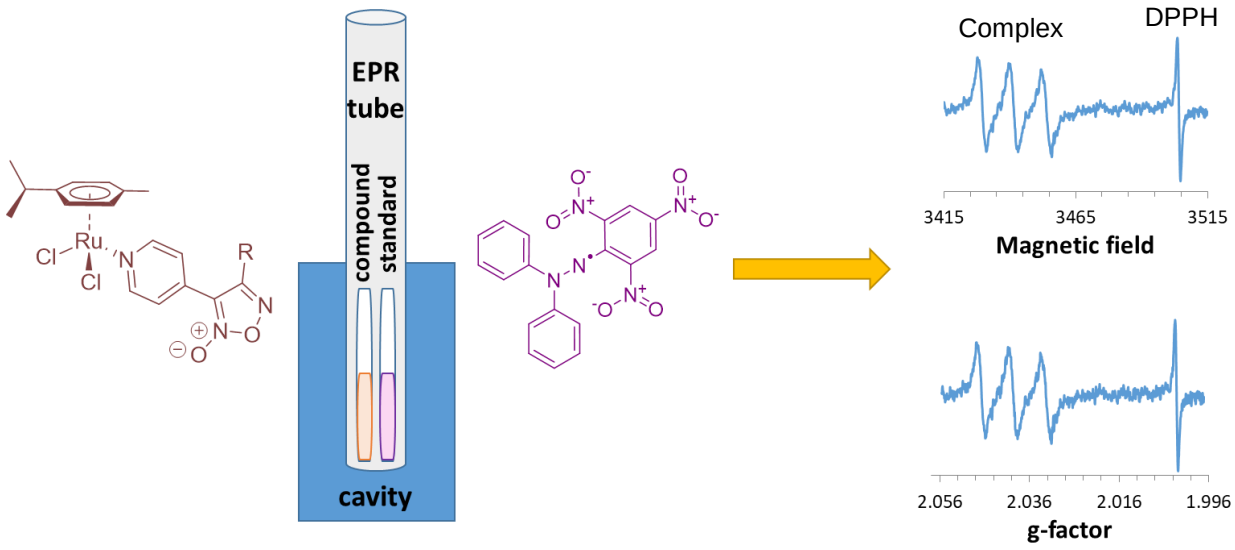

Figure 2.28. The compound of interest and the standard (DPPH) are placed in capillary tubes inside an EPR tube. The signal acquired shows both the NO triplet and DPPH signal.

The value obtained from the second integration of the trapped NO signal was calibrated against the standard (**Figure 2.29**). The DPPH sample was prepared in methanol and had a concentration of 4.77 µM, corresponding to an intensity of 1.38×10^9. As shown in **Figure 2.29**, the EPR signal intensity from nitric oxide released by the compound C4(-OPh) is 2.68×10^9. Therefore, the concentration of nitric oxide released is calculated to be 9.26 µM. It is difficult to estimate the error in the NO concentration since the measurements were not performed in replicates.

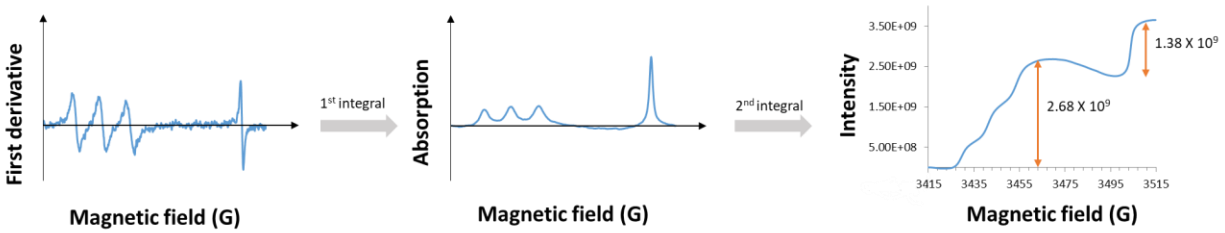

Figure 2.29. The method employed in calculating the amount of nitric oxide released by the complexes.

Using this method, the concentration of nitric oxide released by all the complexes was calculated. **Figure 2.30** shows the change in NO concentration over one hour for complexes 1 – 7. All spectra were obtained at room temperature and in the presence of 5 equivalents of GSH. The amount of NO-released follows the same trend as that obtained using the intensities of the spectra. C7(-SO2Ph) released the highest concentration of NO at 38 µM.

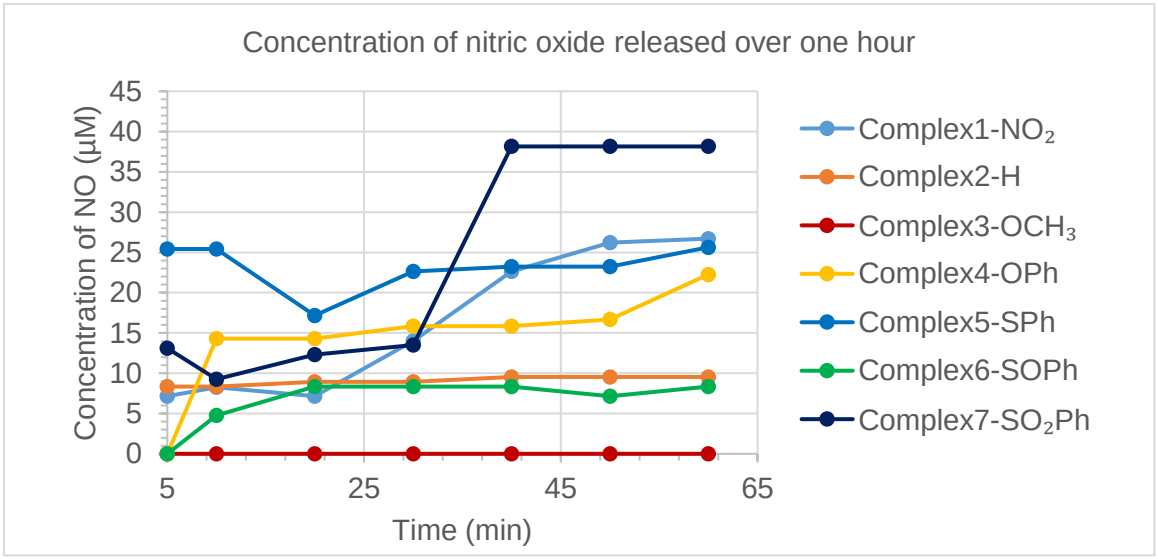

Figure 2.30. Concentration of nitric oxide released by the complexes over one hour.

Comparing NO release of C7(-SO_2Ph) with S-nitrosoglutathione

After calculating the concentration of nitric oxide released by the complexes upon their reaction with excess GSH in one hour, it was important to compare them to an NO-generating standard. Sodium nitrite ($NaNO_2$) was used for this purpose. In this case, 1 equivalent of $NaNO_2$, 1 equivalent of GSH, and 500 equivalent of HCl, leads to the *in situ* formation of S-nitrosoglutathione.[233] Using $Fe(MGD)_2$ and a probe, these measurements were compared to the NO release of C7(-SO_2Ph) at room temperature using 5 mM of the compound C7 and 25 mM of GSH. The aim of this experiment is to compare the amount of NO released by both solutions (i.e., the complex and the reference) following their reaction with GSH. The concentration of nitric oxide can be calculated by calibrating the intensity of the EPR signal for each of the samples against the intensity of the standard, DPPH, (**Figure 2.31**). As can be seen from the EPR spectra, the amount of nitric oxide released after five minutes by the reference is approximately 14 times higher than that of C7(-SO_2Ph). This demonstrates that the furoxan complex produces less NO than the reference, but that the amount detected is still significant. In addition, the concentration of NO donated by C7(-SO_2Ph) reaches a plateau after 40 min (see **Figure 2.30**) and thus the highest amount of NO that can be released by this complex is 38 μM which is at most 3 times less than that released by the reference (123 μM) in 5 minutes. This suggests that the complex does not react completely with GSH. Nevertheless, the amount released is promising in terms of being able to influence biological processes.

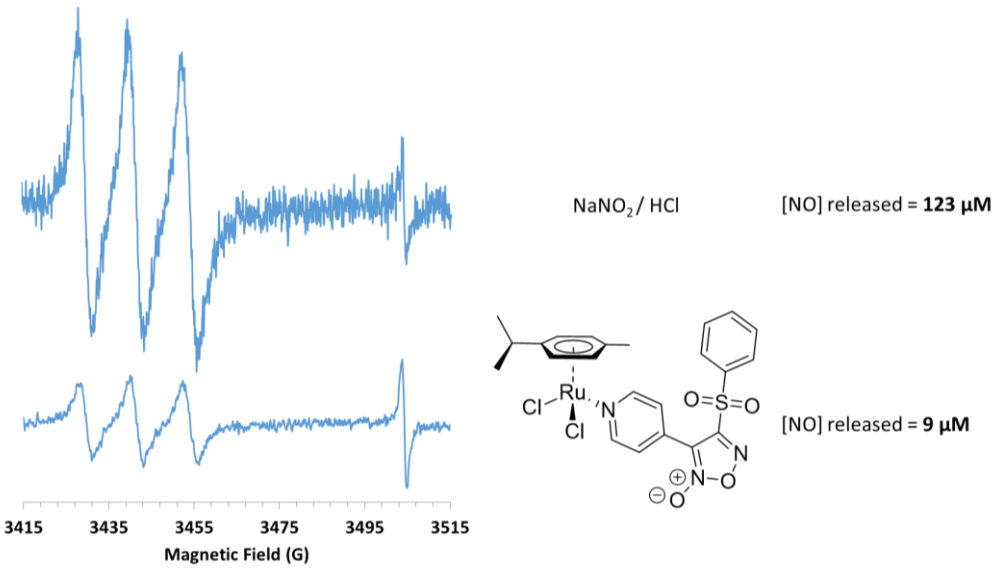

Figure 2.31. Comparing the concentration of nitric oxide released by 5 mM of C7(-SO_2Ph) and 5 mM of $NaNO_2$ under similar reaction conditions.

Comparing the concentration of nitric oxide released by the ligand versus the complex

As stated earlier, the ligands were found to release less nitric oxide than the complexes based on the intensities of the EPR signals (see **Table 1**). Therefore, a quantitative analysis of the amount of nitric oxide released by complex C1(-NO_2) and its corresponding ligand L1(-NO_2) was performed. The experiment was done at room temperature using 5 mM of Ru(II) compound and 25 mM GSH in degassed PBS, pH 7.4. The concentration of nitric oxide was calibrated against DPPH (**Figure 2.32**). C1(-NO_2) was found to release 26 µM of NO, while the ligand released 11 µM, under the same conditions. Therefore, the Ru(II) complex is more reactive than the ligand. This might be attributed to the presence of the Lewis acidic, Ru(II), which can withdraw electrons from the pyridyl moiety, making the complex more susceptible to nucleophilic attack by thiolate.

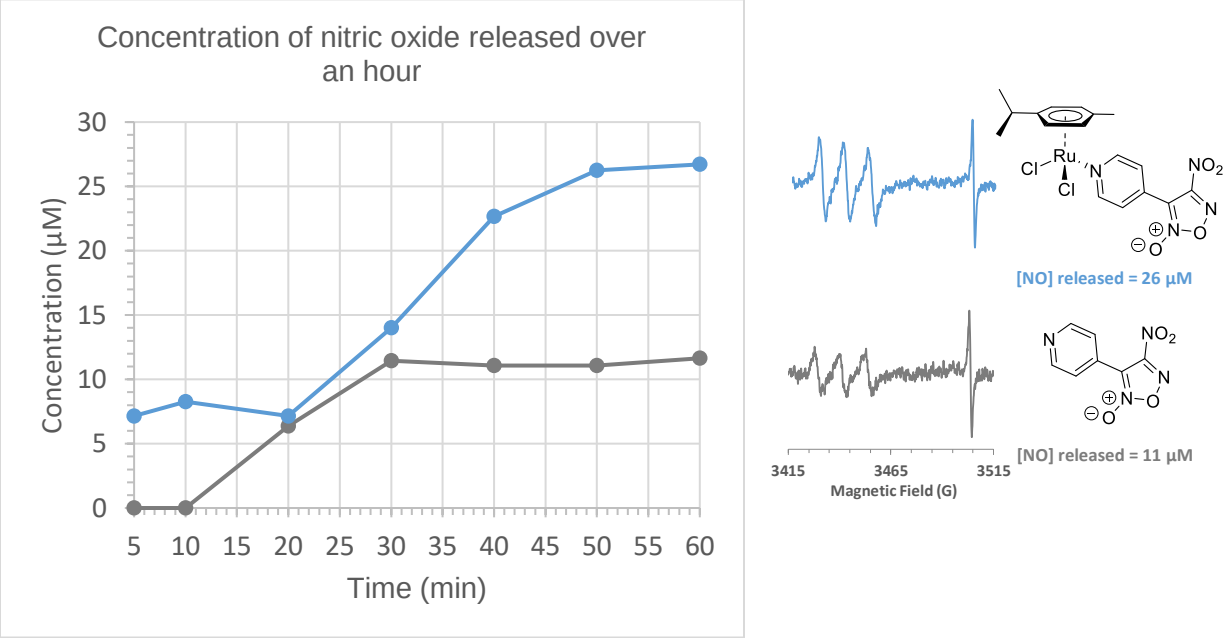

Figure 2.32. Comparing the concentration of nitric oxide released by the complex versus the ligand.

2.3.5. Nitric oxide anticancer activity

Cytostatic cells (i.e., cells that are not growing or dividing) have active NOS and low activity of ribonucleotide reductase (RR).[269] RR is an enzyme required for the synthesis of DNA. The activity of RR in tumour cells, which are fast dividing cells, is higher than in normal cells.[269] When tumour cell cultures are exposed to NO, RR activity is inhibited, and thus the proliferation of cells is also inhibited.[269] These results confirmed the ability of NO to stimulate cytostasis in cancer cells.

Electron withdrawing groups in furoxan derivatives, such as $-NO_2$ and $-SO_2Ph$, exhibit better biological activity than electron donating substituents.[205, 270] The $-NO_2$ and $-SO_2Ph$ were found to be good activators of sGC when they are positioned closer to the nitrone functional group (position 3).[267] In addition, nitrite, nitrate and S-nitrosothiols were found to be generated as side-products when furoxans were tested in biological systems containing sGC.[256] It has been suggested that furoxans containing ($-NO_2$) can also assist in the formation of ROS in biological systems.[270]

Unfortunately, due to time constraints, anticancer studies were not completed in this thesis. However, four of the furoxan derivatives L1($-NO_2$), L5(-SPh), L6(-SOPh), and L7($-SO_2Ph$) were sent to the National Cancer Institute (NCI) to investigate their anticancer activity via NCI-60 screening. The screening results are still unavailable.

2.3.6. Nitric oxide antibacterial activity

Nitrite salts exhibit antimicrobial activity in meat and are commonly used as food preservatives.[201] The commonly used food additive and preservative, sodium nitrite, can inhibit the growth of both aerobic and anaerobic microorganisms.[201] Researchers have studied the effect of NO formed from nitrite salts on the growth of bacteria in food. They concluded that NO can bind to the iron in heme enzymes of the respiratory chain located in the membrane of Gram-negative bacteria and thus impairing aerobic respiration.[201] However, since some bacterial strains can grow anaerobically, and they do not require the presence or activity of the respiratory chain. This suggests a different mechanism for bacterial growth inhibition in the presence of nitrite. It has been reported that nitrite can bind to sulfhydryl enzymes in bacteria and thereby inhibit their growth.[201] Nitrite-cured meat was found to contain more Gram-positive, catalase-negative bacteria than Gram-negative bacteria. This was a crucial observation that provided insight into the effect of NO on both bacterial types. If bacteria are treated with a source of NO in the presence of oxygen, NO can react with oxygen to form NO_2^- which can then generate nitrous acid. Nitrous acid is a strong antimicrobial agent.[201] In addition, NO can act as an antimicrobial agent since it can penetrate the cellular membrane because it is hydrophobic.[109, 271-273] NO has low solubility in water; it was measured to be 56.3 ppm at 25 °C and 1 atm.[201] Different strains of bacteria may have different response to NO because the permeability of this small molecule will vary depending on the structure of the cellular membrane.[201]

Due to the antibacterial activity of NO, the furoxan derivatives and the corresponding complexes described in this thesis were tested in the model Gram-positive bacterium *Bacillus subtilis* (*B. subtilis*) and in the model Gram-negative bacterium *Escherichia coli* (*E. coli*). Gram-negative bacteria are characterized by having an outer membrane as opposed to Gram-positive bacteria, which do not (**Figure 2.33**).[274] The permeability of small molecules into Gram-negative bacteria is hindered or lowered, which is expected to cause higher resistance to many antibiotics. The following diagram shows the membrane structure of both bacterial strains:

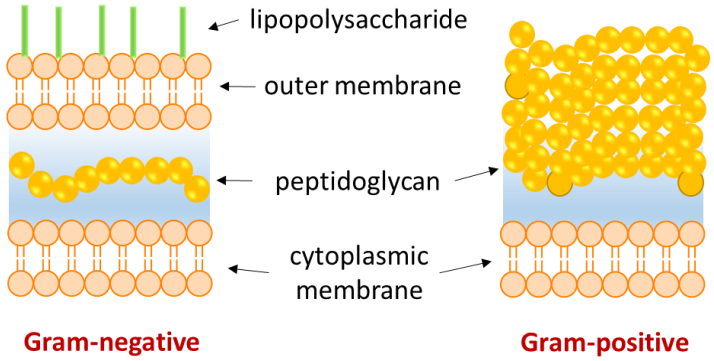

Figure 2.33. The cell envelope structure of Gram-negative and Gram-positive bacteria.

To monitor the microbial growth under the effect of the new compounds, a turbidity assay was performed. As bacteria grow, the growth medium becomes more turbid due to increased cell concentration and therefore a spectrophotometer can be used to determine the optical density (O.D.). The Optical density is a quantitative measurement of the light that is scattered by the cells present in the liquid culture.[275] If the O.D. value decreases, then the growth of cells is inhibited. A schematic diagram describing how the assay was performed is presented in **Figure 2.34**. The compound of interest was incubated with bacteria in a microplate. A spectrophotometer was used to measure the absorbance during the log phase of bacterial growth. There are four phases of bacterial growth (**Figure 2.35**).[275] Bacteria are in the log phase when the rate of cells produced is higher than the rate of cell death and thus the growth is exponential and follows the equation (**2.3**) below:[275]

$$N = N^o 2^n \qquad 2.3$$

Where *N* is the final cell number, *N*° is the initial cell number, and *n* is the number of generations. During this phase the bacterial cells are most susceptible to environmental factors, such as antibiotics.[275] Therefore, the antibacterial activity of the furoxan derivatives and complexes was tested during the log phase.

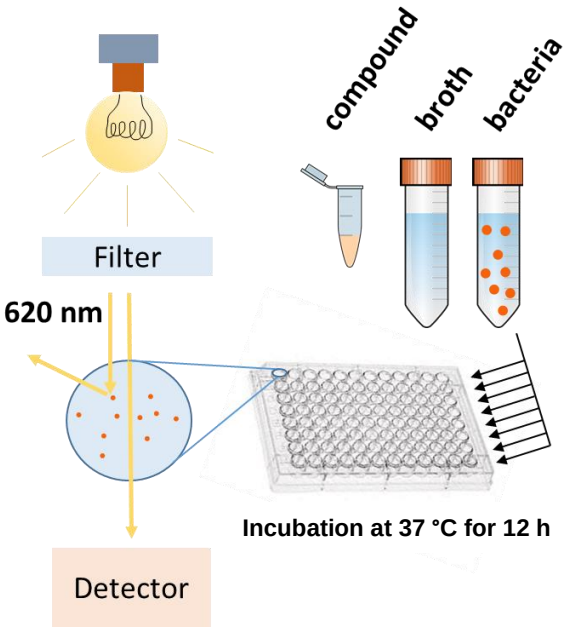

Figure 2.34. **Schematic diagram showing how the turbidity assay was performed. The compound of interest was incubated with the bacterial strains in a microplate for 12 h at 37 °C. The cell growth was monitored using a spectrophotometer to evaluate the absorbance at 620 nm.**

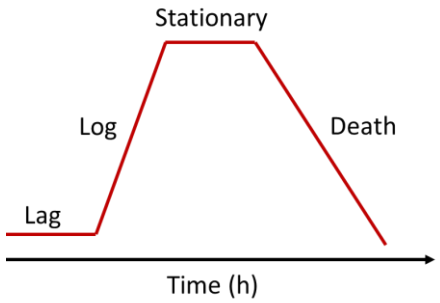

Figure 2.35. **The four phases of bacterial growth. Lag phase: no cell division or slow cell division. Log phase: the number of cells increases at a logarithmic rate. Stationary phase: the number of cells produced equal the number of cells dying. Death phase: the number of cells decreases at a logarithmic rate.**

The antibacterial activity of a compound can be assessed at different concentrations to evaluate efficacy. An example of this type of study using the turbidity assay to measure the inhibitory effect of C2(-H) against *B. subtilis* is shown in **Figure 2.36**.

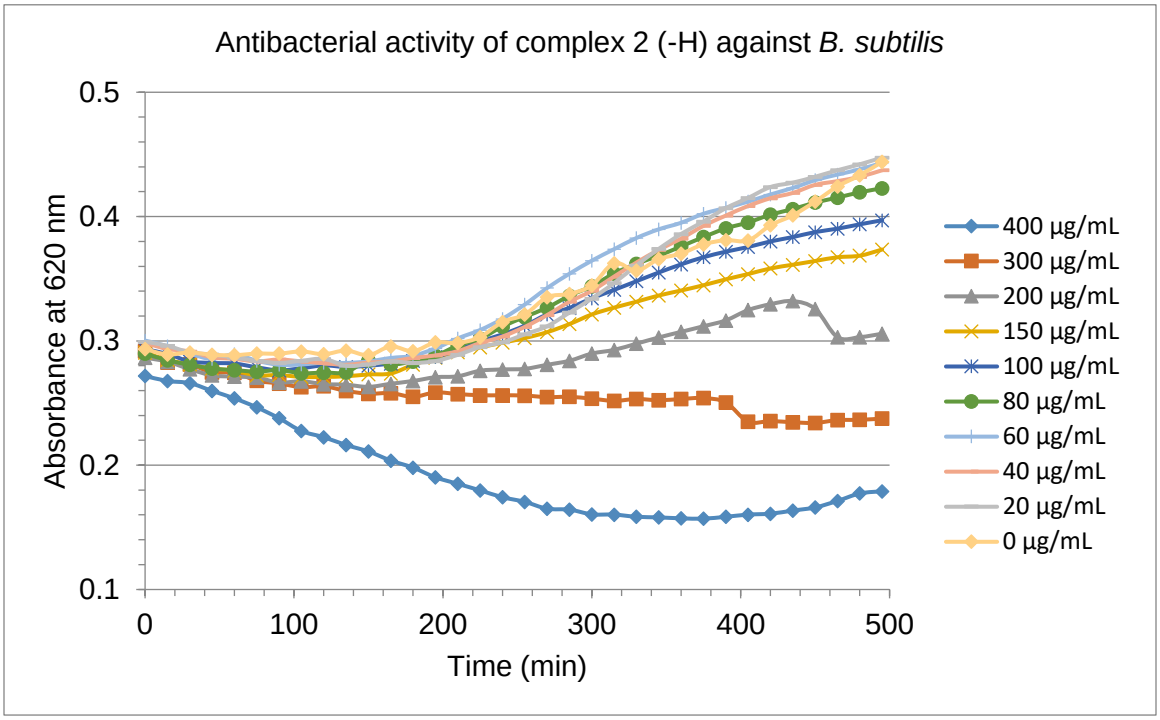

Figure 2.36. Antibacterial activity of C2(-H) against *B. subtilis*. The compound concentration was in the range of (0 – 400 µg/mL). The absorbance was measured at 620 nm over 8 hours and was found to be in the range of (0.45 – 0.15).

The inhibitory concentration (IC_{50}) of the compounds was determined after 12 hours of incubation by plotting the log of the concentration of compound against the percentage of cell growth inhibition, which is measured according to the following formula:

$$actual\ cell\ growth\ inhibition\ (\%) = 100 - \left(\frac{A - NC}{PC - NC} \times 100\right) \qquad 2.4$$

Where *A* is the absorbance measured for a specific compound concentration, which is the average of four replicates. *NC* is the negative control (i.e., media without culture or compound) and *PC* is the positive control (i.e., culture in media without compound). The actual inhibitory concentration data is fitted to a sigmoidal curve, described by equation

(**2.5**), to interpolate the concentration required to inhibit the growth of 50% of the bacterial population (IC_{50}):[276]

$$theoretical\ cell\ growth\ inhibition\ (\%) = \frac{\exp(slope \times (\log[compound] - IP))}{1 + \exp(slope \times (\log[compound] - IP))} \times SP \qquad 2.5$$

Where *IP* and *SP* are the inflection and saturation points, respectively. Both ligands and complexes were found to be ineffective against *E. coli,* however, they exhibited some activity against *B. subtilis*. Concentration-response curves for *B. subtilis* incubated with different concentrations of the ligands is presented in **Figure 2.37**. The IC_{50} values of the ligands against *B. subtilis* were determined from the concentration-response curves (**Table 2**). However, the IC_{50} values of the ligands against *E. coli* were higher than the highest concentration of the ligands used in the assay, since none of the ligands exhibited a significant inhibitory effect (**Table 2**). The reported uncertainty values are one standard deviation, as calculated from the fitting algorithm in *Excel 365* program.[276]

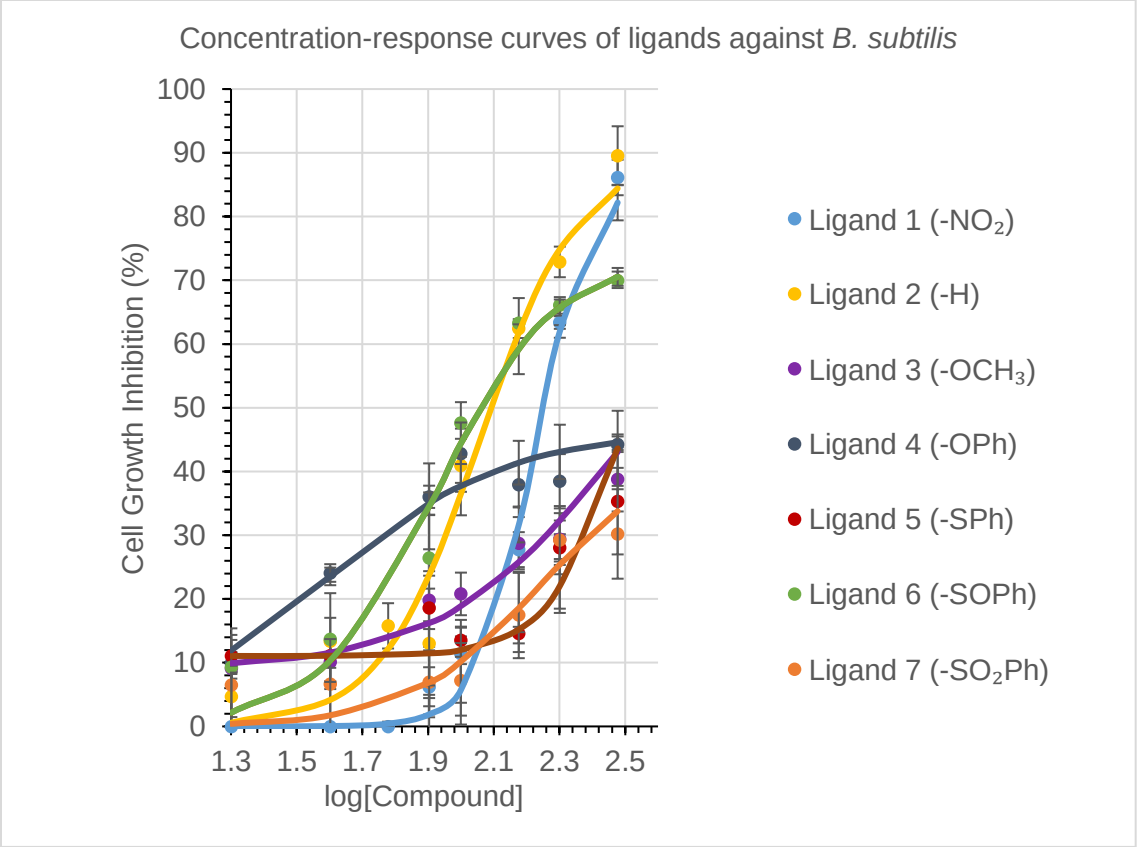

Figure 2.37. The concentration-response curves of ligands against *B. subtilis*.

Table 2. Antibacterial cytotoxicity (IC_{50}) results

Compound	*B. subtilis*	*E. coli*
	IC_{50} (μM) ± SD	
Ligand 1 (-NO_2)	835 ± 7	>1441 ± 10
Ligand 2 (-H)	754 ± 4	>1839 ± 10
Ligand 3 (-OCH_3)	>1553 ± 10	>1553 ± 22
Ligand 4 (-OPh)	>1175 ± 4	>1175 ± 16
Ligand 5 (-SPh)	807 ± 10	>1106 ± 18
Ligand 6 (-SOPh)	396 ± 4	>1044 ± 15
Ligand 7 (-SO_2Ph)	>989 ± 7	>989 ± 13

SD, standard deviation. This measurement was calculated by determining how much the actual value deviates from the fitting curve.

According to the results in **Table 2**, the IC_{50} values for the ligands are high, indicating low to moderate cytotoxicity against *B. subtilis*. The IC_{50} of L6(-SOPh) was found to be the lowest (396 ± 4 μM), which indicates that it possesses the highest antibacterial activity of all the ligands. The ligands L2(-H) and L5(-SPh) exhibited low, but measurable, cytotoxicity with IC_{50} values of 754 ± 4 μM and 807 ± 10 μM, respectively.

The complexes displayed greater antibacterial activity against *B. subtilis* than the ligands. The concentration-response curves for *B. subtilis* are presented in **Figure 2.38** from which the IC_{50} values in **Table 3** were interpolated. As with the ligands, the complexes were found to be ineffective against *E. coli*. Furthermore, the IC_{50} values of the complexes against *E. coli* were higher than the highest concentration of the complexes used in the assays (**Table 3**).

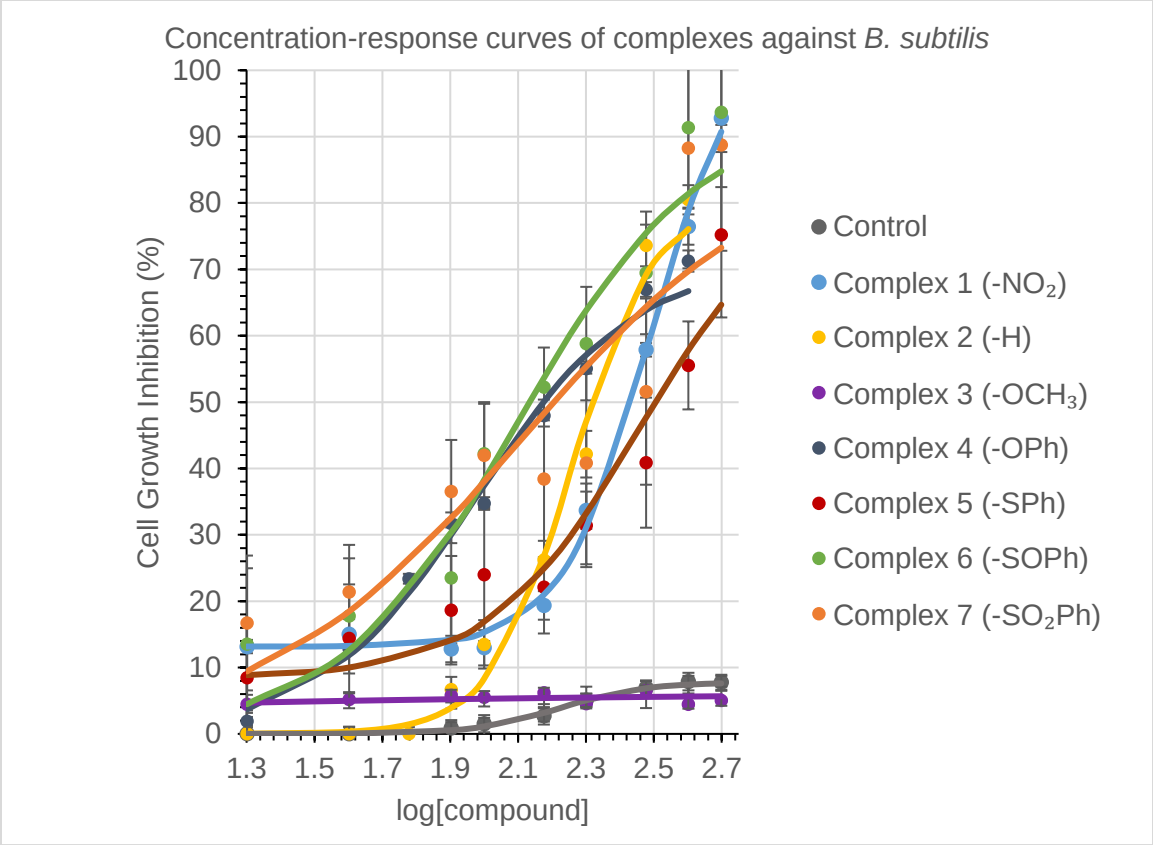

Figure 2.38. The concentration-response curves of complexes against *B. subtilis*.

Table 3. Antibacterial cytoxicity (IC_{50}) results for the complexes.

Compound	*B. subtilis*	*E. coli*
	IC_{50} (μM) ± SD	
Control (Ru(η^6-*p*-cymene)(Pyridine)Cl_2)	>1297 ± 13	>1297 ± 11
Complex 1 (-NO_2)	511 ± 5	>972 ± 12
Complex 2 (-H)	425 ± 4	>1065 ± 10
Complex 3 (-OCH_3)	>1001 ± 11	>1001 ± 7
Complex 4 (-OPh)	267 ± 4	>891 ± 15
Complex 5 (-SPh)	548 ± 10	>866 ± 6
Complex 6 (-SOPh)	200 ± 7	>842 ± 5
Complex 7 (-SO_2Ph)	260 ± 15	>820 ± 7

SD, standard deviation

The IC_{50} values of the complexes indicate a moderate cytotoxicity against *B. subtilis*. In general, the complexes were found to have lower IC_{50} values than their corresponding ligands indicating a higher cytotoxicity. C6(-SOPh) was found to be the most cytotoxic with an IC_{50} of 200 ± 7 μM. The sulfone derivative C7(-SO_2Ph) exhibited similar cytotoxicity to C6(-SOPh) with an IC_{50} of 260 ± 15 μM. This agrees with the general prediction that furoxans with a sulfone substituent tend to have biological activities, for instance acting as antimicrobial agents.[209] It is interesting to note that the sulfoxide derivative C6(-SOPh) was the most cytotoxic. According to the author's knowledge, furoxans with sulfoxide substituents are not well examined in the literature in terms of their biological role. Therefore, this finding suggests a new class of furoxans that exhibit biological activity.

To assess the role of the Ru(II)-arene moiety, the unfunctionalized complex, Ru(η^6-*p*-cymene)(Pyridine)Cl_2, was also tested for antibacterial activity as a control. It was determined that the control complex was not cytotoxic (**Table 3**), demonstrating that the Ru(II)-arene was not solely responsible for the observed antibacterial activity of the furoxan complexes. Assessment of the cytotoxicity of the control complex revealed that the antibacterial activity is not only due to the presence of the Ru(II)-arene moiety, since the control was not cytotoxic. As was mentioned earlier, arene rings are lipophilic, which promote internalization by cells. Once the compound is internalized, if it only contains the Ru(II)-arene moiety, such as the control, it will not be cytotoxic.[75] However, if it contains the NO releasing moiety (furoxan derivatives), then it can be cytotoxic, because it can attack the cysteine protease enzymes, hindering the replication and growth of cells.[277-279] It seems likely that the furoxan ligands exhibited lower cytotoxicity than the complexes because they were not internalized by cells. In conclusion, both the Ru(II)-arene moiety and the NO-releasing moiety are crucial in providing cytotoxic compounds.

2.3.7. Crystal structure of decomposed C1(-NO_2)

The complex C1(-NO_2) was not stable and a crystal structure was obtained for the decomposed product (**Figure 2.39**). The ligand L1(-NO_2) has decomposed to give 4-cyanopyridine. Decomposition of furoxan ring is a common phenomenon.[280, 281] This process occurs over time and might be caused by exposure to heat or light.

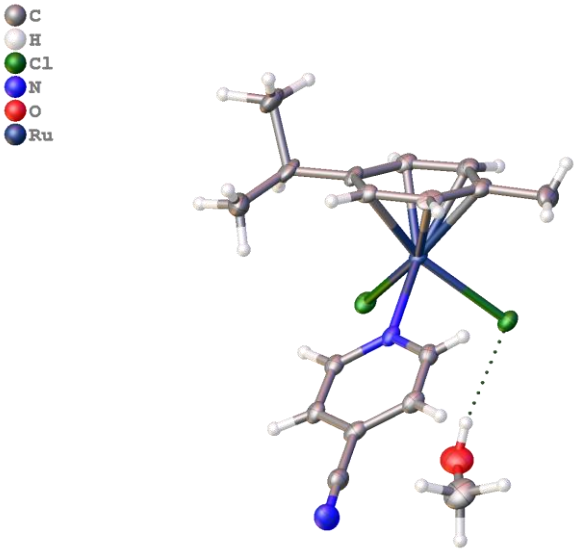

Figure 2.39. Crystal structure of decomposed C1(-NO_2).

2.4. Conclusion and future work

This chapter described the synthesis and application of furoxan derivatives which were used as ligands on a Ru(II)-arene moiety based on the structure of RAPTA-C. The complexes exhibited different abilities to release nitric oxide due to the difference in the functional groups on the furoxan ring. Electron withdrawing groups (-NO_2 and -SO_2Ph) lower the electron density in the furoxan ring and make it susceptible to nucleophilic attack by thiols present in physiological systems, such as glutathione. The antibacterial activity of the complexes and their corresponding ligands was also investigated by performing a turbidity assay. The furoxan derivative with the sulfoxide substituent, L6(-SOPh), exhibited the highest cytotoxicity among the seven derivatives. To the author's knowledge, a sulfoxide substituent has never been attached to furoxan derivatives. Therefore, this new derivative needs to be studied further in terms of its bioactivity. Furthermore, future work will focus on analysing the anticancer activity of the compounds.

Chapter 3. Synthesis and Characterization of New Ruthenium(II)-Gold(III) Heterobimetallic Complex

3.1. Introduction

3.1.1. Gold-based chemotherapeutics and thioredoxin reductase inhibitors

In recent years, there has been an increase in studies focused on the utilization of gold complexes as anticancer therapeutics.[282-286] However, development of Au(III)-based coordination complexes as medicinal agents is challenged by their poor stability in biological systems.[165, 287] These compounds can undergo redox reactions in hypoxic tumour environments, which can result in the reduction of Au(III) to Au(I) and elemental Au.[164, 287, 288] Furthermore, intracellular hydrolysis of Au(III) typically occurs at a faster rate than that for Pt(II).[165] Nonetheless, some Au(III) complexes are stable under physiological conditions and exhibit cytotoxic effects against several cancer cell lines, including cisplatin-resistant cells.[289-293] This class of complexes provides a suitable alternative to Pt(II)-based therapeutics due to their mode of action, which is usually different from cisplatin.[65, 167] Au(III) complexes can inhibit enzymes containing thiol and/or selenol groups, particularly thioredoxin reductase (TrxR), by undergoing ligand-exchange reactions and forming new Au-S bonds, due to the strong affinity of gold ions for thiols.[65, 287, 294] The resulting gold-protein interactions lead to apoptosis.[167, 287] TrxR and a number of other thiol containing enzymes, such as cysteine proteases and glutathione reductase, are often upregulated in cancer cells; therefore, Au(III) complexes can selectively target these cells.[294-298] In addition, the most abundant intracellular thiol-containing molecule, reduced glutathione (GSH), with a concentration ranging between 0.5 – 10 mM in tumour cells, was also found to interact with some Au(III) complexes.[223, 288]

The thioredoxin system regulates redox reactions in living cells.[299] It consists of: 1) thioredoxin, which is a small protein (12 kDa) that acts as a scavenger of hydrogen peroxide and hydroxyl radicals; 2) NADPH (reduced **N**icotinamide **A**denine **D**inucleotide **P**hosphate), which controls the level of reduced thioredoxin; and 3) TrxR, an enzyme that reduces the disulfide bond between two cysteines present in the active site of thioredoxin.[299-301] Cancer cells often exhibit oxidative stress (i.e., an imbalance between ROS production and depletion) and consequently overexpress TrxR.[299, 302] TrxR isoforms

are found in the cell cytosol and mitochondria.[299, 301] Studies have shown that this enzyme improves the survival rate of tumour cells.[299, 301, 302] Furthermore, TrxR in the cytosol can promote metastasis in breast cancer cells.[299, 303] The Au(I) complex, auranofin (*discussed earlier in Chapter 1*) was found to inhibit the activity of TrxR in multiple myeloma (i.e., cancer in plasma cells, which are a type of white blood cells).[299, 304] Inhibition of TrxR increased the amount of reactive oxygen species (ROS) resulting in apoptosis.[299, 305] Therefore, TrxR can serve as a target for chemotherapeutics (**Figure 3.1**).[301, 302, 304]

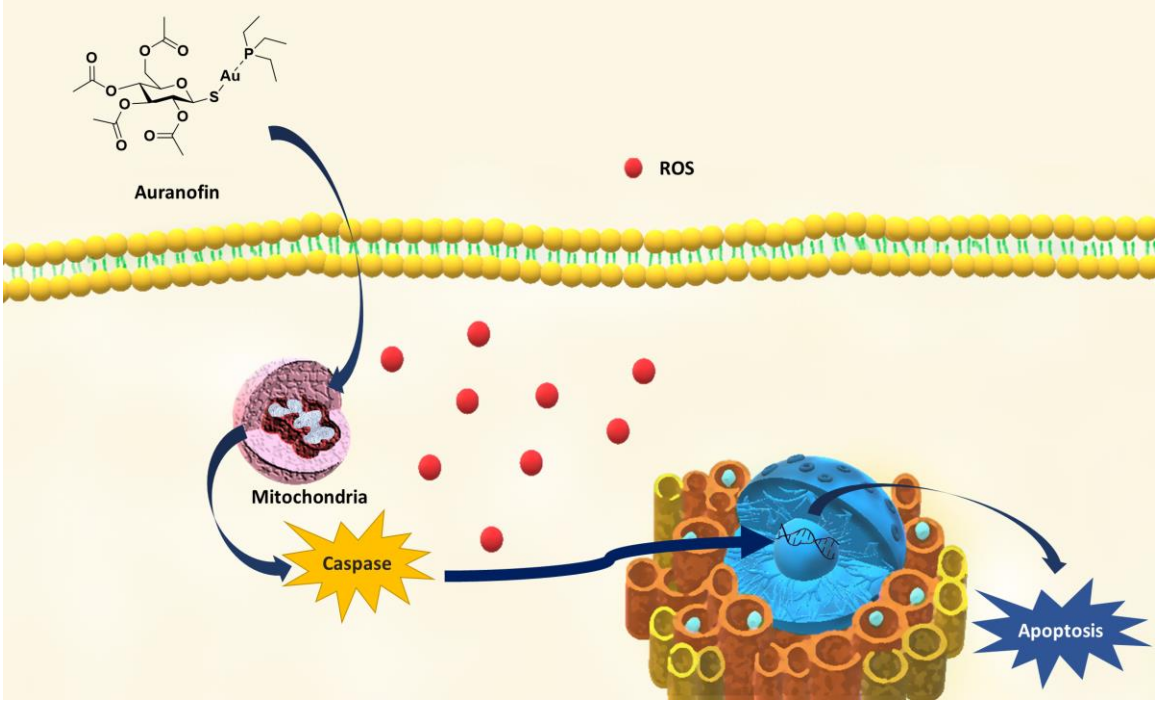

Figure 3.1. **Proposed mechanism of action of auranofin in cancer cells.1) auranofin inhibits the TrxR enzyme, which is present in the cytosol and mitochondria; 2) the concentration of reactive oxygen species (ROS) increases and triggers the mitochondria to activate caspase; 3) activated caspase degrades cellular components and prepares the cell for apoptosis.**

3.1.2. Bimetallic anticancer compounds

Heterobimetallic complexes combine the unique therapeutic features of individual metal centres into one molecule and may generate new activity through synergy between the metal-containing components.[306] Recent developments in this area have included a limited number of ruthenium and gold-based bimetallic complexes. These compounds have demonstrated cytotoxic activity and have been suggested as alternatives to platinum-based therapeutics (**Figure 3.2**).[65, 306, 66] The work in this chapter provides insight into the development of heterobimetallic chemotherapeutic candidates designed around Au(III) centre coupled to Ru(II)-arene scaffold.

A previously published example of a related compound is a Ru(II)-arene linked through a spacer to auranofin to generate a hybrid molecule (**Figure 3.2-A**) that targets TrxR and/or DNA.[66] In another example, a Ru(II)-arene was combined with derivatives of Au(I)-NHC*** (**Figure 3.2-b**). These complexes were found to be cytotoxic to renal and colon cancer cell lines and exhibited higher selectivity than the mononuclear moieties due to a synergistic interaction between Ru and Au.[307] Recently, one derivative of these complexes, [Ru (*p*-cymene)Cl_2(μ-dppm)Au(IMes)]ClO_4, known as RANCE-1, was studied further *in vitro* to investigate its activity in renal cancer cells.†††[306] The binuclear complex manifests the therapeutic features of Au-NHC-based compounds (antiproliferative and cytotoxic), as well as, Ru(II)-based compounds (anti-metastatic and anti-angiogenic).[306]

*** NHC = N-Heterocyclic Carbene

††† R' = 1,2,4-trimethylbenzene is the ligand coordinated to Au(I)

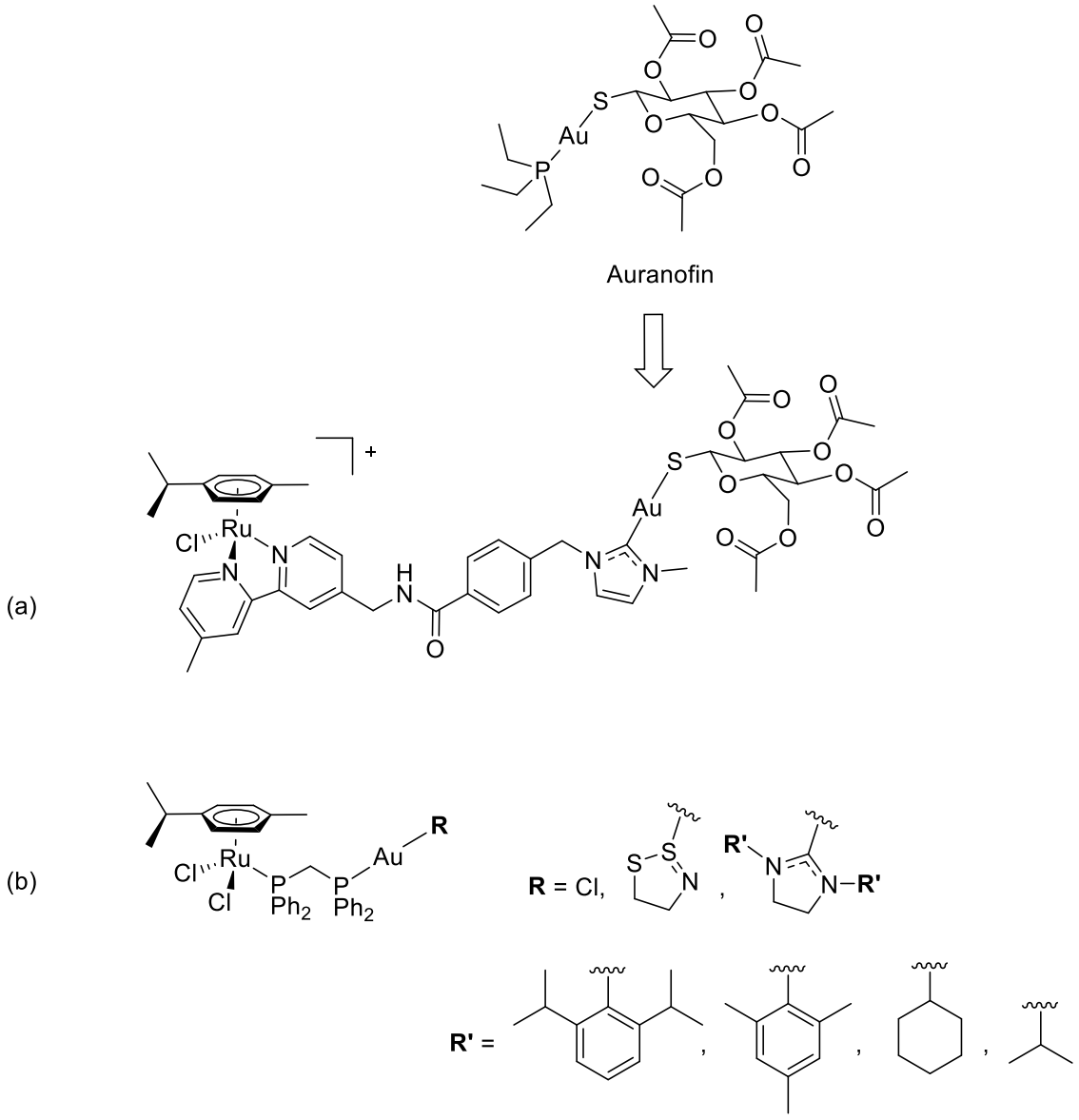

Figure 3.2. Heterobimetallic Ru(II)-arene-Au(I) complexes that exhibit anticancer activity.

Besides ruthenium and gold-based compounds, copper complexes are also known to exhibit anticancer activity.[308-312] The coordination number for Cu(II) complexes can vary based on the ligands employed in the structure.[313] Typically, Cu(II) has four-coordinate square-planar geometry.[313] However, it could also exist as five-coordinate trigonal bipyramidal or square pyramidal; or six-coordinate octahedral.[313]

There are different modes of action by which Cu complexes can act as chemotherapeutics, this includes inhibition of proteasome, DNA damage, and ROS generation leading to apoptosis.[308, 314] Copper is an endogenous metal that is involved in the development and growth of cells.[313] It is a cofactor for several enzymes, such as superoxide dismutase and ascorbate oxidase.[313] When not bound to proteins, free copper ions can participate in Fenton's reaction, which leads to the generation of ROS.[315, 316] In biological systems, copper exists in two oxidation states: cuprous (Cu^{+}) and cupric (Cu^{2+}).[316] High levels of copper are associated with angiogenesis (i.e., generation of new blood vessels from the tumour site) in several forms of cancer, such as lung and brain cancers.[313] This is because copper is required as a cofactor for the enzymes/proteins involved in angiogenesis and tumorigenesis. Nevertheless, in 2004, Dou and co-workers reported that some copper complexes, such as NCI-109268 (**Figure 3.3**), act as anticancer agents by inhibiting proteasomes, which are protein complexes that hydrolyse unrequired proteins in the cell.[317]

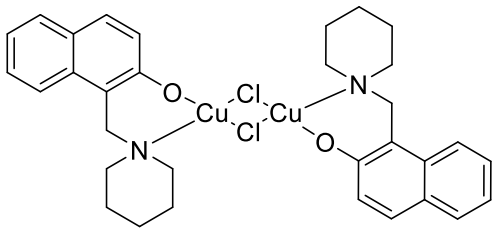

Figure 3.3. The chemical structure of NCI-109268, a Cu(II)-based complex with anticancer properties.

Proteasomes are the target for some chemotherapeutics since their inhibition causes apoptosis.[318] Proteasome inhibition is not caused by the oxidative activity of the copper complex. Instead, the organic ligands bind to the endogenous copper ions present at elevated levels in tumour cells and this leads to proteasome inhibition.[313, 317] Hence, organic copper complexes can be selective toward cancer cells as opposed to healthy cells, which have lower concentrations of copper.[313] The ligands used in this class of complexes need to be labile.[313, 319] Indeed, this brings up the questions: is the metal required, and can the organic compound serve as the anticancer agent by itself? Dou and co-workers found that neither the organic ligand nor Cu(II) chloride can inhibit

proteasomes; the complex is required to manifest anticancer activity.[317] Although there are several studies on the anticancer activity of organic copper complexes, the mechanism by which they inhibit proteasome remains unclear.[313, 317, 320, 321] Aside from these complexes, many copper complexes can generate ROS, which damage DNA and result in apoptosis.[312, 321-323]

In this chapter, the synthesis of a heterobimetallic Ru(II)-arene-Au(III) complex (**Figure 3.4-A**) will be addressed. In addition, a summary will be given of the unsuccessful attempts to synthesize Ru(II)-arene-Cu(II) complex (**Figure 3.4-B**) and a discussion of the problems with the synthesis of these and related compounds is presented.

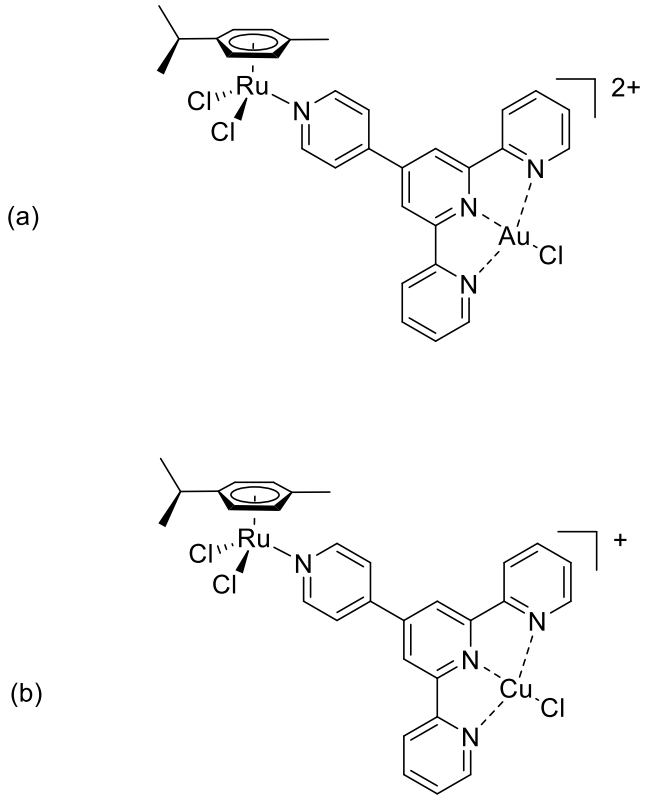

Figure 3.4. Chemical structure of: (a) Ru(II)-arene-Au(III) bimetallic complex; (b) Ru(II)-arene-Cu(II) bimetallic complexes.

3.2. Experimental

3.2.1. Materials and methods.

All reagents were purchased from Sigma-Aldrich except ruthenium(III) chloride trihydrate, $RuCl_3 \cdot 3H_2O$, which was purchased from Pressure Chemical. Reagents were used as received. Nuclear Magnetic Resonance (NMR) spectra were recorded on Bruker-AV (400, 500, or 600 MHz) instruments. Infrared (IR) spectra were recorded in the range of 4000-400 cm^{-1} using a PerkinElmer Spectrum Two FTIR Spectrometer equipped with a UATR Diamond/ ZnSe ATR (Single Reflection) accessory. Mass spectra (positive ion) were obtained on an Agilent 6210 time-of-flight electrospray ionization mass spectrometer.

3.2.2. Synthesis of 4'-(4-pyridyl)-2,2':6',2''-terpyridine (Pterpy) ligand.

Pterpy was prepared according to the literature procedure.[324] 4-pyridinecarboxaldehyde, C_6H_5NO, (2.80 mL, 29.7 mmol), 2-acetylpyridine, C_7H_7NO, (6.70 mL, 59.7 mmol), and NaOH (2.55 g, 63.8 mmol) were mixed and ground using a mortar and pestle until a yellow powder was obtained. The powder was refluxed with ammonium acetate (22.3 g, 289 mmol) in glacial acetic acid (50.0 mL) for 3 h. A mixture of ethanol (30 mL) and H_2O (40 mL) was added and the solution was cooled to room temperature. The product was filtered and then recrystallized from ethanol and dried in vacuo. Yield: 3.22 g (35%). ^{1}H NMR (500 MHz, DMSO-*d6*) δ 8.78 (t, J = 3.4 Hz, $6H_{d+e+g}$), 8.69 (d, J = 7.9 Hz, $2H_a$), 8.06 (t, J = 7.8 Hz, $2H_c$), 7.95 (dd, J = 4.4, 2.5 Hz, $2H_f$), 7.55 (dd, J = 7.9, 4.5 Hz, $2H_b$).

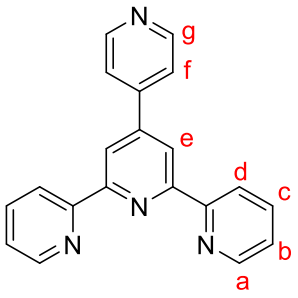

3.2.3. Synthesis of $[Au(Pterpy)Cl]Cl_2$ complex (C1).

C1 was prepared following the literature procedure.[325] **Pterpy** (0.1739 g, 0.563 mmol) was partially dissolved in a mixture of methanol and water (1:4, v/v, 50 mL). $HAuCl_4 \cdot H_2O$ (0.1947 g, 0.5 mmol) was added to the mixture and the pH was adjusted to 3 using $NaHCO_{3(aq)}$. The solution was then refluxed for 2 h. Subsequently, the solution was cooled to room temperature and the product was collected via vacuum filtration and rinsed with cold hexanes (2 mL). Yield: 0.2515 g (93%). ^{1}H NMR (500 MHz, DMSO-d_6) δ 9.08 (d, J = 5.7 Hz, $2H_d$), 9.00 (s, $2H_e$), 8.89 (dd, J = 13.6, 6.4 Hz, $4H_{g+a}$), 8.59 (d, J = 5.7 Hz, $2H_f$), 8.28 (t, J = 7.9 Hz, $2H_c$), 7.75 (t, J = 6.2 Hz, $2H_b$).

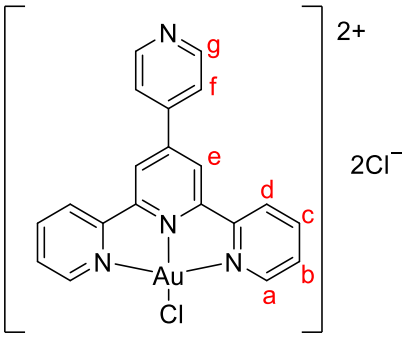

3.2.4. Synthesis of $[Ru(\eta^6\text{-}p\text{-cymene})Cl_2]_2$ (C2).

C2 was prepared according to the literature procedure (*see section 2.2.9*).[227]

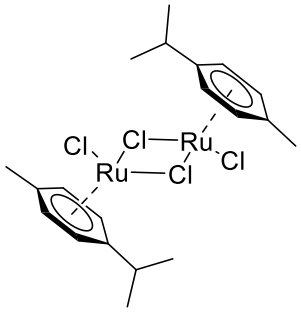

3.2.5. Synthesis of Ru(II)-arene-Au(III) complex (C3).

C1 (0.2042 g, 0.334 mmol) and **C2** (0.1201 g, 0.167 mmol) were refluxed in methanol (40 mL) for 1.5 h. The reaction was left to cool down to room temperature, then the product was collected via vacuum filtration and rinsed with dichloromethane (2 mL). Yield: 0.1001 g (71%). ^{1}H NMR (400 MHz, DMSO-*d6*) δ 9.86 (d, *J* = 4.8 Hz, $2H_g$), 9.05 – 9.00 (m, $2H_f$), 8.92 (s, $2H_e$), 8.83 (dd, *J* = 4.9, 1.6 Hz, $2H_d$), 8.81 – 8.51 (m, $2H_a$), 8.19 (td, *J* = 8.0, 1.6 Hz, $2H_c$), 7.66 (dd, *J* = 8.0, 4.9 Hz, $2H_b$), 5.81 (d, *J* = 6.2 Hz, 2H, benzyl, *p*-cymene), 5.77 (d, *J* = 6.2 Hz, 2H, benzyl, *p*-cymene), 2.86 – 2.80 (m, 1H, isopropyl, *p*-cymene), 2.09 (s, 3H, methyl, *p*-cymene), 1.19 (d, *J* = 6.9 Hz, 6H, isopropyl, *p*-cymene). Positive ESI-MS: $[M+2Na]^{2+}$ calculated 481.9625, found 481.9477; $[M+H]^{+}$ calculated 918.9539, found 918.9388.

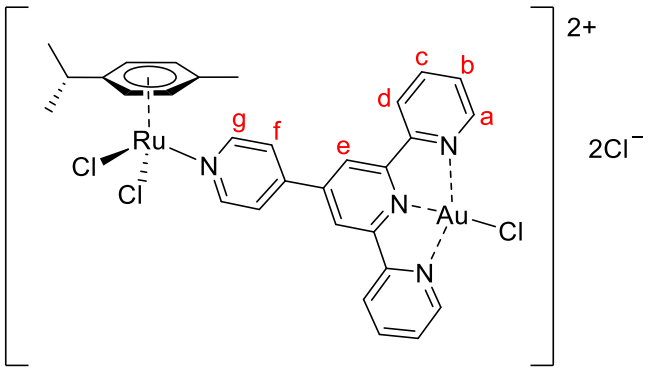

3.2.6. X-ray Crystallography

Single crystals suitable for X-ray diffraction were mounted on 100 μm MiTeGen dual-thickness micromounts. The temperature was regulated by Oxford Cryosystem Cryostream. Bruker SMART DUO was used for data collection, equipped with an APEX II CCD area detector placed 50 mm from the crystals. The radiation sources were either: Mo Kα radiation ($\lambda_{(Mo)}$ = 0.71073 Å) filtered with graphite TRIUMPH-monochromator or Cu Kα radiation ($\lambda_{(Cu)}$ = 1.54178 Å).

3.2.7. Crystal structure determination of Ru(Pterpy)Cl_3.

During the synthesis of C3, an impurity crystalized in the NMR tube containing DMSO. The impurity was found to be Ru(Pterpy)Cl_3. This is a known compound; however, its crystal structure has not been determined before. The crystal data were viewed using Olex2 and solved using SHELXL.[229, 230, 326]

Crystal Data for $C_{20}H_{14}Cl_3N_4Ru$ (M = 517.77 g/mol): monoclinic, space group P21/c (no. 14), a = 10.1597 (2) Å, b = 13.6038(2) Å, c = 13.7817(2) Å, β = 97.0630(10)°, V = 1890.32(5) Å3, Z = 4, T = 150(2) K, μ(Cu Kα) = 10.732 mm-1, D_{calc} = 1.819 g/cm3, 8372 reflections measured (8.77° ≤ 2Θ ≤ 133.29°), 3297 unique (R_{int} = 0.0503, R_{sigma} = 0.0578) which were used in all calculations. The final R1 was 0.0356 (I > 2σ(I)) and wR2 was 0.0806 (all data).

3.2.8. Crystal structure determination of [Ru(η^6-*p*-cymene)$(NH_3)_2Cl]PF_6$.

During the unsuccessful attempts to synthesize Ru(II)-arene-Cu(II), a crystal of [Ru(η^6-*p*-cymene)$(NH_3)_2$Cl]PF_6 was obtained. The crystal was kept at 299.01 K during data collection. Using Olex2, the structure was solved with the SHELXL, structure solution program using Dual Space and refined with the olex2.refine, refinement package using GaussNewton minimisation.[229, 230, 326]

Crystal Data for $C_{40}N_8RuClPFH$ (M = 903.30 g/mol): triclinic, space group P-1 (no. 2), a = 8.1167(13) Å, b = 9.0006(14) Å, c = 11.3836(18) Å, α = 88.140(2)°, β = 88.283(2)°, γ = 77.956(2)°, V = 812.7(2) Å3, Z = 1, T = 299.01 K, μ (Mo Kα) = 1.282 mm-1, Dcalc = 1.8456 g/cm3, 16901 reflections measured (3.58° ≤ 2Θ ≤ 58.42°), 4409 unique (R_{int} = 0.0128, R_{sigma} = 0.0108) which were used in all calculations. The final R1 was 0.0189 (I>=2u(I)) and wR2 was 0.0503 (all data).

3.3. Results and Discussion

3.3.1. Synthesis

Synthesis of 4'-(4-pyridyl)-2,2':6',2''-terpyridine (Pterpy) ligand

The ligand 4'-(4-pyridyl)-2,2':6',2''-terpyridine can be prepared via the Kröhnke pyridine synthesis. The proposed reaction scheme is illustrated below (**Scheme 12**).

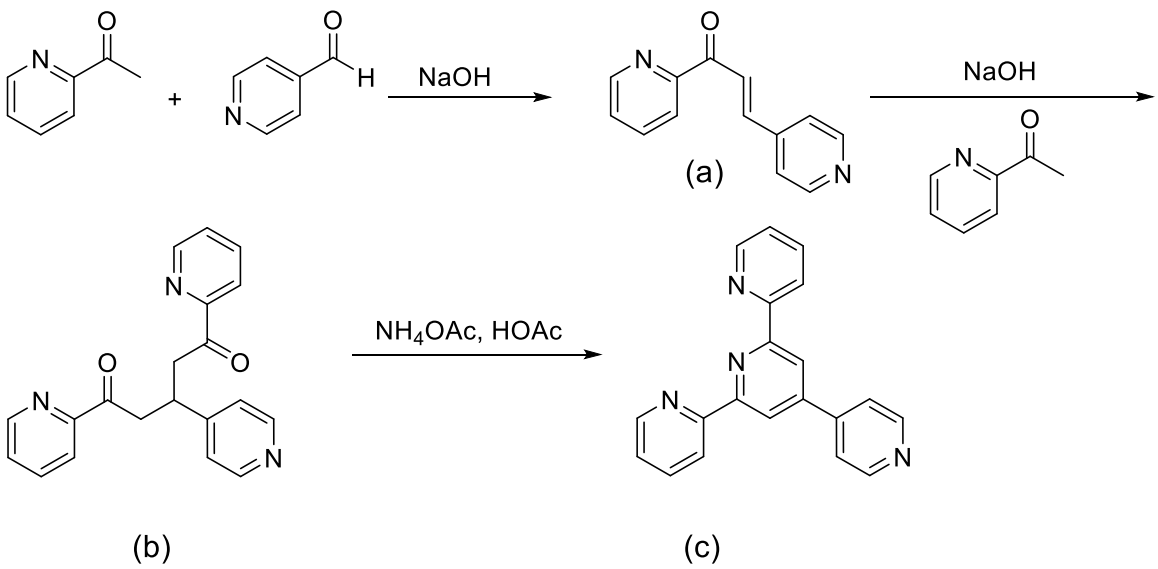

Scheme 12. Proposed reaction scheme for the synthesis of Pterpy via Kröhnke pyridine synthesis.

Initially, 4-pyridinecarboxaldehyde reacts with 2-acetylpyridine to form the α,β-unsaturated compound **(a)** through the Claisen-Schmidt reaction.[327, 328] Subsequently, compound **(a)** reacts with another ketone to form the 1,5-dicarbonyl compound **(b)** via a Michael addition reaction.[327, 328] Compound **(b)** then reacts with ammonium acetate to form a new pyridine ring, which is known as the Kröhnke reaction.[327, 328] This synthetic approach is commonly used in the preparation of 2,4,6-trisubstituted pyridine derivatives.[327, 328]

The unsuccessful synthesis of Ru(II)-arene-Cu(II) heterobimetallic complex

A summary of some of the procedures employed in this synthesis is provided in **Table 4**. The synthesis of the Ru(II)-arene-Cu(II) bimetallic complex was not successful

despite several attempts. The proposed reason for this is that when [Cu(Pterpy)Cl]Cl is reacted with [Ru(η^6-*p*-cymene)Cl_2]$_2$, Ru(II) exchanges with Cu(II) and thus the final product(s) contained Pterpy coordinated to Ru(II), such as: [Ru(Pterpy)$_2$]Cl_2 and/ or [Ru(Pterpy)Cl_2]. Initially, it was speculated that the relatively high temperature used in the initial reaction attempts might have resulted in the dissociation of Ru(II) from the arene, and then the free metal exchanged with Cu(II). Therefore, the reaction was also performed at room temperature or lower (*ca.* 0 °C) but this also was unsuccessful. Ligand exchange kinetics can be related to the electronic and geometrical structures of coordination compounds.[49] The ligand exchange rate for Ru(II) complexes is slow and similar to Pt(II), which is relevant with respect to chemotherapeutic properities.[49, 329] Each Ru(II) in [Ru(η^6-*p*-cymene)Cl_2]$_2$ possesses a pseudo-octahedral geometry, therefore during substitution reactions, it is likely to lose one ligand (chloro) and form a five-coordinate intermediate.[49] Afterwards, the new ligand (the uncoordinated pyridine in [Cu(Pterpy)Cl]Cl will attack and the bimetallic complex can form. It is difficult to explain how Ru(II) in the pseudo-octahedral geometry can lose coordination with *p*-cymene., The rate of ligand-exchange for Cu(II) is high so it is possible to speculate that Cu(II) will lose coordination with Pterpy in solution. Furthermore, since Ru(II) has a high affinity for nitrogen, once it encounters three N-coordination sites, it forms new bonds with Pterpy and dissociates from the arene. This hypothesis assumes that the arene provides lower crystal field stabilization energy than Pterpy.‡‡‡

To determine whether the complex of interest has formed, MALDI-TOF was used to measure the molecular weight of the final products. Ideally, X-ray crystallography would have been used as the primary technique to characterize this compound and to confirm the structure. However, all the attempts to grow crystals failed; only one crystal was obtained from experiment (SJ-100) and did not correspond to the product (**Figure 3.5**). Proton NMR cannot be used in characterizing the product since Cu(II) is paramagnetic, d^9 which results in broad lines.

‡‡‡ There is no direct evidence for this; but it is consistent with the results obtained from the experiments in this chapter.

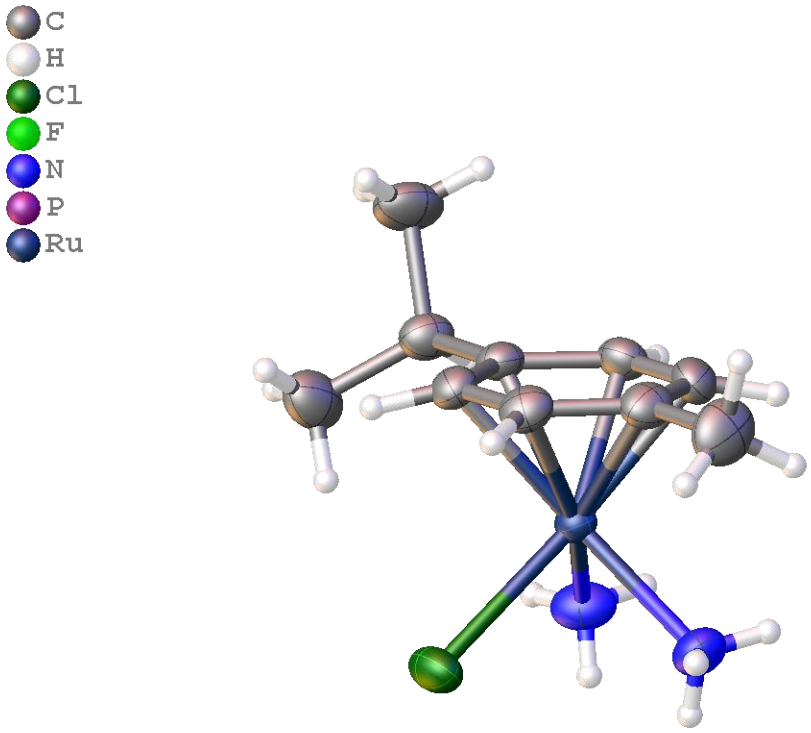

Figure 3.5. Crystal structure obtained from experiment SJ-100, [Ru(η^6-*p*-cymene)$(NH_3)_2$Cl]PF_6. The counterion is omitted for clarity.

After several trials, the Cu^{2+} metal centre, [Cu(Pterpy)Cl]Cl, was replaced with zinc(II) or ruthenium(II). All experiments with these metal ions also proved to be unsuccessful. The goal of using Zn(II) was to determine whether the final product had the skeletal structure of interest. Zn(II) is diamagnetic, d^{10}, and thus NMR spectroscopy can be used to judge the outcome of the experiments. Nevertheless, if stability of the metal complex is the reason for the unsuccessful synthesis of the bimetallic complex, then indeed Zn(II) will not be a better alternative than Cu(II). According to the Irving-Williams series, which predicts the stability of divalent first row transition metal complexes, Zn(II) should form less stable complexes than Cu(II) irrespective of the type and/ or the number of ligands.[330] On the other hand, Ru(II) was expected to provide a stable complex when coordinated to Pterpy. The issue with the synthesis of [Ru(Pterpy)Cl_2] was the possibility of having a mixture of Ru(II) and Ru(III)-based complexes. These experiments were discontinued due to time considerations.

Table 4. Summary of the procedures followed in the attempt to synthesize the Ru(II)-arene-Cu(II) heterobimetallic complex.

abbreviations: SM = starting material; MeOH = methanol; DCM = methylene chloride; DMF = Dimethylformamide; TEA = Triethylamine; eq = equivalents; soln = solution; Rt = room temperature
* MALDI-TOF results are given as: mass – percentage

Exp	Cu-Ru	Solvent(s)	pH	Temp.	Reagent(s)	MALDI*
1	SJ-14	MeOH	-	Reflux 6 h	-	407-100 483-84 720-3
2	SJ-39	Toluene	-	Reflux 6 h	-	SM
3	SJ-64	Acetone, H_2O (1/1; v/v)	~3	Rt	$CuCl_2{\cdot}2H_2O$ (3 eq)	407-100 720-3
4	SJ-70-C	Acetone, DCM (1/1; v/v)	>7	Rt	Na_2CO_3 (1 eq)	SM
5	SJ-72-C	DMF	~12	Rt	TEA (3 eq)	409-93 483-100 577-30 721-32
6	SJ-75-E	DMF	~12	Rt	TEA (3 eq) NH_4PF_6 (>5 eq)	392-41 577-35 721-100
7	SJ-86	CH_3CN	-	Rt	-	407-100 483-66
8	SJ-91	MeOH	-	Mixing at Rt (5 min) ~0 °C before extraction (1 h)	CuPterpy (4 eq) Ru-arene (~1 eq) Ether for extraction	408-82 577-100 651-72 714-16 757-5 1053-2 1223-3
9	SJ-94	MeOH CH_3CN	-	0 °C when RuL was added & during extraction	CuPtpy (4 eq) Ru-arene (1 eq)	410-100 482-45 579-8 720-0.7
10	SJ-95	MeOH	-	Stirring at Rt ~0 °C during extraction	CuPtpy (4 eq) Ru-arene (1 eq) Ether for extraction	408-100 484-40 579-9 721-2
11		The above crude soln	-	Reflux 4 h	-	No change
13	SJ-100	MeOH CH_3CN	-	Rt (24 h)→ Reflux 4 h	NH_4PF_6 (5 eq)	292-41 447-100 720-60

Exp	Zn-Ru	Solvent(s)	pH	Temp.	Reagent(s)	MALDI
1	SJ-22	MeOH	-	Reflux 6 h	-	446-100 720-87
2	SJ-38	toluene	-	Reflux 4 h	-	446-100 720-79
3	SJ-48	H_2O	-	Rt 12 h	-	482-29 580-100
4	SJ-62	Acetone, H_2O (1/1; v/v)	~3	Rt	$ZnCl_2$ (3 eq)	447-100 720-91
5	SJ-70-A	Acetone, ether (4/1; v/v)	-	Rt	$ZnCl_2$ (3 eq)	SM
6	SJ-70-B	Acetone, ether (3/2; v/v)	>7	Rt	$ZnCl_2$ (3 eq) Na_2CO_3 (1 eq)	SM
7	SJ-71-D	DMF	>7	Rt	$ZnCl_2$ (3 eq) Na_2CO_3 (3 eq)	268-100 446-70 720-90
8	SJ-70A2	Acetone, ether (4/1; v/v)	~3	Rt	$ZnCl_2$ (3 eq) NH_4PF_6 (>5 eq)	578-16 721-100
Exp	Ru-Ru	Solvent(s)	pH	Temp.	Reagent(s)	MALDI
1	SJ-35	MeOH	-	Reflux 6 h	-	578-100
2	SJ-76-G	DCM, acetone (1/1)	~13	Rt	TEA (3 eq)	447-100 720-72
3	SJ-95	CH_3CN	-	Reflux 4 h ~0 °C before extraction	RuPtpy(4 eq) RuL (1 eq) Ether for extraction	447-88 578-60 754-14 721-100

Synthesis of Ru(II)-arene-Au(III) heterobimetallic complex

Initially, Au(III) was coordinated to the tridentate Pterpy ligand. The resulting complex was reacted with the dimeric starting material, [Ru(η^6-*p*-cymene)Cl_2]$_2$, which breaks into monomers in solution and coordinates via Ru(II) to the pyridyl moiety in the Au(III) complex. It is important to do the reaction in this order, because if Pterpy was reacted with Ru(II) dimer prior to its reaction with Au(III), it will have multiple sites capable of acting as Lewis bases and thus can become a bidentate ligand on the Ru(II) metal centre (two chloro ligands in the Ru(II)-arene monomer will exchange with two pyridines in Pterpy).

According to the procedure reported in the **Experimental (3.2.5)** section of this chapter, the crude product was rinsed with dichloromethane. However, during the initial experimental trials, the crude was not rinsed with any solvent. In one of these experiments,

crystals were observed after approximately two months at room temperature in the NMR tube containing the crude product dissolved in DMSO-D_6. The crystals were identified as Ru(Pterpy)Cl_3 (**Figure 3.6**) from the X-ray crystal structure. Although it is a minor product, it is interesting since the absence of counterion in the crystal structure means that the Ru ion is in the (3+) oxidation state, despite the dimeric starting compound containing two Ru(II) centres. The presence of this product could be due to: a) traces of the Ru(III) ion was present in the reaction solution as an impurity that was carried along with Ru(II) dimer, [Ru(η^6-*p*-cymene)Cl_2]$_2$, in addition to traces of unreacted Pterpy; and/or b) the Ru(II) monomer lost its coordination to the arene ring, *p*-cymene, reducing the stability of its 2+ oxidation state, and enabling oxidization and exchange with Au(III) in [Au(Pterpy)Cl]Cl_2. The first hypothesis can be refuted, since Ru(III), d^5, is paramagnetic and thereby results in broad signals in the ^{1}H NMR spectrum. This distinctive feature was not observed in the NMR spectra of the starting material [Ru(η^6-*p*-cymene)Cl_2]$_2$ or the final product, Ru(II)-arene-Au(III). The second hypothesis suggests that Ru(II)/(III) has a higher affinity for Pterpy than the arene. It is important to keep in mind that the crystals were observed after a long period of time which allows slow metal-ligand exchange reactions to take place.

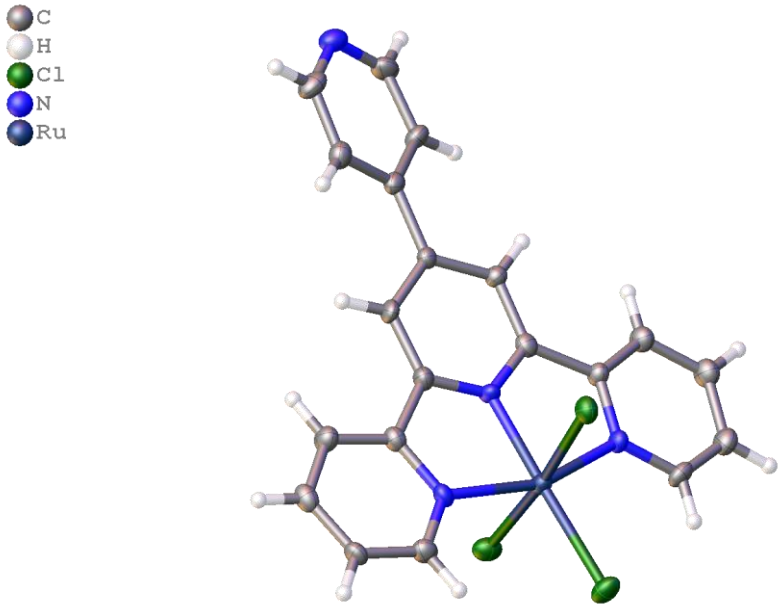

Figure 3.6. Crystal structure of the by-product obtained from the synthesis of Ru(II)-arene-Au(III).

Au(III), d^8, is isoelectronic and isostructural with Pt(II), d^8, which has been suggested it could have anticancer properities.[331] Au(III) complexes assume square-planar geometry, which is the same geometry that is crucial for Pt(II) bioactivity.[331] However, some of these complexes were found to be unstable in physiological systems due to the high reduction potential of Au(III).[166, 167] To solve this issue, chelating ligands are typically used to stabilize gold in its (3+) oxidation state.[164, 167] In addition, Au(III) is a soft Lewis acid and can form stable coordination complexes with soft bases like phosphorous, and borderline bases like pyridine.[332, 333] Therefore, Au(III) was coordinated to the tridentate ligand Pterpy.

3.3.2. X-ray fluorescence (XRF) analysis

Principle of XRF

X-ray fluorescence (XRF) is a non-destructive technique used to identify or confirm the presence of elements in a sample and their mass or concentration.[334] X-ray radiation is high in energy and thus is used to excite inner-shell electrons (i.e., core electrons in the K, L, or M layer) to a higher energy state.[171, 334] The excited electron can be ejected from the atom or it can relax back to the inner shell while emitting light (fluorescence) at a wavelength that is element-specific.[334] The intensity of the fluorescence emission correlates to the amount of element present in the tested sample.[171, 334]

XRF Results

XRF analysis was performed on the Ru(II)-arene-Au(III) heterobimetallic complex. Unfortunately, due to instrumental uncertainty, the analysis could only confirm the presence of elements, but could not be used to calculate the concentration. The results of XRF analysis are presented in **Figure 3.7** and these results confirm the presence of Au, Ru, and Cl elements.

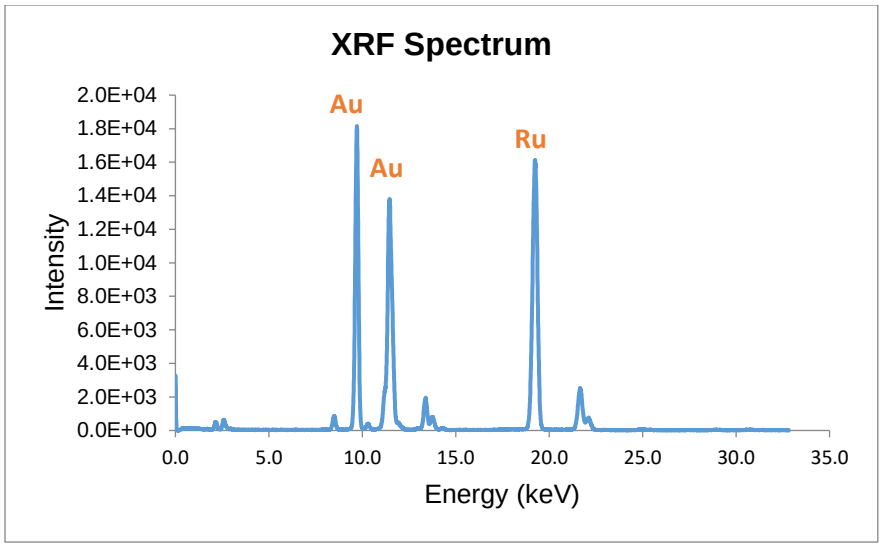

Figure 3.7. XRF spectrum for Ru(II)-arene-Au(III) heterobimetallic complex.

3.4. Conclusion and future work

In this chapter, the synthesis of a heterobimetallic Ru(II) complexes was described. The initial aim of this research was to synthesize a Ru(II)-arene-Cu(II) binuclear complex. After several experimental trials, the synthesis was unsuccessful, mainly because Cu(II) is labile and cannot form a stable complex even when it is coordinated to a tridentate ligand, Pterpy. This heteronuclear complex was intended to be bifunctional, in the sense that the Ru(II) centre targets transport into cancer cells and can eventually interact with DNA when internalized in the cell nucleus, and Cu(II) can generate ROS which results in oxidative stress that induces apoptosis. Recent research tend to emphasize the role of Cu(II) complexes as ROS generators, without considering the fact that many forms of cancer lead to elevated concentrations of Cu ion, which is required as a cofactor for several enzymes involved in angiogenesis and cancer cell proliferation. Since Cu ions are labile, as shown in this work, loss of ligands in biological systems could assist in cancer cell proliferation as opposed to its death. Thus, future research should focus on the stability of Cu(I)/(II) coordination complexes in physiological conditions. Due to the synthetic issues associated with the use of Cu ions, the author turned to Au(III), since it can also generate oxidative stress and exhibit anticancer activity.[167] In addition, Au(III) was shown to form stable complexes under physiological conditions, when coordinated to chelating ligands.[167] This chapter only reports the synthesis of the heterobimetallic complex without investigating its biological activity, because the complex was found to exhibit low solubility in several solvents including DMSO. Therefore, future work should consider enhancing the solubility of this compound by modifying its structure, such as, adding functional groups on the pyridine rings in the spacer ligand, Pterpy, that can form H-bonds.

Chapter 4. Conclusion

In this thesis, the synthesis and characterization of fifteen new compounds were described, in which seven were heterocyclic furoxan derivatives and eight were organometallic complexes. The complexes contain the Ru(II)-arene moiety and belong to the family of RAPTA-C compounds. All the compounds, including the heterocyclic ligands, were intended to be used as anticancer and/ or antibacterial agents. The speculated mode of action for the compounds described in **Chapter 2** was that the Ru(II)-arene moiety will promote transport into cancerous or bacterial cells, enabling cytotoxic nitric oxide to be released from the furoxan ligand inside the cells. The heterobimetallic complex reported in **Chapter 3** was expected to be selective, since it also possesses the Ru(II)-arene moiety. In addition, it was speculated that this complex could have enhanced bioactivity due to synergistic interactions between Ru(II) and Au(III).

Chapter 2 contributes to the synthesis and application of N-heterocyclic oxides. Furoxan derivatives were used as ligands on the Ru(II)-arene moiety to generate compounds that mimic the structure of RAPTA-C. The complexes exhibited different abilities to release nitric oxide and variable cytotoxicity in bacterial cells. These studies demonstrated that altering the electronic properties of the substituents on the furoxan ring can impact its NO-donating character. Electron withdrawing groups (i.e., $-NO_2$, $-SO_2Ph$) lower the electron density in the furoxan ring making it more susceptible to nucleophilic attack by thiol-containing biomolecules, such as glutathione. Antibacterial studies showed that the furoxan derivative with the sulfoxide substituent, L6(-SOPh), demonstrated the highest cytotoxicity among the seven derivatives. According to the author's knowledge, a sulfoxide substituent has not been used as a functional group on furoxan derivatives. Therefore, this new class of compounds need to be studied further in terms of their bioactivity. The NCI will evaluate the anticancer activity of four of the furoxan derivatives, L1($-NO_2$), L5(-SPh), L6(-SOPh), and L7($-SO_2Ph$) using NCI-60 screening.

Chapter 3 introduced the synthesis of a new heterobimetallic complex that consists of a Ru(II)-arene moiety, which is analogous to RAPTA-C, linked to a Au(III) centre coordinated to the tridentate ligand, Pterpy. The structure of this complex still needs to be confirmed via X-ray diffraction. Indeed, the low solubility of this molecule in several solvents, including dimethyl sulfoxide (DMSO), hindered the analysis of its biological

activity. Nevertheless, modifications of the chemical structure may solve this issue. For instance, functionalizing the Pterpy ligand with substituents capable of forming H-bonds could enhance the solubility of the complex in biological systems. In addition, changing the spacer length could modulate the cytotoxicity by altering the synergistic interactions between Ru(II) and Au(III).

Serendipity, "*the faculty of making fortunate discoveries by accident*," revealed three crystal structures, two of which are novel.[96] The first being the by-product for the synthesis of L1(-NO_2) reported in **Chapter 2**, 4-cyanopyridine (**Figure 4.1**), which can be used as a reagent in several reactions.[335-338] The crystal structure of this compound has been reported previously, and is not discussed further in this thesis. However, it is an interesting compound from a synthetic perspective. In 1958-1972, multiple articles reported the synthesis of anti-tuberculosis drug, isonicotinylhydrazide (INH, commonly called Isoniazid) from 4-cyanopyridine and hydrazine hydrate.[339] Isoniazid (**Figure 4.1**) is still manufactured today using the same reagents.[340] Recently, 4-cyanopyridine has been implicated in the synthesis of another anti-tuberculosis drug, ethionamide (**Figure 4.1**).[341] The industrial method for manufacturing 4-cyanopyridine involves ammoxidation of 4-methylpyridine.[342] Ammoxidation (also called Sohio process) is the industrial synthesis of nitriles by using ammonia and molecular oxygen.[343, 344]

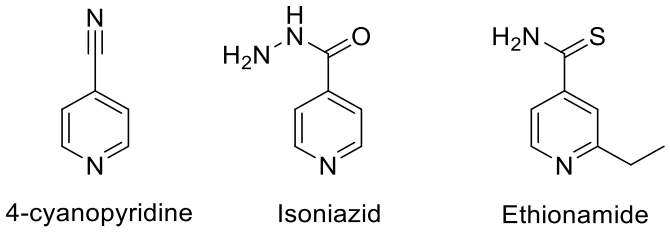

Figure 4.1. Chemical structure of two anti-tuberculosis drugs synthesized from 4-cyanopyridine.

In addition, the synthetic procedure for L1 (-NO_2), described in **Chapter 2**, can be used to provide an alternative route to the synthesis of niacin by replacing the starting material with 3-vinylpyridine (**Scheme 13**). The by-product will be 3-cyanopyridine. Then, by using base hydrolysis, 3-cyanopyridine will be converted to nicotinic acid (i.e., niacin:

a form of vitamin B_3).[342] Typically, niacin is manufactured from 3-picoline (i.e., 3-methylpyridine).[342]

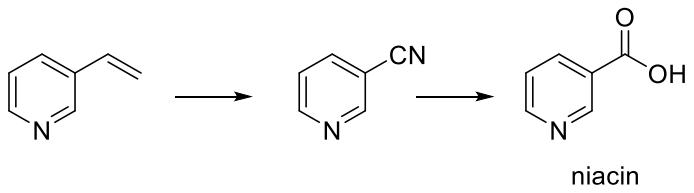

niacin

Scheme 13. Proposed synthetic pathway for niacin.

The second crystal, reported in **Chapter 3**, was identified to be the novel organometallic complex: [Ru(η^6-*p*-cymene)$(NH_3)_2Cl$]PF_6. This compound formed a few crystals while attempting to synthesize the Ru(II)-arene Cu(II) bimetallic compound. In the future, the biological activity of this new complex can be investigated. Furthermore, a third crystal was found to be [Ru(Pterpy)Cl_3] complex, which is the by-product formed during the synthesis of Ru(II)-arene-Au(III). This is a known compound but, its crystal structure has not been reported. In the future, the [Ru(Pterpy)Cl_3] compound can be coordinated to another metal complex through the pyridyl moiety in Pterpy to synthesize binuclear compounds.

In this thesis, the development of new furoxan derivatives and their corresponding Ru(II)-arene complexes was discussed. This research contributes to the field of N-heterocyclic oxides and their application in medicine. Furthermore, the synthesis of the heterobimetallic complex Ru(II)-arene-Au(III) provides insight into the development of binuclear complexes and their potential use as chemotherapeutics.

References

1. Cancer -World Health Organization. http://www.who.int/mediacentre/factsheets/fs297/en/ (accessed Nov-28-2018).

2. Statistics, C. C. http://www.cancer.ca/en/cancer-information/cancer-101/canadian-cancer-statistics-publication/?region=bc (accessed June-23-2018).

3. Alessio, E., *Eur. J. Inorg. Chem.,* **2016**, 1549-1560.

4. Institute, N. C. Types of Cancer Treatment. https://www.cancer.gov/about-cancer/treatment/types (accessed June-23-2018).

5. Society, C. C. Treatment. http://www.cancer.ca/en/cancer-information/diagnosis-and-treatment/treatment/?region=on (accessed June-23-2018).

6. Sadler, P. J.; Li, H.; Sun, H., *Coord. Chem. Rev.,* **1999,** *185*, 689-709.

7. Lotfi, Z.; Mousavi, H. Z.; Sajjadi, S. M., *RSC Adv.,* **2016,** *6*, 90360-90370.

8. Farrer, N. J.; Salassa, L.; Sadler, P. J., *Dalton Trans.,* **2009,** *0*, 10690-10701.

9. Norman, J. F.; Hambley, T. W., Targeting Strategies for Metal-Based Therapeutics. In *Bioinorganic Medicinal Chemistry*, Alessio, E., Ed. Wiley-VCH Verlag GmbH & Co. KGaA: 2011; pp 49-73.

10. Jones, M. R.; Dustin, D.; Storr, T., Introduction to Ligand Design in Medicinal Inorganic Chemistry. In *Ligand Design in Medicinal Inorganic Chemistry*, Storr, T., Ed. Wiley: 2014; pp 1-7.

11. Haas, K. L.; Franz, K. J., *Chem. Rev.,* **2009,** *109*, 4921-4960.

12. Holm, R. H.; Kennepohl, P.; Solomon, E. I., *Chem. Rev.,* **1996,** *96*, 2239-2314.

13. Pizarro, A. M.; Sadler, P. J., *Biochimie,* **2009,** *91*, 1198-1211.

14. Zhang, C. X.; Lippard, S. J., *Curr. Opin. Chem. Biol.,* **2003,** *7*, 481-489.

15. Ferreira, A.; Petersen, P.; Petrilli, H.; Ciriolo, M., O*xidative Stress in Applied Basic Research and Clinical Practice*. In *Redox-Active Therapeutics*, Armstrong, D., Ed. Humana Press: 2016; pp 287-309.

16. Brissos, R. F.; Caubet, A.; Gamez, P., *Eur. J. Inorg. Chem.,* **2015,** *2015*, 2633-2645.

17. Medici, S.; Peana, M.; Nurchi, V. M.; Lachowicz, J. I.; Crisponi, G.; Zoroddu, M. A., *Coord. Chem. Rev.,* **2015,** *284*, 329-350.

18. Johnstone, T. C.; Suntharalingam, K.; Lippard, S. J., *Phil. Trans. R. Soc. A.,* **2015,** *373*, 20140185.

19. Milaeva Elena, R.; Tyurin Vladimir, Y., *Pure Appl. Chem.*, **2017,** *89*, 1065-1088.

20. Dörr, M.; Meggers, E., *Curr. Opin. Chem. Biol.,* **2014,** *19*, 76-81.

21. Mari, C.; Pierroz, V.; Ferrari, S.; Gasser, G., *Chem. Sci.,* **2015,** *6*, 2660-2686.

22. Sinitsyna, O.; Paralikar, P.; Pandit, R.; Rai, M., Platinum in Biomedical Applications. In *Biomedical Applications of Metals*, Rai, M.; Ingle, A. P.; Medici, S., Eds. Springer International Publishing: Cham, 2018; pp 151-165..

23. Johnstone, T. C.; Suntharalingam, K.; Lippard, S. J., *Chem. Rev.,* **2016,** *116*, 3436-3486.

24. Dilruba, S.; Kalayda, G. V., *Cancer Chemother. Pharmacol.,* **2016,** *77*, 1103-1124.

25. Klein, A. V.; Hambley, T. W., Platinum-Based Anticancer Agents. In *Ligand Design in Medicinal inorganic Chemistry*, Storr, T., Ed. Wiley: 2014; pp 9-37.

26. Mejía, C.; Ortega-Rosales, S.; Ruiz-Azuara, L., Mechanism of Action of Anticancer Metallodrugs. In *Biomedical Applications of Metals*, Rai, M.; Ingle, A. P.; Medici, S., Eds. Springer International Publishing: Cham, 2018; pp 213-234.

27. Petruzzella, E.; Curci, A.; Margiotta, N.; Natile, G.; Hoeschele, J. D., *Inorganica Chim. Acta.,* **2016,** *452*, 130-136.

28. Kauffman, G. B.; Pentimalli, R.; Doldi, S.; Hall, M. D., *Platin. Met. Rev.,* **2010,** *54*, 250-256.

29. Rosenberg, B.; Van Camp, L.; Krigas, T., *Nature,* **1965,** *205*, 698-699.

30. Jamieson, E. R.; Lippard, S. J., *Chem. Rev.,* **1999,** *99*, 2467-2498.

31. Ishida, S.; Lee, J.; Thiele, D. J.; Herskowitz, I., *Proc. Natl. Acad. Sci.,* **2002,** *99*, 14298-14302.

32. Wang, D.; Lippard, S. J., *Nat. Rev. Drug Discov.,* **2005,** *4*, 307-320.

33. Tulub, A. A.; Stefanov, V. E., *Int. J. Biol. Macromol.,* **2001,** *28*, 191-198.

34. Papadia, P.; Barozzi, F.; Hoeschele, J. D.; Piro, G.; Margiotta, N.; Di Sansebastiano, G.-P., *Int. J. Mol. Sci.,* **2017,** *18*, 306-319.

35. Herzog, C.; Yang, C.; Holmes, A.; Kaushal, G. P., *Am. J. Physiol. Renal. Physiol.,* **2012,** *303*, F1239-F1250.

36. Florea, A.-M.; Büsselberg, D., *Cancers,* **2011,** *3*, 1351-1371.

37. Ding, L.; Ren, J.; Zhang, D.; Li, Y.; Huang, X.; Ji, J.; Hu, Q.; Wang, H.; Ni, Y.; Hou, Y., *Mol. Cancer Ther.,* **2017**, molcanther. 0454.2016.

38. Zhitomirsky, B.; Assaraf, Y. G., *Drug Resist. Updat.,* **2016,** *24*, 23-33.

39. Riddell, I. A.; Lippard, S. J., *Met. Ions Life Sci.,* **2018,** *18*, 1-52.

40. Kelland, L., *Nat. Rev. Cancer,* **2007,** *7*, 573-584.

41. Knight, K. R. G.; Kraemer, D. F.; Neuwelt, E. A., *J. Clin. Oncol.,* **2005,** *23*, 8588-8596.

42. Minasian Lori, M.; Frazier, A. L.; Sung, L.; O'Mara, A.; Kelaghan, J.; Chang Kay, W.; Krailo, M.; Pollock Brad, H.; Reaman, G.; Freyer David, R., *Cancer Med.,* **2018,** *0*, 0.

43. Coccia, P. F.; Pappo, A. S.; Beaupin, L.; Borges, V. F.; Borinstein, S. C.; Chugh, R.; Dinner, S.; Folbrecht, J.; Frazier, A. L.; Goldsby, R., *J. Natl. Compr. Canc. Netw.,* **2018,** *16*, 66-97.

44. Desoize, B., *Anticancer Res.,* **2004,** *24*, 1529-1544.

45. Bruijnincx, P. C. A.; Sadler, P. J., *Curr. Opin. Chem. Biol.,* **2008,** *12*, 197-206.

46. Deo, K. M.; Pages, B. J.; Ang, D. L.; Gordon, C. P.; Aldrich-Wright, J. R., *Int. J. Mol. Sci.,* **2016,** *17*, 1818.

47. Esteban Leon, I.; Fernando Cadavid-Vargas, J.; Laura Di Virgilio, A.; Beatriz Etcheverry, S., *Curr. Med. Chem.,* **2017,** *24*, 112-148.

48. Montani, M.; Pazmay, G. V. B.; Hysi, A.; Lupidi, G.; Pettinari, R.; Gambini, V.; Tilio, M.; Marchetti, F.; Pettinari, C.; Ferraro, S.; Iezzi, M.; Marchini, C.; Amici, A., *Pharmacol. Res.,* **2016,** *107*, 282-290.

49. Reedijk, B. J., *Platin. Met. Rev.,* **2008,** *52*, 2-11.

50. Hartinger, C. G.; Zorbas-Seifried, S.; Jakupec, M. A.; Kynast, B.; Zorbas, H.; Keppler, B. K., *J. Inorg. Biochem.,* **2006,** *100*, 891-904.

51. Chen, L.; Li, G.; Peng, F.; Jie, X.; Dongye, G.; Cai, K.; Feng, R.; Li, B.; Zeng, Q.; Lun, K., *Oncotarget,* **2016,** *7*, 80716.

52. Wachter, E.; Zamora, A.; Heidary, D. K.; Ruiz, J.; Glazer, E. C., *ChemComm.,* **2016,** *52*, 10121-10124.

53. Sava, G.; Cocchietto, M., *In Vivo,* **2000,** *14*, 741-744.

54. Pluim, D.; van Waardenburg, R. C. A. M.; Beijnen, J. H.; Schellens, J. H. M., *Cancer Chemother. Pharmacol.,* **2004,** *54*, 71-78.

55. Aitken, J. B.; Antony, S.; Weekley, C. M.; Lai, B.; Spiccia, L.; Harris, H. H., *Metallomics,* **2012,** *4*, 1051-1056.

56. Sava, G.; Zorzet, S.; Turrin, C.; Vita, F.; Soranzo, M.; Zabucchi, G.; Cocchietto, M.; Bergamo, A.; DiGiovine, S.; Pezzoni, G.; Sartor, L.; Garbisa, S., *Clin. Cancer Res.,* **2003,** *9*, 1898-1905.

57. Gava, B.; Zorzet, S.; Spessotto, P.; Cocchietto, M.; Sava, G., *J. Pharmacol. Exp. Ther.,* **2006,** *317*, 284-291.

58. Pelillo, C.; Mollica, H.; Eble, J. A.; Grosche, J.; Herzog, L.; Codan, B.; Sava, G.; Bergamo, A., *J. Inorg. Biochem.,* **2016,** *160*, 225-235.

59. Bergamo, A.; Pelillo, C.; Chambery, A.; Sava, G., *J. Inorg. Biochem.,* **2017,** *168*, 90-97.

60. Pillozzi, S.; Gasparoli, L.; Stefanini, M.; Ristori, M.; D'Amico, M.; Alessio, E.; Scaletti, F.; Becchetti, A.; Arcangeli, A.; Messori, L., *Dalton Trans.,* **2014,** *43*, 12150-12155.

61. Hartinger, C. G.; Jakupec, M. A.; Zorbas-Seifried, S.; Groessl, M.; Egger, A.; Berger, W.; Zorbas, H.; Dyson, P. J.; Keppler, B. K., *Chem. Biodivers.,* **2008,** *10*, 2140-2155.

62. Pongratz, M.; Schluga, P.; Jakupec, M. A.; Arion, V. B.; Hartinger, C. G.; Allmaier, G.; Keppler, B. K., *J. Anal. At. Spectrom.,* **2004,** *19*, 46-51.

63. Gomme, P. T.; McCann, K. B.; Bertolini, J., *Drug Discov. Today,* **2005,** *10*, 267-273.

64. Otero, L.; Gambino, D., Ruthenium in Medicinal Chemistry. In *Ruthenium Chemistry*, Mishra, A.; Mishra, L., Eds. Pan Stanford: 2018; pp 11-44.

65. Ndagi, U.; Mhlongo, N.; Soliman, M. E., *Drug Des. Devel. Ther.,* **2017,** *11*, 599-616.

66. Babak, M. V.; Ang, W. H., *Met. Ions Life Sci.,* **2018,** *18*, 171-198.

67. Yip, A. M.-H.; Lo, K. K.-W., *Coord. Chem. Rev.,* **2018,** *361*, 138-163.

68. Gill, M. R.; Jarman, P. J.; Halder, S.; Walker, M. G.; Saeed, H. K.; Thomas, J. A.; Smythe, C.; Ramadan, K.; Vallis, K. A., *Chem. Sci.,* **2018,** *9*, 841-849.

69. Liu, J.; Zhang, C.; Rees, T. W.; Ke, L.; Ji, L.; Chao, H., *Coord. Chem. Rev.,* **2018,** *363*, 17-28.

70. Ganeshpandian, M.; Palaniandavar, M.; Muruganantham, A.; Ghosh Swapan, K.; Riyasdeen, A.; Akbarsha Mohammad, A., *Appl. Organomet. Chem.,* **2017,** *32*, 4154-4171.

71. Hong, W.-X.; Huang, F.; Huan, T.; Xu, X.; Han, Q.; Wang, G.; Xu, H.; Duan, S.; Duan, Y.; Long, X.; Liu, Y.; Hu, Z., *J. Inorg. Biochem.,* **2018,** *180*, 54-60.

72. Mandal, P.; Kundu, B. K.; Vyas, K.; Sabu, V.; Helen, A.; Dhankhar, S. S.; Nagaraja, C. M.; Bhattacherjee, D.; Bhabak, K. P.; Mukhopadhyay, S., *Dalton Trans.,* **2018,** *47*, 517-527.

73. Schmitt, F.; Kasparkova, J.; Brabec, V.; Begemann, G.; Schobert, R.; Biersack, B., *J. Inorg. Biochem.,* **2018,** *184*, 69-78.

74. Martínez-Peña, F.; Infante-Tadeo, S.; Habtemariam, A.; Pizarro, A. M., *Inorg. Chem.,* **2018,** *57*, 5657-5668.

75. Mu, C. Mechanisms of New Ru-Ferrocene and Binuclear Ru Metallochemotherapeutics and the Ru Metastasis Inhibitor NAMI-A. Simon Fraser University, Canada, 2016, pp 65-119.

76. Tan, C.; Lai, S.; Wu, S.; Hu, S.; Zhou, L.; Chen, Y.; Wang, M.; Zhu, Y.; Lian, W.; Peng, W., *J. Med. Chem.,* **2010,** *53*, 7613-7624.

77. Liu, H.-K.; Berners-Price, S. J.; Wang, F.; Parkinson, J. A.; Xu, J.; Bella, J.; Sadler, P. J., *Angew. Chem. Int. Ed.,* **2006,** *45*, 8153-8156.

78. Mu, C.; Walsby, C. J., Ruthenium anticancer compounds with biologically-derived ligands In *Ligand Design in Medicinal inorganic Chemistry*, Storr, T., Ed. Wiley Online Library: 2014; pp 405-437.

79. Suss-Fink, G., *Dalton Trans.,* **2010,** *39*, 1673-1688.

80. Chotard, F.; Dondaine, L.; Balan, C.; Bettaeib, A.; Paul, C.; Le Gendre, P.; Bodio, E., *New J. Chem.,* **2018,** *42*, 8105-8112.

81. Murray, B. S.; Babak, M. V.; Hartinger, C. G.; Dyson, P. J., *Coord. Chem. Rev.,* **2016,** *306*, 86-114.

82. Bergamo, A.; Gaiddon, C.; Schellens, J. H. M.; Beijnen, J. H.; Sava, G., *J. Inorg. Biochem.,* **2012,** *106*, 90-99.

83. Allardyce, C. S.; Dyson, P. J.; Ellis, D. J.; Heath, S. L., *ChemComm.,* **2001,***15*, 1396-1397.

84. Scolaro, C.; Bergamo, A.; Brescacin, L.; Delfino, R.; Cocchietto, M.; Laurenczy, G.; Geldbach, T. J.; Sava, G.; Dyson, P. J., *J. Med. Chem.,* **2005,** *48*, 4161-4171.

85. Nowak-Sliwinska, P.; van Beijnum, J. R.; Casini, A.; Nazarov, A. A.; Wagnières, G.; van den Bergh, H.; Dyson, P. J.; Griffioen, A. W., *J. Med. Chem.,* **2011,** *54*, 3895-3902.

86. Morris, R. E.; Aird, R. E.; del Socorro Murdoch, P.; Chen, H.; Cummings, J.; Hughes, N. D.; Parsons, S.; Parkin, A.; Boyd, G.; Jodrell, D. I.; Sadler, P. J., *J. Med. Chem.,* **2001,** *44*, 3616-3621.

87. Chen, H.; Parkinson, J. A.; Morris, R. E.; Sadler, P. J., *J. Am. Chem. Soc.,* **2003,** *125*, 173-186.

88. Fiers, W.; Beyaert, R.; Declercq, W.; Vandenabeele, P., *Oncogene,* **1999,** *18*, 7719-7730.

89. Mendoza-Ferri, M.-G.; Hartinger, C. G.; Eichinger, R. E.; Stolyarova, N.; Severin, K.; Jakupec, M. A.; Nazarov, A. A.; Keppler, B. K., *Organometallics,* **2008,** *27*, 2405-2407.

90. Farrell, N., *Compr. Coord. Chem.,* **2003,** *9*, 809-840.

91. Boerner, L. J. K.; Zaleski, J. M., *Curr. Opin. Chem. Biol.,* **2005,** *9*, 135-144.

92. K. van der Schilden, F. G., H. Kooijman, A.L. Spek, J.G. Haasnoot, J. Reedijk, *Angew. Chem. Int. Ed. Engl.,* **2004,** *43*, 5668-5670.

93. Williams, R. L.; Toft, H. N.; Winkel, B.; Brewer, K. J., *Inorg. Chem.,* **2003,** *42*, 4394-4400.

94. Bjelosevic, H.; Guzei, I. A.; Spencer, L. C.; Persson, T.; Kriel, F. H.; Hewer, R.; Nell, M. J.; Gut, J.; van Rensburg, C. E. J.; Rosenthal, P. J.; Coates, J.; Darkwa, J.; Elmroth, S. K. C., *J. Organomet. Chem.,* **2012,** *720*, 52-59.

95. Pelletier, F.; Comte, V.; Massard, A.; Wenzel, M.; Toulot, S.; Richard, P.; Picquet, M.; Le Gendre, P.; Zava, O.; Edafe, F.; Casini, A.; Dyson, P. J., *J. Med. Chem.,* **2010,** *53*, 6923-6933.

96. Butler, A.; Nicholson, R., *Life, death and nitric oxide*. RSC: UK, 2003, pp 1-148.

97. Scicinski, J.; Oronsky, B.; Ning, S.; Knox, S.; Peehl, D.; Kim, M. M.; Langecker, P.; Fanger, G., *Redox Biol.,* **2015,** *6*, 1-8.

98. Lundberg, J. O.; Gladwin, M. T.; Weitzberg, E., *Nat. Rev. Drug Discov.,* **2015,** *14*, 623.

99. Garry, P. S.; Ezra, M.; Rowland, M. J.; Westbrook, J.; Pattinson, K. T. S., *Exp. Neurol.,* **2015,** *263*, 235-243.

100. Rodrigues, F. P.; Carneiro, Z. A.; Mascharak, P.; Curti, C.; da Silva, R. S., *Coord. Chem. Rev.,* **2016,** *306*, 701-707.

101. Li, H.; Horke, S.; Förstermann, U., *Atherosclerosis,* **2014,** *237*, 208-219.

102. Zhang, P. Y.; Xu, X.; Li, X. C., *Eur. Rev. Med. Pharmacol. Sci.,* **2014,** *18*, 3091-3096.

103. Cheng, H.; Wang, L.; Mollica, M.; Re, A. T.; Wu, S.; Zuo, L., *Cancer Lett.,* **2014,** *353*, 1-7.

104. Caneba, C. A.; Yang, L.; Baddour, J.; Curtis, R.; Win, J.; Hartig, S.; Marini, J.; Nagrath, D., *Cell Death Dis.,* **2014,** *5*, 1302-1314.

105. Chang, C.-F.; Diers, A. R.; Hogg, N., *Free Radic. Biol. Med.,* **2015,** *79*, 324-336.

106. Fukumura, D.; Kashiwagi, S.; Jain, R. K., *Nat. Rev. Cancer,* **2006,** *6*, 521-534.

107. Burke, A. J.; Sullivan, F. J.; Giles, F. J.; Glynn, S. A., *Carcinogenesis,* **2013,** *34*, 503-512.

108. Thomas, D. D.; Espey, M. G.; Ridnour, L. A.; Hofseth, L. J.; Mancardi, D.; Harris, C. C.; Wink, D. A., *Proc. Natl. Acad. Sci. U. S. A.,* **2004,** *101*, 8894-8899.

109. Ignarro, L. J., Nitric Oxide as a Communication Signal in Vascular and Neuronal Cells. In *Nitric Oxide*, Lancaster, J., Ed. Academic Press: San Diego, 1996; pp 111-137.

110. Ford, P. C.; Lorkovic, I. M., *Chem. Rev.,* **2002,** *102* (4), 993-1018.

111. Liberti, M. V.; Locasale, J. W., *Trends Biochem. Sci.,* **2016,** *41*, 211-218.

112. Otto, A. M., *Cancer Metab.,* **2016,** *4*, 5-13.

113. Cosby, K.; Partovi, K. S.; Crawford, J. H.; Patel, R. P.; Reiter, C. D.; Martyr, S.; Yang, B. K.; Waclawiw, M. A.; Zalos, G.; Xu, X., *Nat. Med.,* **2003,** *9*, 1498-1505.

114. Doyle, M. P.; Pickering, R. A.; DeWeert, T. M.; Hoekstra, J. W.; Pater, D., *J. Biol. Chem.,* **1981,** *256*, 12393-12398.

115. Folkman, J., *N. Engl. J. Med.,* **1971,** *285*, 1182-1186.

116. Hockel, M.; Vaupel, P., *J. Natl. Cancer Inst.,* **2001,** *93*, 266-276.

117. Peitzsch, C.; Perrin, R.; Hill, R. P.; Dubrovska, A.; Kurth, I., *Int. J. Radiat. Biol.,* **2014,** *90*, 636-652.

118. Overgaard, J.; Horsman, M. R. In *Modification of hypoxia-induced radioresistance in tumors by the use of oxygen and sensitizers*, 1996; Elsevier: pp 10-21.

119. Chan, N.; Koritzinsky, M.; Zhao, H.; Bindra, R.; Glazer, P. M.; Powell, S.; Belmaaza, A.; Wouters, B.; Bristow, R. G., *Cancer Res.,* **2008,** *68*, 605-614.

120. Zeman, E. M., Biologic basis of radiation oncology. In *Clinical Radiation Oncology*, Gunderson, L. L.; Tepper, J. E., Eds. Churchill Livingstone: Churchill Livingstone, Harcourt Health Sciences, Philadelphia, 2000; pp 1-41.

121. Horsman, M. R.; Wouters, B. G.; Joiner, M. C.; Overgaard, J., The oxygen effect and fractionated radiotherapy. In *Basic clinical radiobiology*, Edward Arnold, London: 2009; pp 207-216.

122. Gray, L. H.; Conger, A. D.; Ebert, M.; Hornsey, S.; Scott, O. C. A., *Br. J. Radiol.,* **1953,** *26*, 638-648.

123. Mitchell, J. B.; Wink, D. A.; DeGraff, W.; Gamson, J.; Keefer, L. K.; Krishna, M. C., *Cancer Res.,* **1993,** *53*, 5845-5848.

124. Matsumoto, H.; Hayashi, S.; Hatashita, M.; Shioura, H.; Ohtsubo, T.; Kitai, R.; Ohnishi, T.; Yukawa, O.; Furusawa, Y.; Kano, E., *Int. J. Radiat. Biol.,* **2000,** *76*, 1649-1657.

125. De Ridder, M.; Verellen, D.; Verovski, V.; Storme, G., *Nitric oxide,* **2008,** *19*, 164-169.

126. Bhowmick, R.; Girotti, A. W., *Cancer Lett.,* **2014,** *343*, 115-122.

127. Bazak, J.; Fahey, J. M.; Wawak, K.; Korytowski, W.; Girotti, A. W., *Free Radic. Biol. Med.,* **2017,** *102*, 111-121.

128. Ostrowski, A. D.; Ford, P. C., *Dalton Trans.,* **2009,** *48*, 10660-10669.

129. Shao, C.; Stewart, V.; Folkard, M.; Michael, B. D.; Prise, K. M., *Cancer Res.,* **2003,** *63*, 8437-8442.

130. Zhao, H.; Ning, S.; Nolley, R.; Scicinski, J.; Oronsky, B.; Knox, S. J.; Peehl, D. M., *Clin. Epigenetics,* **2017,** *9*, 4-15..

131. Peehl, D.; Zhao, H.; Ning, S., *J. Clin. Oncol.,* **2018,** *36*, 280-280.

132. Institute, N. C. Radiosensitizer RRx-001. https://www.cancer.gov/publications/dictionaries/cancer-drug/def/radiosensitizer-rrx-001 (accessed June-20-2018).

133. Oronsky, B.; Scicinski, J.; Ning, S.; Peehl, D.; Oronsky, A.; Cabrales, P.; Bednarski, M.; Knox, S., *Invest. New Drugs,* **2016,** *34*, 371-377.

134. Yalcin, O.; Oronsky, B.; Carvalho, L. J. M.; Kuypers, F. A.; Scicinski, J.; Cabrales, P., *Malar. J.,* **2015,** *14*, 218-230.

135. National Cancer Institute. https://www.cancer.gov/publications/dictionaries/cancer-drug?cdrid=739669 (accessed Nov-28-2018).

136. Caramori, G. F.; Ortolan, A. O.; Parreira, R. L. T.; da Silva, E. H., *J. Organomet. Chem.,* **2015,** *799*, 54-60.

137. Carneiro, Z. A.; Biazzotto, J. C.; Alexiou, A. D. P.; Nikolaou, S., *J. Inorg. Biochem.,* **2014,** *134*, 36-38.

138. Zhao, J.; Gou, S.; Sun, Y.; Fang, L.; Wang, Z., *Inorg. Chem.,* **2012,** *51*, 10317-10324.

139. Aguirre, G.; Boiani, M.; Cerecetto, H.; Fernández, M.; González, M.; León, E.; Pintos, C.; Raymondo, S.; Arredondo, C.; Pacheco, J., *Pharmazie.,* **2006,** *61*, 54-59.

140. Zaffiri, L.; Gardner, J.; Toledo-Pereyra, L. H., *J. Invest. Surg.,* **2012,** *25*, 67-77.

141. Brown, E. D.; Wright, G. D., *Nature,* **2016,** *529*, 336-343.

142. Naeem, A.; Badshah, S. L.; Muska, M.; Ahmad, N.; Khan, K., *Molecules,* **2016,** *21*, 268-287.

143. Lloyd, N. C.; Morgan, H. W.; Nicholson, B. K.; Ronimus, R. S., *Angew. Chem. Int. Ed.,* **2005,** *44*, 941-944.

144. Levy, S. B.; Marshall, B., *Nat. Med.,* **2004,** *10*, 122-129.

145. Friedman, N. D.; Temkin, E.; Carmeli, Y., *Clin. Microbiol. Infect.,* **2016,** *22*, 416-422.

146. Penchovsky, R.; Traykovska, M., *Expert Opin. Drug Discov.,* **2015,** *10*, 631-650.

147. Ventola, C. L., *Pharm. Ther.,* **2015,** *40*, 277-283.

148. Roca, I.; Akova, M.; Baquero, F.; Carlet, J.; Cavaleri, M.; Coenen, S.; Cohen, J.; Findlay, D.; Gyssens, I.; Heure, O. E., *New Microbes New Infect.,* **2015,** *6*, 22-29.

149. Clardy, J.; Fischbach, M. A.; Walsh, C. T., *Nat. Biotech.,* **2006,** *24*, 1541-1550.

150. Patridge, E.; Gareiss, P.; Kinch, M. S.; Hoyer, D., *Drug Discov. Today,* **2016,** *21*, 204-207.

151. Wenzel, R.; Bate, G.; Kirkpatrick, P., *Nat. Rev. Drug Discov.,* **2005,** *4*, 809-810.

152. Fang, F. C., *J. Clin. Invest.,* **1997,** *99*, 2818-2825.

153. Chakravortty, D.; Hensel, M., *Microb. Infect.,* **2003,** *5*, 621-627.

154. Napoli, C.; Ignarro, L. J., *Arch. Pharm. Res.,* **2009,** *32*, 1103-1108.

155. Carpenter, A. W.; Schoenfisch, M. H., *Chem. Soc. Rev.,* **2012,** *41*, 3742-3752.

156. Carpenter, A. W.; Slomberg, D. L.; Rao, K. S.; Schoenfisch, M. H., *ACS Nano.,* **2011,** *5*, 7235-7244.

157. Hetrick, E. M.; Shin, J. H.; Paul, H. S.; Schoenfisch, M. H., *Biomaterials,* **2009,** *30*, 2782-2789.

158. Fershtat, L.; Makhova, N. N., *ChemMedChem.,* **2017,** *12*, 622-628.

159. Galkina, I. V.; Takhautdinova, G. L.; Tudrii, E. V.; Yusupova, L. M.; Falyakhov, I. F.; Pozdeev, O. K.; Shulaeva, M. P.; Kipenskaya, L. V.; Sakhibullina, V. G.; Krivolapov, D. B., *Russ. J. Org. Chem.,* **2013,** *49*, 591-597.

160. Segretti, N. D.; Serafim, R. A. M.; Segretti, M. C. F.; Miyata, M.; Coelho, F. R.; Augusto, O.; Ferreira, E. I., *Bioorg. Med. Chem. Lett.,* **2016,** *26*, 3988-3993.

161. Boiani, L. a.; Aguirre, G.; González, M.; Cerecetto, H.; Chidichimo, A.; Cazzulo, J. J.; Bertinaria, M.; Guglielmo, S., *Bioorg. Med. Chem.,* **2008,** *16*, 7900-7907.

162. Pricker, S. P., *Gold Bull.,* **1996,** *29*, 53-60.

163. Higby, G. J., *Gold Bull.,* **1982,** *15*, 130-140.

164. Berners-Price, S. J., Gold-Based Therapeutic Agents: A New Perspective. In *Bioinorganic Medicinal Chemistry*, Alessio, E., Ed. Wiley-VCH Verlag GmbH & Co. KGaA: 2011; pp 197-222.

165. Farrer, N. J.; Sadler, P. J., Medicinal Inorganic Chemistry: State of the Art, New Trends, and a vision of the Future. In *Bioinorganic Medicinal Chemistry*, Alessio, E., Ed. John Wiley & Sons: 2011; pp 1-37.

166. Che, C.-M.; Sun, R. W.-Y., *ChemComm.,* **2011,** *47*, 9554-9560.

167. Casini, A.; Sun, R. W.-Y.; Ott, I., Medicinal Chemistry of Gold Anticancer Metallodrugs. In *Metallo-Drugs: Development and Action of Anticancer Agents: Development and Action of Anticancer Agents*, Sigel, A.; Sigel, H.; Freisinger, E.; Sigel, R., Eds. Walter de Gruyter GmbH & Co KG: 2018; pp 199-221.

168. Fung Sin, K.; Zou, T.; Cao, B.; Lee, P. Y.; Fung Yi Man, E.; Hu, D.; Lok, C. N.; Che, C. M., *Angew. Chem.,* **2017,** *129*, 3950-3954.

169. Tan, J.; Sivaram, H.; Huynh, H. V., *Appl. Organomet. Chem.,* **2018,** *32*, 4441-4448.

170. Zhang, C.; Hemmert, C.; Gornitzka, H.; Cuvillier, O.; Zhang, M.; Sun, R. W. Y., *ChemMedChem.,* **2018**, *0*, 1218-1229.

171. Ott, I.; Biot, C.; Hartinger, C., AAS, XRF, and MS Methods in Chemical Biology of Metal Complexes. In *Inorganic Chemical Biology: Principles, Techniques and Applications*, Gasser, G., Ed. Wiley: 2014; pp 63-90.

172. Tu, S.; Wai-Yin Sun, R.; Lin Marie, C. M.; Tao Cui, J.; Zou, B.; Gu, Q.; Kung, H. F.; Che, C. M.; Wong Benjamin, C. Y., *Cancer,* **2009,** *115*, 4459-4469.

173. Messori, L.; Abbate, F.; Marcon, G.; Orioli, P.; Fontani, M.; Mini, E.; Mazzei, T.; Carotti, S.; O'Connell, T.; Zanello, P., *J. Med. Chem.,* **2000,** *43*, 3541-3548.

174. Yang, T.; Tu, C.; Zhang, J.; Lin, L.; Zhang, X.; Liu, Q.; Ding, J.; Xu, Q.; Guo, Z., *Dalton Trans.,* **2003,** *17*, 3419-3424.

175. Beckman, J. S.; Koppenol, W. H., *Am. J. Physiol. Cell Physiol.,* **1996,** *271*, C1424-C1437.

176. Butler, A. R.; Pearson, R. J., Vasodilators for Biological Research. In *Nitric Oxide Donors*, Wiley-VCH Verlag GmbH & Co. KGaA: 2005; pp 201-231.

177. Yetik-Anacak, G.; Catravas, J. D., *Curr. Vasc. Pharmacol.,* **2006,** *45*, 268-276.

178. Bill Cai, T.; Wang, P. G.; Holder, A. A., NO and NO Donors. In *Nitric Oxide Donors: for Pharmacetical and Biological Applications*, Taniguchi, N.; Bill Cai, T., Eds. Wiley-VCH Verlag GmbH & Co. KGaA: 2005; pp 1-31.

179. Investigators, E. T., *The Lancet,* **2015,** *385*, 617-628.

180. Marsh, N.; Marsh, A., *Clin. Exp. Pharmacol. Physiol.,* **2000,** *27*, 313-319.

181. Beckman, J. S., The Physiological and Pathological Chemistry of Nitric Oxide. In *Nitric Oxide*, Lancaster, J., Ed. Academic Press: San Diego, 1996; pp 1-82.

182. McCleverty, J. A., *Chem. Rev.,* **2004,** *104*, 403-418.

183. Lancaster Jr, J.; Stuehr, D. J., The Intracellular Reactions of Nitric Oxide in the Immune System and Its Enzymatic Synthesis. In *Nitric Oxide*, Lancaster, J., Ed. Academic Press: San Diego, 1996; pp 139-175.

184. Nathan, C., *J. Clin. Invest.,* **1997,** *100*, 2417-2423.

185. Dasgupta, T. P.; Aquart, D. V., Metal–NO Complexes: Structures, Syntheses, Properties and NO-Releasing Mechanisms. In *Nitric Oxide Donors: for Pharmaceutical and Biological Applications*, Taniguchi, N.; Bill Cai, T., Eds. Wiley-VCH Verlag GmbH & Co. KGaA: 2005; pp 109-129.

186. Butler, A. R.; Glidewell, C.; Li, M.-H., Nitrosyl Complexes of Iron-Sulfur Clusters. In *Advances in Inorganic Chemistry*, Sykes, A. G., Ed. Academic Press: 1988; pp 335-393.

187. Kobsar, A.; Eigenthaler, M., NO Donors As Antiplatelet Agents. In *Nitric Oxide Donors: for Pharmaceutical and Biological Applications*, Taniguchi, N.; Bill Cai, T., Eds. Wiley-VCH Verlag GmbH & Co. KGaA: 2005; pp 233-253.

188. Janero, D. R.; Garvey, D. S., Nitric Oxide Donors As Anti-Platelet Agents for Thromboembolic Disorders: Clinical Status and Therapeutic Prognosis. In *Nitric Oxide Donors: for Pharmaceutical and Biological Applications*, Taniguchi, N.; Bill Cai, T., Eds. Wiley-VCH Verlag GmbH & Co. KGaA: 2005; pp 299-328.

189. Murphy, S.; Simmons, M. L.; Agullo, L.; Garcia, A.; Feinstein, D. L.; Galea, E.; Reis, D. J.; Minc-Golomb, D.; Schwartz, J. P., *Trends Neurosci.,* **1993,** *16*, 323-328.

190. Law, A.; Gauthier, S.; Quirion, R., *Brain Res. Rev.,* **2001,** *35*, 73-96.

191. MacMicking, J.; Xie, Q.-w.; Nathan, C., *Annu. Rev. Immunol.,* **1997,** *15*, 323-350.

192. Rath, M.; Müller, I.; Kropf, P.; Closs, E. I.; Munder, M., *Front. Immunol.,* **2014,** *5*, 532-542.

193. Garcia-Bonilla, L.; Moore, J. M.; Racchumi, G.; Zhou, P.; Butler, J. M.; Iadecola, C.; Anrather, J., *J. Immunol.,* **2014**, *5*, 2531-2537.

194. Crack, J. C.; Green, J.; Thomson, A. J.; Brun, N. E. L., *Acc. Chem. Res.,* **2014,** *47*, 3196-3205.

195. Fitzpatrick, J.; Kim, E., *Acc. Chem. Res.,* **2015,** *48*, 2453-2461.

196. Yang, T.; Peleli, M.; Zollbrecht, C.; Giulietti, A.; Terrando, N.; Lundberg, J. O.; Weitzberg, E.; Carlström, M., *Free Radic. Biol. Med.,* **2015,** *83*, 159-166.

197. Ignarro, L. J., 3 - Nitric Oxide as a Communication Signal in Vascular and Neuronal Cells A2 - Lancaster, Jack. In *Nitric Oxide*, Academic Press: San Diego, 1996; pp 111-137.

198. Di Silvio, M.; Nussler, A. K.; Geller, D. A.; Billiar, T. R., A Role for Nitric Oxide in Liver Inflammation and Infection. In *Nitric Oxide*, Lancaster, J., Ed. Academic Press: San Diego, 1996; pp 219-236.

199. Lushchak, O. V.; Piroddi, M.; Galli, F.; Lushchak, V. I., *Redox Rep.,* **2014,** *19*, 8-15.

200. Sanchez-Padilla, J.; Guzman, J. N.; Ilijic, E.; Kondapalli, J.; Galtieri, D. J.; Yang, B.; Schieber, S.; Oertel, W.; Wokosin, D.; Schumacker, P. T., *Nat. Neurosci.,* **2014,** *17*, 832-840.

201. Cornforth, D., Role of Nitric Oxide in Treatment of Foods. In *Nitric Oxide*, Lancaster, J., Ed. Academic Press: San Diego, 1996; pp 259-287.

202. Jeney, V.; Ramos, S.; Bergman, M.-L.; Bechmann, I.; Tischer, J.; Ferreira, A.; Oliveira-Marques, V.; Janse, C. J.; Rebelo, S.; Cardoso, S., *Cell Rep.,* **2014,** *8*, 126-136.

203. Hollocher, T. C., The Enzymology and Occurrence of Nitric Oxide in the Biological Nitrogen Cycle. In *Nitric Oxide*, Lancaster, J., Ed. Academic Press: San Diego, 1996; pp 289-344.

204. Fajardo, C.; Mora, M.; Fernández, I.; Mosquera-Corral, A.; Campos, J. L.; Méndez, R., *Chemosphere,* **2014,** *97*, 10-15.

205. Cena, C.; Bertinaria, M.; Boschi, D.; Giorgis, M.; Gasco, A., *Arkivoc.,* **2006,** *7*, 301-309.

206. Burov, O. N.; Kletskii, M. E.; Fedik, N. S.; Lisovin, A. V.; Kurbatov, S. V., *Chem. Heterocycl. Com.,* **2015,** *51*, 951-960.

207. Kletskii, M. E.; Burov, O. N.; Fedik, N. S.; Kurbatov, S. V., *Nitric Oxide,* **2017,** *62*, 44-51.

208. Albini, A., *Heterocyclic N-oxides*. Taylor & Francis: 1991, pp 20-150.

209. Gasco, A.; Schoenafinger, K., The NO-Releasing Heterocycles. In *Nitric Oxide Donors: for Pharmaceutical and Biological Applications*, Taniguchi, N.; Bill Cai, T., Eds. Wiley-VCH Verlag GmbH & Co. KGaA: 2005; pp 131-175.

210. Li, Y.; Zhang, Z.; Ge, Z.; Wang, B.; Lai, W.; Luo, Y., *Chinese J. Chem.,* **2013,** *31*, 520-524.

211. Wang, P. G.; Xian, M.; Tang, X.; Wu, X.; Wen, Z.; Cai, T.; Janczuk, A. J., *Chem. Rev.,* **2002,** *102*, 1091-1134.

212. Manna, K.; Banik, U.; Ghosh, P. S.; Das, M., *Nirma Univ. J. Pharm. Sci.,* **2014,** *1*, 37-49.

213. Serafim, R. A. M.; de Oliveira, T. F.; Loureiro, A. P. M.; Krogh, R.; Andricopulo, A. D.; Dias, L. C.; Ferreira, E. I., *Med. Chem. Res.,* **2017,** *26*, 760-769.

214. Wang, J. a. L. J. a. L. Q. a. H. Y. a. D. H., *Propellants Explos. Pyrotech.,* **2008,** *33*, 347--352.

215. Liu, N.; Li, Y.-n.; Zeman, S.; Shu, Y.-j.; Wang, B.-z.; Zhou, Y.-s.; Zhao, Q.-l.; Wang, W.-l., *CrystEngComm.,* **2016,** *18*, 2843-2851.

216. Schiefer, I. T.; VandeVrede, L.; Fa', M.; Arancio, O.; Thatcher, G. R. J., *J. Med. Chem.,* **2012,** *55*, 3076-3087.

217. Bohn, H. a. B. J. a. M. P. A. a. S. K., *Br. J. Pharmacol.,* **1995,** *114*, 1605--1612.

218. Bian, H.; Feng, J.; Li, M.; Xu, W., *Bioorg. Med. Chem. Lett.,* **2011,** *21*, 7025-7029.

219. Ghosh, P.; Whitehouse, M., *J. Med. Chem.,* **1969,** *12*, 505-507.

220. Wieland, H., *Liebigs Ann.,* **1904**, *0*, 154-255.

221. Sorba, G.; Medana, C.; Fruttero, R.; Cena, C.; Di Stilo, A.; Galli, U.; Gasco, A., *J. Med. Chem.,* **1997,** *40*, 463-469.

222. Gasco, A.; Fruttero, R.; Sorba, G.; Di Stilo, A.; Calvino, R., *Pure Appl. Chem.,* **2004,** *76*, 973-981.

223. Balendiran Ganesaratnam, K.; Dabur, R.; Fraser, D., *Cell Biochem. Funct.,* **2004,** *22*, 343-352.

224. Calvino, R.; Ferrarotti, B.; Gasco, A.; Serafino, A., *J. Heterocycl. Chem.,* **1983,** *20*, 1419-1421.

225. Takayama, H.; Shirakawa, S.; Kitajima, M.; Aimi, N.; Yamaguchi, K.; Hanasaki, Y.; Ide, T.; Katsuura, K.; Fujiwara, M.; Ijichi, K., *Bioorg. Med. Chem. Lett.,* **1996,** *6*, 1993-1996.

226. Bahrami, K., *Tetrahedron Lett.,* **2006,** *47*, 2009-2012.

227. Bennett, M. A.; Smith, A. K., *Dalton Trans.,* **1974,** *2*, 233-241

228. Vock, C. A.; Scolaro, C.; Phillips, A. D.; Scopelliti, R.; Sava, G.; Dyson, P. J., *J. Med. Chem.,* **2006,** *49*, 5552-5561.

229. Dolomanov, O. V.; Bourhis, L. J.; Gildea, R. J.; Howard, J. A. K.; Puschmann, H., *J. Appl. Crystallogr.,* **2009,** *42*, 339-341.

230. Bourhis, L. J.; Dolomanov, O. V.; Gildea, R. J.; Howard, J. A. K.; Puschmann, H., *Acta Cryst.,* **2015,** *71*, 59-75

231. Coats, N.; Katritzky, A., *J. Org. Chem.,* **1959,** *24*, 1836-1837.

232. Xia, Y.; Dawson, V. L.; Dawson, T. M.; Snyder, S. H.; Zweier, J. L., *Proc. Natl. Acad. Sci.,* **1996,** *93*, 6770-6774.

233. Giulivi, C.; Poderoso, J. J.; Boveris, A., *J. Biol. Chem.,* **1998,** *273*, 11038-11043.

234. Matsubara, R.; Ando, A.; Saeki, Y.; Eda, K.; Asada, N.; Tsutsumi, T.; Shin, Y. S.; Hayashi, M., *J. Heterocycl. Chem.,* **2016,** *53*, 1094-1105.

235. Matsubara, R.; Katsuragi, Y.; Sakaguchi, T.; Eguchi, S.; Hayashi, M.; Ando, A., *Tetrahedron,* **2018,** *74*, 3642-3651.

236. Nand, B.; Khanna, G.; Chaudhary, A.; Lumb, A.; Khurana, J., *Curr. Org. Chem.,* **2015,** *19*, 790-812.

237. Quin, L. D.; Tyrell, J. A., *Fundamentals of Heterocyclic Chemistry: Importance in Nature and in the Synthesis of Pharmaceuticals*. Wiley: 2010; pp 189-191.

238. Fershtat, L. L.; Epishina, M. A.; Ovchinnikov, I. V.; Struchkova, M. I.; Romanova, A. A.; Ananyev, I. V.; Makhova, N. N., *Tetrahedron Lett.,* **2016,** *57*, 5685-5689.

239. Muller, P., Glossary of terms used in physical organic chemistry (IUPAC Recommendations 1994). In *Pure and Applied Chemistry*, 1994; p 1077.

240. Ponzio, G., *Gazz. Chim. Ital.,* **1927,** *57*, 117-122.

241. Whitham, G. H., *Organosulfur Chemistry*. Oxford Chemistry Press: 1995; pp 20-27.

242. Caron, S.; Ghosh, A., Nucleophilic Aromatic Substitution. In *Practical Synthetic Organic Chemistry: Reactions, Principles, and Techniques*, Caron, S., Ed. John Wiley & Sons, Inc.: Hoboken, NJ, USA, 2011; pp 237-253.

243. Simpkins, N. S., *Sulphones in Organic Synthesis*. Pergamon Press: England, 1993; pp 120-198.

244. Sato, H., *B. Chem. Soc. JPN.,* **1965,** *38*, 1719-1721.

245. Smith, J. R. L.; Norman, R. O. C.; Walker, W. M., *J. Chem. Soc.,* **1968**, *0*, 269-274.

246. Cerecetto, H.; González, M.; Seoane, G.; Stanko, C.; Piro, O. E.; Castellano, E. E., *J. Braz. Chem. Soc.,* **2004,** *15*, 232-240.

247. Hwang, K.-J.; Jo, I.; Shin, Y. A.; Yoo, S.-e.; Lee, J. H., *Tetrahedron Lett.,* **1995,** *36*, 3337-3340.

248. Brittelli, D. R.; Boswell Jr, G. A., *J. Org. Chem.,* **1981,** *46*, 312-315.

249. Chafin, A. P.; Erickson, E. D., *Org. mass spectrom.,* **1985,** *20*, 276-280.

250. Ungnade, H. E.; Loughran, E. D., *J. Heterocycl. Chem.,* **1964,** *1*, 61-66.

251. Boyer, N. E.; Czerniak, G. M.; Gutowsky, H. S.; Snyder, H. R., *J. Am. Chem. Soc.,* **1955,** *77*, 4238-4241.

252. Mallory, F. B.; Cammarata, A., *J. Am. Chem. Soc.,* **1966,** *88*, 61-64.

253. Eaton, G. R.; Eaton, S. S.; Barr, D. P.; Weber, R. T., *Quantitative EPR*. Springer Science & Business Media: 2010.

254. Chu, G., *J. Biol. Chem.,* **1994,** *269*, 787-790.

255. Cairns, R. A.; Harris, I. S.; Mak, T. W., *Nat. Rev. Cancer,* **2011,** *11*, 85-95.

256. Feelisch, M.; Schönafingeri, K.; Noack, H., *Biochem. Pharmacol.,* **1992,** *44*, 1149-1157.

257. Schnelldorfer, T.; Gansauge, S.; Gansauge, F.; Schlosser, S.; Beger, H. G.; Nussler, A. K., *Cancer,* **2000,** *89*, 1440-1447.

258. Honda, T.; Coppola, S.; Ghibelli, L.; Cho, S. H.; Kagawa, S.; Spurgers, K. B.; Brisbay, S. M.; Roth, J. A.; Meyn, R. E.; Fang, B., *Cancer Gene Ther.,* **2004,** *11*, 249-255.

259. Hamilton, T. C.; Winker, M. A.; Louie, K. G.; Batist, G.; Behrens, B. C.; Tsuruo, T.; Grotzinger, K. R.; McKoy, W. M.; Young, R. C.; Ozols, R. F., *Biochem. Pharmacol.,* **1985,** *34*, 2583-2586.

260. Xie, X.; Zhao, Y.; Ma, C. Y.; Xu, X. M.; Zhang, Y. Q.; Wang, C. G.; Jin, J.; Shen, X.; Gao, J. L.; Li, N., *Br. J. Pharmacol.,* **2015,** *172*, 3929-3943.

261. Eisenberg, R.; Meyer, C. D., *Acc. Chem. Res.,* **1975,** *8*, 26-34.

262. Salerno, J. C., Nitric Oxide Complexes of Metalloproteins: An Introductory Overview. In *Nitric Oxide*, Lancaster, J., Ed. Academic Press: San Diego, 1996; pp 83-110.

263. Hogg, N., *Free Radic. Biol. Med.,* **2010,** *49*, 122-129.

264. Vanin, A. F.; Huisman, A.; Van Faassen, E. E., Iron dithiocarbamate as spin trap for nitric oxide detection: pitfalls and successes. In *Methods in Enzymology*, Elsevier: 2002; pp 27-42.

265. Komarov, A.; Mattson, D.; Jones, M. M.; Singh, P. K.; Lai, C. S., *Biochem. Biophys. Res. Commun.,* **1993,** *195*, 1191-1198.

266. Petit, C.; Bernardes-Genisson, V.; Hoffmann, P.; Souchard, J. P.; Labidalle, S., *Braz. J. Med. Biol. Res.,* **1999,** *32*, 1407-1412.

267. Oae, S.; Yoshihara, M.; Tagaki, W., *B. Chem. Soc. JPN.,* **1967,** *40*, 951-958.

268. Kukolich, S. G.; Huffman, D. R., *Chem. Phys. Lett.,* **1991,** *182*, 263-265.

269. Hoffman, R. A.; Langrehr, J. M.; Simmons, R. L., Role of Nitric Oxide in Allograft Rejection. In *Nitric Oxide*, Lancaster, J., Ed. Academic Press: San Diego, 1996; pp 237-257.

270. Kolomeichuk, S. N.; Nizhnik, Y. P.; Makhova, N. N.; Ovchinnikov, I. V., *Chem. Heterocycl. Com.,* **2018,** *54*, 70-75.

271. Ischiropoulos, H.; Zhu, L.; Beckman, J. S., *Arch. Biochem. Biophys.,* **1992,** *298*, 446-451.

272. Gross, S. S.; Wolin, M. S., *Ann. Rev. Physiol.,* **1995,** *57*, 737-769.

273. Davis, K. L.; Martin, E.; Turko, I. V.; Murad, F., *Ann. Rev. Pharmacol. Toxicol.,* **2001,** *41*, 203-236.

274. Silhavy, T. J.; Kahne, D.; Walker, S., *Cold Spring Harb. Perspect. Biol.,* **2010,** *2*, 414-430.

275. Monod, J., *Annu. Rev. Microbiol.,* **1949,** *3*, 371-394

276. Verschuuren, G.; M., *Regression and Curve In Excel 2013 for Scientists*. 3 ed.; Holy Macro! Books: 2014, pp. 220-224.

277. Dimmeler, S.; Haendeler, J.; Nehls, M.; Zeiher, A. M., *J. Exp. Med.,* **1997,** *185*, 601-608.

278. Li, J.; Billiar, T. R.; Talanian, R. V.; Kim, Y. M., *Biochem. Biophys. Res. Commun.,* **1997,** *240*, 419-424.

279. Colasanti, M.; Salvati, L.; Venturini, G.; Ascenzi, P.; Gradoni, L., *Trends Parasitol.,* **2001,** *17*, 575.

280. Wu, Q.; Zhu, W.; Xiao, H., *RSC Adv.,* **2014,** *4*, 34454-34459.

281. Guo, T.; Liu, M.; Huang, X.-C.; Wang, Z.-j.; Qiu, S.-j.; Ge, Z.-x.; Meng, Z.-h., *J. Anal. Appl. Pyrolysis,* **2017,** *128*, 451-458.

282. Abadeer, N. S.; Murphy, C. J., *J. Phys. Chem. C.,* **2016,** *120*, 4691-4716.

283. Azimzadeh, M.; Rahaie, M.; Nasirizadeh, N.; Ashtari, K.; Naderi-Manesh, H., *Biosens. Bioelectron.,* **2016,** *77*, 99-106.

284. Her, S.; Jaffray, D. A.; Allen, C., *Adv. Drug Deliv. Rev.,* **2017,** *109*, 84-101.

285. Arambula, J. F.; McCall, R.; Sidoran, K. J.; Magda, D.; Mitchell, N. A.; Bielawski, C. W.; Lynch, V. M.; Sessler, J. L.; Arumugam, K., *Chem. Sci.,* **2016,** *7*, 1245-1256.

286. Chaves, J. D. S.; Tunes, L. G.; de J. Franco, C. H.; Francisco, T. M.; Corrêa, C. C.; Murta, S. M. F.; Monte-Neto, R. L.; Silva, H.; Fontes, A. P. S.; de Almeida, M. V., *Eur. J. Med. Chem.,* **2017,** *127*, 727-739

287. Casini, A.; Hartinger, C.; Gabbiani, C.; Mini, E.; Dyson, P. J.; Keppler, B. K.; Messori, L., *J. Inorg. Biochem.,* **2008,** *102*, 564-575.

288. Zou, T.; Lum, C. T.; Lok, C.-N.; Zhang, J.-J.; Che, C.-M., *Chem. Soc. Rev.,* **2015,** *44*, 8786-8801.

289. Lum, C. T.; Sun, R. W.-Y.; Zou, T.; Che, C.-M., *Chem. Sci.,* **2014,** *5*, 1579-1584.

290. Altaf, M.; Monim-ul-Mehboob, M.; Kawde, A.-N.; Corona, G.; Larcher, R.; Ogasawara, M.; Casagrande, N.; Celegato, M.; Borghese, C.; Siddik, Z. H., *Oncotarget,* **2017,** *8*, 490-505.

291. Fung Sin, K.; Zou, T.; Cao, B.; Lee, P. Y.; Fung Yi Man, E.; Hu, D.; Lok, C. N.; Che, C. M., *Angew. Chem.,* **2017,** *129*, 3950-3954.

292. Lammer, A. D.; Cook, M. E.; Sessler, J. L., *J. Porphyr. Phthalocyanines,* **2015,** *19*, 398-403.

293. Amani, V.; Abedi, A.; Ghabeshi, S.; Khavasi, H. R.; Hosseini, S. M.; Safari, N., *Polyhedron,* **2014,** *79*, 104-115.

294. Bindoli, A.; Rigobello, M. P.; Scutari, G.; Gabbiani, C.; Casini, A.; Messori, L., *Coord. Chem. Rev.,* **2009,** *253*, 1692-1707.

295. Mohamed, M. M.; Sloane, B. F., *Nat. Rev. Cancer,* **2006,** *6*, 764-775.

296. Urig, S.; Fritz-Wolf, K.; Réau, R.; Herold-Mende, C.; Tóth, K.; Davioud-Charvet, E.; Becker, K., *Angew. Chem. Int. Ed.,* **2006,** *45*, 1881-1886.

297. Schmidt, C.; Karge, B.; Misgeld, R.; Prokop, A.; Franke, R.; Brönstrup, M.; Ott, I., *Chem. Eur. J.,* **2016,** *23*, 1869-1880.

298. Joyce, J. A.; Baruch, A.; Chehade, K.; Meyer-Morse, N.; Giraudo, E.; Tsai, F.-Y.; Greenbaum, D. C.; Hager, J. H.; Bogyo, M.; Hanahan, D., *Cancer Cell,* **2004,** *5*, 443-453.

299. Short, S. P.; Williams, C. S., *Adv. Cancer Res. Treat.,* **2017,** *136*, 49-83.

300. Messner, D. J.; Murray, K. F.; Kowdley, K. V., Mechanisms of Hepatocyte Detoxification. In *Physiology of the Gastrointestinal Tract*, 5 ed.; Ghishan, F. K.; Kaunitz, J. D.; Merchant, J. L.; Said, H. M.; Wood, J. D., Eds. Academic Press: Boston, 2012; pp 1507-1527.

301. Arnér, E. S. J.; Holmgren, A., *Semin. Cancer Biol.,* **2006,** *16*, 420-426.

302. Mukherjee, A.; Martin, S. G., *Br. J. radiol.,* **2008,** *81*, S57-S68.

303. Urig, S.; Becker, K., *Semin. Cancer Biol.,* **2006,** *16*, 452-465.

304. Ott, I.; Qian, X.; Xu, Y.; Vlecken, D. H. W.; Marques, I. J.; Kubutat, D.; Will, J.; Sheldrick, W. S.; Jesse, P.; Prokop, A., *J. Med. Chem.,* **2009,** *52*, 763-770.

305. Liu, C.; Liu, Z.; Li, M.; Li, X.; Wong, Y.-S.; Ngai, S.-M.; Zheng, W.; Zhang, Y.; Chen, T., *PLOS one,* **2013,** *8*, e53945.

306. Elie, B. T.; Pechenyy, Y.; Uddin, F.; Contel, M., *J. Biol. Inorg. Chem.,* **2018,** *23*, 399-411.

307. Fernandez-Gallardo, J.; Elie, B. T.; Sanau, M.; Contel, M., *ChemComm.,* **2016,** *52*, 3155-3158.

308. Santini, C.; Pellei, M.; Gandin, V.; Porchia, M.; Tisato, F.; Marzano, C., *Chem. Rev.,* **2013,** *114*, 815-862.

309. Jaividhya, P.; Dhivya, R.; Akbarsha, M. A.; Palaniandavar, M., *J. Inorg. Biochem.,* **2012,** *114*, 94-105.

310. Rajarajeswari, C.; Loganathan, R.; Palaniandavar, M.; Suresh, E.; Riyasdeen, A.; Akbarsha, M. A., *Dalton Trans.,* **2013,** *42*, 8347-8363.

311. Usman, M.; Zaki, M.; Khan, R. A.; Alsalme, A.; Ahmad, M.; Tabassum, S., *RSC Adv.,* **2017,** *7*, 36056-36071.

312. Boodram Janine, N.; McGregor Iain, J.; Bruno Peter, M.; Cressey Paul, B.; Hemann Michael, T.; Suntharalingam, K., *Angew. Chem.,* **2016,** *128*, 2895-2900.

313. Tisato, F.; Marzano, C.; Porchia, M.; Pellei, M.; Santini, C., *Med. Res. Rev.,* **2010,** *30*, 708-749.

314. Wehbe, M.; Leung, A. W. Y.; Abrams, M. J.; Orvig, C.; Bally, M. B., *Dalton Trans.,* **2017,** *46*, 10758-10773.

315. Wardman, P.; Candeias, L. P., *Radiat. Res.,* **1996,** *145*, 523-531.

316. Mawani, Y.; Orvig, Essential Metal Related Metabolic Disorders. In *Bioinorganic Medicinal Chemistry*, Alessio, E., Ed. Wiley-VCH Verlag GmbH &Co. KGaA, 2011; pp 315-318.

317. Daniel, K. G.; Gupta, P.; Harbach, R. H.; Guida, W. C.; Dou, Q. P., *Biochem. Pharmacol.,* **2004,** *67*, 1139-1151.

318. Rajkumar, S. V.; Richardson, P. G.; Hideshima, T.; Anderson, K. C., *J. Clin. Oncol.,* **2005,** *23*, 630-639.

319. Adsule, S.; Barve, V.; Chen, D.; Ahmed, F.; Dou, Q. P.; Padhye, S.; Sarkar, F. H., *J. Med. Chem.,* **2006,** *49*, 7242-7246.

320. Liu, N.; Liu, C.; Li, X.; Liao, S.; Song, W.; Yang, C.; Zhao, C.; Huang, H.; Guan, L.; Zhang, P.; Liu, S.; Hua, X.; Chen, X.; Zhou, P.; Lan, X.; Yi, S.; Wang, S.; Wang, X.; Dou, Q. P.; Liu, J., *Sci. Rep.,* **2014,** *4*, 5240.

321. Low, M. L.; Chan, C. W.; Ng, P. Y.; Ooi, I. H.; Maah, M. J.; Chye, S. M.; Tan, K. W.; Ng, S. W.; Ng, C. H., *J. Coord. Chem.,* **2017,** *70*, 223-241.

322. Sîrbu, A.; Palamarciuc, O.; Babak, M. V.; Lim, J. M.; Ohui, K.; Enyedy, E. A.; Shova, S.; Darvasiová, D.; Rapta, P.; Ang, W. H., *Dalton Trans.,* **2017,** *46*, 3833-3847.

323. Chan, C. W.; Lai, J. W.; Ooi, H.; Er, H. M.; Chye, S. M.; Tan, K. W.; Ng, S. W.; Maah, M. J.; Ng, C. H., *Inorg. Chim. Acta,* **2016,** *450*, 202-210.

324. Feng, D.-Q.; Zhou, X.-P.; Zheng, J.; Chen, G.-h.; Huang, X.-C.; Li, D., *Dalton Trans.,* **2012,** *41*, 4255-4261.

325. Czerwińska, K.; Golec, M.; Skonieczna, M.; Palion-Gazda, J.; Zygadło, D.; Szlapa-Kula, A.; Krompiec, S.; Machura, B.; Szurko, A., *Dalton Trans.,* **2017,** *46*, 3381-3392.

326. Sheldrick, G. M., *Acta Crystall. C.,* **2015,** *71*, 3-8.

327. Li, J. J., Kröhnke pyridine synthesis. In *Name Reactions*, Springer: 2009; pp 323-324.

328. Scheme, B. G. R., **2010**.

329. Bratsos, I.; Gianferrara, T.; Alessio, E.; Hartinger, C.; Jakupec, M.; Keppler, B., Ruthenium and other Non-platinum Anticancer Compounds. Alessio, E., Ed. Wiley-VCH Verlag GmbH & Co. KGaA: Weinheim, 2011; pp 151-170.

330. Irving, H.; Williams, R., *Dalton Trans.,* **1953**, *0*, 3192-3210.

331. Kostova, I., *Anticancer Agents Med. Chem.,* **2006,** *6*, 19-32.

332. Uson, R.; Laguna, A.; Laguna, M.; Briggs, D. A.; Murray, H. H.; Fackler Jr, J. P., *Inorg. Synth.,* **1989,** *26*, 85-91.

333. Ayers, P. W.; Parr, R. G.; Pearson, R. G., *J. Chem. Phys.,* **2006,** *124*, 194107-194115.

334. Bambynek, W.; Crasemann, B.; Fink, R. W.; Freund, H. U.; Mark, H.; Swift, C. D.; Price, R. E.; Rao, P. V., *Rev. Mod. Phys.,* **1972,** *44*, 716-813.

335. Sun, D.; Wei, Z.-H.; Yang, C.-F.; Wang, D.-F.; Zhang, N.; Huang, R.-B.; Zheng, L.-S., *CrystEngComm.,* **2011,** *13*, 1591-1601.

336. Mautner, F. A.; Gspan, C.; Gatterer, K.; Goher, M. A. S.; Abu-Youssef, M. A. M.; Bucher, E.; Sitte, W., *Polyhedron,* **2004,** *23*, 1217-1224.

337. Zhu, X.-Y.; Gong, J.-S.; Li, H.; Lu, Z.-M.; Shi, J.-S.; Xu, Z.-H., *Chem. Pap.,* **2014,** *68*, 739-744.

338. Wang, G.; Zhang, H.; Zhao, J.; Li, W.; Cao, J.; Zhu, C.; Li, S., *Angew. Chem. Int. Ed.,* **2016,** *55*, 5985-5989.

339. Sycheva, T. P.; Pavlova, T. N.; Shchukina, M. N., *Pharm. Chem. J.,* **1972,** *6*, 696-698.

340. Publishing, W. A., Isoniazid. In *Pharmaceutical Manufacturing Encyclopedia (Third Edition)*, 3rd ed.; William Andrew, P., Ed. William Andrew Publishing: Oxford, 2007; pp 1969-1970.

341. Liang, Z.; He, L.; Wang, W.; Zhou, Z.; Ren, Z., *Can. J. Chem. Eng.,* **2018,** *96*, 679-687.

342. Scriven, E. F. V.; Murugan, R., *Kirk-Othmer Encyclopedia of Chemical Technology,* **2000**.

343. Grasselli, R. K., *J. Chem. Educ.,* **1986,** *63*, 216-221.

344. Cavani, F.; Centi, G.; Marion, P., Catalytic ammoxidation of hydrocarbons on mixed oxides. In *Metal oxide catalysis*, Jackson, D.; Hargreaves, J., Eds. Wiley Online Library: 2008; pp 771-818.

Appendix A. Supplementary Information for Chapter 2

^{1}H NMR spectrum for L1(-NO_2)

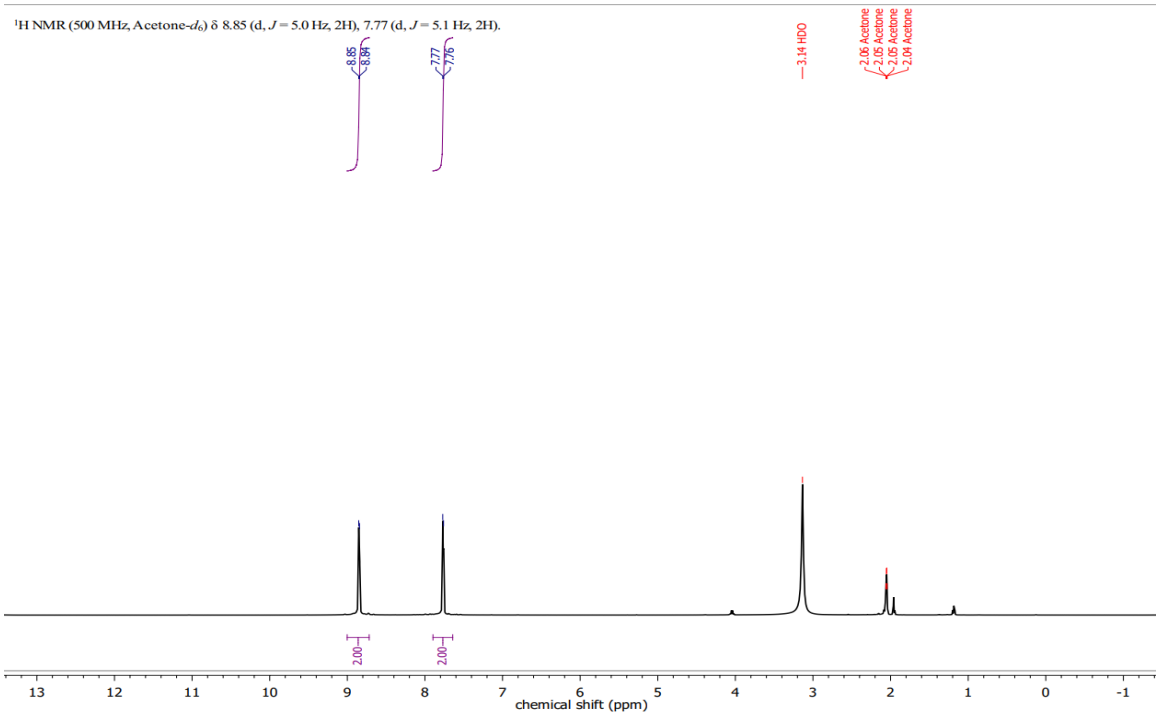

Solvent impurities: δ 1.20 (t, $CH_2C\boldsymbol{H}_3$, ethyl acetate), 1.96 (s, CH_3, acetic acid), 4.05 (q, $C\boldsymbol{H}_2CH_3$, ethyl acetate).

^{13}C NMR spectrum for L1(-NO_2)

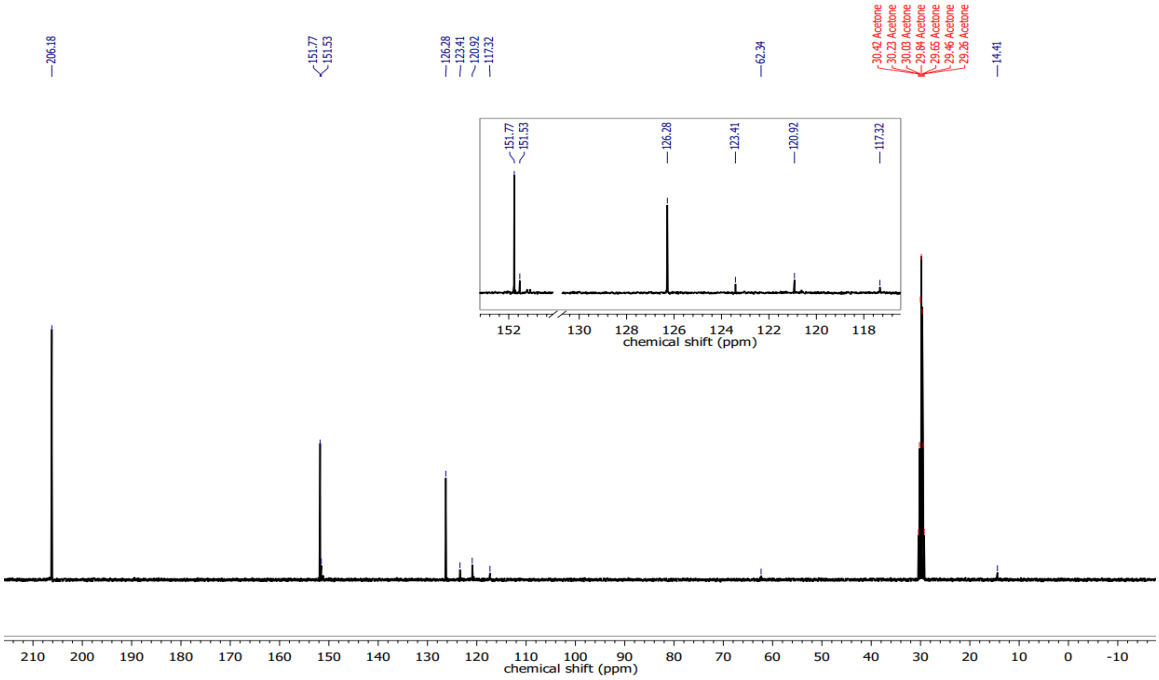

Solvent impurities: δ 14.41 (CH_3, ethyl acetate), 62.34 (CH_2, ethyl acetate), 206.18 (CO, $(CD_3)_2CO$ signal).

HMBC spectra for L1(-NO_2)

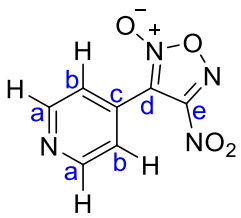

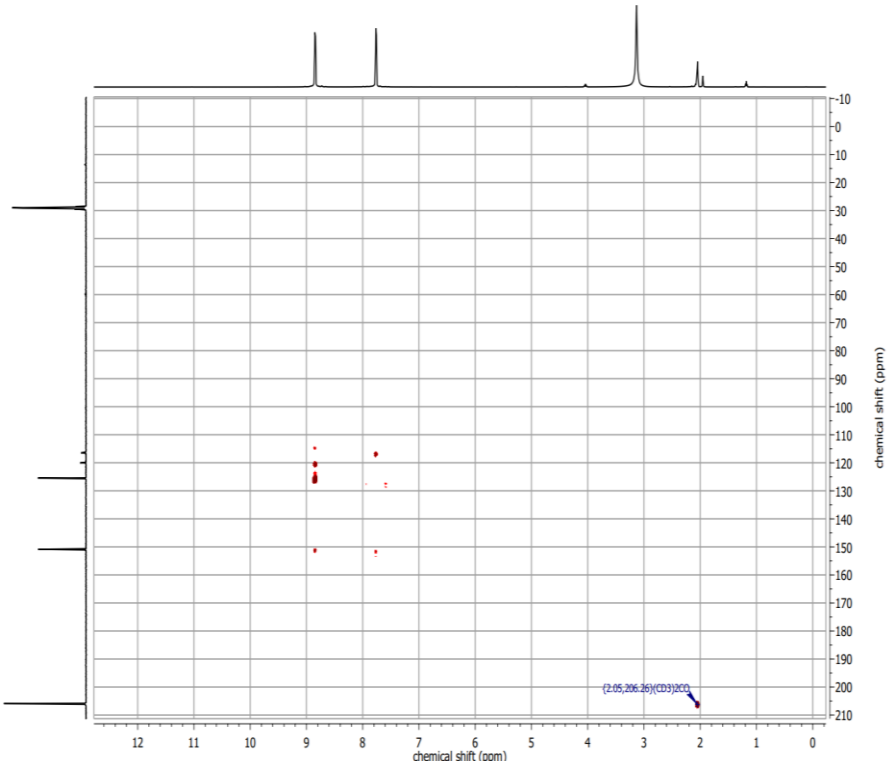

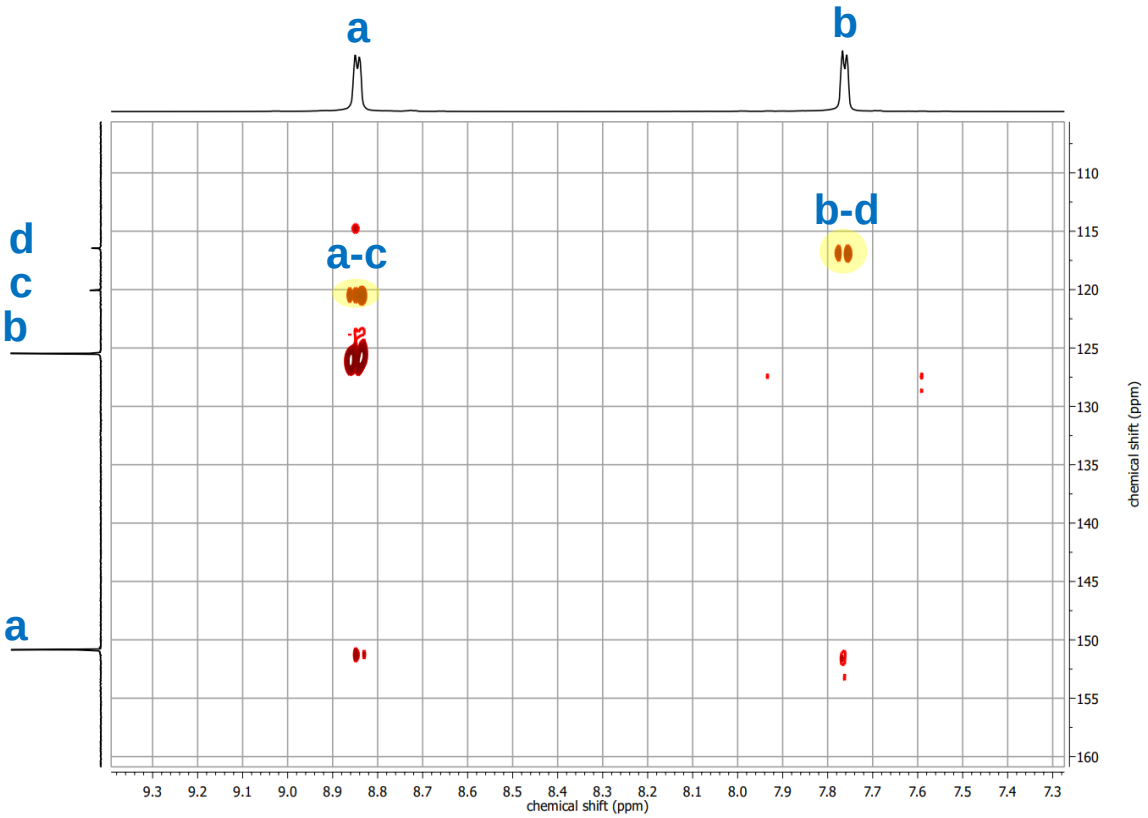

^{1}H-^{15}N HMBC spectrum of L1(-NO_2) at 300 K

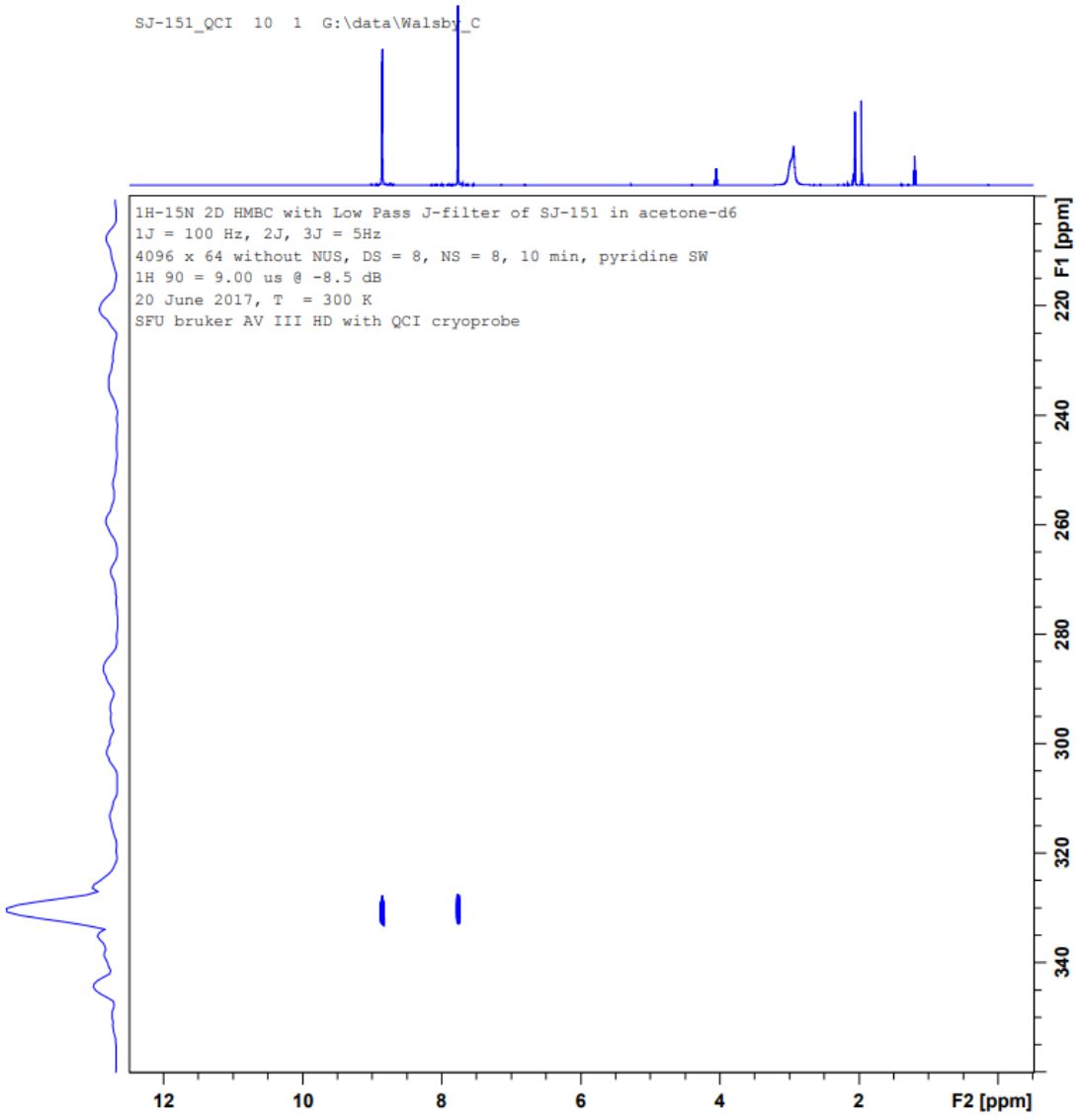

Electrospray ionization mass spectrum (positive) for L1(-NO_2)

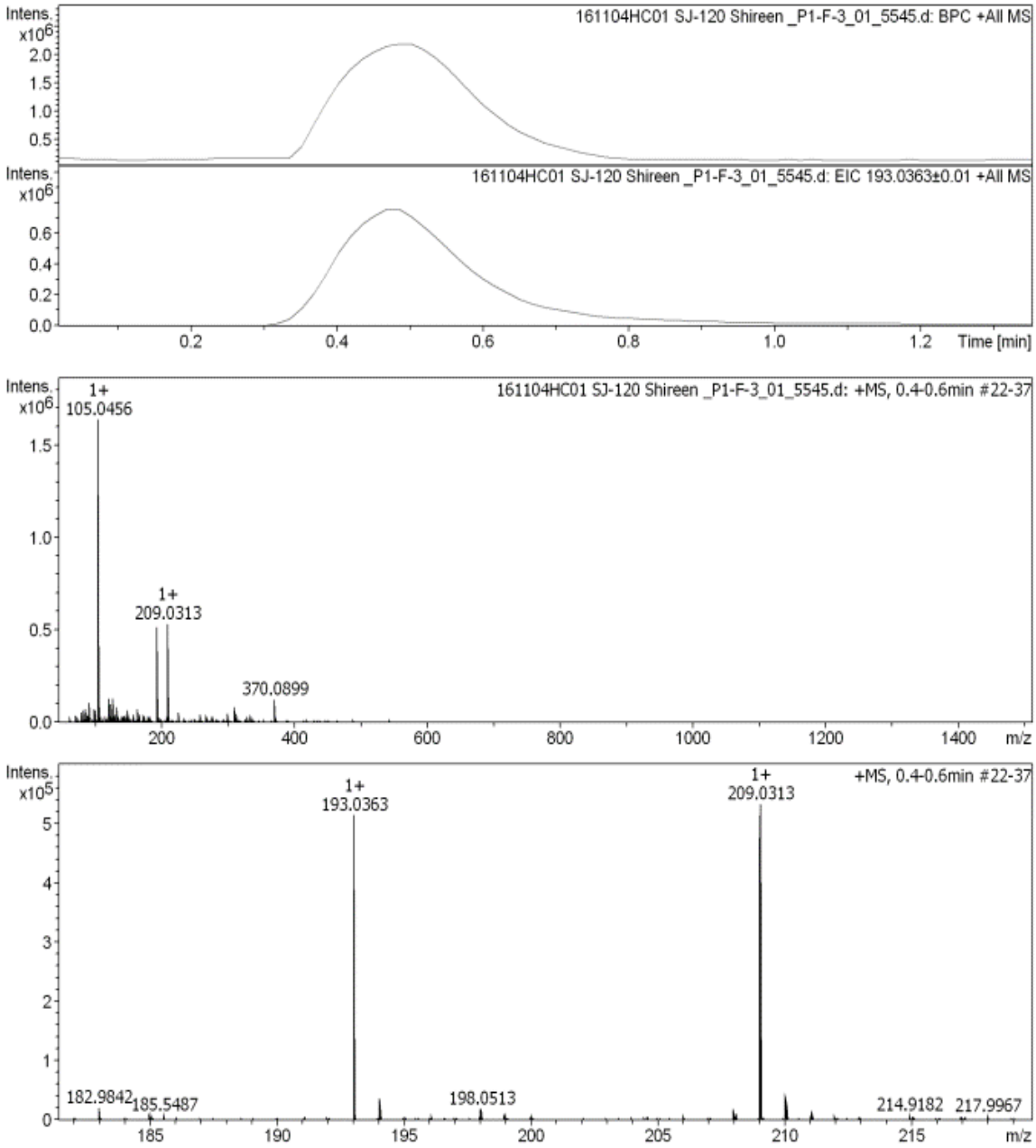

$[M+H]^+$ calculated 209.0311 found 209.0313; $[M+H-O]^+$ calculated 193.0362 found 193.0363; [M-NO-CNO_2+H] calculated 105.0453 found 105.0456.

^{1}H NMR spectrum for L2(-H)

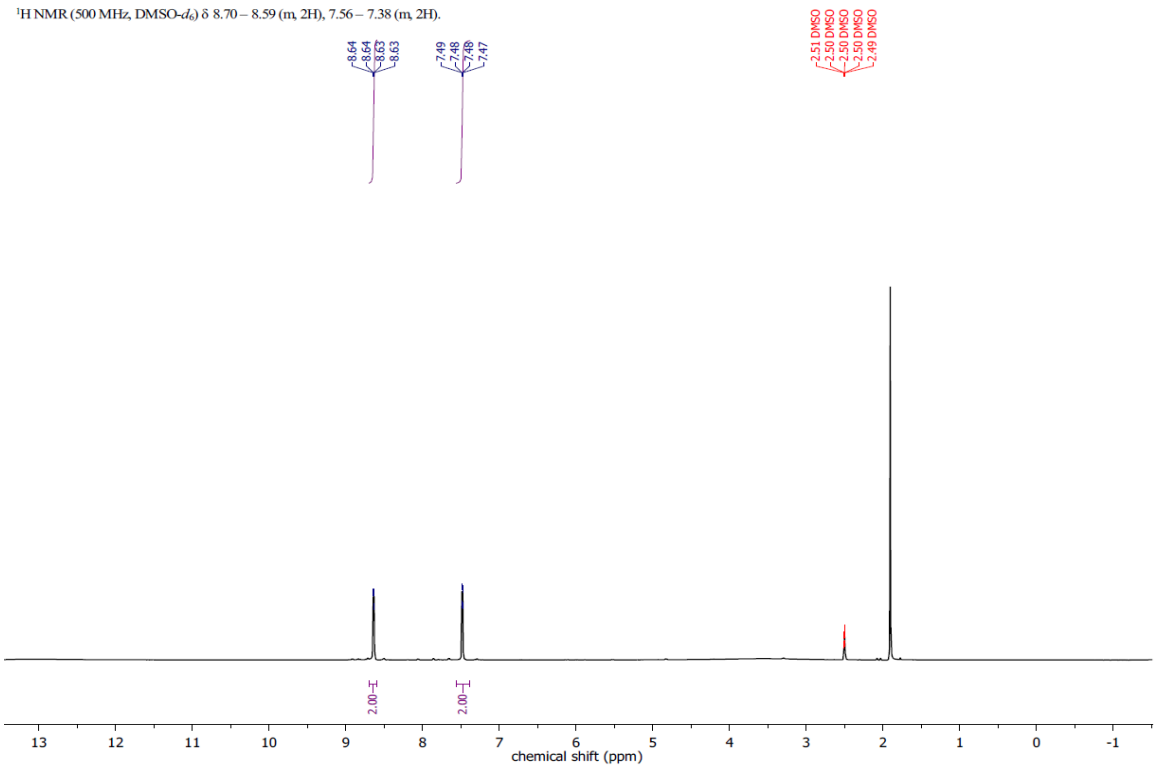

Solvent impurities: δ 1.96 (s, CH_3, acetic acid).

^{13}C NMR spectrum for L2(-H)

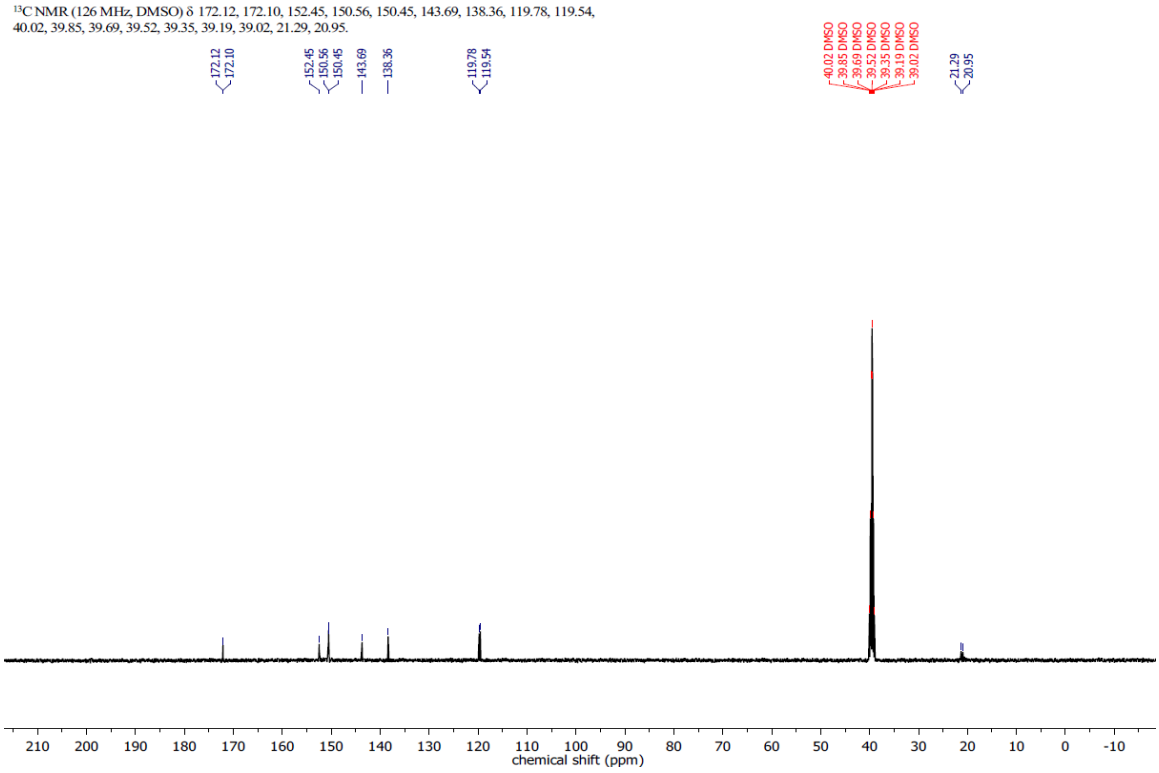

Solvent impurities: δ 172.10 (CO, acetic acid).

HMBC spectra for L2(-H)

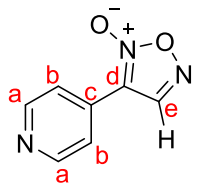

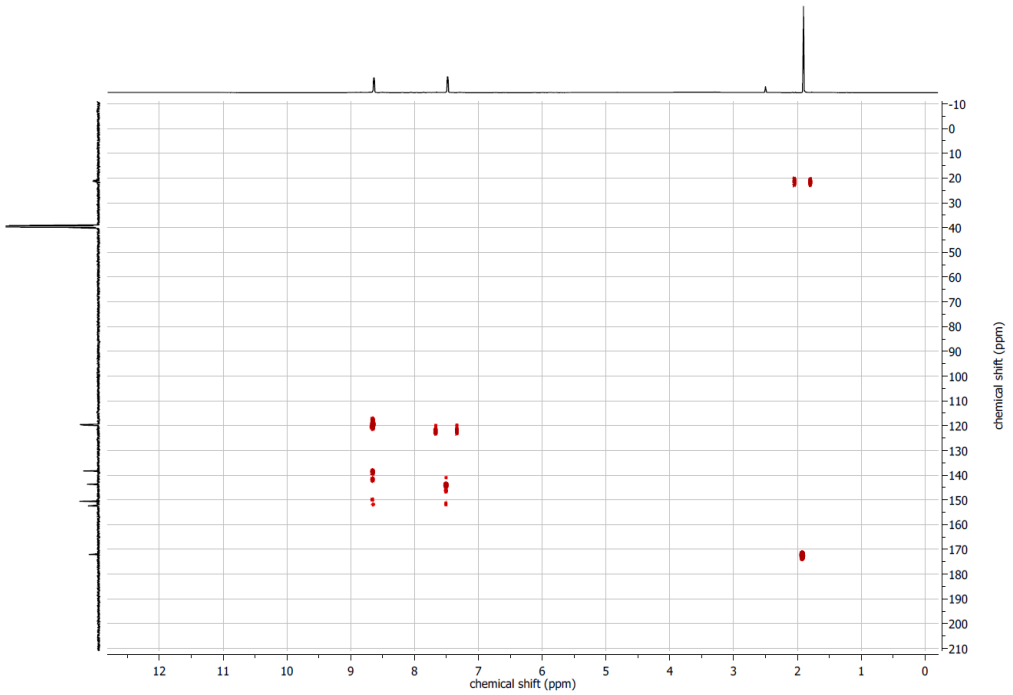

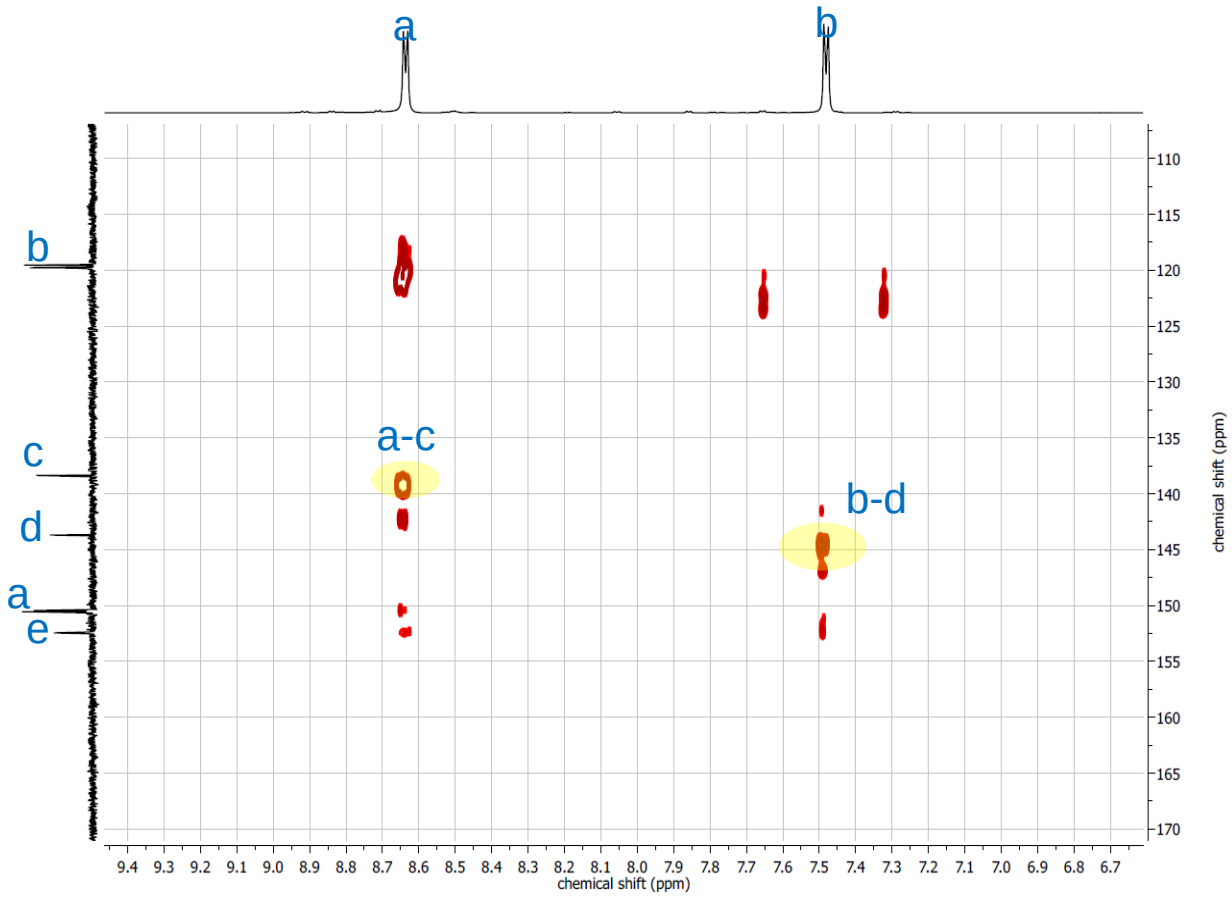

Electrospray ionization mass spectrum (positive) for L2(-H)

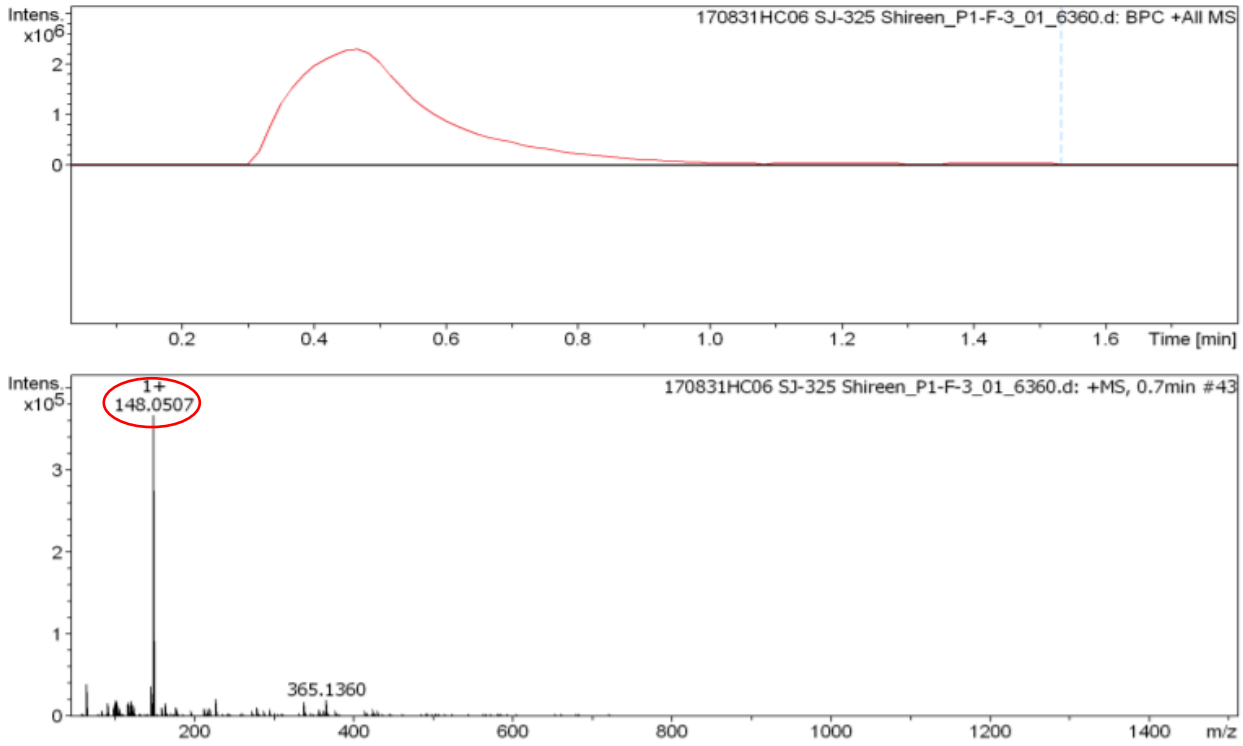

$[M+H-O]^+$ calculated 148.0511 found 148.0507.

Electrospray ionization mass spectrum (positive) for L2(-H)

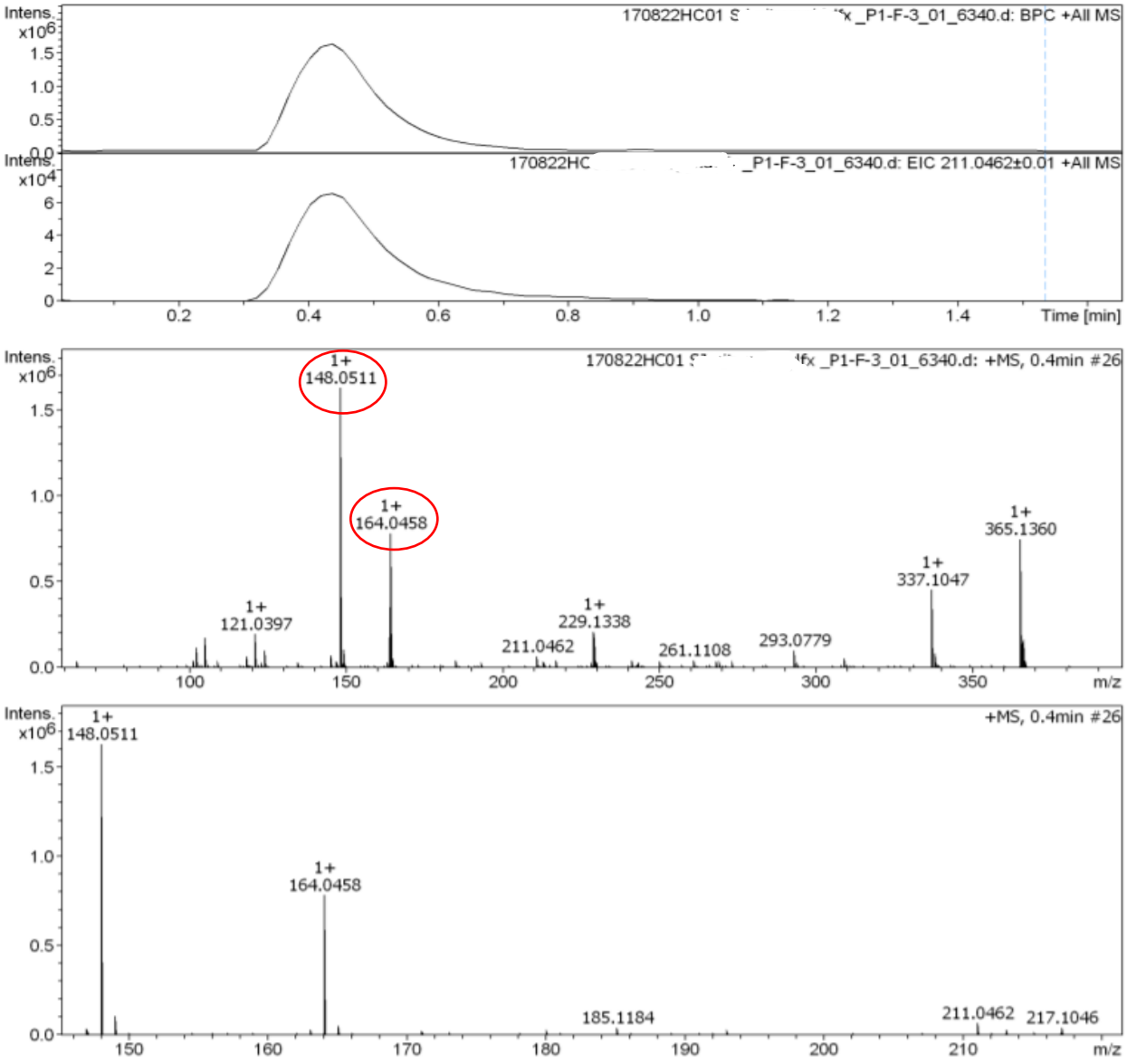

$[M+H]^+$ calculated 164.0460 found 164.0458; $[M+H-O]^+$ calculated 148.0511 found 148.0511.

^{1}H NMR spectrum for L3(-OCH_3)

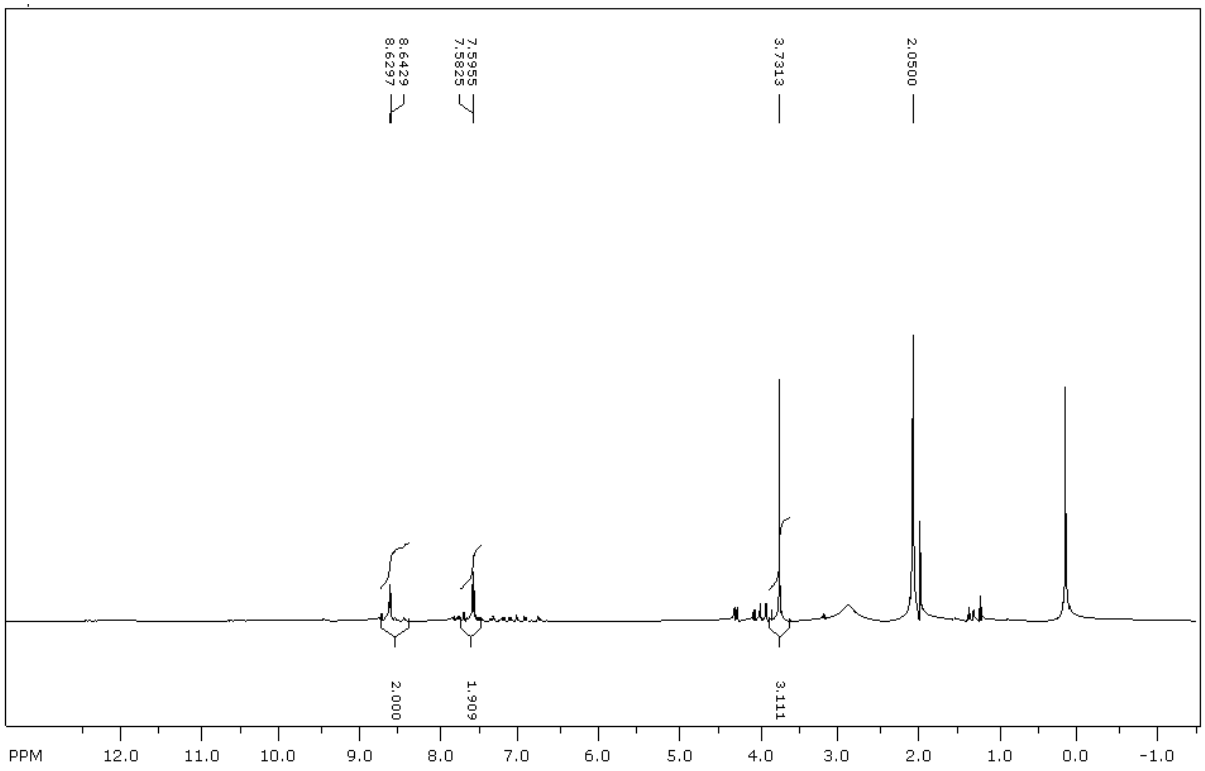

Solvent impurities: δ 1.3 (s, silicon grease), 1.96 (s, CH_3, acetic acid), 4.05 (q, C***H***$_2CH_3$, ethyl acetate).

^{13}C NMR spectrum for L3(-OCH_3)

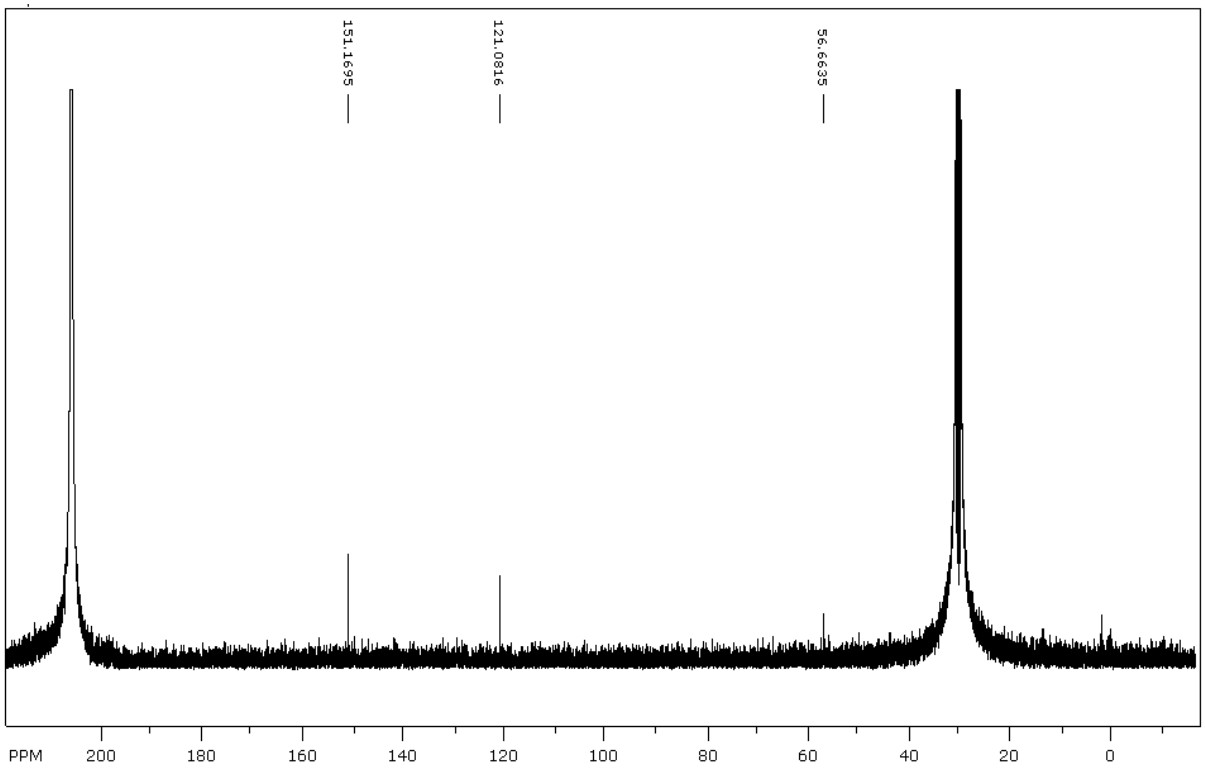

Electrospray ionization mass spectrum (positive) for L3(-OCH_3)

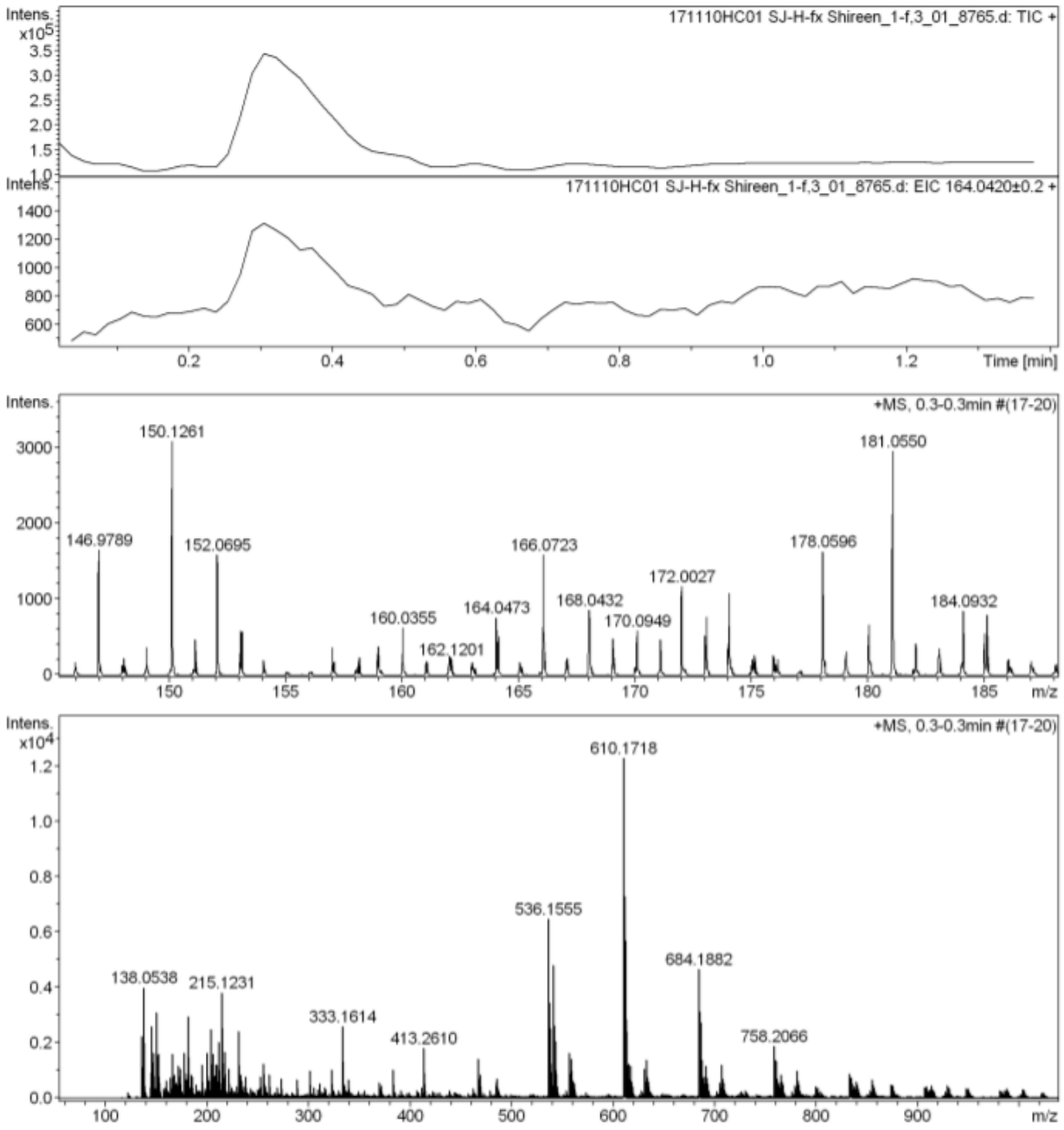

$[M+H-NO]^+$ calculated 164.0586 found 164.0473; $[M+H-O]^+$ calculated 178.0617 found 178.0596; $[M+H-NO-Me]^+$ calculated 152.0586 found 152.0695.

^{1}H NMR spectrum for L4(-OPh)

^{1}H NMR (400 MHz, Chloroform-*d*) δ 8.85 – 8.78 (m, 2H), 7.61 – 7.51 (m, 2H), 7.25 – 7.18 (m, 2H), 6.99 – 6.73 (m, 3H).

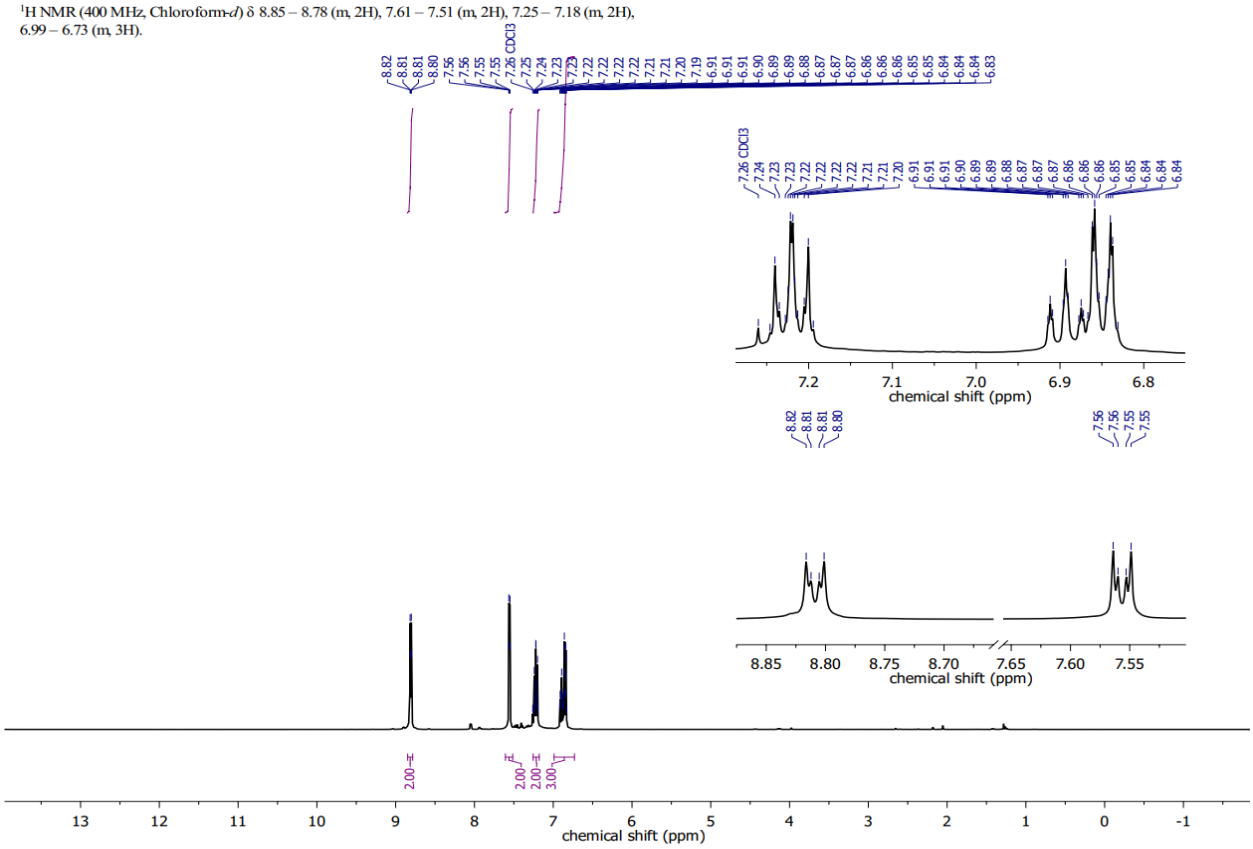

^{13}C NMR spectrum for L4(-OPh)

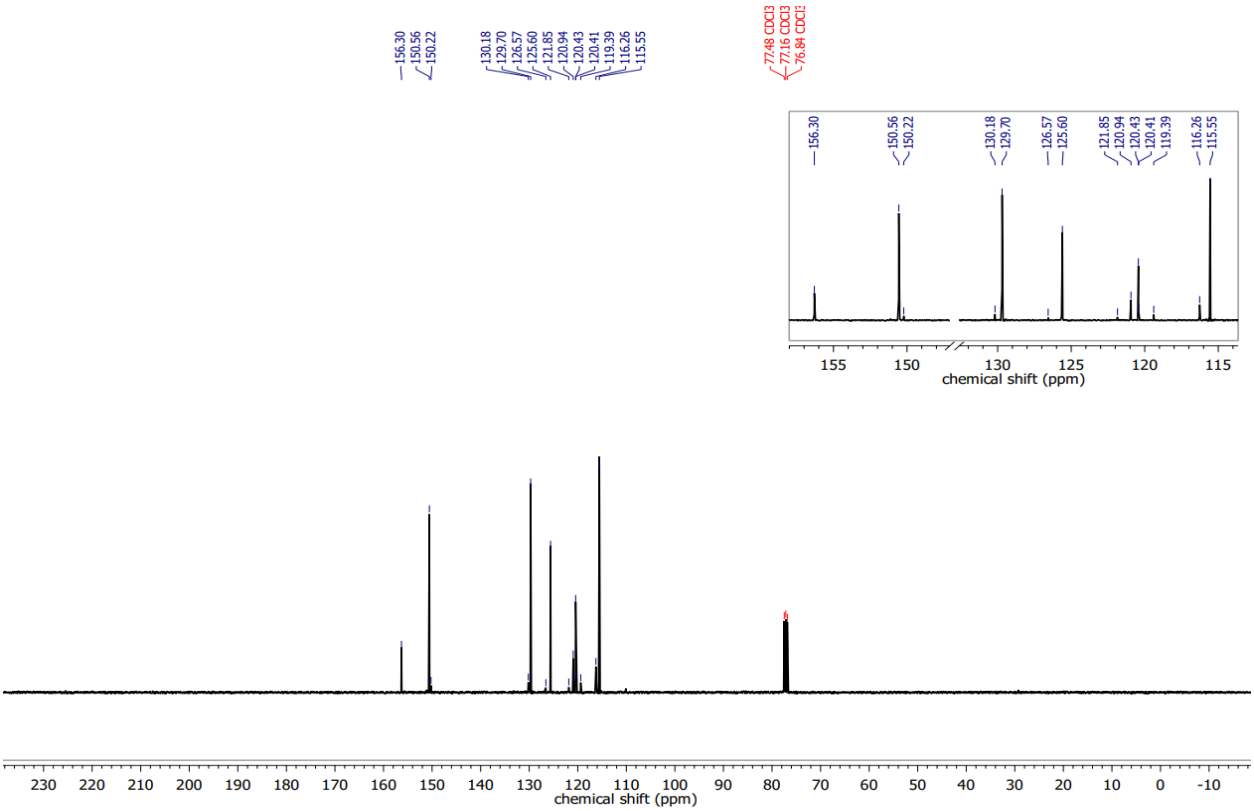

HMBC spectra for L4(-OPh)

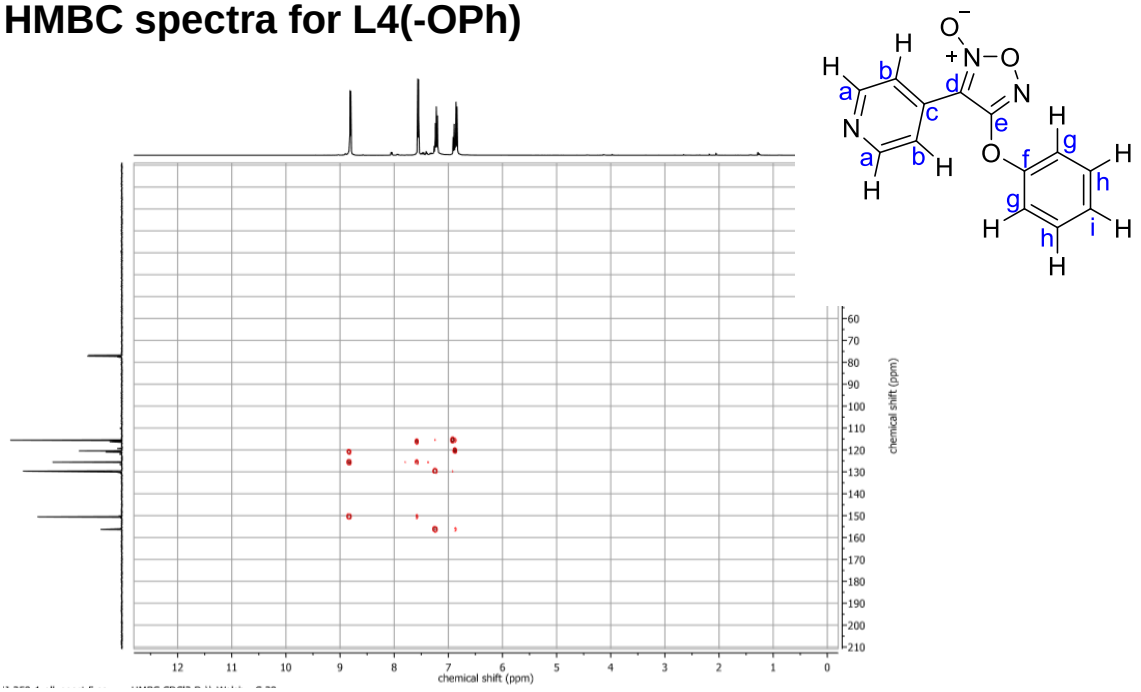

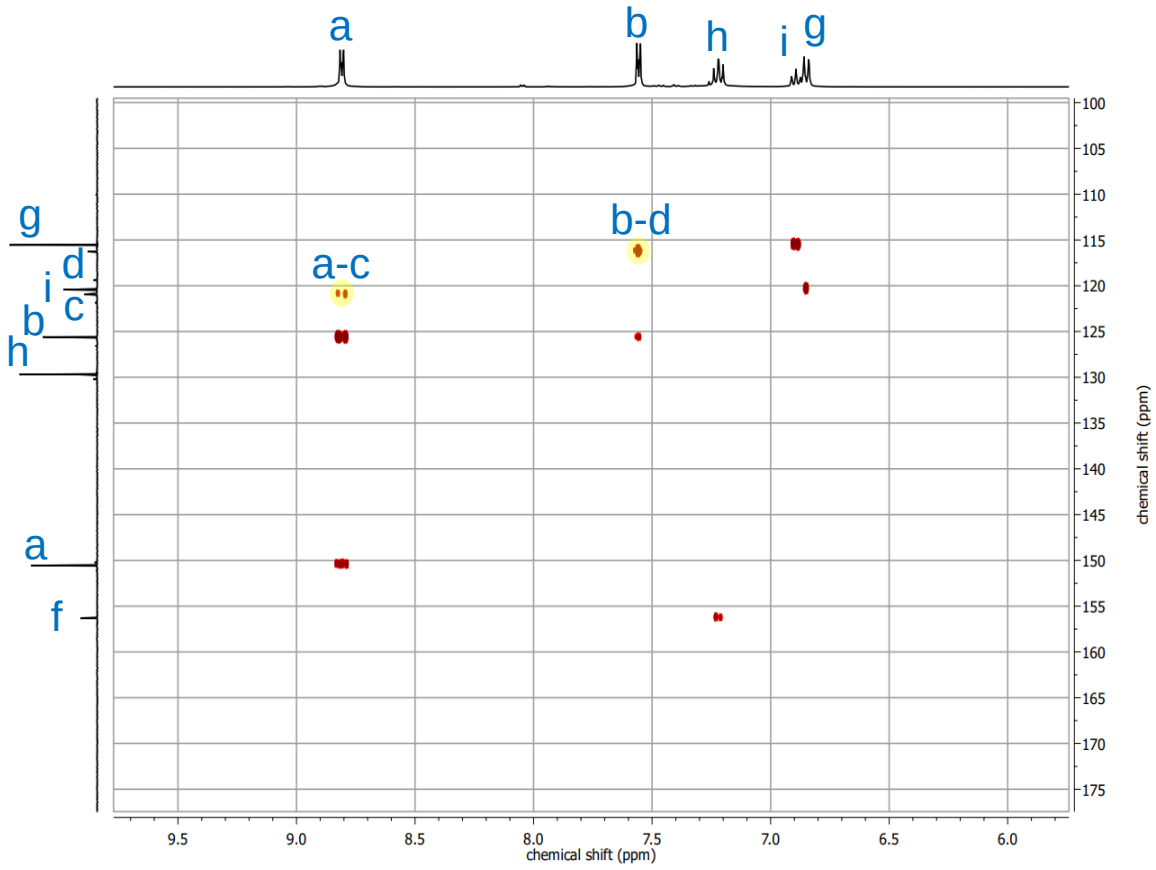

Electrospray ionization mass spectrum (positive) for L4(-OPh)

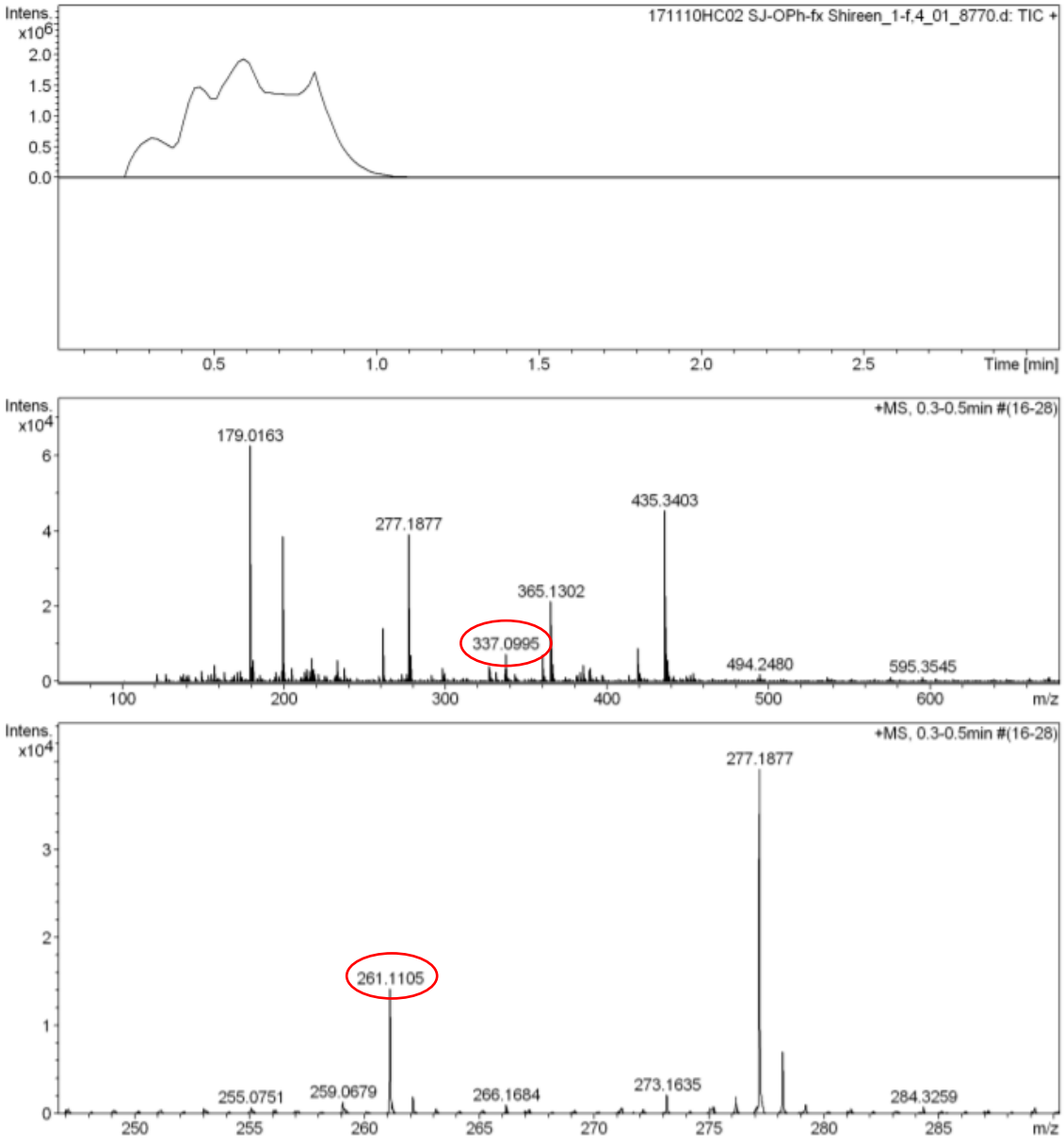

$[M - O + Na]^+$ calculated mass 261.0522, found 261.1105; $[C_{13}H_{11}N_3O_4 + ACN + Na]^+$ calculated 337.0908, found 337.0995.

^{1}H NMR spectrum for L5(-SPh)

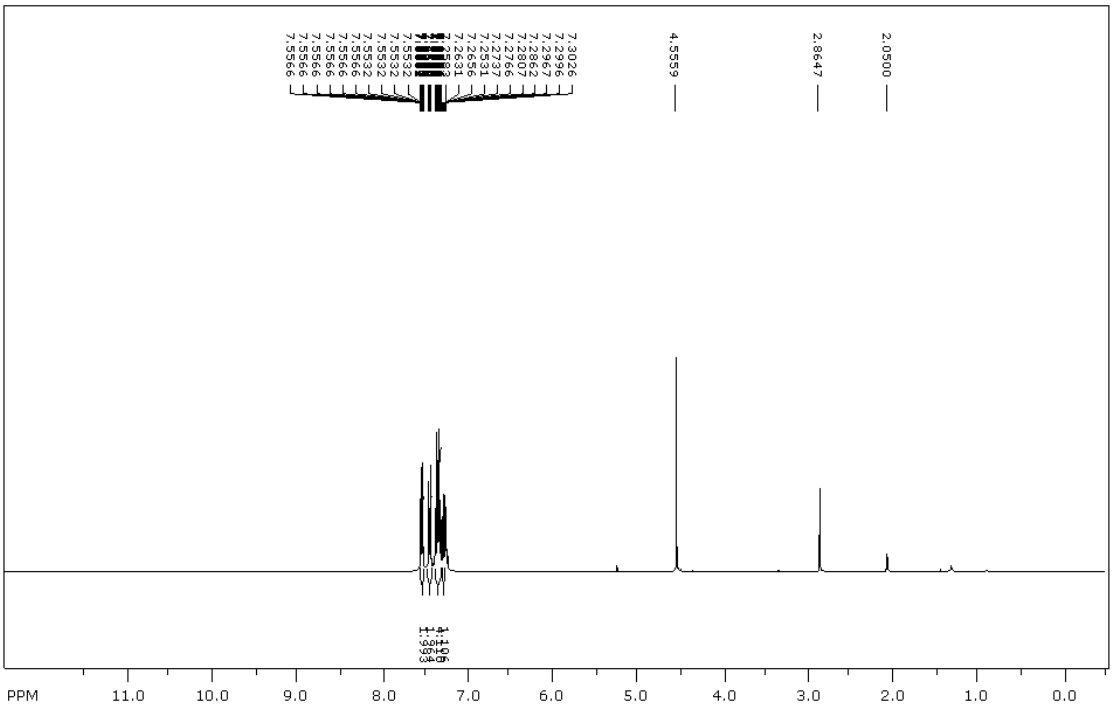

Solvent impurities: δ 2.84 (s, OH, water).

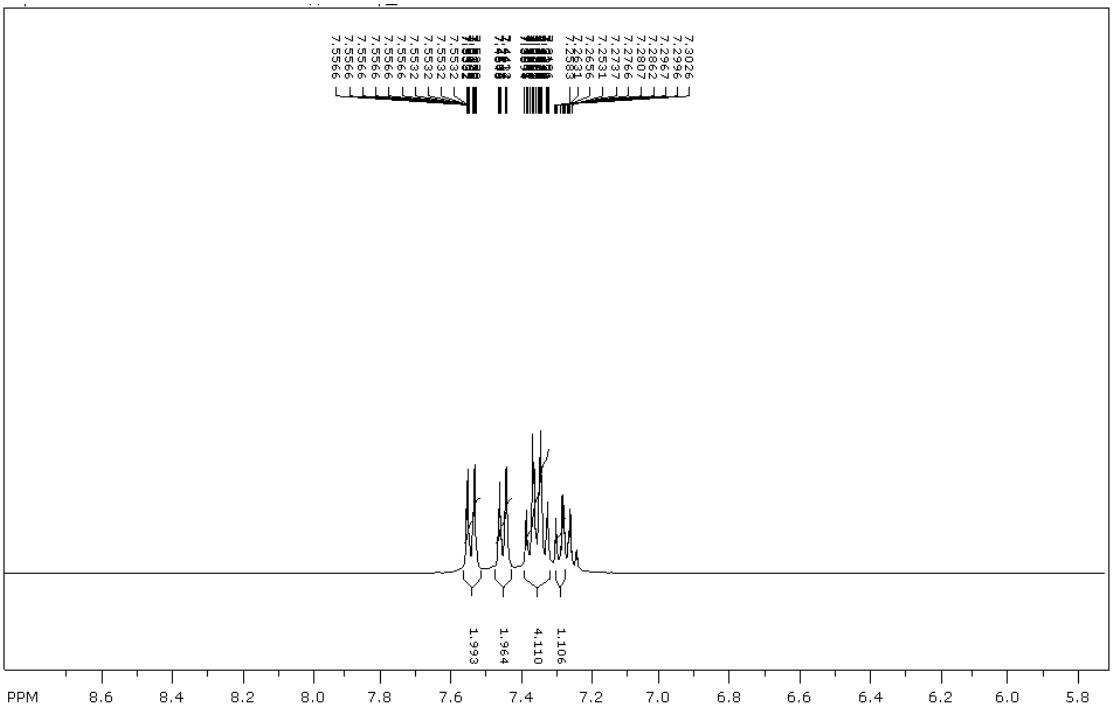

^{13}C NMR spectrum for L5(-SPh)

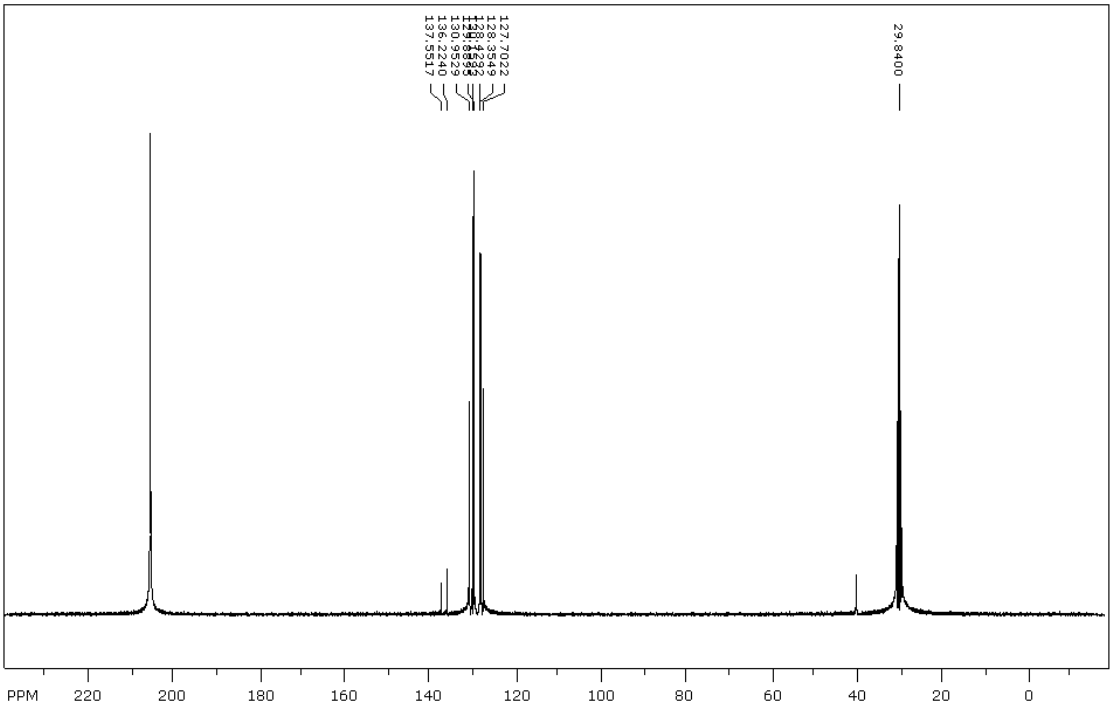

Electrospray ionization mass spectrum (positive) for L5(-SPh)

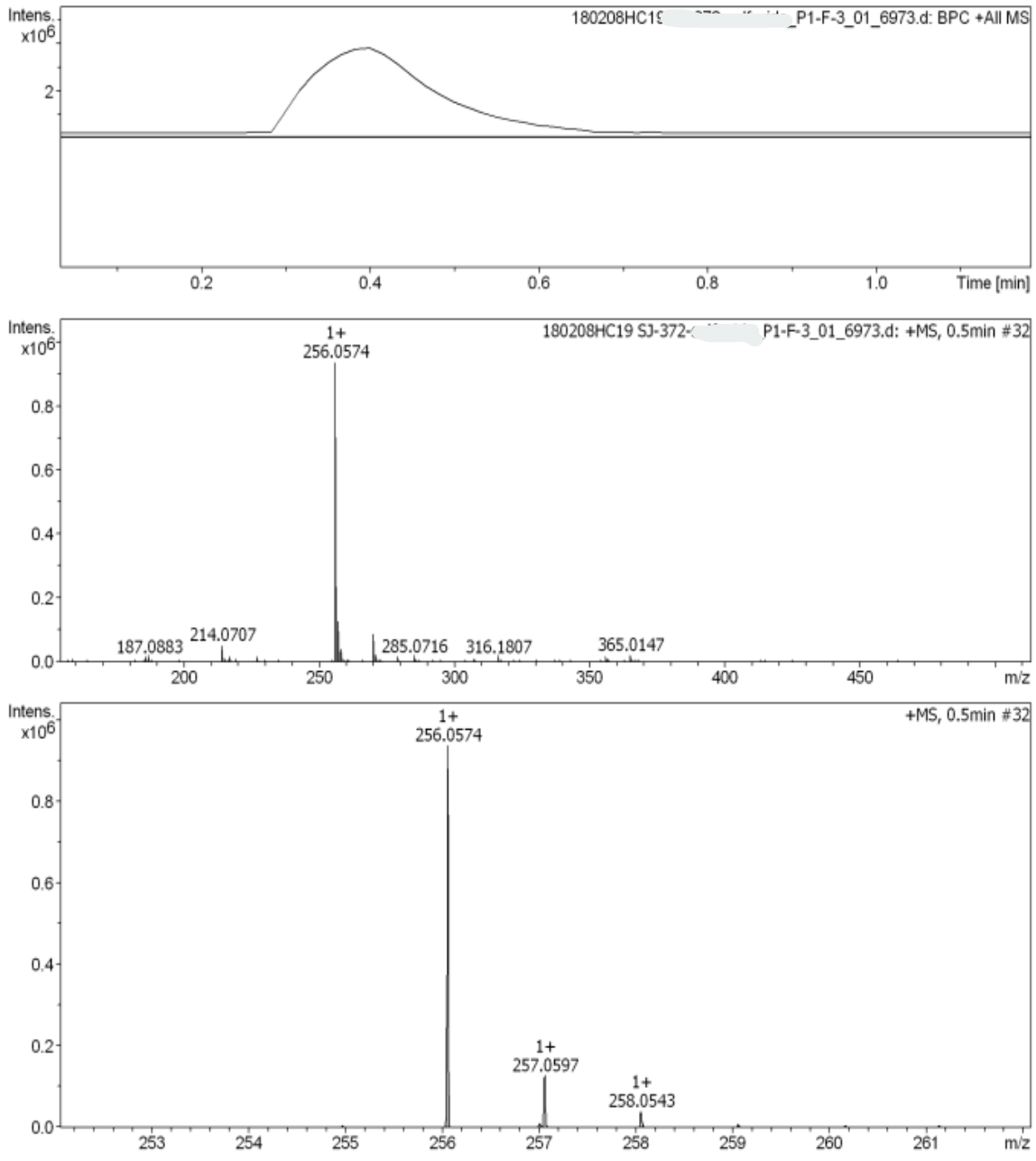

Formula Confirmation

Meas. m/z	#	Ion Formula	Score	m/z	err [mDa]	err [ppm]	mSigma	rdb	e⁻ Conf	N-Rule	Adduct
256.057432	1	C13H10N3OS	100.00	256.053909	-3.5	-13.8	15.5	10.5	even	ok	M
	1	C13H10N3OS	100.00	256.053909	-3.5	-13.8	15.5	10.5	even	ok	M+H

^{1}H NMR spectrum for L6(-SOPh)

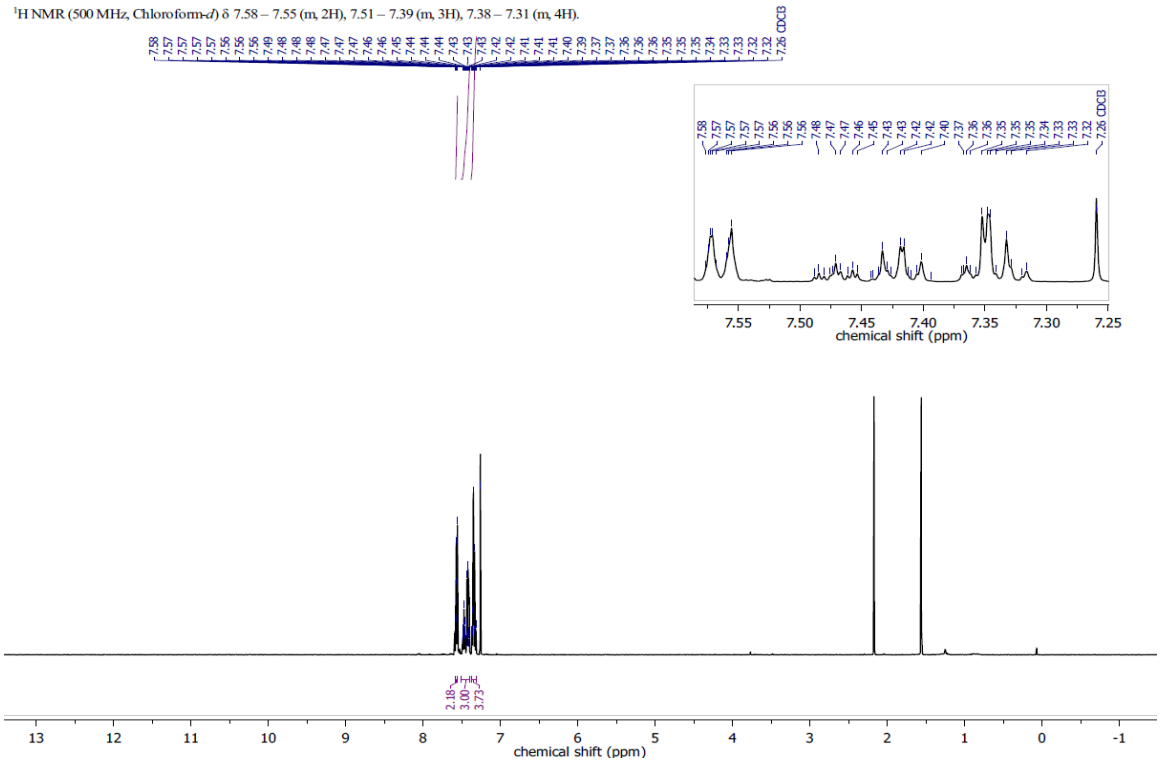

^{13}C NMR spectrum for L6(-SOPh)

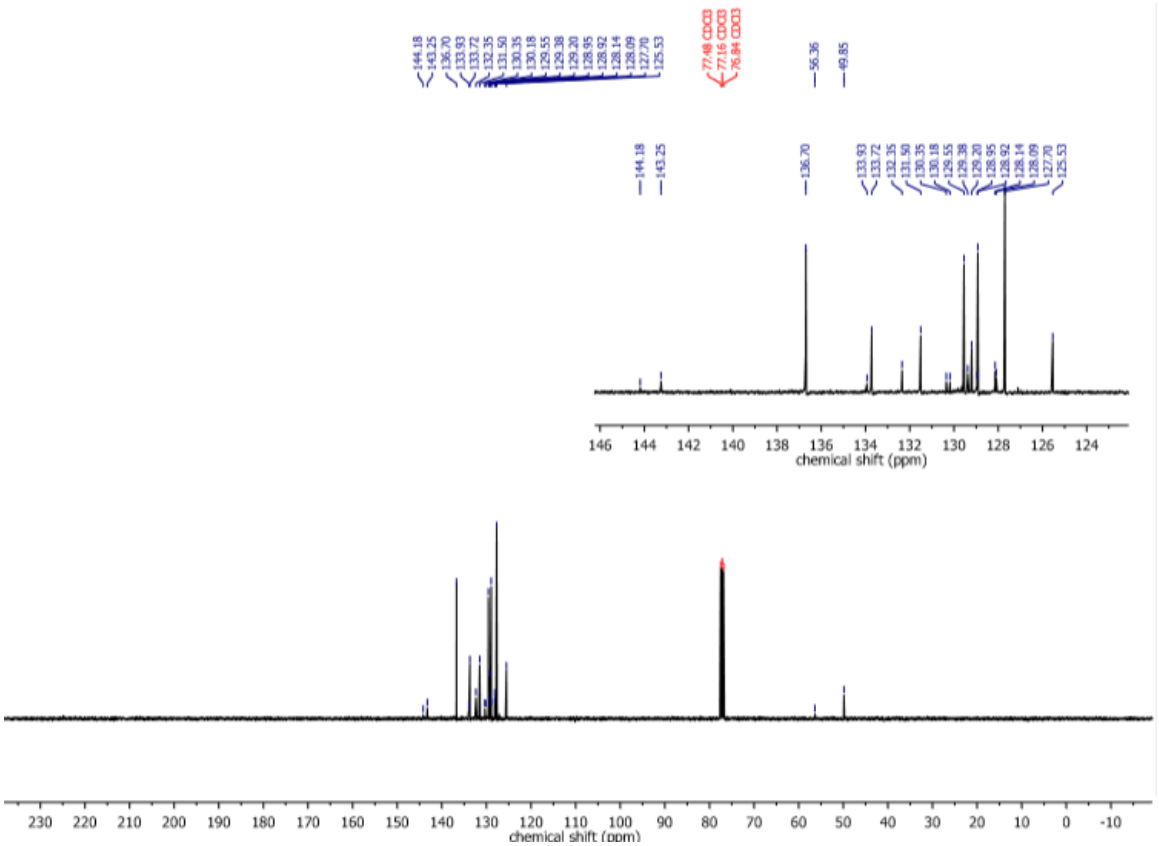

Electrospray ionization mass spectrum (positive) for L6(-SOPh)

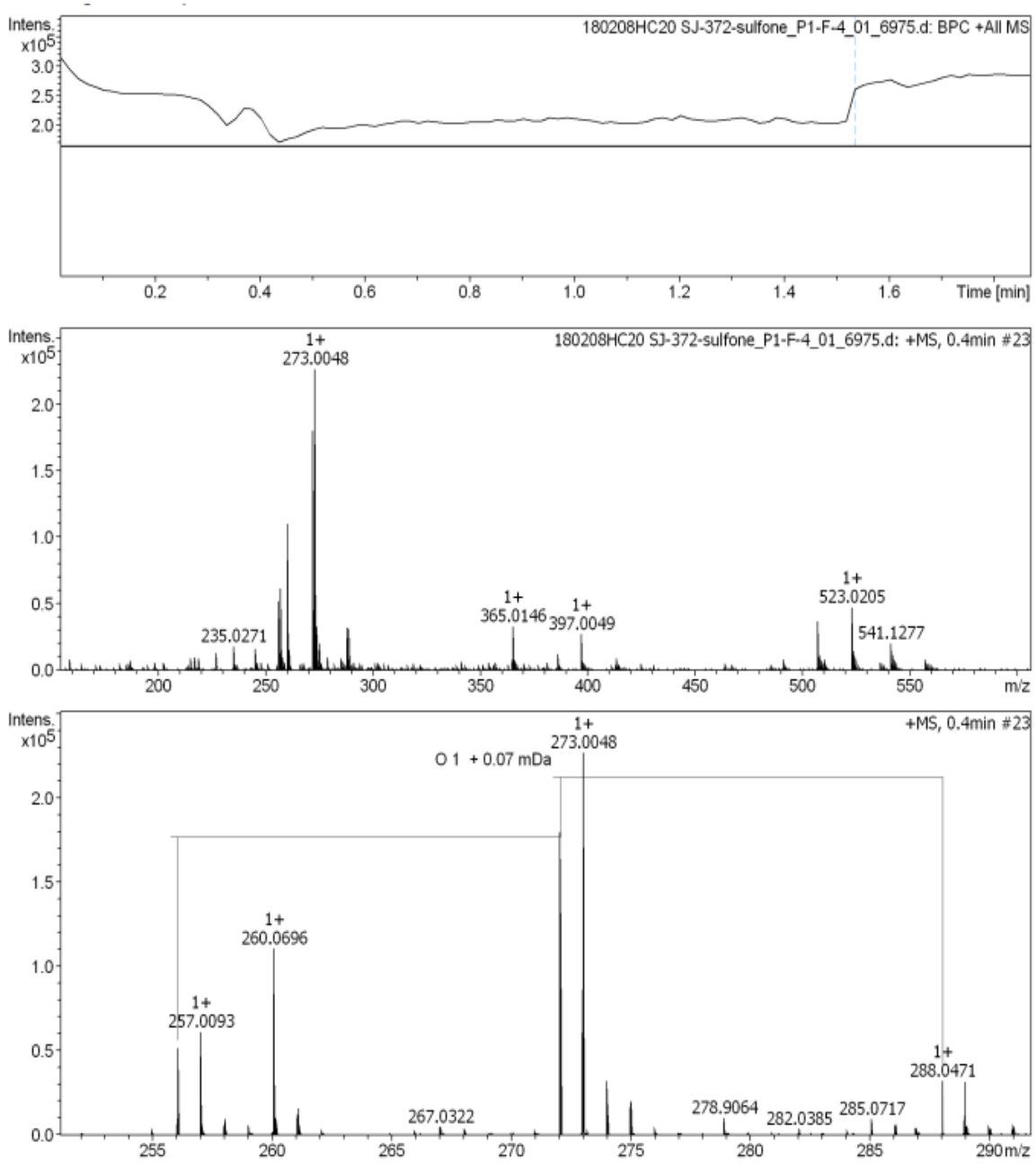

Formula Confirmation

Meas. m/z	#	Ion Formula	Score	m/z	err [mDa]	err [ppm]	mSigma	rdb	e⁻ Conf	N-Rule	Adduct
256.056699	1	C13H10N3OS	38.60	256.053909	2.8	10.9	4.4	10.5	even	ok	M
272.052241	1	C13H10N3O2S	100.00	272.048824	3.4	12.6	8.3	10.5	even	ok	M+H
288.047088	1	C13H10N3O3S	100.00	288.043739	3.3	11.6	33.6	10.5	even	ok	M+H

^{1}H NMR spectrum for L7(-SO_2Ph)

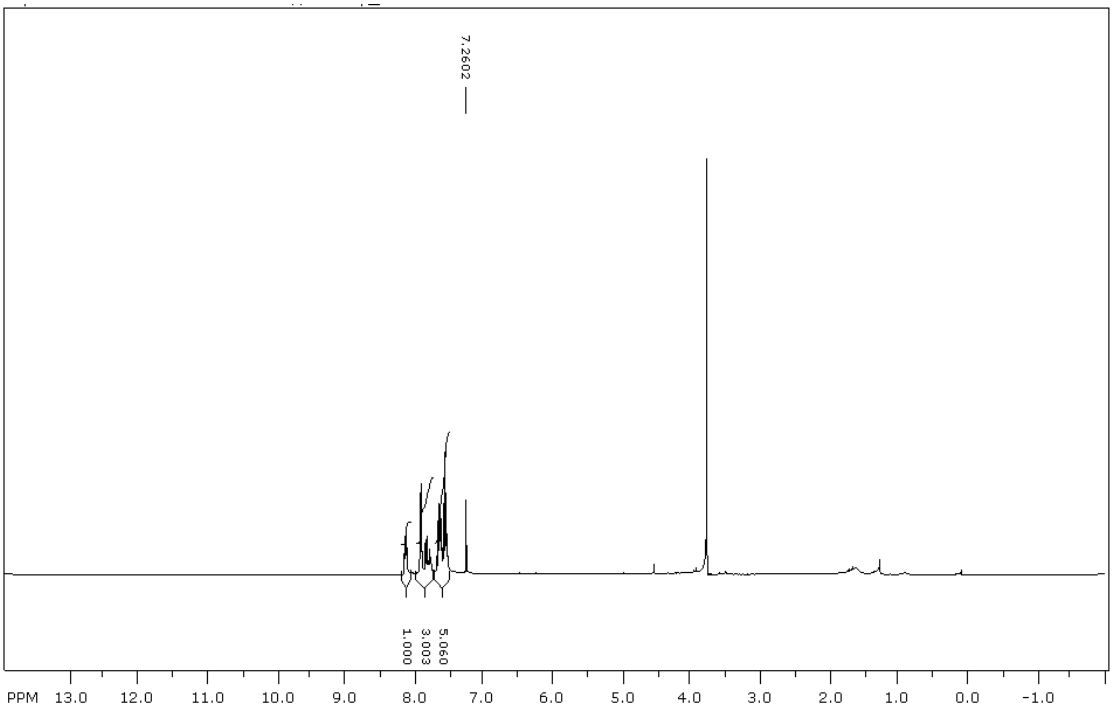

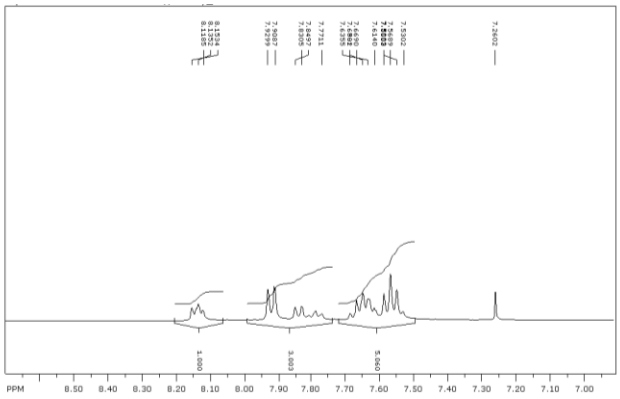

^{13}C NMR spectrum for L7(-SO_2Ph)

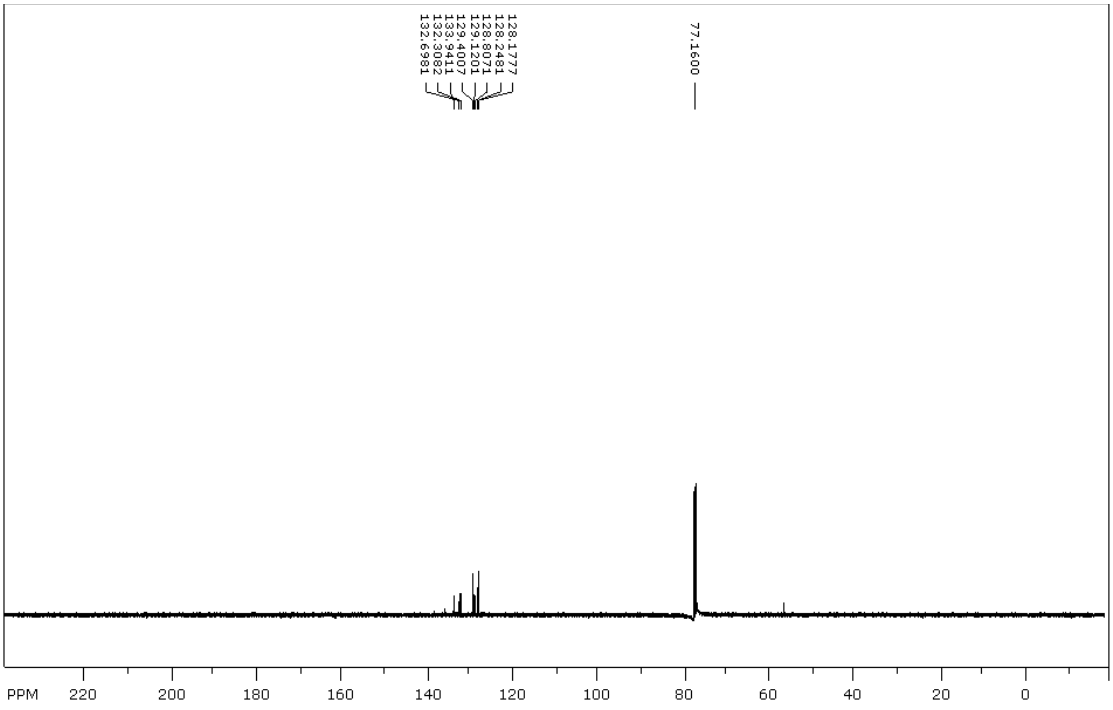

MALDI-TOF spectrum for L7(-SO_2Ph)

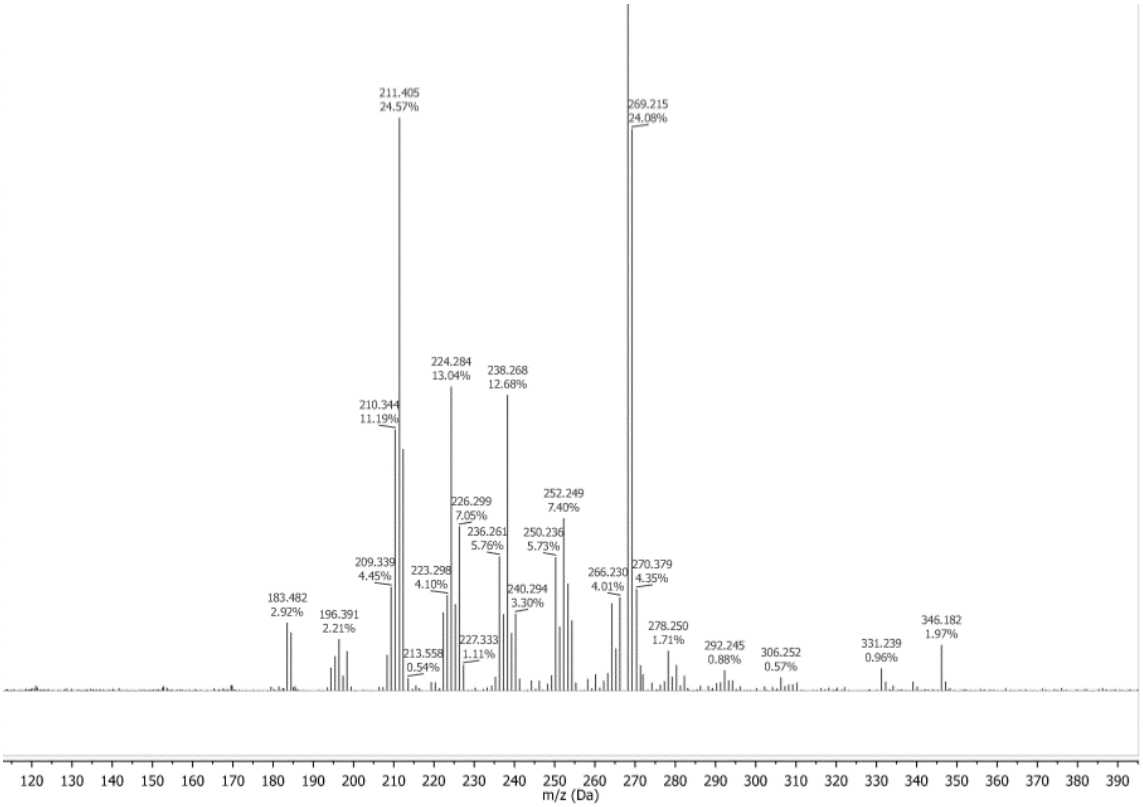

Electrospray ionization mass spectrum (positive) for L7(-SO_2Ph).

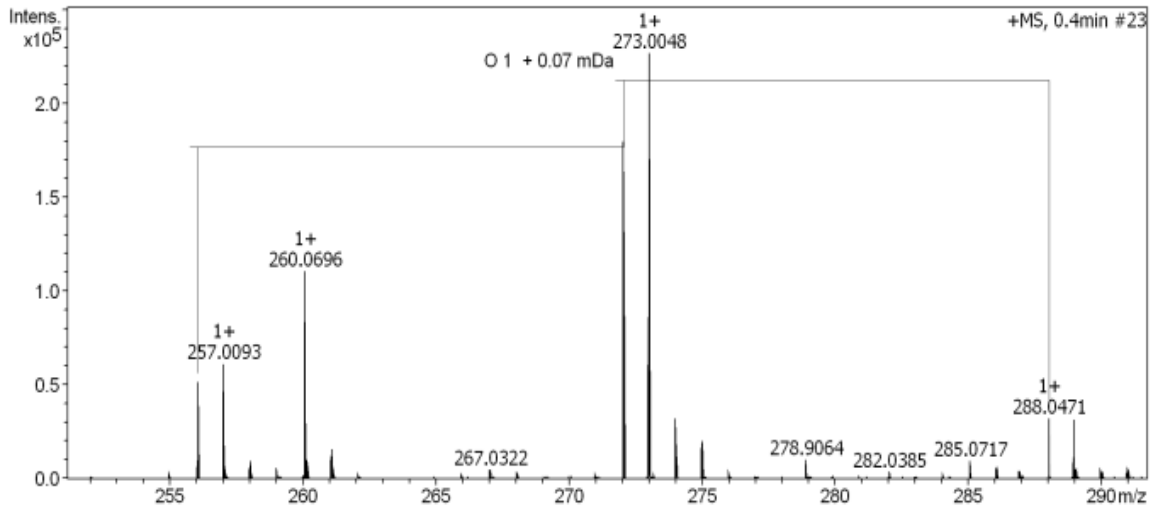

Formula Confirmation

Meas. m/z	#	Ion Formula	Score	m/z	err [mDa]	err [ppm]	mSigma	rdb	e⁻ Conf	N-Rule	Adduct
256.056699	1	C13H10N3OS	38.60	256.053909	2.8	10.9	4.4	10.5	even	ok	M
272.052241	1	C13H10N3O2S	100.00	272.048824	3.4	12.6	8.3	10.5	even	ok	M+H
288.047088	1	C13H10N3O3S	100.00	288.043739	3.3	11.6	33.6	10.5	even	ok	M+H

^{1}H NMR spectrum for C1(-NO_2)

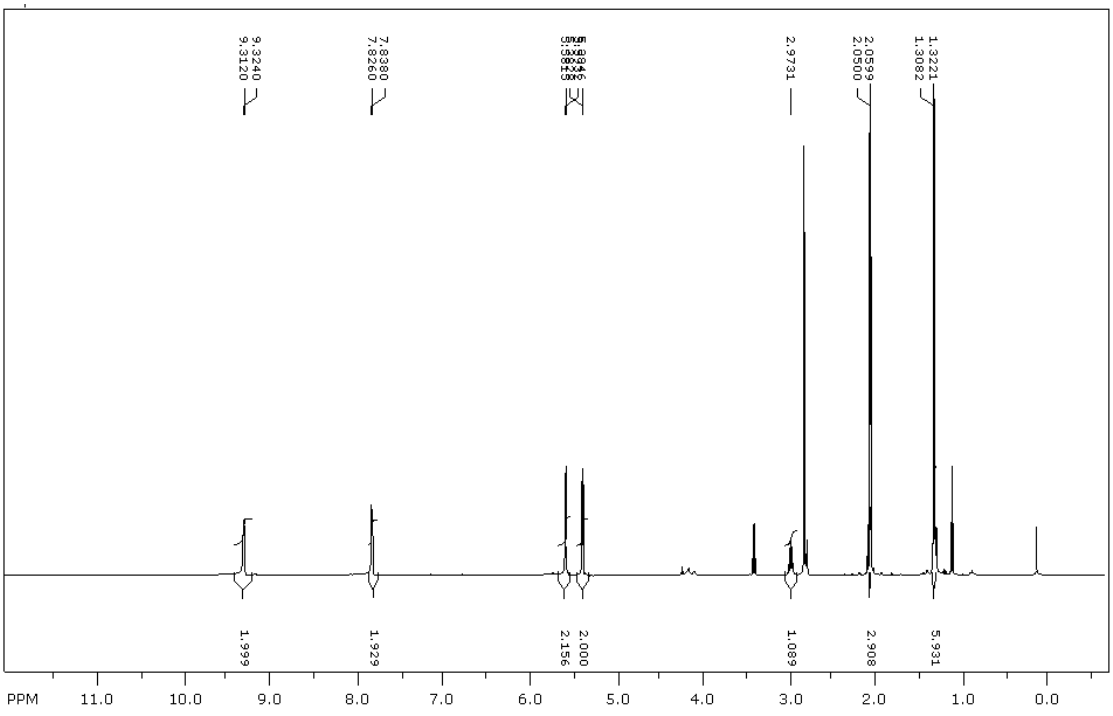

^{13}C NMR spectrum for C1(-NO_2)

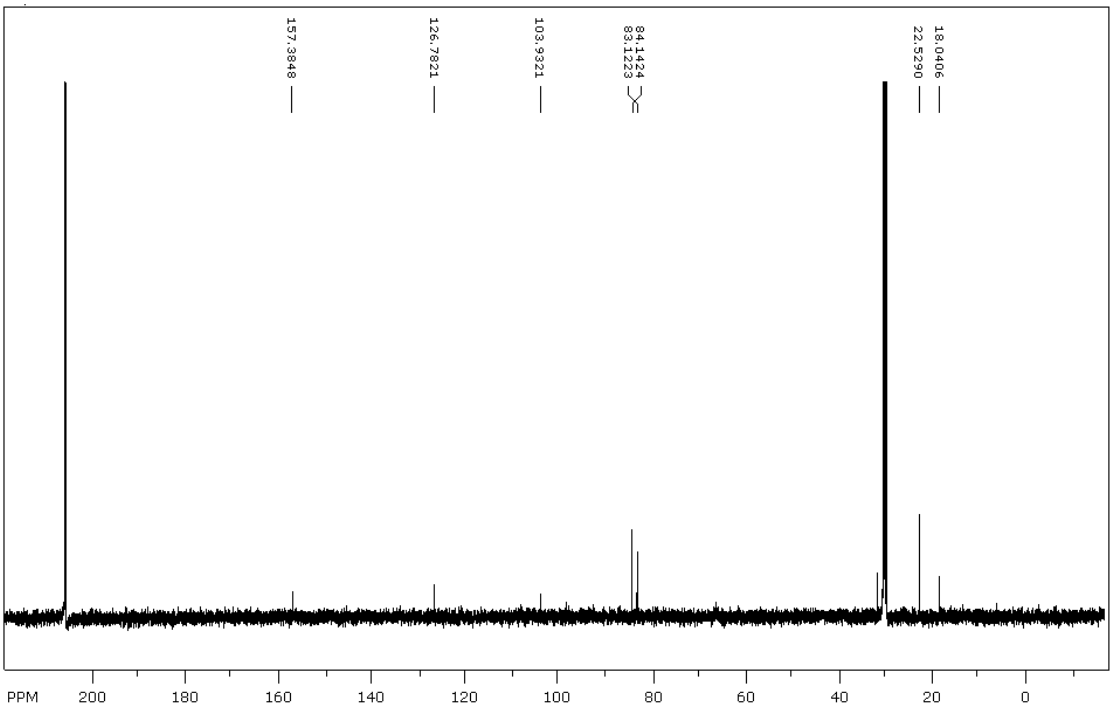

Electrospray ionization mass spectrum (positive) for C1(-NO_2)

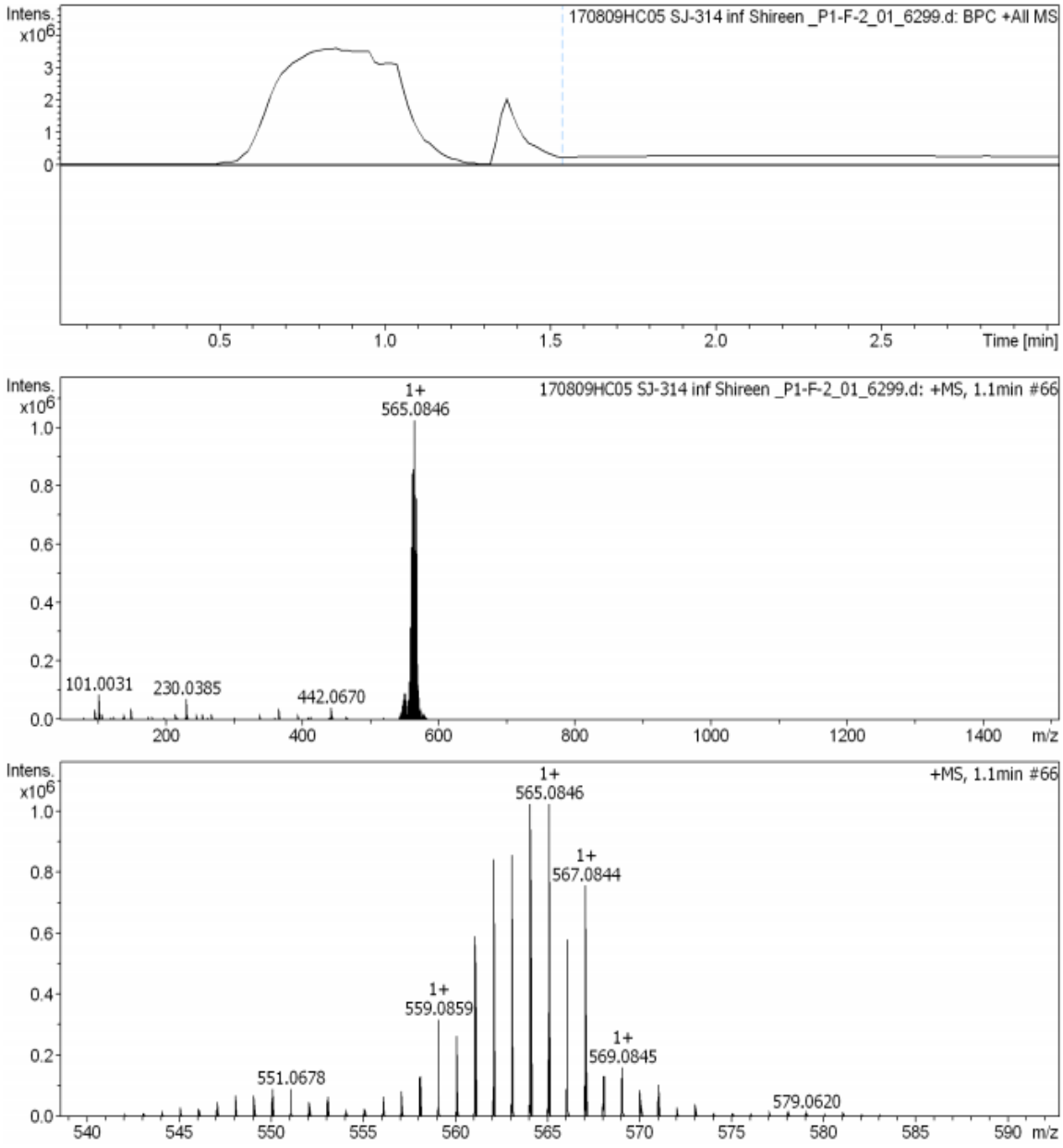

^{1}H NMR spectroscopy for C2(-H)

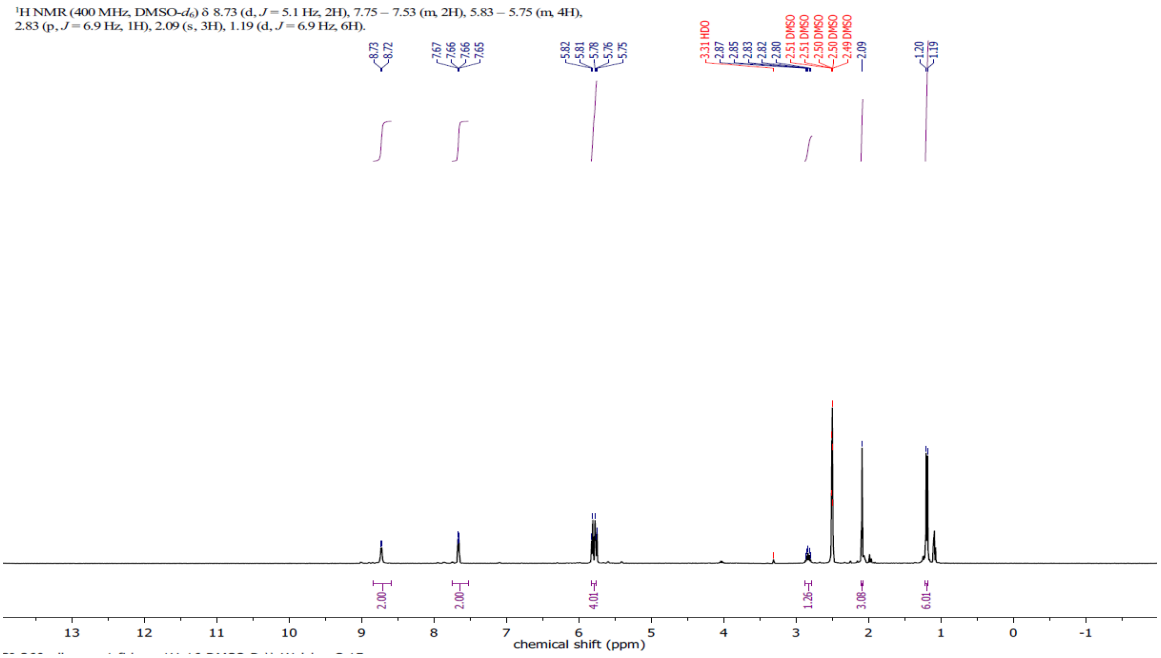

Solvent impurities: δ 1.09 (t, CH_3, diethyl ether), 1.25 (m, CH_2, n-hexane), 1.99 (s, CH_3CO, ethyl acetate), 3.31 (s, HDO, suppressed), 4.03 (q, C***H*****$_2$**CH_3, ethyl acetate).

^{13}C NMR spectrum for C2(-H)

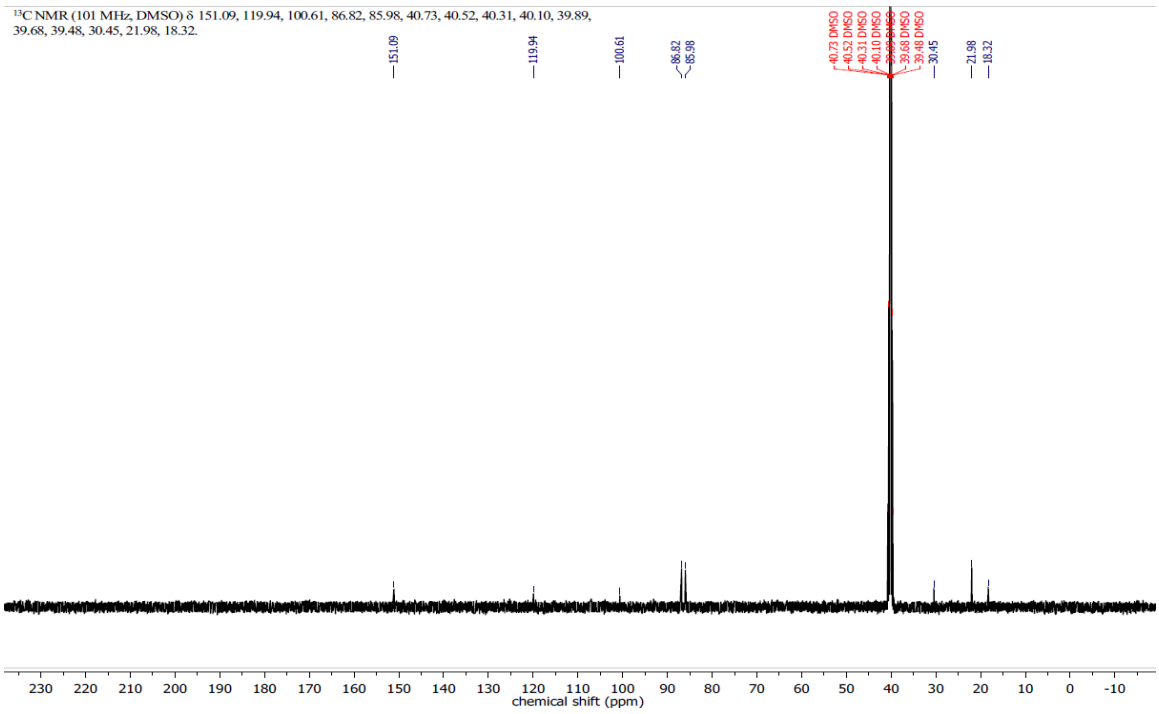

Electrospray ionization mass spectrum (negative) for C2(-H)

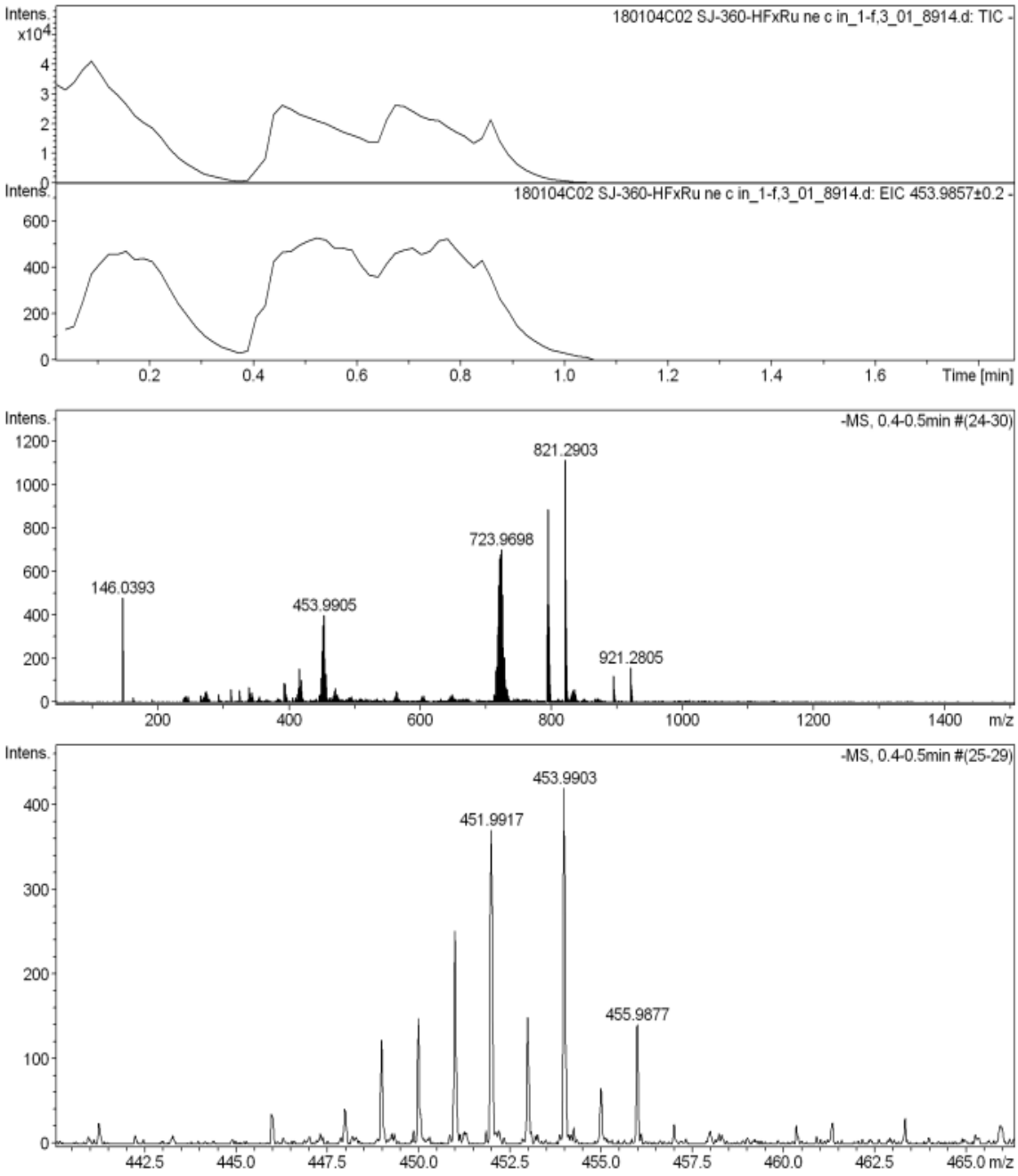

$[M - O - H]^+$ calculated 451.9876 found 451.9917; $[M - 2NO + \text{formic acid} - H]^+$ calculated 453.9920 found 453.9903; $[\text{deoxygenated ligand} - H]^+$ calculated 146.0360 found 146.0393.

^{1}H NMR spectrum for C3(-OCH_3)

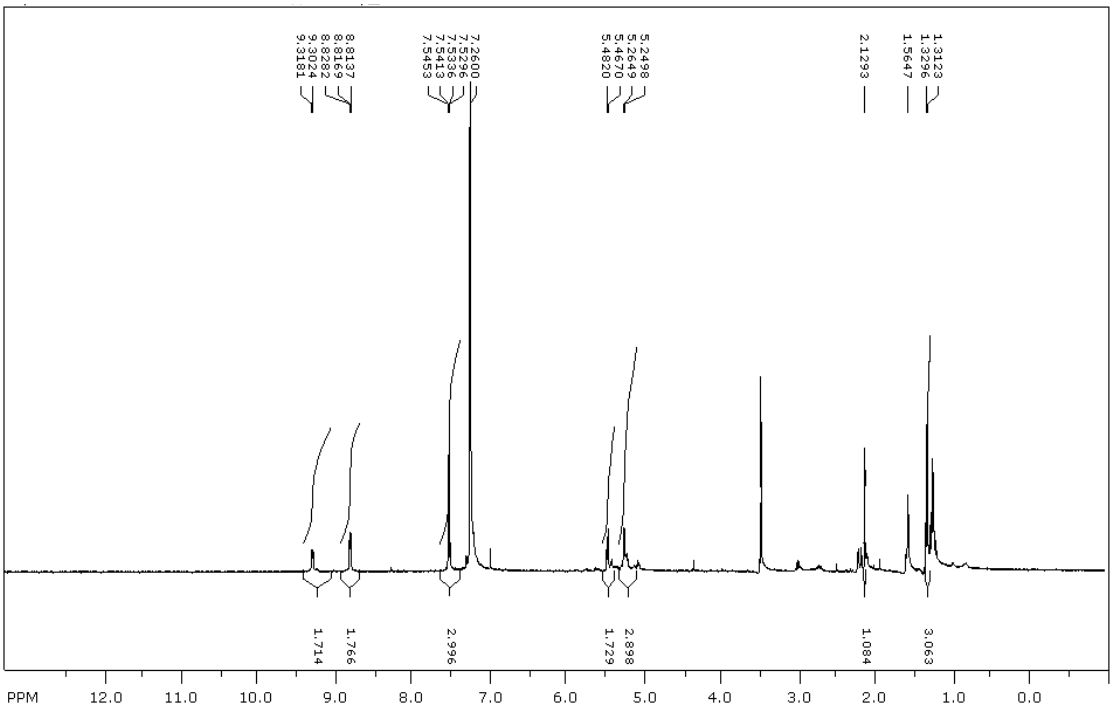

Solvent impurities: δ 1.25 (t, C***H*****$_3$**, EtOH), 1.56 (s, O***H***, water), 2.17 (s, C***H*****$_3$**, acetone), 3.49 (s, C***H*****$_3$**, MeOH).

Electrospray ionization mass spectrum (positive) for C3(-OCH_3)

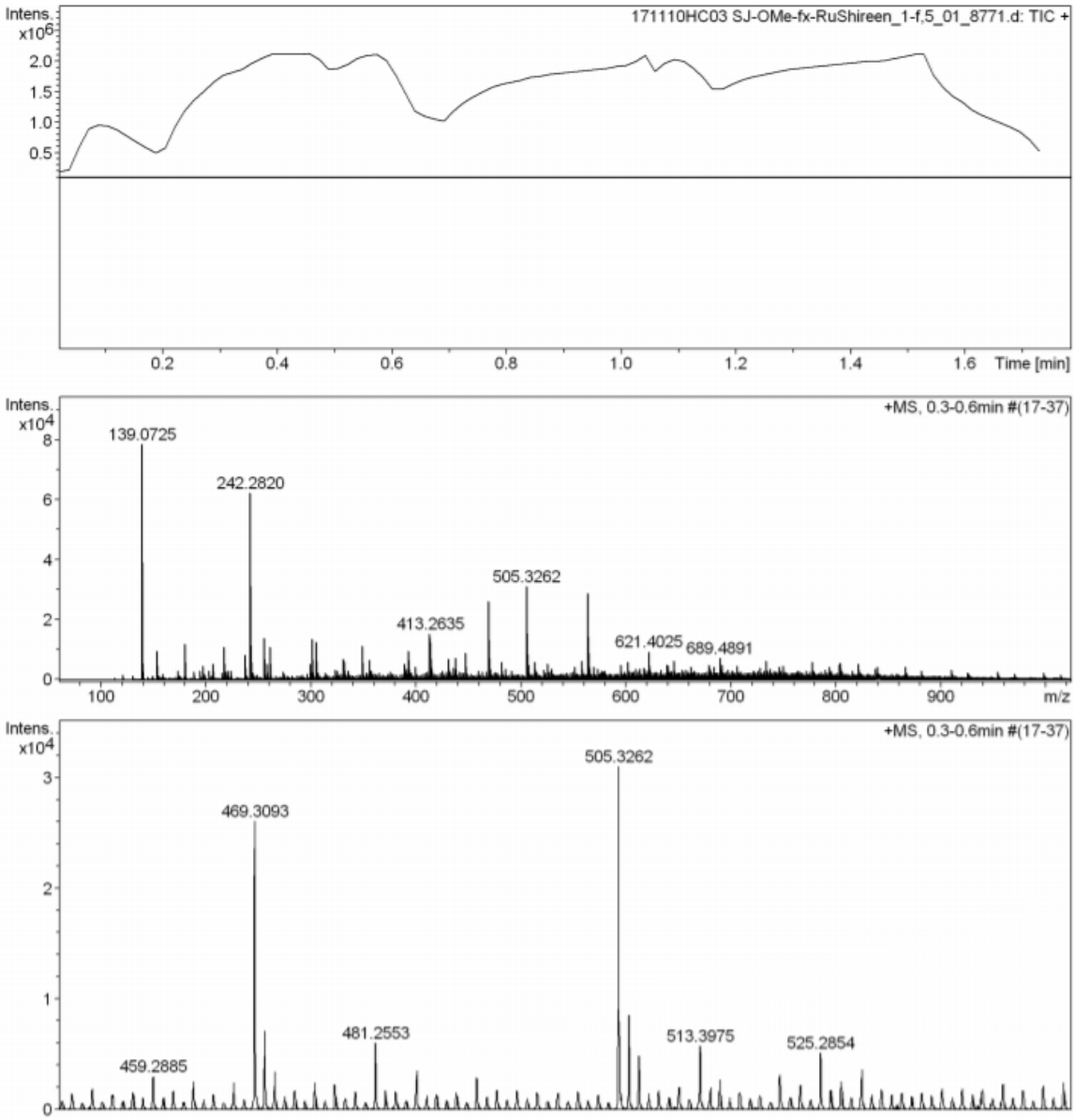

Reverse $[M+ K]^+ = M_2$ adduct, calculated $[M_2- CH_3 + NH_4]^+$ 505.0414 found 505.3262.

^{1}H NMR spectrum for C4(-OPh)

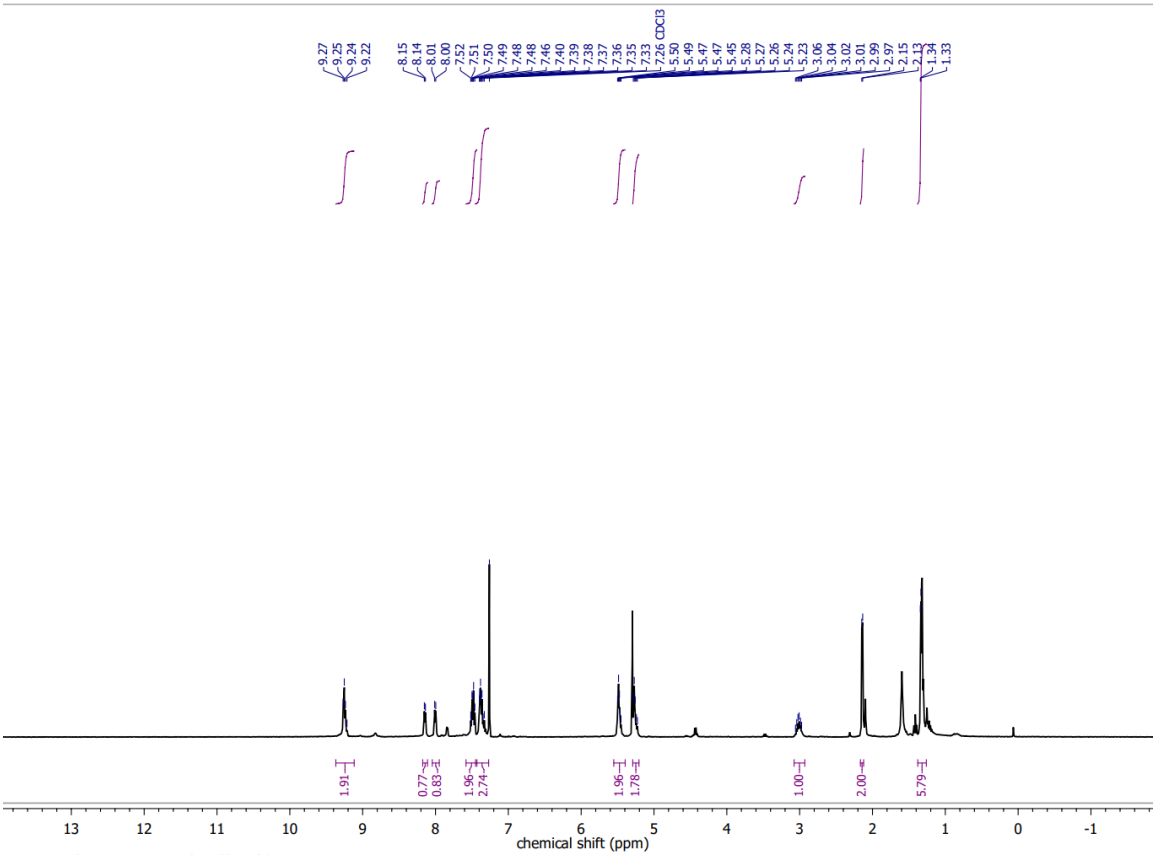

^{13}C NMR spectrum for C4(-OPh)

^{13}C NMR (151 MHz, $CDCl_3$) δ 155.92, 152.19, 143.20, 134.05, 130.29, 126.81, 122.03, 120.19, 119.97, 119.43, 105.74, 83.12, 82.50, 77.37, 77.16, 76.95, 30.84, 22.42, 18.46.

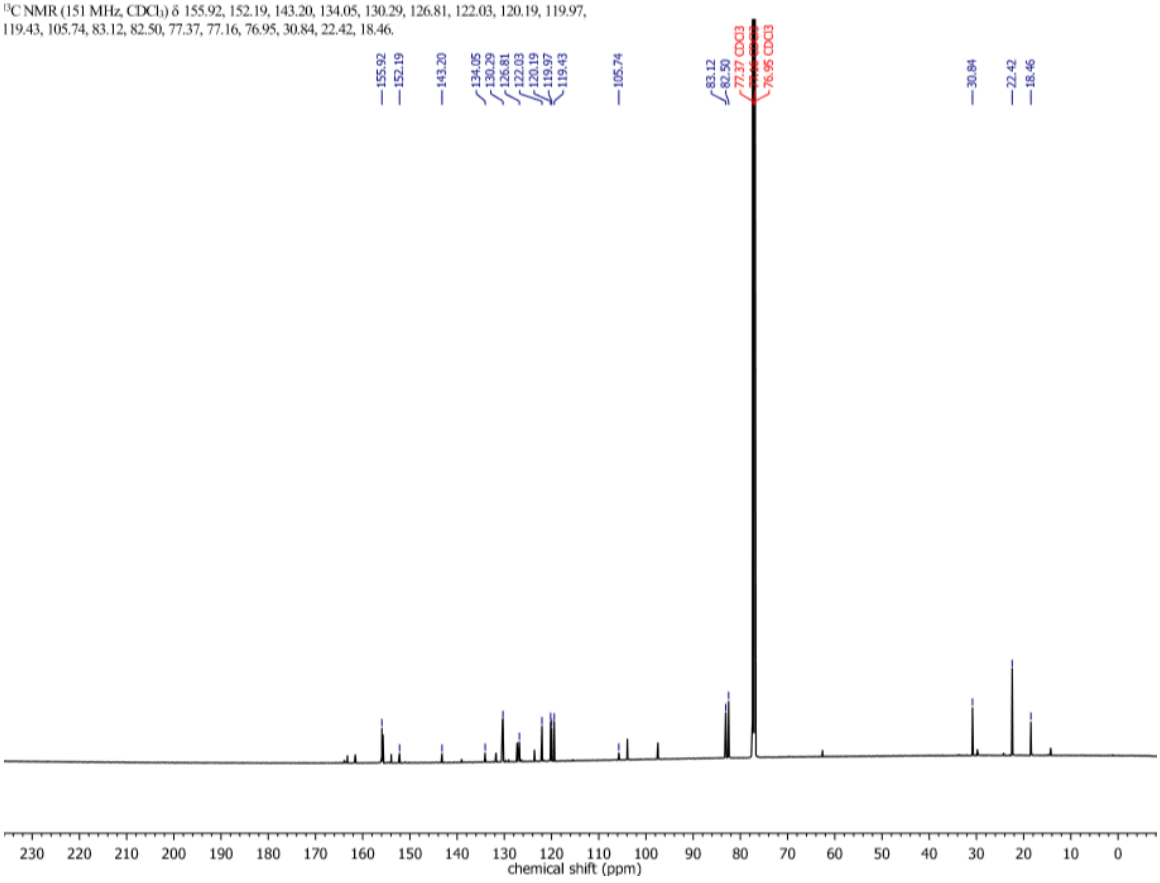

MALDI-TOF spectrum for C4(-OPh)

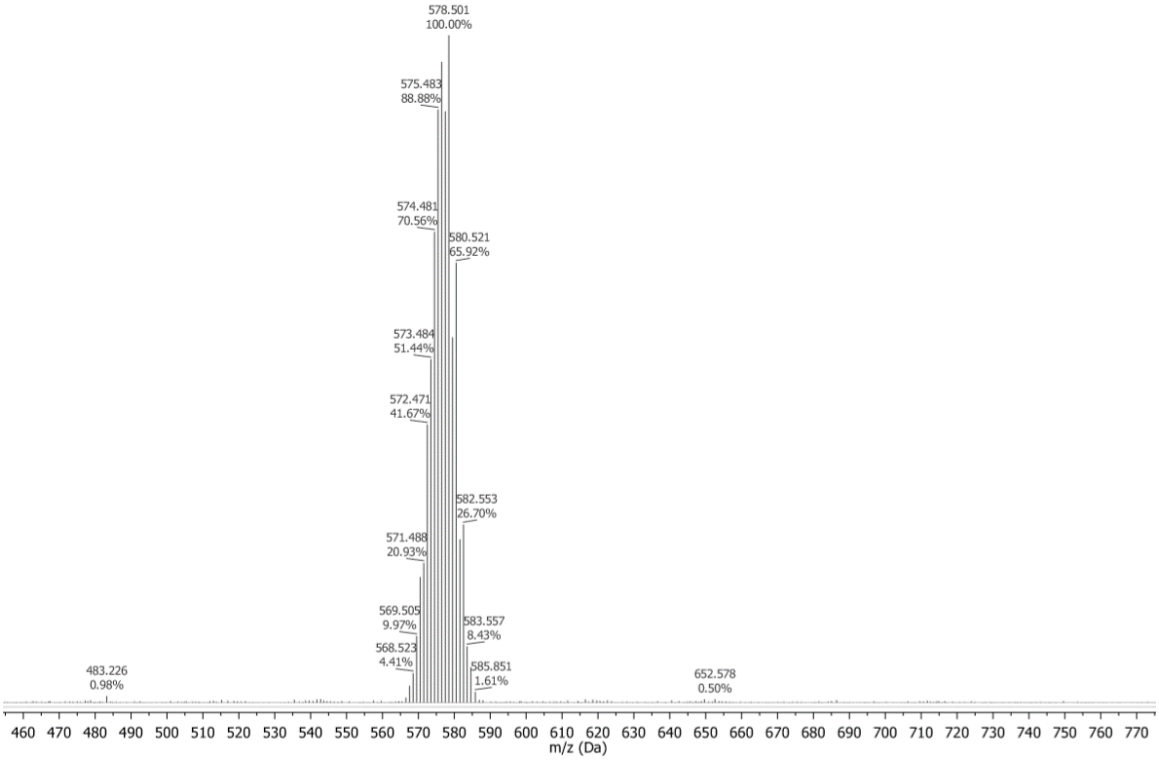

$[M\text{-}O+CH_3OH+H]^+$ calculated 578.054 Da, found 578.501 Da

^{1}H NMR spectrum for C5(-SPh)

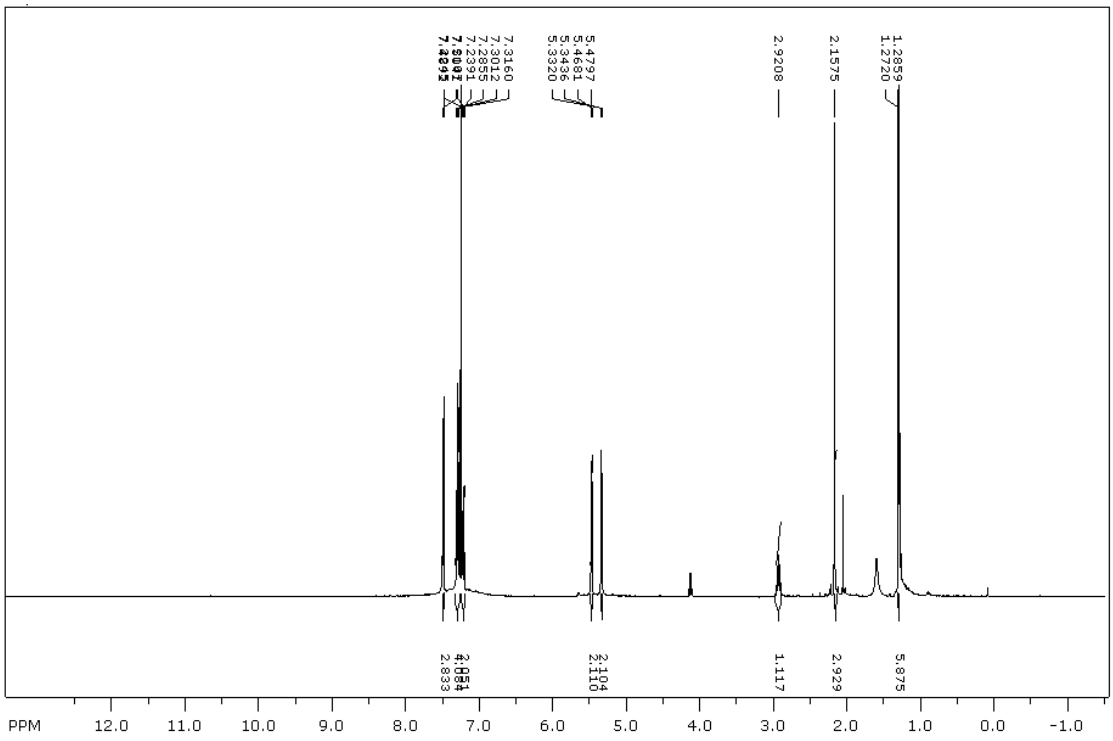

^{13}C NMR spectrum for C5(-SPh)

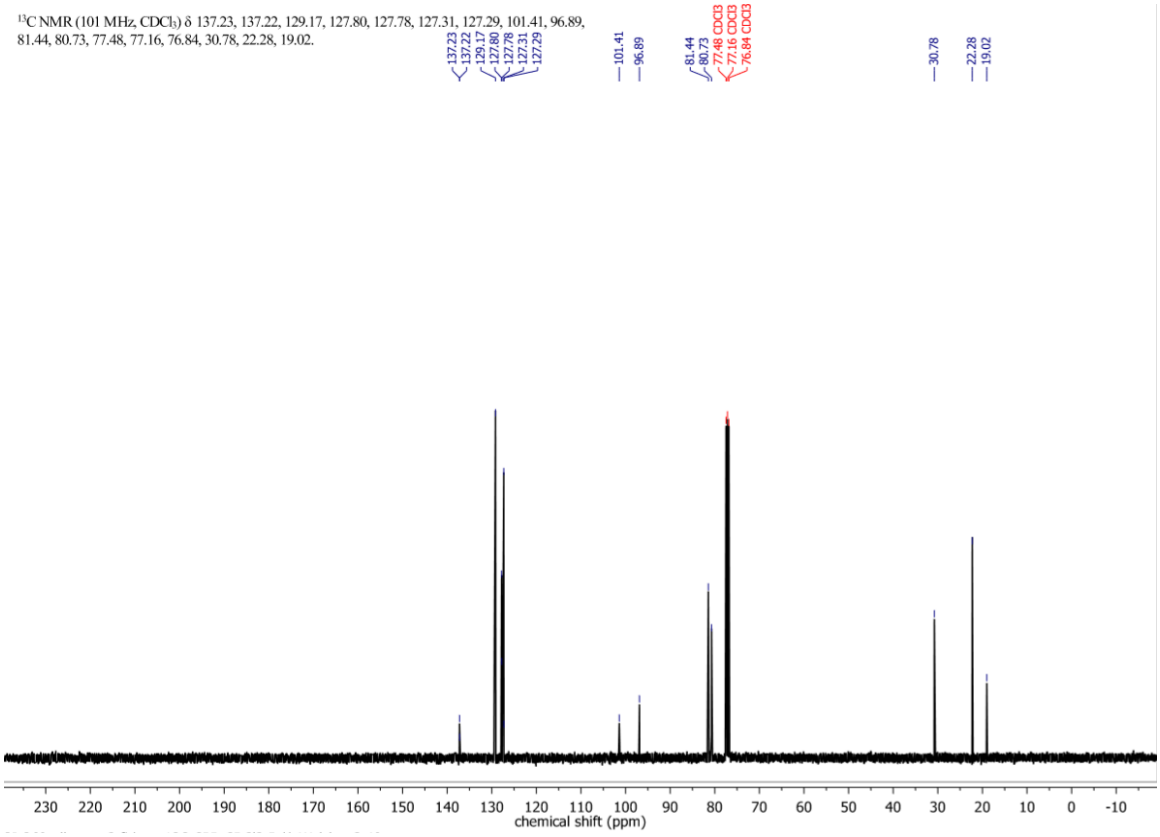

MALDI-TOF spectrum for C5(-SPh)

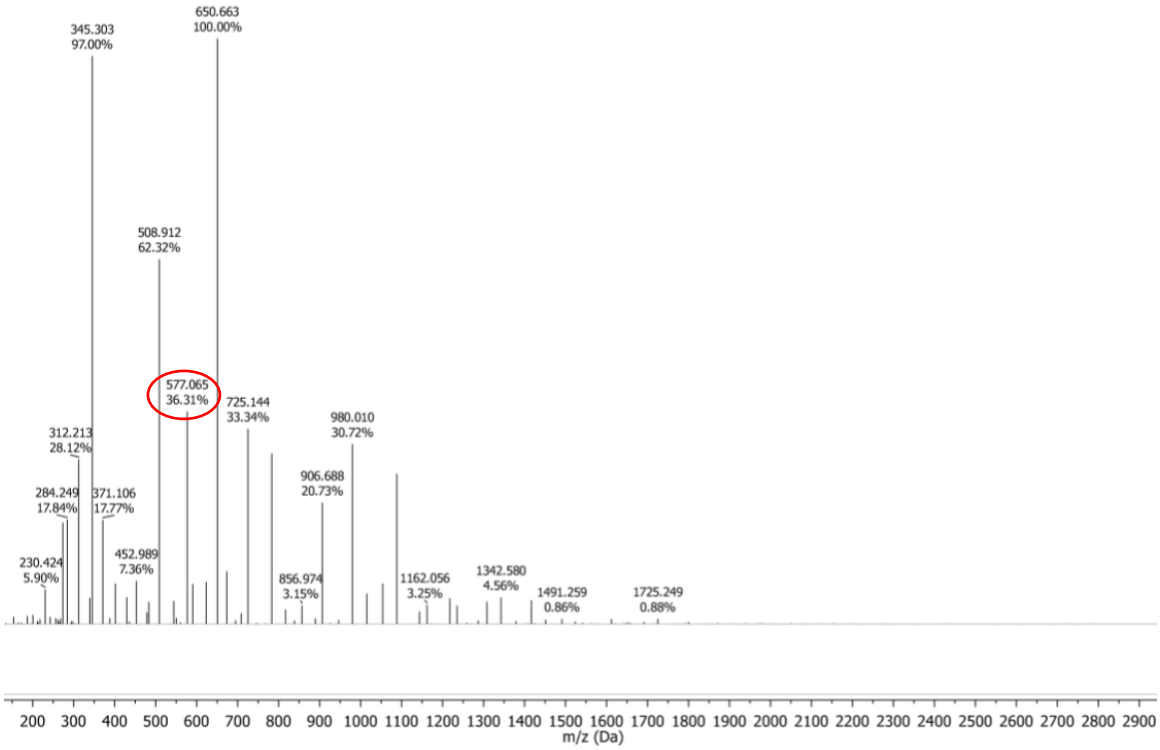

[M] calculated 577.49 Da found 577.055 Da.

^{1}H NMR spectrum for C6(-SOPh)

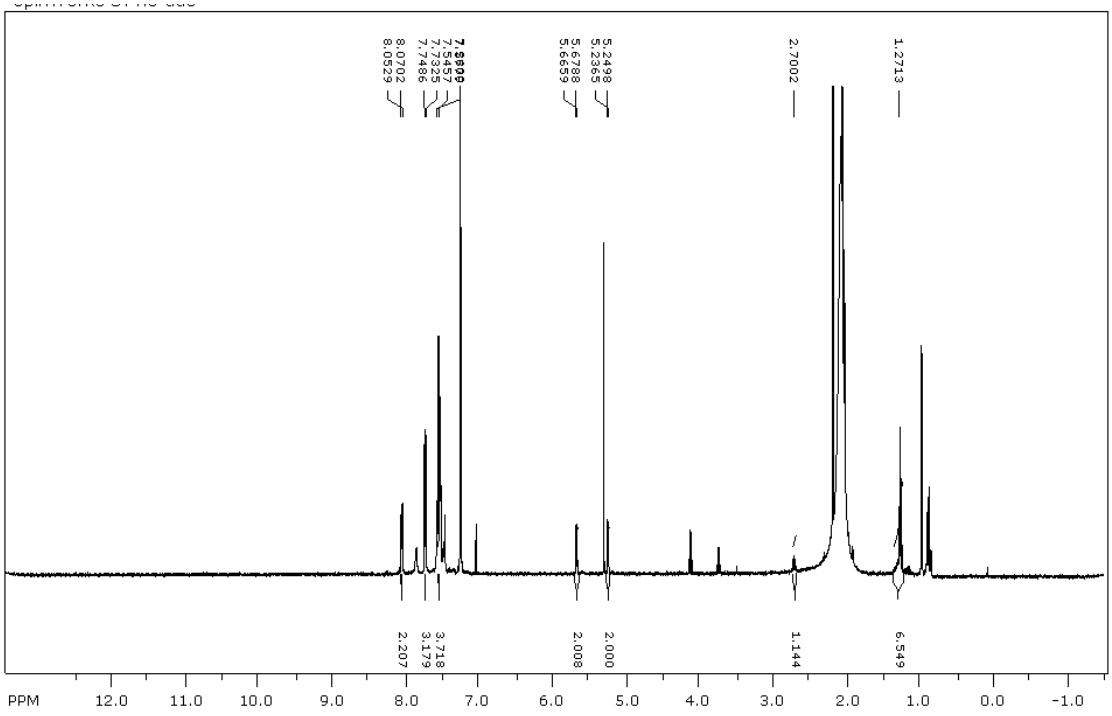

MALDI-TOF spectrum for C6(-SOPh)

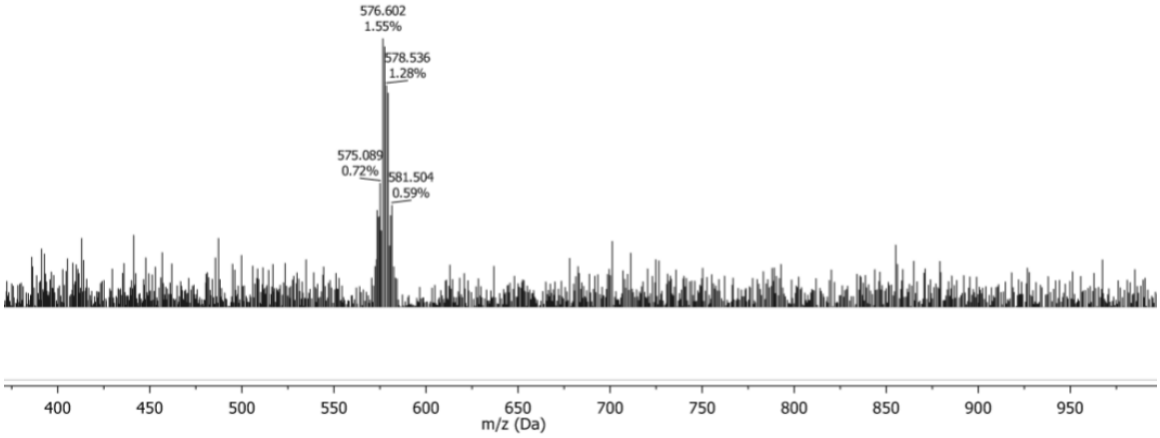

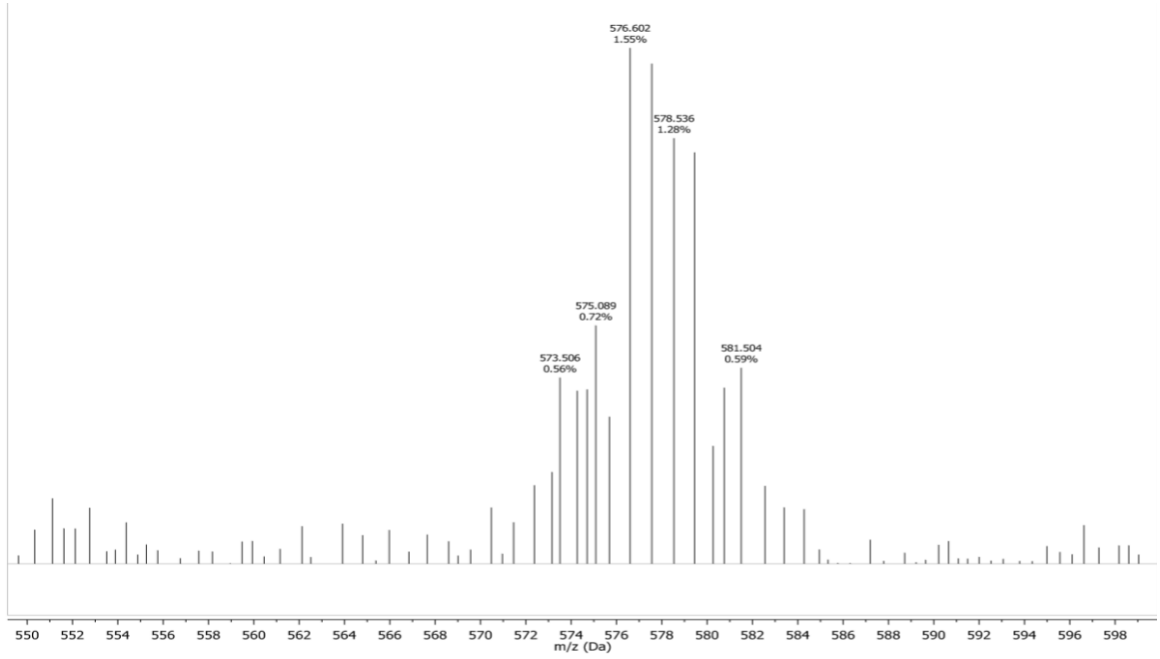

[M-O] calculated 576.9932 Da, found 576.602 Da

^{1}H NMR spectrum for C7(-SO_2Ph)

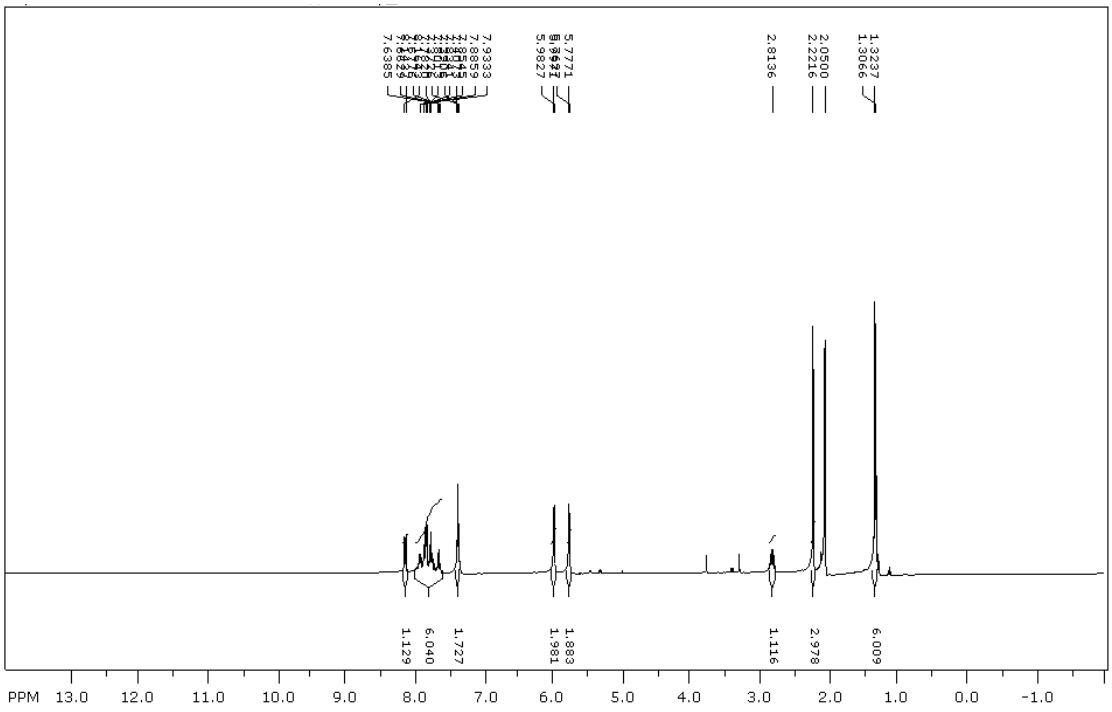

^{13}C NMR spectrum for C7(-SO_2Ph)

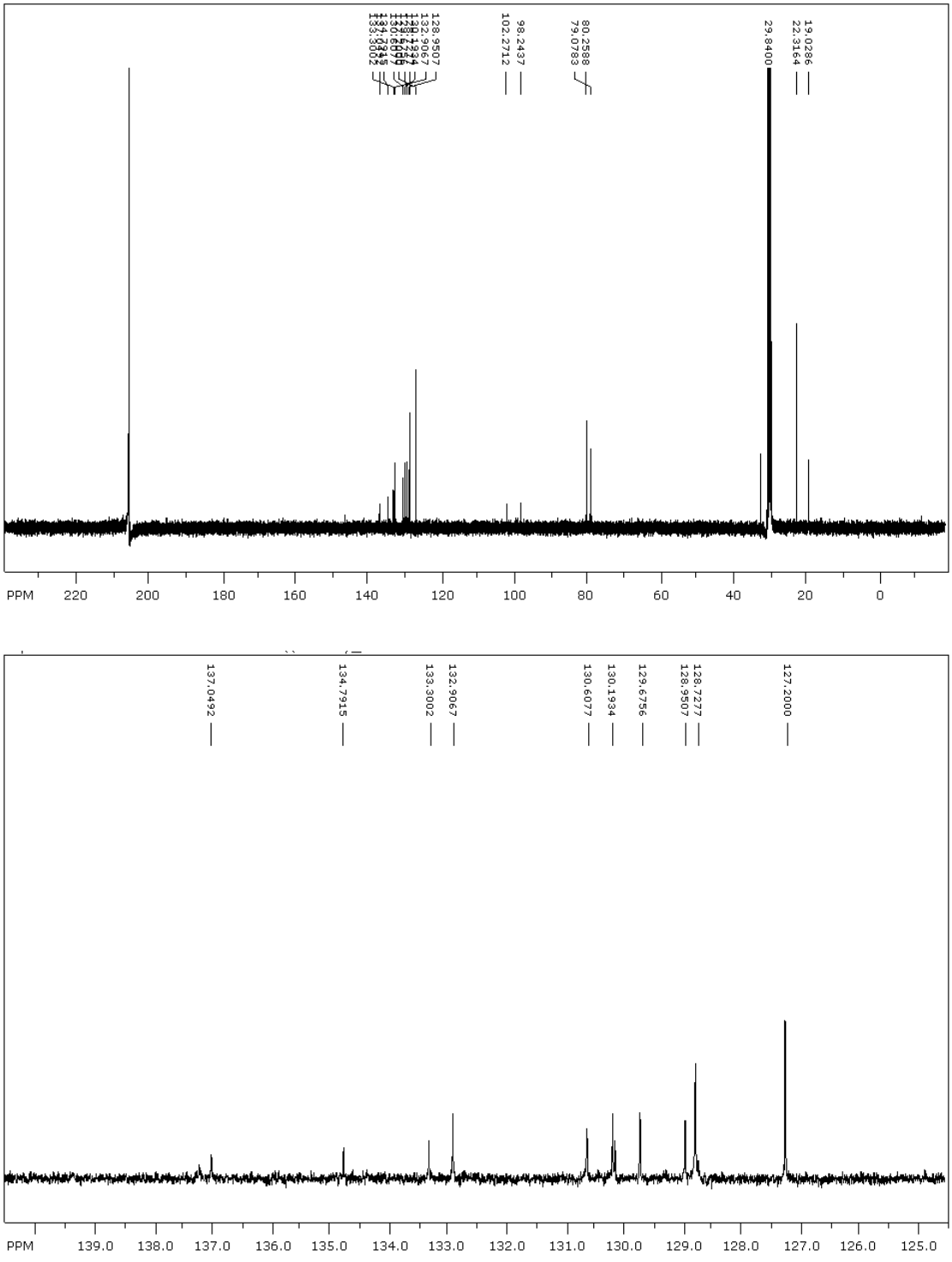

^{1}H NMR spectrum for Ru(η^{6}-*p*-cymene)(Pyridine) – control

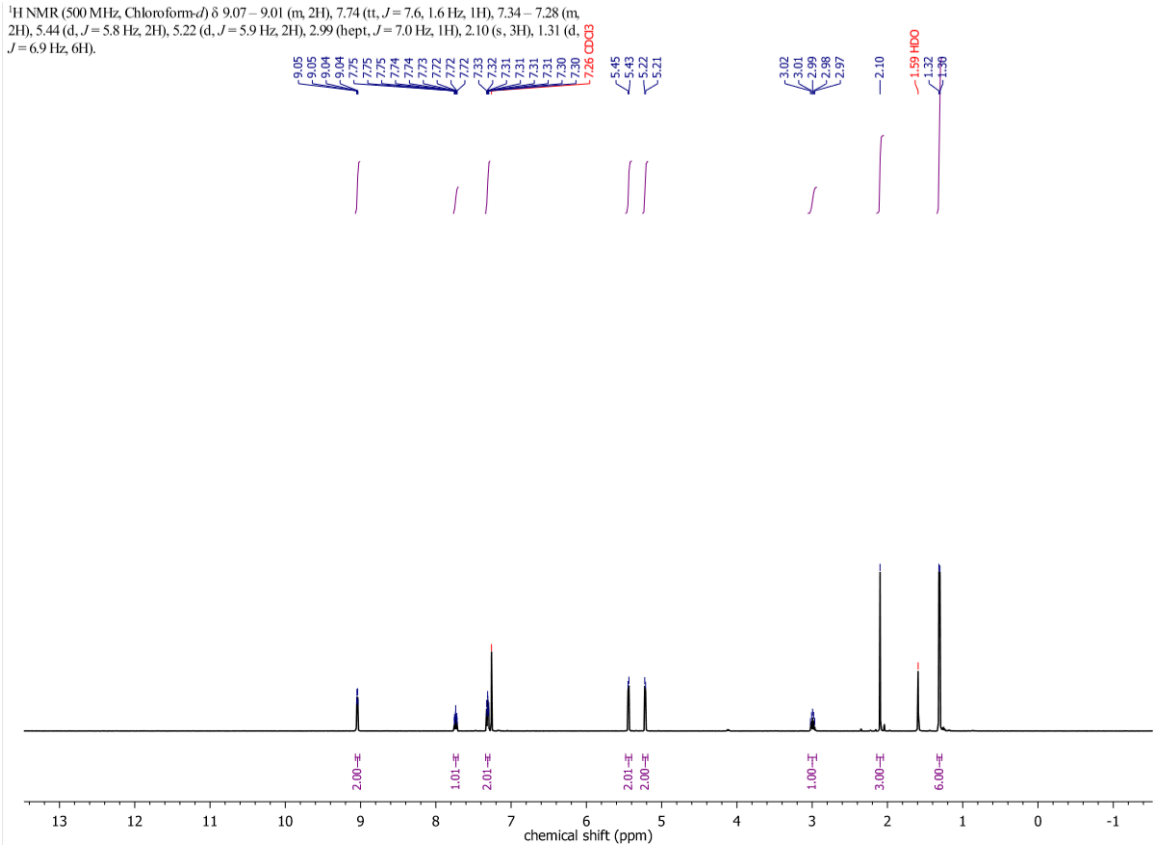

Electrospray ionization mass spectrum (positive) for 4-nitro-3-phenyl-1,2,5-oxadiazole 2-oxide

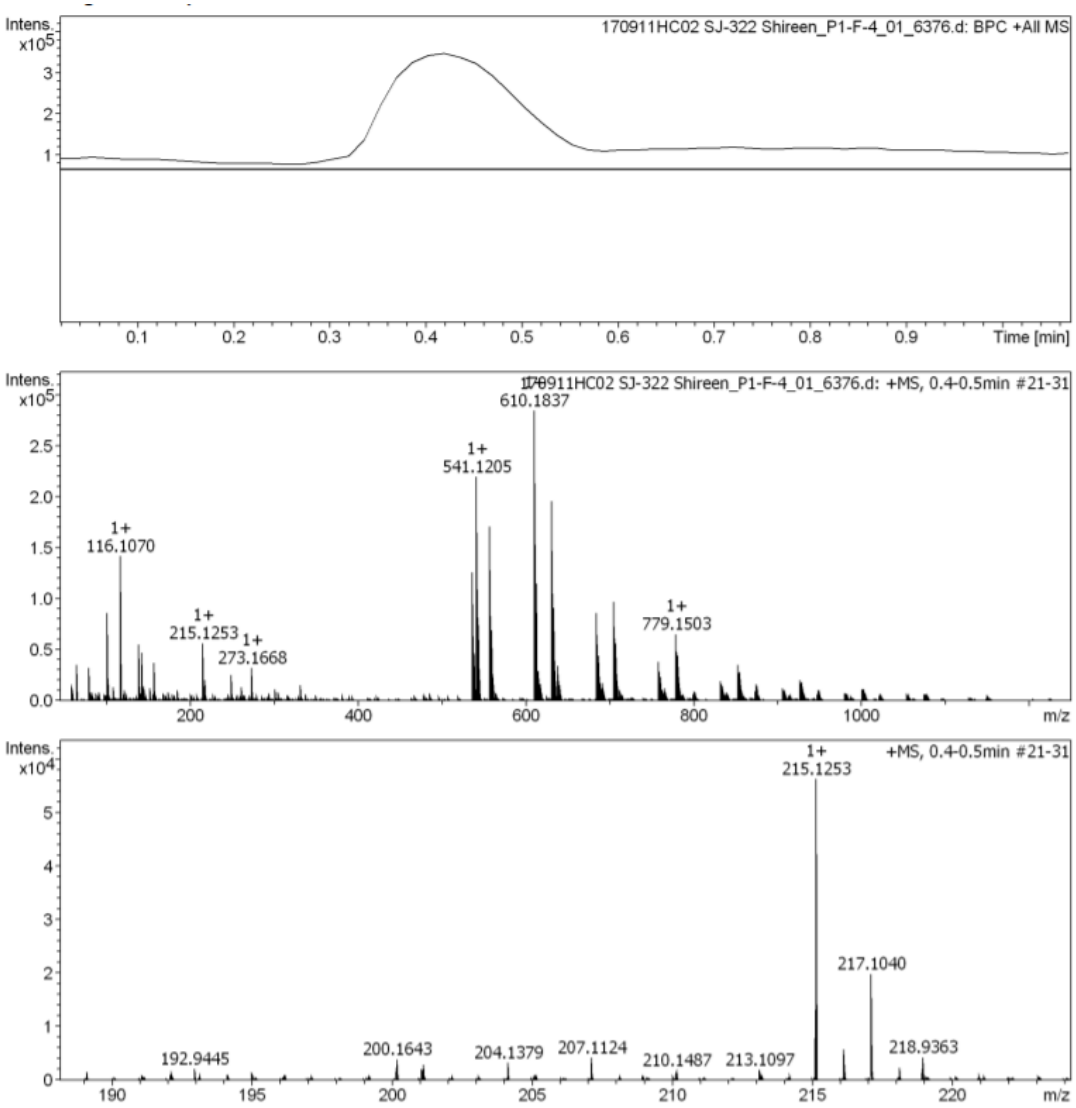

Formula Confirmation

Meas. m/z	#	Ion Formula	Score	m/z	err [mDa]	err [ppm]	mSigma	rdb	e¯ Conf	N-Rule	Adduct
64.015602	1	C2H3NNa	100.00	64.015770	-0.2	-2.6	0.6	1.5	even	ok	M+Na
116.107009	1	C6H14NO	100.00	116.106990	0.0	0.2	4.8	0.5	even	ok	M+H
	1	C6H14NO	100.00	116.106990	0.0	0.2	4.8	0.5	even	ok	M+NH4
139.072908	1	C4H7N6	100.00	139.072671	0.2	1.7	4.2	4.5	even	ok	M+H
	1	C4H7N6	100.00	139.072671	0.2	1.7	4.2	4.5	even	ok	M+NH4
	1	C6H12NaO2	100.00	139.072950	-0.0	-0.3	0.9	0.5	even	ok	M+Na
156.138159	1	C9H18NO	100.00	156.138291	-0.1	-0.8	7.9	1.5	even	ok	M+H
	1	C9H18NO	100.00	156.138291	-0.1	-0.8	7.9	1.5	even	ok	M+NH4
215.125293	1	C7H15N6O2	100.00	215.125100	-0.2	-0.9	5.3	3.5	even	ok	M+H
	1	C7H15N6O2	100.00	215.125100	-0.2	-0.9	5.3	3.5	even	ok	M+NH4
	1	C9H20NaO4	100.00	215.125380	-0.1	-0.4	7.5	-0.5	even	ok	M+Na
249.109413	1	C10H13N6O2	100.00	249.109450	-0.0	-0.2	7.8	7.5	even	ok	M+H
	1	C10H13N6O2	100.00	249.109450	-0.0	-0.2	7.8	7.5	even	ok	M+NH4
	1	C12H18NaO4	100.00	249.109730	-0.3	-1.3	35.7	3.5	even	ok	M+Na
273.166834	1	C10H21N6O3	100.00	273.166965	0.1	0.5	10.4	3.5	even	ok	M+H
	1	C10H21N6O3	100.00	273.166965	0.1	0.5	10.4	3.5	even	ok	M+NH4
	1	C12H26NaO5	100.00	273.167245	-0.4	-1.5	8.1	-0.5	even	ok	M+Na

C1 Crystal data Tables

C1

Table 1 Crystal data and structure refinement for C1.

Identification code	C1
Empirical formula	$C_{17}H_{21}Cl_2N_2ORu$
Formula weight	441.34
Temperature/K	273.15
Crystal system	triclinic
Space group	P-1
a/Å	7.2742(13)
b/Å	11.827(2)
c/Å	12.046(2)
α/°	64.300(5)
β/°	89.453(5)
γ/°	77.446(5)
Volume/Å^3	907.3(3)
Z	2
ρ_{calc}g/cm^3	1.6155
μ/mm^{-1}	1.163
F(000)	444.2
Crystal size/mm^3	0.26 × 0.2 × 0.03
Radiation	Mo Kα (λ = 0.71073)
2Θ range for data collection/°	3.94 to 56
Index ranges	$-9 \leq h \leq 9$, $-13 \leq k \leq 15$, $0 \leq l \leq 15$
Reflections collected	4361
Independent reflections	4361 [R_{int} = 0.0000, R_{sigma} = 0.0623]
Data/restraints/parameters	4361/0/289
Goodness-of-fit on F^2	1.040
Final R indexes [I>=2σ (I)]	R_1 = 0.0631, wR_2 = 0.1680
Final R indexes [all data]	R_1 = 0.0706, wR_2 = 0.1739
Largest diff. peak/hole / e Å^{-3}	1.62/-2.64

Table 2 Fractional Atomic Coordinates ($\times 10^4$) and Equivalent Isotropic Displacement Parameters ($Å^2 \times 10^3$) for C1. U_{eq} is defined as 1/3 of of the trace of the orthogonalised U_{IJ} tensor.

Atom	*x*	*y*	*z*	U(eq)
Cl2	6376.3(16)	2651.9(11)	4747.6(11)	20.2(3)
Cl3	5992.7(16)	5033.4(11)	1892.2(11)	20.6(3)
Ru1	3713.8(5)	4123.3(3)	3258.0(3)	15.90(16)
N1	4097(5)	2680(4)	2622(4)	17.9(8)
C	4407(7)	1984(5)	1019(5)	20.0(9)
C1	680(7)	4771(5)	2596(5)	19.4(9)
C2	4359(7)	2909(5)	1433(5)	20.0(9)
C0aa	2425(7)	5999(5)	3192(5)	20.9(10)
N2	4159(8)	-1066(5)	1241(5)	32.0(11)
C5	3932(7)	525(5)	3077(5)	21.5(10)
C6	3893(7)	1499(5)	3414(5)	21.1(10)
C7	4181(8)	-245(5)	1486(5)	23.6(10)
C8	1464(6)	5878(5)	2236(5)	19.3(9)
O2	9468(7)	1578(6)	3289(5)	47.8(12)
C10	4194(7)	769(5)	1853(5)	21.3(10)
C11	933(6)	3809(5)	3848(5)	22.5(10)
C12	1298(8)	6911(6)	918(5)	29.0(12)
C13	2233(9)	2900(7)	6106(5)	32.0(13)
C14	-179(9)	8115(6)	791(6)	35.4(14)
C15	836(10)	6480(7)	-47(6)	37.6(15)
C3	9091(10)	431(8)	3387(8)	43.4(16)
C16	1897(7)	3930(5)	4782(5)	22.8(10)
C17	2613(7)	5064(5)	4432(5)	22.4(10)

Table 3 Anisotropic Displacement Parameters ($Å^2 \times 10^3$) for C1. The Anisotropic displacement factor exponent takes the form: $-2\pi^2[h^2a^{*2}U_{11}+2hka^*b^*U_{12}+\ldots]$.

Atom	U_{11}	U_{22}	U_{33}	U_{12}	U_{13}	U_{23}
Cl2	13.8(5)	19.6(5)	22.3(6)	-3.1(4)	-1.8(4)	-5.2(5)
Cl3	11.7(5)	21.3(6)	24.2(6)	-6.9(4)	3.0(4)	-4.7(5)
Ru1	8.7(2)	17.2(2)	18.8(2)	-3.41(14)	0.23(14)	-5.02(16)
N1	10.6(18)	17.6(19)	19.2(19)	-3.4(14)	-1.4(14)	-2.4(16)
C	13(2)	22(2)	21(2)	-3.7(17)	-3.4(17)	-5.3(19)
C1	11(2)	23(2)	26(2)	-2.9(17)	-1.9(18)	-13(2)
C2	12(2)	21(2)	21(2)	-3.8(17)	-0.2(17)	-5(2)
C0aa	12(2)	20(2)	27(3)	-3.5(18)	1.5(18)	-7(2)
N2	40(3)	25(2)	31(2)	-11(2)	6(2)	-11(2)
C5	15(2)	18(2)	27(2)	-6.2(18)	0.6(18)	-5(2)
C6	16(2)	24(2)	19(2)	-5.2(18)	1.6(18)	-5(2)
C7	22(2)	21(2)	23(2)	-5.4(19)	2.7(19)	-5(2)
C8	8.4(19)	21(2)	20(2)	-0.3(17)	-0.8(16)	-2.9(19)
O2	29(2)	61(3)	56(3)	-6(2)	5(2)	-30(3)
C10	13(2)	17(2)	30(3)	-3.0(17)	-2.6(18)	-8(2)
C11	6.0(19)	25(3)	36(3)	-8.2(18)	8.0(19)	-11(2)
C12	15(2)	25(3)	30(3)	5(2)	-4(2)	-1(2)
C13	27(3)	36(3)	21(3)	-2(2)	9(2)	-5(2)
C14	28(3)	27(3)	31(3)	7(2)	-1(2)	0(2)
C15	33(3)	44(4)	25(3)	7(3)	-1(2)	-12(3)
C3	21(3)	51(4)	57(4)	-11(3)	-2(3)	-22(4)
C16	14(2)	24(2)	25(2)	-0.9(18)	2.5(18)	-7(2)
C17	13(2)	25(2)	28(3)	-1.2(18)	-1.5(18)	-12(2)

Table 4 Bond Lengths for C1.

Atom	Atom	Length/Å	Atom	Atom	Length/Å
Cl2	Ru1	2.4274(12)	C1	C11	1.424(8)
Cl3	Ru1	2.4085(12)	C0aa	C8	1.427(7)
Ru1	N1	2.123(4)	C0aa	C17	1.407(8)
Ru1	C1	2.205(5)	N2	C7	1.134(8)
Ru1	C0aa	2.179(5)	C5	C6	1.373(8)
Ru1	C8	2.201(5)	C5	C10	1.393(8)
Ru1	C11	2.192(5)	C7	C10	1.450(7)
Ru1	C16	2.211(5)	C8	C12	1.511(7)
Ru1	C17	2.198(5)	O2	C3	1.397(10)
N1	C2	1.357(6)	C11	C16	1.406(8)
N1	C6	1.347(7)	C12	C14	1.535(8)
C	C2	1.380(7)	C12	C15	1.523(9)
C	C10	1.392(7)	C13	C16	1.509(8)
C1	C8	1.434(7)	C16	C17	1.434(8)

Table 5 Bond Angles for C1.

Atom	Atom	Atom	Angle/°	Atom	Atom	Atom	Angle/°
Cl3	Ru1	Cl2	87.17(4)	C6	N1	Ru1	118.0(3)
N1	Ru1	Cl2	83.86(11)	C6	N1	C2	118.0(5)
N1	Ru1	Cl3	88.00(11)	C10	C	C2	118.8(5)
C1	Ru1	Cl2	152.21(14)	C8	C1	Ru1	70.9(3)
C1	Ru1	Cl3	120.05(14)	C11	C1	Ru1	70.6(3)
C1	Ru1	N1	91.17(17)	C11	C1	C8	121.0(5)
C0aa	Ru1	Cl2	121.48(14)	C	C2	N1	122.3(5)
C0aa	Ru1	Cl3	90.67(14)	C8	C0aa	Ru1	71.8(3)
C0aa	Ru1	N1	154.55(18)	C17	C0aa	Ru1	72.0(3)
C0aa	Ru1	C1	67.66(19)	C17	C0aa	C8	121.4(5)
C8	Ru1	Cl2	159.48(15)	C10	C5	C6	118.4(5)
C8	Ru1	Cl3	91.49(13)	C5	C6	N1	123.3(5)
C8	Ru1	N1	116.58(18)	C10	C7	N2	177.6(6)
C8	Ru1	C1	37.97(19)	C1	C8	Ru1	71.1(3)
C8	Ru1	C0aa	38.03(19)	C0aa	C8	Ru1	70.1(3)
C11	Ru1	Cl2	114.83(15)	C0aa	C8	C1	117.1(4)
C11	Ru1	Cl3	157.83(15)	C12	C8	Ru1	130.1(3)
C11	Ru1	N1	91.61(18)	C12	C8	C1	123.6(5)
C11	Ru1	C1	37.8(2)	C12	C8	C0aa	119.3(5)
C11	Ru1	C0aa	80.3(2)	C5	C10	C	119.3(5)
C11	Ru1	C8	68.93(19)	C7	C10	C	122.2(5)
C16	Ru1	Cl2	90.17(13)	C7	C10	C5	118.5(5)
C16	Ru1	Cl3	153.81(15)	C1	C11	Ru1	71.6(3)
C16	Ru1	N1	117.62(18)	C16	C11	Ru1	72.1(3)
C16	Ru1	C1	67.98(19)	C16	C11	C1	121.5(5)
C16	Ru1	C0aa	68.68(19)	C14	C12	C8	108.7(5)
C16	Ru1	C8	82.05(18)	C15	C12	C8	113.8(5)
C16	Ru1	C11	37.2(2)	C15	C12	C14	111.2(5)
C17	Ru1	Cl2	93.95(14)	C11	C16	Ru1	70.6(3)
C17	Ru1	Cl3	116.26(15)	C13	C16	Ru1	128.5(4)
C17	Ru1	N1	155.57(19)	C13	C16	C11	122.2(5)
C17	Ru1	C1	79.46(19)	C17	C16	Ru1	70.5(3)
C17	Ru1	C0aa	37.5(2)	C17	C16	C11	117.6(5)
C17	Ru1	C8	68.34(19)	C17	C16	C13	120.2(5)
C17	Ru1	C11	67.2(2)	C0aa	C17	Ru1	70.5(3)
C17	Ru1	C16	38.0(2)	C16	C17	Ru1	71.5(3)
C2	N1	Ru1	123.7(3)	C16	C17	C0aa	121.4(5)

Table 6 Hydrogen Atom Coordinates (Å×10^4) and Isotropic Displacement Parameters (Å^2×10^3) for C1.

Atom	*x*	*y*	*z*	U(eq)
H2a	8630(80)	1920(50)	3580(90)	71.6(19)
H11	530(90)	3150(60)	4060(50)	16(14)
H0aa	2990(80)	6600(60)	2900(50)	10(13)
H1	240(100)	4840(70)	1920(70)	32(18)
H17	3470(110)	5150(80)	4960(80)	50(20)
H5	3810(80)	-310(60)	3640(50)	11(13)
H2	4420(80)	3730(50)	820(50)	8(12)
H	4540(100)	2250(70)	150(70)	31(17)
H6	3790(110)	1410(70)	4130(70)	40(20)
H15a	1750(100)	5770(70)	-70(60)	31(17)
H15b	-390(90)	6310(60)	-120(60)	20(15)
H15c	960(120)	7160(80)	-850(80)	50(20)
H14a	-480(100)	8830(70)	-160(70)	35(19)
H14b	190(80)	8340(60)	1500(50)	13(13)
H12	2480(140)	7340(90)	570(90)	60(30)
H14c	-1370(100)	8040(60)	870(60)	22(16)
H13a	1760(130)	3200(90)	6550(80)	50(20)
H13b	1890(130)	2220(100)	6120(90)	60(30)
H3a	8230(150)	710(100)	2710(90)	70(30)
H3b	10210(150)	-140(100)	3240(90)	70(30)
H3c	8710(180)	-220(120)	4330(120)	110(40)

Experimental

Single crystals of $C_{17}H_{21}Cl_2N_2ORu$ **[C1]** were **[]**. A suitable crystal was selected and **[]** on a diffractometer. The crystal was kept at 273.15 K during data collection. Using Olex2 [1], the structure was solved with the olex2.solve [2] structure solution program using Charge Flipping and refined with the olex2.refine [3] refinement package using Gauss-Newton minimisation.

1. Dolomanov, O.V., Bourhis, L.J., Gildea, R.J, Howard, J.A.K. & Puschmann, H. (2009), J. Appl. Cryst. 42, 339-341.
2. Bourhis, L.J., Dolomanov, O.V., Gildea, R.J., Howard, J.A.K., Puschmann, H. (2015). Acta Cryst. A71, 59-75.
3. Bourhis, L.J., Dolomanov, O.V., Gildea, R.J., Howard, J.A.K., Puschmann, H. (2015). Acta Cryst. A71, 59-75.

Crystal structure determination of [C1]

Crystal Data for $C_{17}H_{21}Cl_2N_2ORu$ (M=441.34 g/mol): triclinic, space group P-1 (no. 2), a = 7.2742(13) Å, b = 11.827(2) Å, c = 12.046(2) Å, α = 64.300(5)°, β = 89.453(5)°, γ = 77.446(5)°, V = 907.3(3) Å^3, Z = 2, T = 273.15 K, μ(Mo Kα) = 1.163 mm^{-1}, *Dcalc* = 1.6155 g/cm^3, 4361 reflections measured (3.94° ≤ 2Θ ≤ 56°), 4361 unique (R_{int} = 0.0000, R_{sigma} = 0.0623) which were used in all calculations. The final R_1 was 0.0631 (I>=2u(I)) and wR_2 was 0.1739 (all data).

Refinement model description

Number of restraints - 0, number of constraints - 2.

Details:

```
1. Fixed Uiso
 At 1.5 times of:
  All O(H) groups
2.a Idealised tetrahedral OH refined as rotating group:
 O2(H2a)
```

Appendix B. Supplementary Information for Chapter 3

^{1}H NMR spectrum for Pterpy

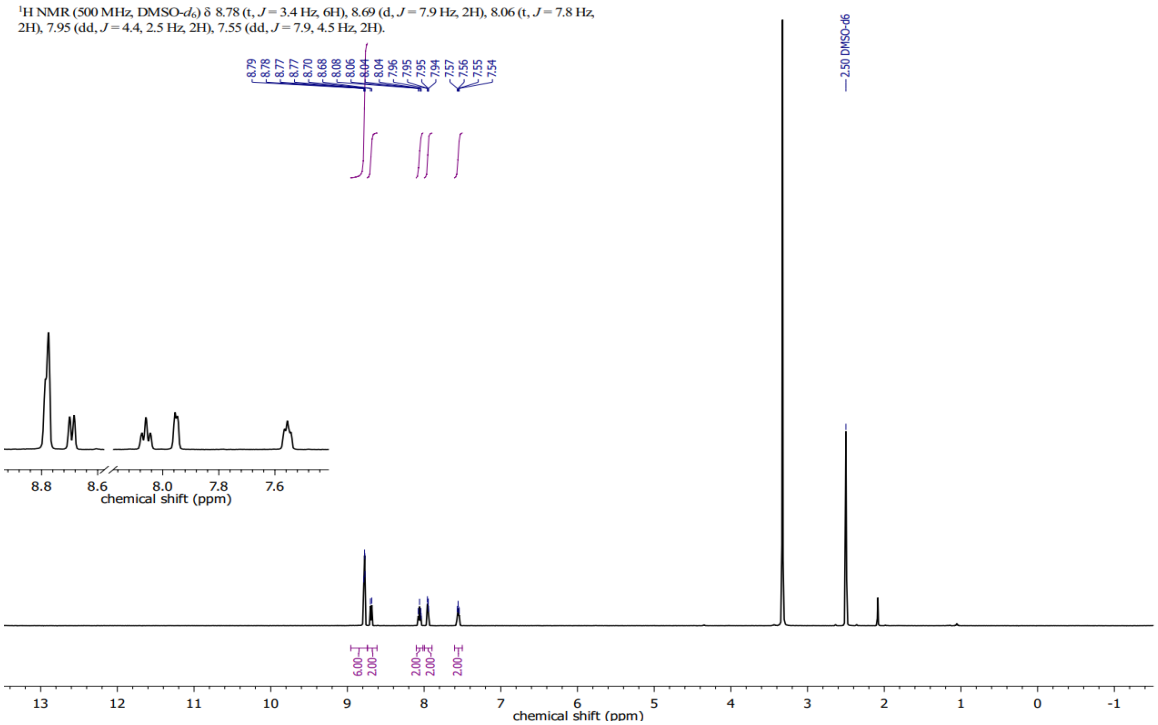

Solvent impurities: δ 1.06 (t, CH_3, ethanol), 2.09 (s, CH_3, acetone), 3.33 (s, HDO).

^{1}H NMR spectrum for [Au(Pterpy)Cl$_2$]Cl

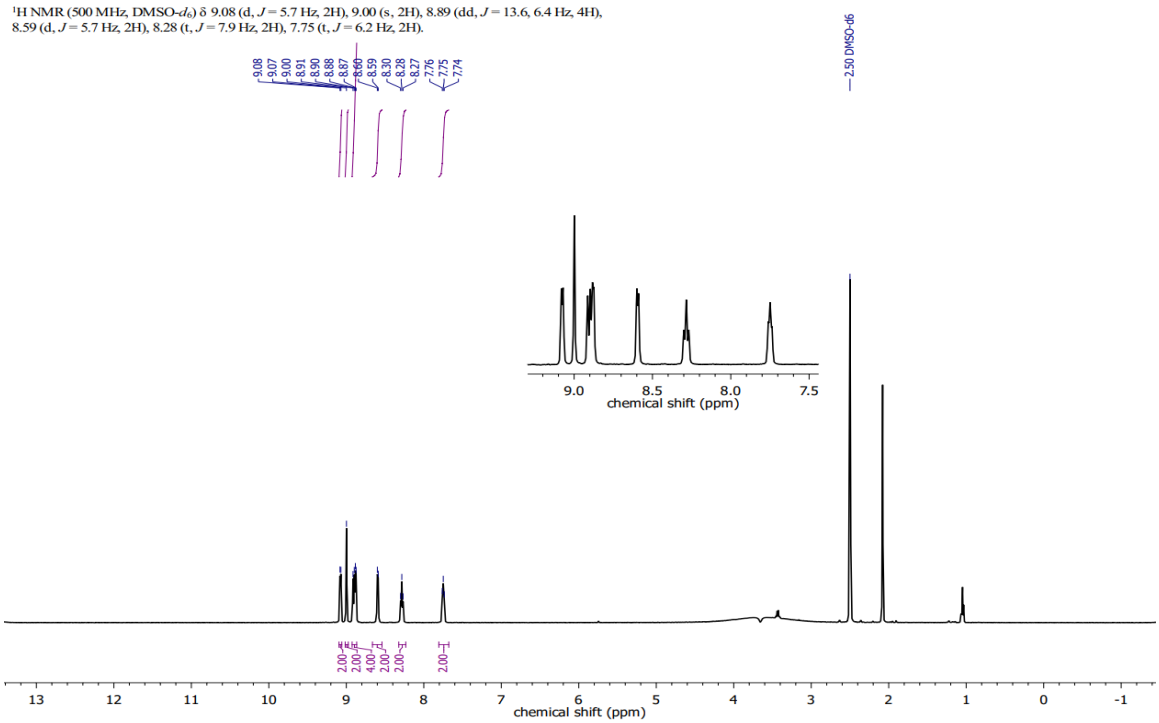

Solvent impurities: δ 1.06 (t, CH_3, ethanol), 2.09 (s, CH_3, acetone), 3.44 (q, CH_2, ethanol), 3.66 (suppressed, s, HDO).

MALDI-TOF for $[Au(Ptepy)Cl_2]Cl$

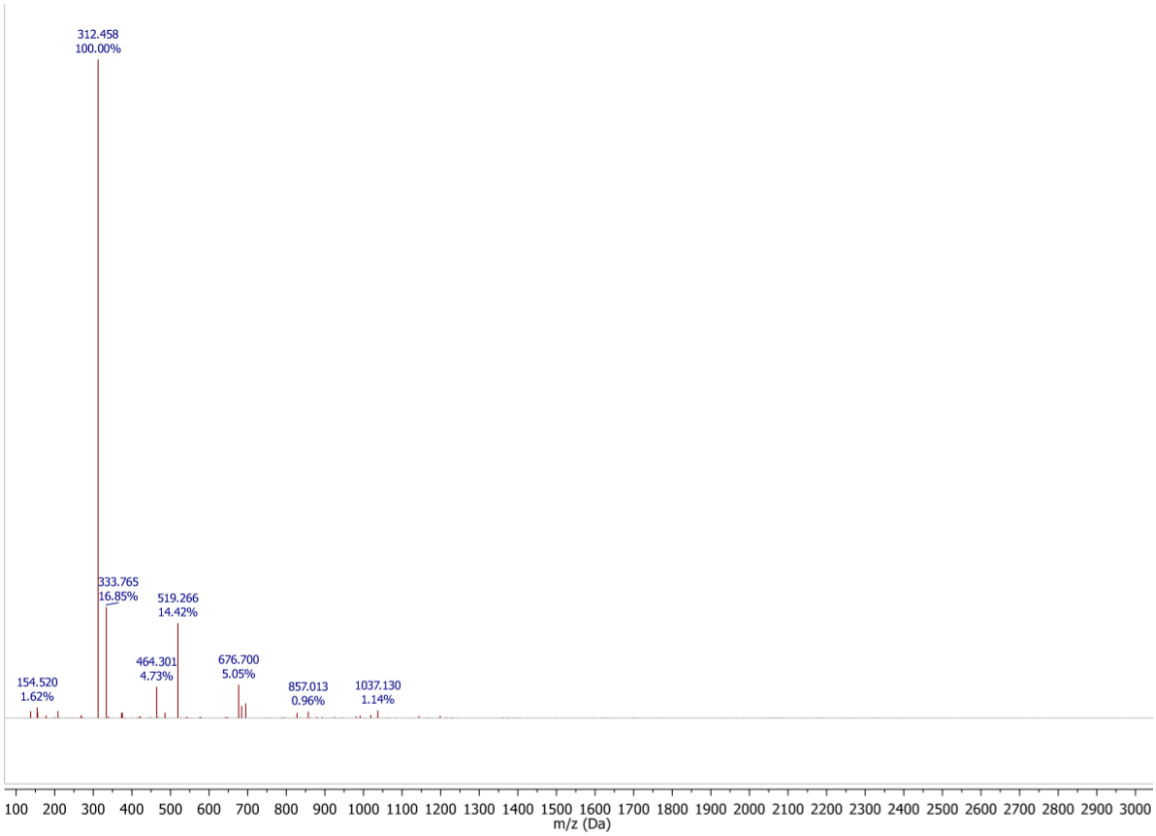

^{1}H NMR spectrum for Ru(II)-arene-Au(III)

^{1}H NMR (400 MHz, DMSO-d_6) δ 9.86 (d, J = 4.8 Hz, 2H), 9.05 – 9.00 (m, 2H), 8.92 (s, 2H), 8.83 (dd, J = 4.9, 1.6 Hz, 2H), 8.81 (d, J = 8.0 Hz, 2H), 8.51 – 8.47 (m, 2H), 8.19 (td, J = 7.8, 1.8 Hz, 2H), 7.66 (dd, J = 7.5, 4.9 Hz, 2H), 5.81 (d, J = 6.2 Hz, 2H), 5.77 (d, J = 6.3 Hz, 2H), 2.86 – 2.80 (m, 1H), 2.09 (s, 3H), 1.19 (d, J = 6.9 Hz, 6H).

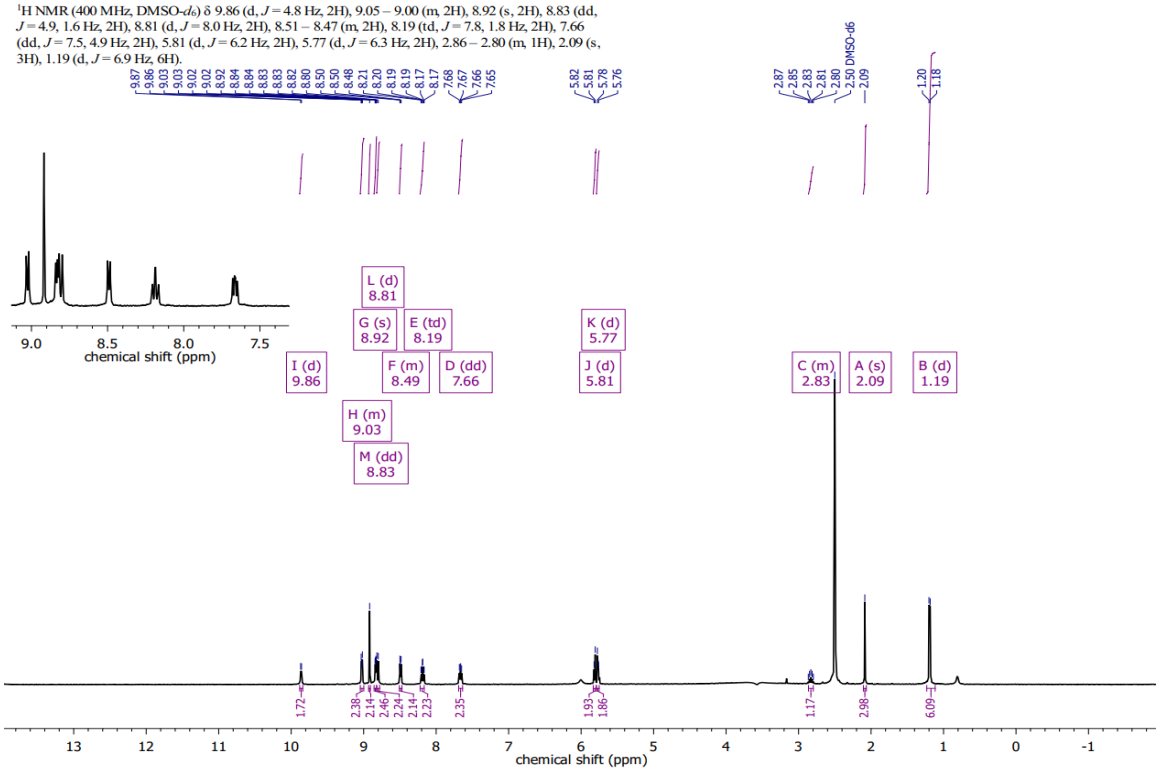

Electrospray ionization mass spectrum for (positive) Ru(II)-arene-Au(III)

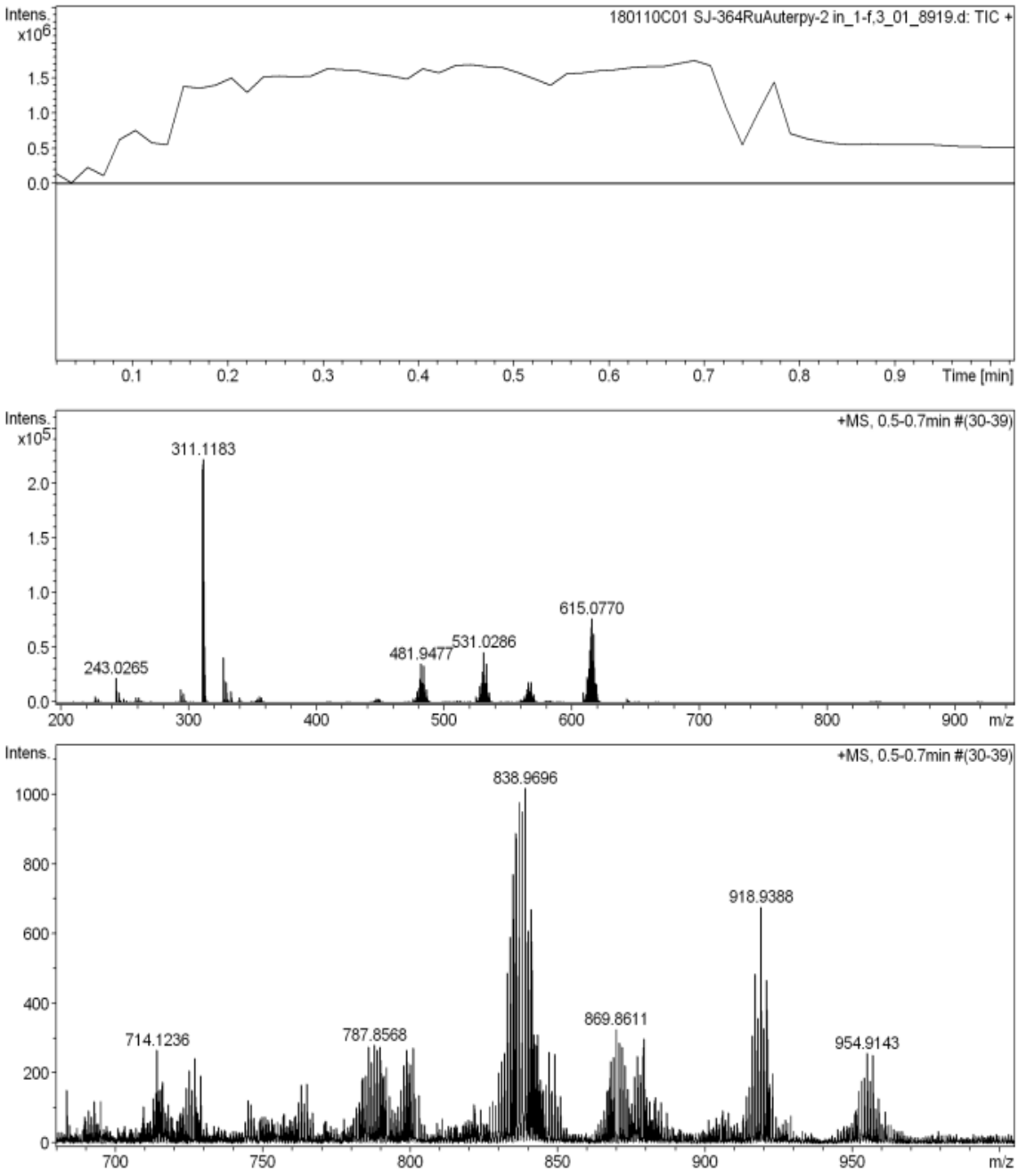

[pterpy+H] calculated 311.1291 found 311.1183, $[M+2Na]^{2+}$ calculated 481.9625 found 481.9477, $[M+H]^{+}$ calculated 918.9539 found 918.9388.

IR spectra for {Au(Pterpy)Cl_2]Cl and Ru(II)-arene-Au(III)

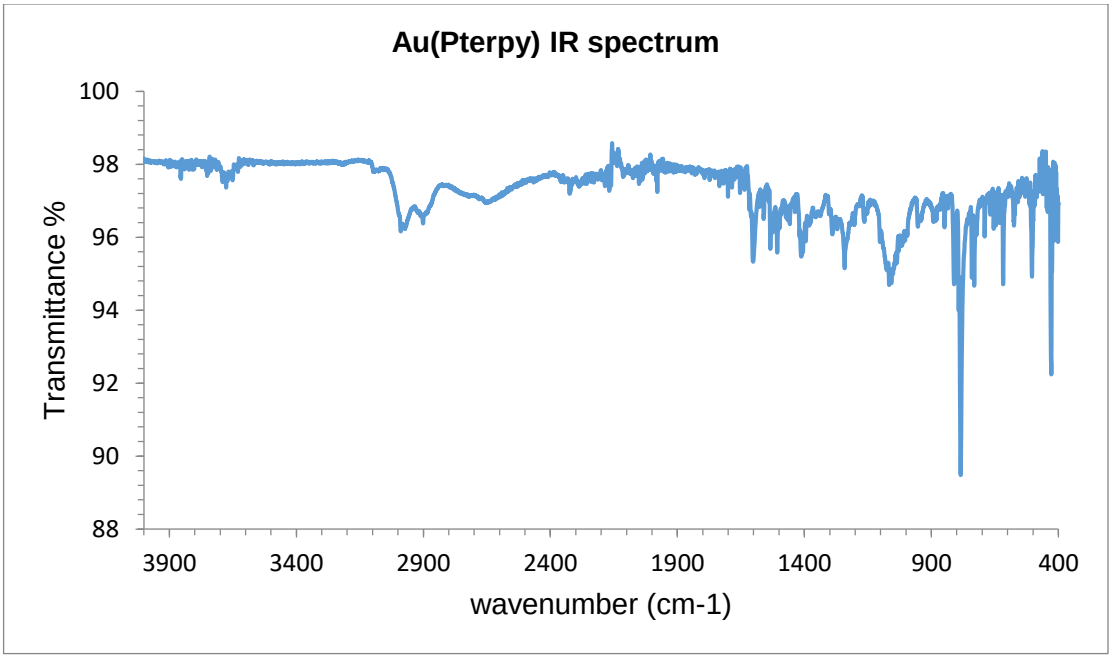

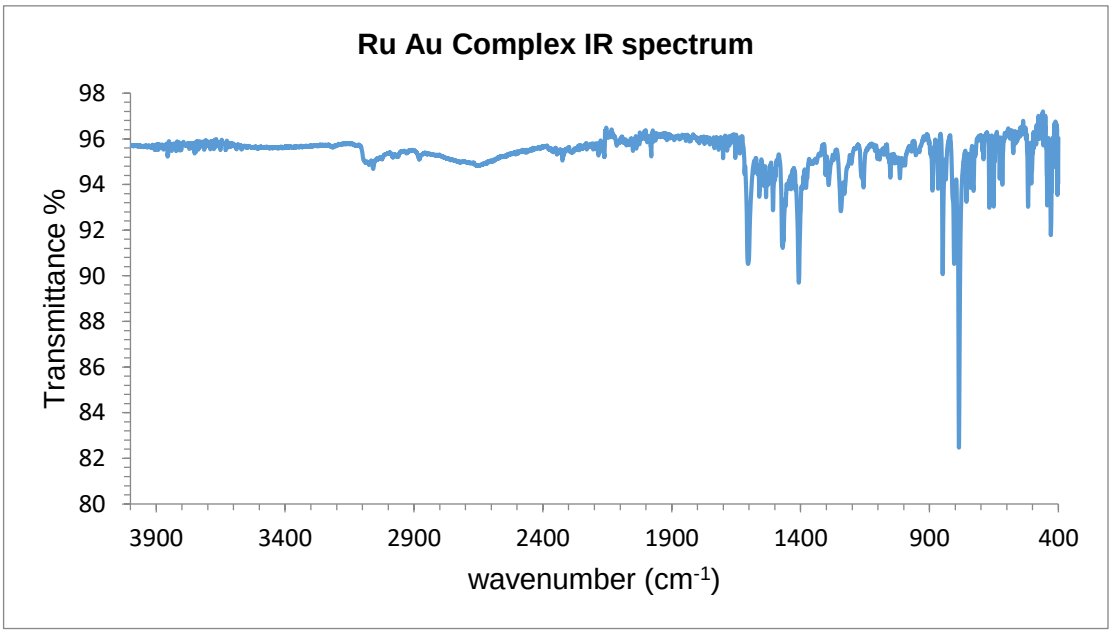

[Ru(Pterpy)Cl_3] Crystal data Tables

Table 1 Crystal data and structure refinement for [Ru(Pterpy)Cl3].

Identification code	[Ru(Pterpy)Cl3]
Empirical formula	$C_{20}H_{14}AuCl_3N_4ORu$
Formula weight	517.77
Temperature/K	150(2)
Crystal system	monoclinic
Space group	$P2_1/c$
a/Å	10.1597(2)
b/Å	13.6038(2)
c/Å	13.7817(2)
α/°	90
β/°	97.0630(10)
γ/°	90
Volume/$Å^3$	1890.32(5)
Z	4
$\rho_{calc}g/cm^3$	1.819
μ/mm^{-1}	10.732
F(000)	1028.0
Crystal size/mm^3	? × ? × ?
Radiation	CuKα (λ = 1.54178)
2Θ range for data collection/°	8.77 to 133.29
Index ranges	$-11 \leq h \leq 12$, $-15 \leq k \leq 16$, $-16 \leq l \leq 16$
Reflections collected	8372
Independent reflections	3297 [R_{int} = 0.0503, R_{sigma} = 0.0578]
Data/restraints/parameters	3297/0/253
Goodness-of-fit on F^2	1.005
Final R indexes [I>=2σ (I)]	R_1 = 0.0356, wR_2 = 0.0740
Final R indexes [all data]	R_1 = 0.0549, wR_2 = 0.0806
Largest diff. peak/hole / e $Å^{-3}$	0.50/-0.46

Table 2 Fractional Atomic Coordinates ($\times 10^4$) and Equivalent Isotropic Displacement Parameters ($Å^2 \times 10^3$) for [Ru(Pterpy)Cl3]. U_{eq} is defined as 1/3 of of the trace of the orthogonalised U_{IJ} tensor.

Atom	*x*	*y*	*z*	U(eq)
Ru01	6944.1(4)	9191.1(2)	2949.6(2)	19.18(11)
Cl02	6875.2(12)	10833.7(8)	2375.7(8)	28.0(3)
Cl03	8960.0(12)	8873.4(8)	2325.0(8)	24.3(2)
Cl04	4901.8(12)	9349.5(8)	3556.4(8)	26.9(3)
N005	7070(4)	7822(3)	3401(3)	18.8(8)
N006	7884(4)	9392(3)	4357(3)	18.8(8)
N007	5972(4)	8492(3)	1732(3)	19.3(8)
N008	8560(4)	2884(3)	4649(3)	28.3(10)
C009	6595(5)	7115(3)	2783(3)	21.5(10)
C00A	5898(5)	7504(3)	1835(3)	20.5(10)
C00B	7578(4)	5900(3)	3920(3)	17.4(9)
C00C	7769(4)	7629(3)	4285(3)	19.6(10)
C00D	8044(5)	6668(3)	4551(3)	18.3(9)
C00E	6813(5)	6141(3)	3028(3)	21.6(10)
C00F	8154(5)	10251(3)	4822(3)	22.6(10)
C00G	7908(5)	4860(3)	4172(3)	20.5(10)
C00H	8316(5)	4561(3)	5132(3)	23.1(10)
C00I	4758(5)	8364(3)	147(3)	21.9(10)
C00J	8767(5)	8529(3)	5803(3)	23.1(10)
C00K	8175(5)	8529(3)	4846(3)	18.9(10)
C00L	5420(5)	8914(3)	906(3)	22.5(10)
C00M	4651(5)	7374(4)	265(3)	23.8(10)
C00N	7844(5)	4132(3)	3461(3)	24.8(10)
C00O	8736(5)	10280(3)	5774(3)	25.7(11)
C00P	8175(5)	3178(4)	3729(4)	30.0(12)
C00Q	9058(5)	9416(3)	6270(3)	26.9(11)
C00R	5248(5)	6929(4)	1111(3)	25.1(11)
C00S	8602(5)	3591(4)	5324(4)	27.6(11)

Table 3 Anisotropic Displacement Parameters ($Å^2 \times 10^3$) for [Ru(Pterpy)Cl3]. The Anisotropic displacement factor exponent takes the form: $-2\pi^2[h^2a^{*2}U_{11}+2hka^*b^*U_{12}+\ldots]$.

Atom	U_{11}	U_{22}	U_{33}	U_{23}	U_{13}	U_{12}
Ru01	24.26(19)	14.10(16)	18.04(17)	0.11(14)	-1.95(14)	-0.36(15)
Cl02	41.7(7)	17.0(5)	24.8(5)	2.7(4)	2.7(5)	-0.7(5)
Cl03	24.3(6)	25.5(5)	22.2(5)	-3.7(4)	-0.8(5)	-3.0(5)
Cl04	28.4(6)	24.1(6)	27.9(5)	5.9(4)	2.4(5)	4.1(5)
N005	22(2)	13.4(18)	19.1(18)	1.6(14)	-5.1(17)	1.3(15)
N006	22(2)	15.9(19)	16.8(18)	-2.0(14)	-2.5(17)	-1.5(15)
N007	15.5(19)	22(2)	19.0(19)	0.9(15)	-3.1(17)	-1.8(15)
N008	27(2)	21(2)	37(2)	3.6(18)	4(2)	4.2(18)
C009	20(3)	20(2)	23(2)	-0.3(18)	-3(2)	-2.3(18)
C00A	19(2)	24(2)	18(2)	-1.3(18)	0(2)	-1.3(19)
C00B	15(2)	17(2)	20(2)	-0.2(18)	0.3(19)	-1.7(18)
C00C	16(2)	23(2)	20(2)	-1.2(18)	2(2)	-0.6(19)
C00D	20(2)	16(2)	19(2)	-0.8(17)	1(2)	0.6(19)
C00E	22(2)	15(2)	25(2)	-6.0(19)	-3(2)	-1.9(19)
C00F	29(3)	13(2)	28(2)	0.1(18)	7(2)	-2.8(19)
C00G	17(2)	17(2)	27(2)	-1.0(18)	2(2)	-1.3(18)
C00H	27(3)	14(2)	28(2)	0.1(19)	3(2)	-1.6(19)
C00I	19(2)	25(2)	19(2)	1.4(19)	-4(2)	1.0(19)
C00J	27(3)	23(2)	19(2)	-2.2(18)	-1(2)	0(2)
C00K	22(2)	17(2)	17(2)	-0.9(17)	0(2)	-1.5(18)
C00L	23(3)	23(2)	22(2)	4.6(18)	1(2)	-0.1(19)
C00M	20(2)	32(3)	19(2)	-5.3(19)	1(2)	-1(2)
C00N	24(2)	23(2)	27(2)	-2(2)	2(2)	-4(2)
C00O	28(3)	22(2)	27(2)	-5.9(19)	2(2)	-1(2)
C00P	35(3)	18(2)	38(3)	-4(2)	9(3)	1(2)
C00Q	30(3)	28(3)	21(2)	-3.4(19)	-1(2)	-1(2)
C00R	30(3)	21(2)	23(2)	-2.1(19)	-2(2)	-1(2)
C00S	27(3)	25(3)	29(3)	10(2)	-3(2)	1(2)

Table 4 Bond Lengths for [Ru(Pterpy)Cl3].

Atom	Atom	Length/Å	Atom	Atom	Length/Å
Ru01	N005	1.962(4)	C00B	C00D	1.404(6)
Ru01	N007	2.070(4)	C00B	C00E	1.409(6)
Ru01	N006	2.072(3)	C00B	C00G	1.485(6)
Ru01	Cl04	2.3406(13)	C00C	C00D	1.378(6)
Ru01	Cl03	2.3571(13)	C00C	C00K	1.479(6)
Ru01	Cl02	2.3686(12)	C00F	C00O	1.371(7)
N005	C009	1.335(6)	C00G	C00N	1.388(6)
N005	C00C	1.358(6)	C00G	C00H	1.398(6)
N006	C00F	1.345(6)	C00H	C00S	1.370(6)
N006	C00K	1.367(5)	C00I	C00M	1.363(7)
N007	C00L	1.336(6)	C00I	C00L	1.390(6)
N007	C00A	1.355(6)	C00J	C00K	1.380(6)
N008	C00S	1.335(6)	C00J	C00Q	1.381(6)
N008	C00P	1.341(6)	C00M	C00R	1.384(6)
C009	C00E	1.379(6)	C00N	C00P	1.380(7)
C009	C00A	1.504(6)	C00O	C00Q	1.379(7)
C00A	C00R	1.372(6)			

Table 5 Bond Angles for [Ru(Pterpy)Cl3].

Atom	Atom	Atom	Angle/°	Atom	Atom	Atom	Angle/°
N005	Ru01	N007	80.04(15)	N007	C00A	C009	114.4(4)
N005	Ru01	N006	79.84(14)	C00R	C00A	C009	124.4(4)
N007	Ru01	N006	159.72(14)	C00D	C00B	C00E	118.3(4)
N005	Ru01	Cl04	90.01(12)	C00D	C00B	C00G	121.0(4)
N007	Ru01	Cl04	88.63(11)	C00E	C00B	C00G	120.7(4)
N006	Ru01	Cl04	88.84(11)	N005	C00C	C00D	119.3(4)
N005	Ru01	Cl03	85.18(12)	N005	C00C	C00K	113.0(4)
N007	Ru01	Cl03	88.25(11)	C00D	C00C	C00K	127.7(4)
N006	Ru01	Cl03	92.59(11)	C00C	C00D	C00B	120.0(4)
Cl04	Ru01	Cl03	174.66(4)	C009	C00E	C00B	119.5(4)
N005	Ru01	Cl02	177.61(12)	N006	C00F	C00O	121.3(4)
N007	Ru01	Cl02	99.85(11)	C00N	C00G	C00H	116.4(4)
N006	Ru01	Cl02	100.36(10)	C00N	C00G	C00B	121.6(4)
Cl04	Ru01	Cl02	92.37(4)	C00H	C00G	C00B	122.0(4)
Cl03	Ru01	Cl02	92.43(4)	C00S	C00H	C00G	119.6(4)
C009	N005	C00C	122.7(4)	C00M	C00I	C00L	118.7(4)
C009	N005	Ru01	118.5(3)	C00K	C00J	C00Q	119.2(4)
C00C	N005	Ru01	118.3(3)	N006	C00K	C00J	120.9(4)
C00F	N006	C00K	119.5(4)	N006	C00K	C00C	115.0(4)
C00F	N006	Ru01	127.2(3)	C00J	C00K	C00C	124.1(4)
C00K	N006	Ru01	113.3(3)	N007	C00L	C00I	121.6(4)
C00L	N007	C00A	119.5(4)	C00I	C00M	C00R	120.0(4)
C00L	N007	Ru01	127.0(3)	C00P	C00N	C00G	119.6(5)
C00A	N007	Ru01	113.4(3)	C00F	C00O	C00Q	119.8(4)
C00S	N008	C00P	115.2(4)	N008	C00P	C00N	124.5(5)
N005	C009	C00E	120.1(4)	C00O	C00Q	C00J	119.3(4)
N005	C009	C00A	113.3(4)	C00A	C00R	C00M	119.1(5)
C00E	C009	C00A	126.5(4)	N008	C00S	C00H	124.8(5)
N007	C00A	C00R	121.1(4)				

Table 6 Hydrogen Atom Coordinates (Å×10^4) and Isotropic Displacement Parameters (Å^2×10^3) for [Ru (Pterpy)Cl3].

Atom	*x*	*y*	*z*	U(eq)
H00D	8549.47	6524.63	5160.69	22
H00E	6450.53	5635.81	2599.85	26
H00F	7938.32	10849	4484.57	27
H00H	8393.37	5028.17	5648.82	28
H00I	4387.66	8672.93	-442.26	26
H00J	8971.02	7926.89	6136.57	28
H00L	5481.18	9606.51	834.83	27
H00M	4167.41	6989.19	-231.78	29
H00N	7573.16	4290.27	2794.9	30
H00O	8916.37	10894.09	6090.79	31
H00P	8125.75	2695.38	3227.16	36
H00Q	9475.39	9429.37	6925.48	32
H00R	5207.37	6236.61	1187.76	30
H00S	8849.64	3407.83	5986.63	33

Experimental

Single crystals of $C_{20}H_{14}AuCl_3N_4ORu$ **[[Ru(Pterpy)Cl3]]** were **[]**. A suitable crystal was selected and **[]** on a diffractometer. The crystal was kept at 150(2) K during data collection. Using Olex2 [1], the structure was solved with the Unknown [2] structure solution program using Unknown and refined with the Unknown [3] refinement package using Unknown minimisation.

1.
2.
3.

Crystal structure determination of [[Ru(Pterpy)Cl3]]

Crystal Data for $C_{20}H_{14}AuCl_3N_4ORu$ (M=517.77 g/mol): monoclinic, space group $P2_1/c$ (no. 14), a = 10.1597 (2) Å, b = 13.6038(2) Å, c = 13.7817(2) Å, β = 97.0630(10)°, V = 1890.32(5) Å^3, Z = 4, T = 150(2) K, μ(CuKα) = 10.732 mm^{-1}, *Dcalc* = 1.819 g/cm^3, 8372 reflections measured (8.77° ≤ 2Θ ≤ 133.29°), 3297 unique (R_{int} = 0.0503, R_{sigma} = 0.0578) which were used in all calculations. The final R_1 was 0.0356 (I > 2σ(I)) and wR_2 was 0.0806 (all data).

Refinement model description

Number of restraints - 0, number of constraints - unknown.

Details:

N/A

This report has been created with Olex2, compiled on 2017.08.10 svn.r3458 for OlexSys. Please let us know if there are any errors or if you would like to have additional features.

References for the experimental section:

1. Bourhis, L.J., Dolomanov, O.V., Gildea, R.J., Howard, J.A.K., Puschmann, H. (2015). Acta Cryst. A71, 59-75.

2. Dolomanov, O.V., Bourhis, L.J., Gildea, R.J, Howard, J.A.K. & Puschmann, H. (2009), J. Appl. Cryst. 42, 339-341.

[Ru(η^6-*p*-cymene)(NH_3)$_2$Cl]PF_6 Crystal data tables

SJ100

Table 1 Crystal data and structure refinement for SJ100.

Identification code	SJ100
Empirical formula	$C_{40}N_8RuClPFH$
Formula weight	903.30
Temperature/K	299.01
Crystal system	triclinic
Space group	P-1
a/Å	8.1167(13)
b/Å	9.0006(14)
c/Å	11.3836(18)
α/°	88.140(2)
β/°	88.283(2)
γ/°	77.956(2)
Volume/Å^3	812.7(2)
Z	1
ρ_{calc}g/cm^3	1.8456
μ/mm^{-1}	1.282
F(000)	448.1
Crystal size/mm^3	N/A × N/A × N/A
Radiation	Mo Kα (λ = 0.71073)
2Θ range for data collection/°	3.58 to 58.42
Index ranges	$-10 \leq h \leq 11$, $-12 \leq k \leq 12$, $-15 \leq l \leq 15$
Reflections collected	16901
Independent reflections	4409 [R_{int} = 0.0128, R_{sigma} = 0.0108]
Data/restraints/parameters	4409/115/274
Goodness-of-fit on F^2	1.067
Final R indexes [I>=2σ (I)]	R_1 = 0.0189, wR_2 = 0.0490
Final R indexes [all data]	R_1 = 0.0205, wR_2 = 0.0503
Largest diff. peak/hole / e Å^{-3}	0.63/-0.31

Table 2 Fractional Atomic Coordinates ($\times 10^4$) and Equivalent Isotropic Displacement Parameters ($Å^2 \times 10^3$) for SJ100. U_{eq} is defined as 1/3 of of the trace of the orthogonalised U_{IJ} tensor.

Atom	*x*	*y*	*z*	U(eq)
Ru1	4078.85(13)	2926.38(12)	3160.68(9)	26.23(4)
F1	-867(16)	8281(9)	1609(14)	114(3)
P1	-973.6(6)	6747.5(5)	2240.7(4)	45.66(11)
Cl1	6177.9(6)	2828.1(5)	4637.0(4)	44.44(10)
N2	4498(3)	5172.8(18)	2786.9(15)	44.6(3)
F3	-2149(9)	6306(9)	1349(5)	126(2)
N1	2365(2)	4070(2)	4464.7(14)	42.5(3)
F2	619(6)	5926(7)	1549(6)	97(2)
F4	-2579(7)	7482(6)	3020(5)	88.7(17)
C008	5102.1(19)	1982.4(17)	1464.1(13)	31.6(3)
F6	164(11)	7122(7)	3232(7)	131(3)
F5	-1053(14)	5199(7)	2938(9)	65.7(19)
C00A	4277(2)	461.2(17)	3146.7(15)	36.9(3)
C00B	5532(2)	876.6(17)	2367.9(14)	33.5(3)
C00C	3368(2)	2703.5(19)	1366.6(13)	35.6(3)
C00D	6397(2)	2439(2)	612.7(14)	39.0(3)
C00E	2129(2)	2308(2)	2138.1(15)	38.9(3)
C00F	2567(2)	1163.4(19)	3037.8(15)	38.9(3)
C00I	6503(3)	1488(3)	-488.7(17)	58.4(5)
C00J	8118(3)	2298(3)	1135.4(19)	55.9(5)
C00K	1247(3)	777(3)	3878(2)	59.2(5)
F6a	-2698(15)	6637(18)	1745(14)	177(7)
F2a	-60(20)	5760(13)	1212(10)	139(6)
F3a	781(12)	6829(13)	2737(16)	144(6)
F4a	-1850(20)	7832(10)	3232(7)	98(4)
F1a	-1130(30)	8214(14)	1416(14)	112(5)
F5a	-882(18)	5248(11)	3052(11)	60(2)

Table 3 Anisotropic Displacement Parameters ($Å^2 \times 10^3$) for SJ100. The Anisotropic displacement factor exponent takes the form: $-2\pi^2[h^2a^{*2}U_{11}+2hka^*b^*U_{12}+\ldots]$.

Atom	U_{11}	U_{22}	U_{33}	U_{12}	U_{13}	U_{23}
Ru1	27.64(6)	24.71(6)	25.64(6)	-3.33(4)	-1.63(4)	-3.08(4)
F1	94(4)	57(3)	172(8)	8(3)	51(4)	50(4)
P1	43.2(2)	40.1(2)	48.2(2)	1.57(18)	7.43(19)	5.14(19)
Cl1	46.9(2)	41.1(2)	43.8(2)	-2.34(17)	-18.24(17)	-7.53(16)
N2	65.2(11)	31.2(7)	38.9(8)	-13.6(7)	-2.2(7)	-2.0(6)
F3	124(5)	192(5)	66(2)	-37(4)	-46(3)	4(3)
N1	43.5(8)	45.6(8)	36.6(7)	-4.3(7)	5.0(6)	-10.6(7)
F2	78(2)	67(3)	123(4)	22.3(18)	59(2)	23(3)
F4	86(3)	63(2)	93(3)	29.8(17)	45(2)	19.2(18)
C008	35.4(7)	32.0(7)	28.5(6)	-8.3(6)	0.7(5)	-8.8(5)
F6	139(5)	110(4)	158(4)	-51(4)	-52(4)	-38(3)
F5	87(4)	46(3)	68(4)	-24(3)	11(2)	1(2)
C00A	44.8(9)	26.6(7)	39.4(8)	-7.4(6)	0.3(6)	-2.8(6)
C00B	33.8(7)	28.1(7)	37.3(7)	-2.7(5)	-0.0(6)	-8.1(5)
C00C	38.6(8)	37.8(8)	30.5(7)	-6.9(6)	-7.7(6)	-4.6(6)
C00D	43.7(9)	41.4(8)	34.3(7)	-14.3(7)	5.1(6)	-5.9(6)
C00E	30.0(7)	43.4(9)	44.4(8)	-8.1(6)	-5.8(6)	-10.3(7)
C00F	39.2(8)	36.5(8)	44.6(8)	-15.4(7)	4.2(7)	-9.5(6)
C00I	66.7(13)	77.9(15)	37.2(9)	-29.0(11)	12.3(9)	-18.9(9)
C00J	44.9(10)	78.1(15)	51.3(10)	-27.3(10)	3.7(8)	-7.3(10)
C00K	51.9(11)	59.7(12)	70.8(14)	-24.8(10)	17.6(10)	-3.9(10)
F6a	83(6)	279(12)	187(13)	-94(7)	-62(7)	144(10)
F2a	251(15)	76(4)	82(5)	-23(8)	92(8)	-15(4)
F3a	62(4)	91(6)	278(15)	-15(4)	-55(7)	51(8)
F4a	167(10)	54(3)	55(3)	13(5)	32(5)	-3(2)
F1a	153(12)	66(5)	84(7)	37(6)	56(5)	42(3)
F5a	66(4)	57(5)	40(3)	22(4)	9(2)	17(3)

Table 4 Bond Lengths for SJ100.

Atom	Atom	Length/Å
Ru1	Cl1	2.4154(5)
Ru1	N2	2.1466(15)
Ru1	N1	2.1393(15)
Ru1	C008	2.2040(14)
Ru1	C00A	2.1915(15)
Ru1	C00B	2.1785(14)
Ru1	C00C	2.1655(15)
Ru1	C00E	2.1656(15)
Ru1	C00F	2.2093(16)
F1	P1	1.553(6)
P1	F3	1.530(4)
P1	F2	1.554(4)
P1	F4	1.591(3)
P1	F6	1.567(4)
P1	F5	1.593(6)
P1	F6a	1.548(7)
P1	F2a	1.567(7)
P1	F3a	1.564(7)
P1	F4a	1.570(6)
P1	F1a	1.580(10)
P1	F5a	1.600(8)
C008	C00B	1.408(2)
C008	C00C	1.428(2)
C008	C00D	1.519(2)
C00A	C00B	1.431(2)
C00A	C00F	1.407(2)
C00C	C00E	1.409(2)
C00D	C00I	1.532(2)
C00D	C00J	1.514(3)
C00E	C00F	1.427(3)
C00F	C00K	1.503(2)

Table 5 Bond Angles for SJ100.

Atom	Atom	Atom	Angle/°
N2	Ru1	Cl1	84.40(5)
N1	Ru1	Cl1	84.65(5)
N1	Ru1	N2	82.77(7)
C008	Ru1	Cl1	114.06(4)
C008	Ru1	N2	95.68(6)
C008	Ru1	N1	161.07(7)
C00A	Ru1	Cl1	95.01(5)
C00A	Ru1	N2	162.53(7)
C00A	Ru1	N1	114.60(7)
C00A	Ru1	C008	68.55(6)
C00B	Ru1	Cl1	91.15(4)
C00B	Ru1	N2	124.31(7)
C00B	Ru1	N1	152.12(7)
C00B	Ru1	C008	37.46(6)
C00B	Ru1	C00A	38.22(6)
C00C	Ru1	Cl1	151.49(5)
C00C	Ru1	N2	91.67(6)
C00C	Ru1	N1	122.95(7)
C00C	Ru1	C008	38.12(6)
C00C	Ru1	C00A	80.50(6)
C00C	Ru1	C00B	67.87(6)
C00E	Ru1	Cl1	160.76(5)
C00E	Ru1	N2	114.61(7)
C00E	Ru1	N1	94.51(7)
C00E	Ru1	C008	68.88(6)
C00E	Ru1	C00A	67.82(7)
C00E	Ru1	C00B	80.61(6)
C00E	Ru1	C00C	37.98(6)
C00F	Ru1	Cl1	122.69(5)
C00F	Ru1	N2	151.56(7)
C00F	Ru1	N1	90.80(7)
C00F	Ru1	C008	81.59(6)
C00F	Ru1	C00A	37.30(6)
C00F	Ru1	C00B	68.41(6)
C00F	Ru1	C00C	68.70(6)
C00F	Ru1	C00E	38.07(7)
F3	P1	F1	94.9(7)
F2	P1	F1	90.7(4)
F2	P1	F3	92.0(3)
F4	P1	F1	93.4(4)
F4	P1	F3	89.1(3)
F4	P1	F2	175.6(3)

Atom	Atom	Atom	Angle/°
F5	P1	F3	87.5(5)
F5	P1	F2	89.9(4)
F5	P1	F4	85.9(4)
F5	P1	F6	88.4(5)
F2a	P1	F6a	89.8(6)
F3a	P1	F6a	179.0(6)
F3a	P1	F2a	89.4(6)
F4a	P1	F6a	91.6(6)
F4a	P1	F2a	176.0(5)
F4a	P1	F3a	89.2(6)
F1a	P1	F6a	84.9(10)
F1a	P1	F2a	89.5(7)
F1a	P1	F3a	95.7(10)
F1a	P1	F4a	86.9(6)
F5a	P1	F6a	92.7(7)
F5a	P1	F2a	90.2(6)
F5a	P1	F3a	86.6(7)
F5a	P1	F4a	93.4(5)
F5a	P1	F1a	177.6(8)
C00B	C008	Ru1	70.28(8)
C00C	C008	Ru1	69.48(8)
C00C	C008	C00B	117.61(14)
C00D	C008	Ru1	131.00(10)
C00D	C008	C00B	122.89(14)
C00D	C008	C00C	119.49(14)
C00B	C00A	Ru1	70.40(8)
C00F	C00A	Ru1	72.04(9)
C00F	C00A	C00B	120.72(15)
C008	C00B	Ru1	72.25(8)
C00A	C00B	Ru1	71.38(9)
C00A	C00B	C008	121.41(14)
C008	C00C	Ru1	72.40(8)
C00E	C00C	Ru1	71.01(9)
C00E	C00C	C008	121.19(15)
C00I	C00D	C008	108.59(14)
C00J	C00D	C008	113.61(15)
C00J	C00D	C00I	110.97(17)
C00C	C00E	Ru1	71.01(9)
C00F	C00E	Ru1	72.62(9)
C00F	C00E	C00C	120.98(15)
C00A	C00F	Ru1	70.66(9)
C00E	C00F	Ru1	69.30(9)

F6	P1	F1	89.3(8)	C00E C00F C00A	118.07(15)
F6	P1	F3	175.3(4)	C00K C00F Ru1	129.23(13)
F6	P1	F2	90.2(3)	C00K C00F C00A	121.13(17)
F6	P1	F4	88.4(3)	C00K C00F C00E	120.74(17)
F5	P1	F1	177.6(6)		

Table 6 Hydrogen Atom Coordinates (Å×10^4) and Isotropic Displacement Parameters (Å^2×10^3) for SJ100.

Atom	*x*	*y*	*z*	U(eq)
H00A	4634(2)	-146.5(17)	3859.3(15)	44.3(4)
H00B	6721(2)	539.6(17)	2565.8(14)	40.1(4)
H00C	3070(2)	3621.2(19)	865.6(13)	42.7(4)
H00D	5988(2)	3507(2)	377.5(14)	46.8(4)
H00E	998(2)	2958(2)	2154.5(15)	46.7(4)
H00f	5406(5)	1623(17)	-820(9)	87.7(8)
H00g	7267(18)	1809(15)	-1055(7)	87.7(8)
H00h	6900(20)	434(4)	-282(3)	87.7(8)
H00i	8832(8)	2726(19)	593(7)	83.9(8)
H00j	8007(4)	2833(18)	1859(8)	83.9(8)
H00k	8606(10)	1245(3)	1286(15)	83.9(8)
H00l	350(12)	1651(7)	3969(13)	88.8(8)
H00m	807(17)	-41(14)	3575(8)	88.8(8)
H00n	1739(6)	470(20)	4628(5)	88.8(8)
H1a	2250(30)	3450(30)	5000(30)	71(8)
H1b	2660(40)	4750(40)	4790(30)	87(10)
H1c	1390(40)	4440(30)	4190(20)	76(9)
H2a	3690(40)	5720(30)	2380(30)	78(9)
H2b	5330(40)	5270(30)	2410(30)	83(10)
H2c	4500(40)	5660(30)	3370(30)	76(8)

Table 7 Atomic Occupancy for SJ100.

Atom	*Occupancy*	Atom	*Occupancy*	Atom	*Occupancy*
F1	0.61(5)	F3	0.649(13)	F2	0.649(13)
F4	0.649(13)	F6	0.649(13)	F5	0.61(5)
F6a	0.384(13)	F2a	0.384(13)	F3a	0.384(13)
F4a	0.351(13)	F1a	0.39(5)	F5a	0.39(5)

Experimental

Single crystals of $C_{40}N_8RuClPFH$ **[SJ100]** were **[]**. A suitable crystal was selected and **[]** on a diffractometer. The crystal was kept at 299.01 K during data collection. Using Olex2 [1], the structure was solved with the ShelXD [2] structure solution program using Dual Space and refined with the olex2.refine [3] refinement package using Gauss-Newton minimisation.

1. Dolomanov, O.V., Bourhis, L.J., Gildea, R.J, Howard, J.A.K. & Puschmann, H. (2009), J. Appl. Cryst. 42, 339-341.
2. Sheldrick, G.M. (2008). Acta Cryst. A64, 112-122.
3. Bourhis, L.J., Dolomanov, O.V., Gildea, R.J., Howard, J.A.K., Puschmann, H. (2015). Acta Cryst. A71, 59-75.

Crystal structure determination of [SJ100]

Crystal Data for $C_{40}N_8RuClPFH$ (M=903.30 g/mol): triclinic, space group P-1 (no. 2), a = 8.1167(13) Å, b = 9.0006(14) Å, c = 11.3836(18) Å, α = 88.140(2)°, β = 88.283(2)°, γ = 77.956(2)°, V = 812.7(2) Å^3, Z = 1, T = 299.01 K, μ (Mo Kα) = 1.282 mm^{-1}, *Dcalc* = 1.8456 g/cm^3, 16901 reflections measured (3.58° ≤ 2Θ ≤ 58.42°), 4409 unique (R_{int} = 0.0128, R_{sigma} = 0.0108) which were used in all calculations. The final R_1 was 0.0189 (I>=2u(I)) and wR_2 was 0.0503 (all data).

Refinement model description

Number of restraints - 115, number of constraints - 25.

Details:

```
1. Fixed Uiso
 At 1.2 times of:
  All C(H) groups
 At 1.5 times of:
  All C(H,H,H) groups
2. Restrained distances
 P1-F3 ≈ P1-F3a
 with sigma of 0.02
 P1-F2 ≈ P1-F2a
 with sigma of 0.02
 P1-F4 ≈ P1-F4a
 with sigma of 0.02
 P1-F6 ≈ P1-F6a
 with sigma of 0.02
 F3-F2 ≈ F3-F4 ≈ F6a-F2a ≈ F6a-F4a ≈ F2-F6 ≈ F6-F4 ≈
F2a-F3a ≈ F3a-F4a
 with sigma of 0.04
 P1-F3 ≈ P1-F6a ≈ P1-F2 ≈ P1-F1 ≈ P1-F6 ≈ P1-F2a ≈
P1-F3a ≈ P1-F4a ≈ P1-F4 ~
 P1-F5
 with sigma of 0.02
 F3-F2 ≈ F3-F4 ≈ F6a-F4a ≈ F6a-F2a ≈ F2-F6 ≈ F3a-F4a ≈
F3a-F2a ≈ F6-F4
 with sigma of 0.04
 P1-F3 ≈ P1-F6a ≈ P1-F2 ≈ P1-F1 ≈ P1-F3a ≈ P1-F4a ≈
P1-F6 ≈ P1-F2a ≈ P1-F4
 with sigma of 0.02
 F1-P1 ≈ F1a-P1
 with sigma of 0.02
 P1-F5 ≈ P1-F5a
```

```
 with sigma of 0.02
 F3-F2 ≈ F3-F1 ≈ F3-F4 ≈ F3-F5 ≈ F6a-F1a ≈ F6a-F2a ≈
F6a-F4a ≈ F2-F1 ≈ F2-F6 ~
 F2-F5 ≈ F1-F6 ≈ F1-F4 ≈ F1a-F2a ≈ F1a-F4a ≈ F3a-F2a ≈
F3a-F4a ≈ F3a-F5a ≈ F2a-
 F5a ≈ F4a-F5a ≈ F6-F4 ≈ F6-F5 ≈ F4-F5
 with sigma of 0.04
 P1-F3 ≈ P1-F6a ≈ P1-F2 ≈ P1-F1 ≈ P1-F1a ≈ P1-F3a ≈
P1-F2a ≈ P1-F4a ≈ P1-F6 ~
 P1-F4 ≈ P1-F5 ≈ P1-F5a
 with sigma of 0.02
 N1-N2 = N1-C00E = N1-C00F = N1-Cl1 = N2-C00C = N2-C00E
≈ N2-C008 ≈ N2-Cl1 ~
 C00C-C00E ≈ C00C-C00B ≈ C00C-C00A ≈ C00C-C008 ≈ C00C-C00F
≈ C00E-C00B ≈ C00E-
 C00A = C00E-C008 = C00E-C00F = C00B-C00A = C00B-C008 =
C00B-C00F ≈ C00B-Cl1 ~
 C00A-C008 ≈ C00A-C00F ≈ C00A-Cl1 ≈ C008-C00F
 with sigma of 0.04
 Ru1-N1 = Ru1-N2 = Ru1-C00C = Ru1-C00E = Ru1-C00B =
Ru1-C00A ≈ Ru1-C008 ≈ Ru1-
 C00F ≈ Ru1-Cl1
 with sigma of 0.02
3. Rigid body (RIGU) restrains
 F3, F2, F4, F6, P1, F5
 with sigma for 1-2 distances of 0.004 and sigma for 1-3 distances of 0.004
 F3, F2, F4, F6, P1, F5, F1
 with sigma for 1-2 distances of 0.004 and sigma for 1-3 distances of 0.004
 F6a, F2a, F3a, F4a, P1, F1, F5
 with sigma for 1-2 distances of 0.004 and sigma for 1-3 distances of 0.004
 F1, F3, F2, F4, F6, F5, P1
 with sigma for 1-2 distances of 0.004 and sigma for 1-3 distances of 0.004
 F6a, F2a, F3a, F4a, F1a, F5a, P1
 with sigma for 1-2 distances of 0.004 and sigma for 1-3 distances of 0.004
4. Others
 Sof(F4a)=1-FVAR(1)
 Sof(F3)=Sof(F2)=Sof(F4)=Sof(F6)=FVAR(1)
 Sof(F6a)=Sof(F2a)=Sof(F3a)=FVAR(2)
 Sof(F1a)=Sof(F5a)=1-FVAR(3)
 Sof(F1)=Sof(F5)=FVAR(3)
5.a Ternary CH refined with riding coordinates:
 C00A(H00A), C00B(H00B), C00C(H00C), C00D(H00D), C00E(H00E)
5.b Idealised Me refined as rotating group:
 C00I(H00f,H00g,H00h), C00J(H00i,H00j,H00k), C00K(H00l,H00m,H00n)
```